SURFACE FUNCTIONALIZED MAGNETIC NANOPARTICLES FOR SEPARATION OF CHIRAL BIOMOLECULES, PHARMACEUTICALS AND ENDOCRINE DISRUPTING COMPOUNDS

SUDIPA GHOSH

NATIONAL UNIVERISTY OF SINGAPORE
2012

SURFACE FUNCTIONALIZED MAGNETIC NANOPARTICLES FOR SEPARATION OF CHIRAL BIOMOLECULES, PHARMACEUTICALS AND ENDOCRINE DISRUPTING COMPOUNDS

SUDIPA GHOSH

B.Sc. (Chemical Engineering)

Bangladesh University of Engineering & Technology

A THESIS SUBMITTED
FOR THE DEGREE OF DOCTOR OF PHILOSOPHY
DEPARTMENT OF CHEMICAL & BIOMOLECULAR
ENGINEERING

NATIONAL UNIVERSITY OF SINGAPORE

2012

Acknowledgements

I would like to take this opportunity to express my heartfelt gratefulness and admiration to my supervisors, Professor Mohammad Shahab Uddin (International Islamic Univeristy, Malaysia) and Associate Professor Kus Hidajat, whose encouragement, guidance and full support from the initial level enabled me to come up to this point.

I would give much credit to my husband, beloved parents and family members for their endless love, understanding, moral support and inspiration during my research.

I would like to thank all staff members in the Department of Chemical and Biomolecular Engineering and my laboratory colleagues who have supported me throughout this project work.

Finally, I would like to thank National University of Singapore for providing me the Research Scholarship and department of Chemical and Biomolecular Engineering for providing all the facilities for carrying out this research work.

Sudipa Ghosh

December, 2012

Table of contents

Summary

In the past decade, synthesis of superparamagnetic nanoparticles has been intensively developed not only for its fundamental scientific interest but also for many technological applications. A wide range of metal, magnetic, semiconductor and polymer nanoparticles with tunable sizes and properties can be synthesized by wet-chemical techniques. Magnetic nanoparticles (MNPs) have the advantages of good dispersibility in various solvents, high surface area and strong magnetic responsivity. These magnetic nanoparticles have emerged as excellent materials in many fields, such as immobilized catalysis, labelling and sorting of biological species, targeted drug or gene delivery, magnetic resonance imaging, and hyperthermia treatment. An important application of these nanoparticles is magnetic separation. Because of strong magnetism, these MNPs can be used as separable supports for adsorbent, which makes profound contribution to green chemistry. The surfaces of these particles are often modified by capping agents such as polymers, inorganic metals or oxides, and surfactants to make them stable, biocompatible, and suitable for further functionalization and applications.

Cyclodextrins (CDs) are natural products which are produced from starch by means of enzymatic conversion. Typical cyclodextrins contain a number of glucose monomers ranging from six to eight units in a ring, creating a cone shape. CDs are promising tools for applications in drug carrier systems, nano reactors, bioactive supramolecular assemblies, molecular recognition and catalysis. The combination of CDs and inorganic nanoparticles has attracted increasing attention. These particles can be utilized for sensing, chiroselective analysis, controlled hydrophobic drug delivery and so on. In this work, magnetite silica particles coated with carboxymethyl-β-cyclodextrin (CMCD) are

synthesized via layer-by-layer method. Cyclodextrin derivatives are synthesized and applied as chiral selectors because of their favorable properties (stability, low cost, UV transparency, inertness, etc.). The bare MNPs are prepared by chemical precipitation of Fe^{2+} and Fe^{3+} salts in the ratio of 1:2 under alkaline and inert condition. Afterwards, surface of these particles are modified by silica to achieve stability against agglomeration and further modification of the particles' surface is done by coating with CMCD. The functionalized magnetic nanoparticles (core-shell) are characterized using several analytical methods namely Fourier Transform Infra-Red (FTIR) spectroscopy, Transmission Electron Microscopy (TEM), X-ray Photoelectron Spectroscopy (XPS), X-ray Diffraction (XRD) and Vibrating Sample Magnetometer (VSM). The thickness of silica shell is about 9 nm and average size of $Fe_3O_4/SiO_2/CMCD$ MNP (silica and CMCD coated magnetic nanoparticle) is around 29 nm.

The as-synthesized particles are used to adsorb single amino acid enantiomers namely D- and L- tryptophan (Trp), D- and L-phenylalanine (Phe) and D- and L-tyrosine (Tyr). Adsorption of these amino acid enantiomers on $Fe_3O_4/SiO_2/CMCD$ MNPs are also studied in detail as function of initial solution pH and temperature. High adsorption capacities of these MNPs are observed at pH around isoelectric points (pI) of the amino acids and at temperature 25°C. Noteworthy, remarkable differences are observed between adsorption capacities of the particles toward the above mentioned D- and L-enantiomers of amino acids. At low concentration of amino acids, adsorption capacities are compared and in same conditions, adsorption capacities of the particles toward amino acids are in the order of tryptophan> phenylalanine>tyrosine. It seems that structure and hydrophobicity of amino acid molecules are responsible for difference in adsorption, by influencing the strength of interactions between amino acid molecules and the particles. It has been shown that adsorption of amino acids are consistent with

Freundlich isotherm equation. Finally, desorption of amino acids is carried out using methanol as eluent and it is found that around 90% desorption of L-amino acids and (75-80) % desorption of D-amino acids are achieved under described condition.

Moreover, chiral resolution of racemic aromatic amino acids, DL-tryptophan (Trp), DL-phenylalanine (Phe), DL- tyrosine (Tyr) from phosphate buffer solution is achieved in present study employing the concept of selective adsorption by surface functionalized magnetic nanoparticles. Resolution of enantiomers from racemic mixture is quantified in terms of enantiomeric excess using chromatographic methods. The nanoparticles selectively adsorb L-enantiomer of Trp, Tyr, and Phe from racemic mixture and the enantiomeric excesses (e.e) are determined as 94%, 73% and 58% for Trp, Phe and Tyr enantiomers, respectively. Furthermore, XPS studies explore that interaction of the enantiomers is mainly attributed to the formation of hydrogen bond between amino group of the amino acid molecule and secondary hydroxyl group of CMCD on the particle surface. Noteworthy, FTIR studies prove that the enantiomers interact with hydrophobic cavity of cyclodextrin molecule to from inclusion complex. Furthermore, higher binding constants are obtained for inclusion complexation of CMCD with L-enantiomers compared to D-enantiomers using flurometric titrations which might have yielded enantioselective properties of the CMCD functionalized magnetite silica nanoparticles.

Afterwards, synthetic strategies are developed for grafting of amino-β-cyclodextrin (β-CDen) onto superparamagnetic Fe_3O_4 nanoparticles by layer-by-layer methods. β-CDen (en:-$NHCH_2CH_2NH_2$) functionalized magnetic nanoparticles are fabricated by grafting mono-6-ethylenediamino-6-deoxy-β-CD (β-CDen) onto thiodiglycolic acid (TDGA) modified magnetic nanoparticles. For confirmation of grafting of β-CDen onto nano-

sized magnetic particles, characterizations are carried out using FTIR spectroscopy, TEM, XPS, XRD analysis, VSM and Thermogravimetric Analysis (TGA). Characterizations by these methods reveal that CDen-MNPs are superparamagnetic nanoparticles with mean diameter of around 11.5 nm. Thermogravimetric analysis indicates that the amount of β-CDen grafted onto the CDen-MNPs is 0.050 mmolg^{-1}. These as-synthesized β-CDen bonded magnetic nanoparticles with combined effect of inclusion properties of CD and magnetic properties of iron oxide are used as potential adsorbent for removal of two pharmaceuticals, carbamazepine (CBZ) and naproxen (NAP) and an endocrine disrupting agent, bisphenol A (BPA) from aqueous solution. Adsorption of the pharmaceuticals and endocrine disrupting compound is found to be pH dependent. β-CDen being grafted on TDGA-coated Fe_3O_4 nanoparticle contributes to an enhancement of adsorption capacities because of the inclusion abilities of its hydrophobic cavity with organic contaminants through host-guest interactions. Experimental data for adsorption of these three chemicals are fitted well to Freundlich isotherm model. Under same experimental conditions (pH 7 and 25°C), adsorption capacities of β-CDen-MNPs toward the three above mentioned targets are found to be in the order of carbamazepine> naproxen> bisphenol A. For better understanding of the interaction between target molecules and CDen MNPs, their inclusion complexes are studied by FTIR spectroscopy which confirms formation of inclusion complexes through van der Waals interaction. Desorption study of pharmaceuticals and EDC shows that ethanol could be used as desorbing agent but for complete desorption multiple steps may be required.

Adsorption of beta-blocker, propranolol utilizing silica and CMCD modified magnetic nanoparticles (Fe_3O_4/SiO_2/CMCD MNPs) from phosphate buffer solution is also studied as function of initial solution pH and initial concentration of sorbate.

Adsorption capacity of the adsorbent increases as pH is increased from 3 to 9 and then reaches the plateau at pH 11. It appears that hydrophobicity of beta-blocker, propranolol affects the interaction with cyclodextrin functionalized magnetic nanoparticles as well as adsorption capacity of the MNPs. Sorption capacity of the nanoadsorbents bearing cyclodextrin is compared and is found to be higher than that of bare magnetic nanoparticles, which is due to presence of cyclodextrin on nanoparticles' surface. Kinetic studies reveal that adsorption of propranolol on the nanoadsorbents is very fast and is completed within 1 hr. The kinetic data of propranolol adsorption is found to follow pseudo-second-order kinetic model. Equilibrium data in aqueous solution is well represented by Freundlich isotherm model. XPS analysis reveals that propranolol adsorption onto the magnetic nanoparticle mainly involve nitrogen atoms to form surface complexes. In addition, FTIR spectroscopy is applied to investigate adsorption mechanism. Finally, desorption studies are carried out and 50% methanol solution is found to be effective for almost complete desorption. All these experimental results show that β-cyclodextrin derivative conjugated MNPs could be promising tools for separation of chiral molecules as well as separation/ removal of pharmaceuticals, endocrine disrupting compounds and beta-blockers from waste-water.

Nomenclature

Symbols

H	Magnetic field strength
B	Magnetic flux density
μ_0	Permeability of free space
M	Magnetic moment per unit volume
M_s	Saturation magnetization
M_r	Residual magnetization
H_c	Coercive field
F_m	Magnetic force
χ	Magnetic susceptibility
r	Radius of particle
k_B	Boltzmann constant
T	Temperature
Tc	Curie temperature
T_N	Neel temperature
C	Material specific curie constant
K_u	Crystalline magneto anisotropy
C_i	Initial concentration (mM or ppm)
C_e	Equilibrium concentration (mM or ppm)
Q_m	Maximum adsorption capacity (mg/g)
Q_e	Adsorption capacity at equilibrium (mg/g)
Q_t	Adsorption capacity at any time (mg/g)
k_L	Langmuir constant

k_F	Freundlich constant
n	Empirical constant
k_1	Pseudo first order rate constant
k_2	Pseudo second order rate constant
θ	Half diffraction angle (deg)
λ	Wavelength of X-ray (nm)
β	Half width of XRD diffraction line (red)

Abbreviations

CD	Cyclodextrin
α-CD	α-cyclodextrin
β-CD	β-cyclodextrin
γ-CD	γ-cyclodextrin
S-β-CD	Sulfated-β-cyclodextrin
CMCD	Carboxymethyl-β-cyclodextrin
Ts-β-CD	Monotosyl- β-cyclodextrin
β-CDen	6 deoxy-6-ethylenediamino-β-cyclodextrin (amino-cyclodextrin)
MNP	Magnetic nanoparticle
CMP	as-synthesized citric acid modified particle
Fe_3O_4/SiO_2 MNP	as-synthesized silica coated magnetic nanoparticle
$Fe_3O_4/SiO_2/CMCD$ MNP	as-synthesized silica and CMCD coated magnetic nanoparticle
CDen MNP	as-synthesized β-CDen coated magnetic nanoparticle
TDGA MNP	as-synthesized thiodiglycolic acid coated magnetic nanoparticle
PhAC	Pharmaceutically active compound
EDC	Endocrine disrupting compound

Trp	Tryptophan
Phe	Phenylalanine
Tyr	Tyrosine
CBZ	Carbamazepine
NAP	Naproxen
BPA	Bisphenol A
CSP	Chiral Stationary Phase
Dns	Dansyl (5-(dimethyl amino)naphthalene-1-sulfonyl)
DNB	3, 5-dinitrobenzoyl
DNFB	2, 4 dinitroflurobenzene
FITC	Fluorescein isothiocyanate
Fmoc	Fluorenylmethyl chloroformate
Ala	Alanine
Arg	Arginine
Asn	Asparagine
Asp	Aspartic acid
Cys	Cysteine
Eth	Ethionine
Glu	Glutamic acid
Gln	Glutamine
Gly	Glycine
His	Histidine
Ile	Isoleucine
Leu	Leucine
Nle	Norleucine

Pro	Proline
Met	Methionine
Ser	Serine
Thr	Threonine
Val	Valine
Nva	Norvaline
Lys	Lysine
TEOS	Tetraethyl orthosilicate
TDGA	Thiodiglycolic acid
FTIR	Fourier-transform Infrared Spectroscopy
TEM	Transmission Electron Microscopy
XPS	X-ray Photoelectron Spectroscopy
XRD	X-ray Diffraction
TGA	Thermogravimetric Analysis
VSM	Vibrating Sample Magnetometer
BET	Brunauer-Emmett-Teller method
HPLC	High Performance Liquid Chromatography

List of figures

List of tables

Chapter 1: Introduction

1.1 Background on magnetic separation

Separation is an important process in chemical engineering which is used to enrich one of the components from the feed solution. Magnetic separation is a process in which magnetically susceptible material is extracted from a mixture using magnetic force. Magnetic separation techniques are used in several different areas ranging from steel production to biotechnology, since they are rapid, cost effective and highly efficient. The process, magnetic separation involves magnetic particles, carrier liquids, complexes and target molecules. In a standard process, magnetic particles are compounded with some intermediate to form a complex. These complex particles can interact with the target molecules and can be separated using magnetic field gradient. The basic concept is to utilize physical interactions between magnetic complex particles and target molecules as well as the specific chemical interactions between the particles and target molecules. The interaction forces involved in magnetic separation process could be electrostatic, hydrophobic and specific ligand interactions.

In 1987, Wikström reported the use of magnetically susceptible additives (ferrofluids or iron oxide particles) and an external magnetic field induced faster phase separations in liquid–liquid extraction procedures than the more conventional methods like chromatography, filtration and distillation processes [1]. Since the introduction of magnetic separation techniques employing small magnetic particles in the 1970s, increased attention has been paid to their development and applications in different areas such as medical imaging, magnetic field assisted transport, separations analysis, biomedical and biotechnological applications including drug delivery, biosensors,

chemical and biochemical separation and concentration of trace amounts of specific targets, such as bacteria, enzyme encapsulation and contrast enhancement in magnetic resonance imaging (MRI) [2-11].

1.2 Surface functionalization of magnetic particles

Over the last few years, synthesis of superparamagnetic nanoparticles (NPs) was intensively developed for various applications because of the advantages of good dispersibility in various solvents, high surface area, and strong magnetic responsivity [12, 13]. However, several unavoidable problems are associated with magnetic NPs, such as their intrinsic instability over long periods due to their tendency to aggregate in order to reduce their surface energy, as well as the ease with which they are oxidised in air. The aggregation of magnetic nanoparticles can significantly decrease their interfacial area, thus resulting in the loss of magnetism and dispersibility. It is therefore crucial to develop new strategies to chemically stabilize the bare magnetic nanoparticles against degradation during or after the synthesis processes [14]. Surface functionalization allows immobilized affinity ligands to capture target biomaterials.

Research has shown that coatings of polymer, silica, or other materials over magnetic nanoparticles can prevent aggregation and functionalize the magnetic nanoparticles to extend their applications in catalysis and biomedicine. Various materials such as surfactant, dextran, polyethylene glycol (PEG), organic acids, polyoxoamines, metal oxide and silica have been used for coating and stabilizing magnetic nanoparticles. Among the materials studied for coating, silica is particularly attractive as it exhibits high biocompatibility and stability, low toxicity, and simple functionality [14-16]. Unlike polymers, it is not subjected to microbial attack and it neither swells nor changes porosity in response to the environmental pH values [17].

Now-a-days, cyclodextrins (CDs) play major roles in many disciplines such as supramolecular chemistry, analytical chemistry, catalysis and biomedicine [18-24]. Since their discovery, parent CDs and their derivatives have served as multi-purpose prototypes for novel host compounds. The CD molecules assume shape of a truncated cone in aqueous environment, exposing their hydroxyl groups to the solvent while the relatively more hydrophobic remainder of the molecule constitutes internal cavity. Properly sized and shaped guests can enter the cavity to form inclusion complexes that can be stabilized by hydrophobic interactions, van der Waals forces and hydrogen bonds [18-25]. All these properties account for their aqueous solubility and ability to encapsulate hydrophobic moieties into their cavities. The incorporation of guest molecules in CD inclusion complexes in aqueous media has been the basis for their most biomedical applications [20, 21, 26]. Recently, some researchers have started using cyclodextrin coated particles using their inclusion complex formation property for various applications [27-30].

Initially in this work, we have coated bare magnetic nanoparticles with silica and carboxymethyl-β-cyclodextrin (CMCD) and have utilized the as-synthesized particles to separate single chiral amino acid enantiomers from aqueous solutions. Benefit of using cyclodextrin bonded magnetic silica particles is tributed by the combined properties of the particles such as magnetic properties of Fe_3O_4, biocompatibility of silica shell and chiral recognition and inclusion complex formation properties of cyclodextrin.

Afterwards, silica and CMCD coated magnetic nanoparticles have been applied to separate chiral amino acid enantiomers from their racemic mixture in aqueous solution. Moreover, superparamagnetic nanoparticles have been coated with amino-CD (β-CDen) and these nanoparticles have been utilized as potential adsorbent for separation of

pharmaceuticals and endocrine disrupting compound. Recently, magnetic nanoparticles coated with silica and CMCD have been used for adsorption separation of beta-blocker, propranolol from aqueous solution. These as-prepared β-CD derivative coated magnetic nanoparticles with inclusion complex formation capabilities and magnetic properties, would be of great use for chiral separation and separation of emerging contaminants (pharmaceuticals, EDCs and beta-blockers) from waste-water.

1.3 Research objectives

Currently established chiral chromatographic separation methods are able to resolve most of the protein amino acids, but there is still need for a rapid, highly efficient and cost effective method for enantioseparation of amino acids. To the best of our knowledge, no such work has been published for enantioseparation of amino acids using coated/ uncoated magnetic nanoparticle which will be a promising way to separate the enantiomers and also inexpensive. Although the magnetic separation processes are increasingly appealing due to their simplicity, efficiency and versatility, there is still a need to study these separation processes in a systemically and detailed way. Firstly, previous published work focused on application of chromatographic methods for chiral separation. So, separation of chiral enantiomers can be studied utilizing surface functionalized magnetic particles. Secondly, for batch adsorption mode, adsorption equilibrium, adsorption kinetics and effects of various parameters (such as pH, temperature, etc.) on adsorption need to be studied in details. Furthermore, enantioselective separation/ chiral resolution of racemic amino acids should be investigated. Lastly, exploration of interaction forces involved and enantioseparation mechanism of the racemic amino acids onto $Fe_3O_4/SiO_2/CMCD$ MNPs is very important.

Research on the effects of chemical pollution in the environment related to urban waste-waters' discharge and reuse until recently was focused almost exclusively on conventional pollutants. Thousands of tons of pharmacologically active substances being used annually are ending up in waste-waters. In addition, during last several years there has been a growing level of concern related to the hypothesis that various chemicals may exhibit endocrine disrupting effects. In many countries facing prolonged droughts and implementing waste-water reuse schemes for irrigation and groundwater discharge, existence of xenobiotic compounds in the tertiary treated waste-waters constitutes a new concern. To the best of our knowledge, no such research work has been found which utilizes cyclodextrin functionalized magnetic nanoparticles for removal of pharmaceutically active compound, endocrine disruptors and beta-blockers. Thus the application of cyclodextrin derivative functionalized magnetic nanoparticles for removal of pharmaceuticals, endocrine disrupting compound and beta-blocker should be investigated. Furthermore, adsorption equilibrium, detailed adsorption kinetics and effect of operating condition on adsorption should be studied in batch adsorption mode. Desorption of the adsorbed molecules and regeneration of the nano adsorbents should be studied as well.

The overall objectives of this research program are to study the application of nanosized magnetic particles for separation of chiral amino acids, pharmaceuticals, endocrine disrupting compound and beta-blocker and the evaluation of effectiveness of the separation method. The desired goals of different procedures could be divided into the following:

1) Preparation of nano-sized magnetic particles, and modify the surface with silica and carboxymethyl-β-cyclodextrin.

2) Characterization of as-synthesized magnetic particle coated with silica and carboxymethyl-β-cyclodextrin (Fe_3O_4/SiO_2/CMCD MNPs).

3) Study on adsorption equilibrium, adsorption kinetics and effects of various parameters on adsorption of single amino acid enantiomers.

4) Study on selective adsorption of the enantiomers of chiral amino acids and analysis of chiral separation of enantiomers.

5) Exploration of chiral separation mechanism of the amino acids onto Fe_3O_4/SiO_2/CMCD MNPs using several analytical techniques.

6) Synthesis of thiodiglycolic acid (TDGA) and amino-cyclodextrin (β-CDen) functionalized magnetic nanoparticle and characterization of the synthesized particle.

7) Detailed study of adsorptive removal of pharmaceuticals (carbamazepine, naproxen) and endocrine disrupting compound (bisphenol-A) using β-CDen coated particle.

8) Study of adsorption behaviour of beta-blocker, propranolol onto Fe_3O_4/SiO_2/CMCD MNPs in details.

9) Study on desorption of adsorbed targets using different chemicals.

1.4 Organization of the Thesis

The thesis is organized into nine chapters. Chapter 1 gives an introduction to the magnetic separation method. The objectives of the present work are introduced and structural organization of the whole thesis is also presented in this chapter. Chapter 2 describes the background of magnetic separation, reviews previous work on magnetic separation and introduces the recent progress in separation of chiral biomolecules, pharmaceuticals, endocrine disrupting compounds and beta-blockers. Based on the detailed review on past work, scope of this study is presented. In Chapter 3, description

on experimental materials and methods are presented. Chapter 4 describes the detailed characterization of silica and carboxymethyl-β-cyclodextrin coated magnetic nanoparticles. In Chapter 5, adsorption results of single amino acid enantiomers of Trp, Phe and Tyr on silica and CMCD coated MNPs under different operating conditions are presented and kinetics of the batch adsorption studies are investigated. In Chapter 6, chiral separation of racemic amino acids utilizing silica and CMCD coated MNPs is explored. Selective adsorption capacities of the magnetic particles towards the enantiomers are studied, enantiomeric excesses of the amino acids are determined and some insights are presented regarding chiral separation mechanism. In Chapter 7, adsorption results of pharmaceuticals and endocrine disrupting compounds are presented. Effect of operating conditions, kinetics of sorption separation and desorption conditions of pharmaceuticals and endocrine disruptor onto β-CDen modified MNPs are explored in this chapter. Chapter 8 covers detailed adsorption studies of beta-blocker, propranolol which include effect of operating parameters, kinetic studies of adsorption onto CMCD functionalized magnetite silica nanoparticles and desorption studies. Adsorption mechanism is also described using different analytical methods in Chapter 8. Finally, in Chapter 9 conclusions obtained from the research work are presented and trends for future works are presented.

Chapter 2: Literature review

In this chapter, literature review on magnetic separation, magnetic nanoparticles, their properties and surface modification, cyclodextrin and its structural properties and applications, chiral amino acid separation, separation of pharmaceuticals, endocrine disrupting compounds and beta-blockers are presented.

2.1 Magnetic separation

Economical separation from bioprocesses is important for purification of bioproducts. However, mechanical separation techniques such as centrifugation or filtration have some disadvantages; i.e. centrifugation requires a lot of energy and filtration sometimes becomes very troublesome by clogging of filters. Among the other separation techniques, chromatography is a powerful technology for purification of biological substances in both analytical and preparative scales. But, packed bed chromatographic column is prone to clogging. To overcome this drawback, various alternative separation techniques have been developed, including fluidizing bed adsorption [31], expanded bed adsorption [32] and magnetic separations [33, 34]. Compared with mechanical separation, magnetic separation is particularly attractive since less energy is needed and strong magnetic force can be generated easily.

There have been several separation approaches performed under magnetic field. The most well-known technique is the magnetically stabilized fluidized bed [34]. The others involve high gradient magnetic filtration [35], magnetophoresis [36] and magnetic split-flow thin fractionation [37].

2.1.1 Classifications of magnetic separation

The technique magnetic separation can be classified as follows-

1. Magnetic separation: In a narrow sense, magnetic separation is a technique whose goal is to concentrate a magnetic material, to remove magnetic impurity or to extract valuable magnetic materials by discharging the particles captured by a magnet at a position depending on their magnetic properties.

2. Magnetic filtration: Magnetic filtration is the method to separate magnetic particles by capturing them in a filter.

3. Magnetic flotation: Magnetic interactions are used to separate materials of different density by magnetic flotation.

4. Magnetohydrostatic separation: When the separation target is non-magnetic or an ion, the magnetic reagent method, in which separation target is sprinkled with a magnetic reagent, is employed. Magnetohydrostatic separation is used to separate non-magnetic materials suspended in a magnetic fluid by adjusting the magnetic buoyant force on materials with a magnetic gradient field.

These techniques are all based on the magnetic feature of the solid-phase employed to achieve a desired separation. Thus, the availability of inexpensive magnetic supports with high selectivity and magnetic responsiveness is crucial to the large-scale application of the above-mentioned techniques.

2.1.2 Principle of magnetic separation

Magnetic separations fall into two general types: (1) those in which the material to be separated is intrinsically magnetic, (2) those in which one or more components of a mixture have been rendered magnetic by the attachment of a magnetically responsive entity.

Large-scale industrial magnetic separations are based on the intrinsic magnetic properties of materials. For example, low grade iron ores can be separated magnetically into hematite and waste; iron sulfide is paramagnetic and can be extracted from pulverized coal [38, 39]. Furthermore, red blood cells [40, 41] (which contain high concentrations of paramagnetic haemoglobin) and magnetic bacteria [42] (which contain small magnetite particles) provide examples of intrinsically magnetic responsive biological particles. So, in this method, magnetic separation of the target molecule can be achieved without further modification of magnetic materials.

In biological systems, magnetic separations generally involve conferring magnetism upon a non-magnetic (diamagnetic) molecule by attaching or adsorbing it to a magnetically responsive particle. Magnetic support materials have been widely used in the field of biotechnology in bioseparations and immunoassays and as immobilizers of enzymes and drug carriers [43-49], separation and purification of protein [50, 51]. The principle of this method is to utilize magnetic particles, which bind the target molecules via intermediates to form complexes that subsequently can be separated from the bulk solution in a gradient magnetic field. Thus, the non-magnetic targets firstly interact with the surfactants; polymer or ligand coated on magnetic particles, and then form a magnetic complex, which can magnetically respond to an external magnetic field. Separation process of non-magnetic target molecules is presented in Figure 2-1.
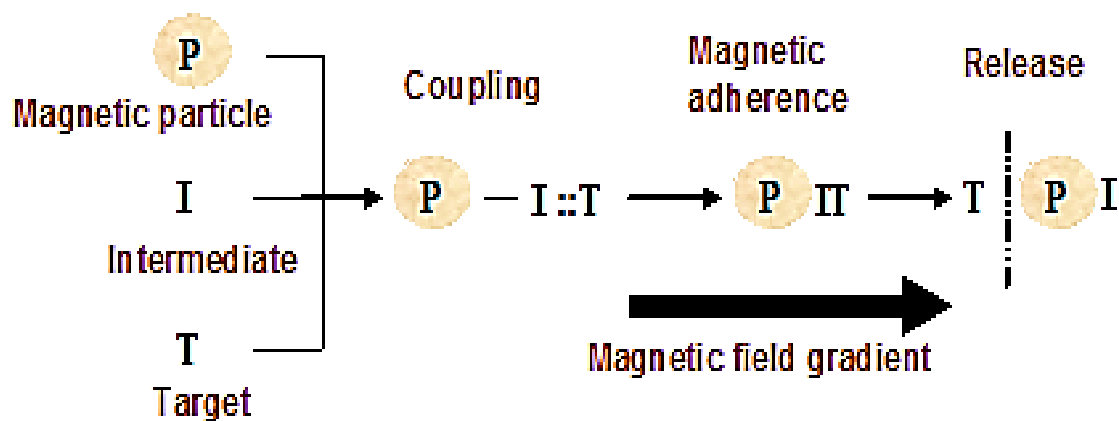
Figure 2-1 Schematic diagram of separation of non-magnetic targets.

2.1.3 Interaction forces involved in magnetic separation

Amino acid is a molecule containing an amine group, a carboxylic acid group and a side-chain that varies between different amino acids. Amino acids are usually classified by the properties of their side-chain into four groups. The side-chain can make an amino acid a weak acid or a weak base, and a hydrophile if the side-chain is polar or a hydrophobe if it is nonpolar. The amine and carboxylic acid functional groups found in amino acids allow them to have amphiprotic properties. An amphoteric species is a molecule or ion that can react as an acid as well as a base. Amino acids are found in all living organisms. Proteins are made in association of 20 primary amino acids [52]. It was found that molecular recognition plays important role in adsorption of amino acids [53].

Carbamazepine (CBZ) is a drug generally used for treatment of epilepsy and referred as neutral drug. Naproxen (NAP) is used for relief from fever, pain and exists as free acid which is practically insoluble in water. On the other hand, bisphenol A (BPA) is an endocrine disruptor and has two phenol functional groups in its structure. CBZ and BPA have pK_a >10 and they exist in neutral form below their pK_a. On the other hand,

NAP has pK_a of 4.15 and exists in neutral form below pH 4.15 and exists as negatively charged molecule above pH 4.15.

Propranolol is a sympatholytic non-selective beta-blocker. Sympatholytic is used to treat hypertension, anxiety and panic. Propranolol is available in generic form as propranolol hydrochloride. Propranolol (pK_a = 9.42), exists as a positively charged molecule in the tested pH below its pK_a and it exists as negatively charged molecule above its pK_a. Because of differences in surface charge, structure and physicochemical properties of the adsorbate and adsorbent, their uptake may differ significantly [54]. The adsorption behavior of the adsorbates at solid surfaces of magnetic nanoparticles is the net result of hydrogen bonding, ionic interaction, van der Waals interaction or hydrophobic effect which is described below.

1. Electrostatic interaction: If biomolecules have positive or negative surface charges, electrostatic interaction may guide the molecule to orient in the unique direction to bond with the oppositely charged surface of magnetic particles. Electrostatic interaction between amino acid and magnetic particle also exists at the isoelectric point of the amino acid. Some researchers studied the electrostatic aspects of the interaction of the amino acids utilizing different adsorbents [55, 56]. It was observed that, adsorption of acidic and basic pharmaceuticals on acrylic aster resin were attributed by electrostatic interaction [57]. Some researchers found that adsorption was dominated by electrostatic interaction using modified attapulgites for sorptive removal of beta-blocker propranolol [58].

2. Hydrophobic interaction: Hydrophobic interactions between biomolecules and magnetic particles also contribute to the adsorption process. Basically, non-polar side chain of biomolecules influence hydrophobic interaction with the magnetic particles'

surface. Some researchers found that the structure and hydrophobicity of amino acid molecules were responsible for the difference in adsorption, by influencing the strength of interactions between amino acid molecule and non-ionic polymeric adsorbent [53]. Furthermore, some work demonstrated the rational use of hydrophobic and electrostatic ligand-polymer interactions for recognition of D-Phe in a novel molecular imprinting system [55, 56]. Also, uptake of some pharmaceuticals and EDCs on some adsorbents was observed to be governed by the hydrophobicity of the compounds [54].

3. Hydrogen bonding and van der Waals interaction: Hydrogen bonds are formed between amino-carbonyl, hydroxyl-amino or hydroxyl-carbonyl groups of the amino acid and the adsorbent [52]. van der Waals force is the sum of attractive or repulsive forces between molecules other than those due to covalent bonds or the electrostatic interaction of ions with one another or with neutral molecules. van der Waals forces are relatively weak compared to normal chemical bonds. It was observed that very little van der Waals interaction was involved in chemical shifting of some amino acids, L-alanine (Ala) and L-leucine (Leu) [59]. Some studies showed that, adsorption of neutral pharmaceutical on acrylic ester resin was solely attributable to nonelectrostatic interaction involving hydrogen bonding (probably through the oxygen groups of the adsorbents) and van der Waals interactions [57]. While studying adsorption of beta-blockers pinodolol and propranolol using β-cyclodextrin polymer, some researchers estimated that once the aromatic rings of pinodolol and propranolol were included within the CD cavities, their bulky chains might have interacted with the polymer network through hydrogen bonding [60].

2.1.4 Advantages and disadvantages of magnetic separation

Magnetic separation is a technology involving the transport of magnetic or magnetically susceptible particles in a gradient magnetic field. Compared to the conventional separation methods, such as centrifugation and filtration, magnetic separation has the following advantages:

1. Magnetic separation process is simple and relatively easy to carry out in batch adsorption on magnetic particles. Separation of solid and liquid phases can be easily achieved only by manipulating an external magnetic field.

2. Since nano-sized magnetic particles have larger specific surface area, adsorption of target molecules at the surface of magnetic particles occurs at high rate. Meanwhile, transfer of magnetic particles in magnetic field is also fast by applying strong magnetic field.

3. The magnetic nanoparticles provide lower mass transfer resistance and less fouling [61].

4. Surface of magnetic nanoparticles' can be easily modified to contain different surface functional groups which are highly useful for separating wide range of sample molecules. For example, magnetic particles can be used to sort cells, recover antibodies/ enzymes, purify proteins etc.

5. Size of nanoparticles can be controlled manipulating various reaction parameters from nanometer to micrometer range.

6. Conventional separation methods need the use of expensive centrifuges or vacuum equipment, there is no such need for magnetic separation methods.

However, disadvantages of magnetic separation technique are-

1. The components of the system to be separated must have different magnetic susceptibilities [39].

2. Most of the present magnetic separation processes, especially in biotechnology, are studied only on lab-scale.

2.2 Magnetic particle

Most of the adsorption separation processes, including ion exchange, affinity, hydrophobic and reverse phase chromatography are performed in packed bed of particles typically having diameters on the order of tens of microns [62]. But because of the problems of 'high-pressure' and fouling in the packed bed systems, there was ample necessity to use alternative adsorbent. Magnetic particles are such an adsorptive separation media which can provide large interfacial areas, small diffusional resistances, high selectivity, capacity for large products and can be easily recovered and regenerated, even in the presence of colloidal contaminants. The most commonly used magnetic particles are magnetite (Fe_3O_4) and maghemite (γ- Fe_2O_3). Other types of magnetic particles are $MeO\bullet Fe_2O_3$, where Me= Ni, Co, Mg, Zn, Mn, Fe.

The attractive or repulsive forces between magnetic materials can be described in terms of magnetic dipoles- tiny bar magnets with opposite poles. Materials can be classified into diamagnetic, paramagnetic, ferromagnetic, ferrimagnetic, and antiferromagnetic according to the arrangement of their magnetic dipoles in the absence and presence of an external magnetic field [63, 64]. Figure 2-2 shows schematic diagrams of these five different situations.
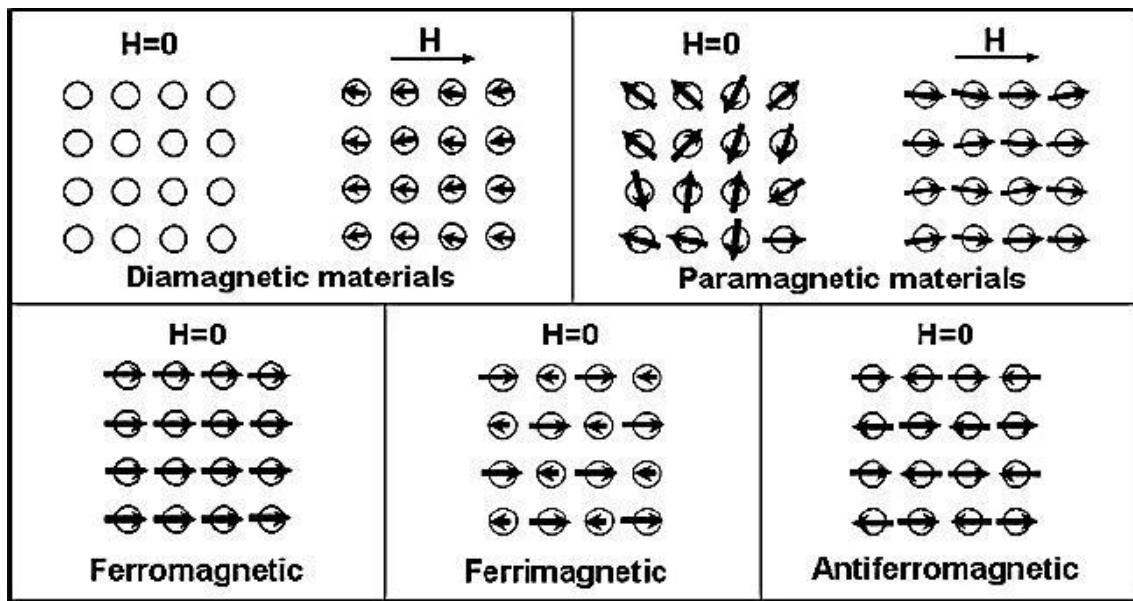
Figure 2-2 Schematic illustrating the arrangements of magnetic dipoles for five different types of materials in the absence or presence of an external magnetic field (H) [4].

If a material does not have magnetic dipoles in the absence of an external field and has weak induced dipoles in the presence of a field, the material is referred as diamagnetic. The magnetization of a diamagnet responds in the opposite direction to the external field. If a material has randomly oriented dipoles that can be aligned in an external field, it is paramagnetic. The magnetization of a paramagnet responds in the same direction as the external field. The magnetic interactions derived from the above two types of materials are very weak. For a ferromagnetic material, the magnetic dipoles always exist in the absence and presence of an external field and exhibit long-range order. Macroscopically, such a material displays a permanent magnetic moment. In a ferrimagnetic material there are always weaker magnetic dipoles aligned antiparallel to the adjacent, stronger dipoles in the absence of an external magnetic field. For an antiferromagnetic material, the adjacent dipoles are antiparallel in the absence of an

external field and cancel each other. In general, magnetic materials are referred to those characterized by either ferro- or ferrimagnetic features.

2.2.1 Magnetic forces

When a magnetic material is placed in a magnetic field of strength H, the magnetic induction/magnetic flux density can be expressed as:

$$B = \mu_0(H + M) \tag{2-1}$$

where, μ_0 is the permeability of free space, and magnetization $M = m/V$ is the magnetic moment per unit volume, where, m is the magnetic moment on a volume V of the material. Relationship between magnetization and magnetic field strength is:

$$M = \chi H \tag{2-2}$$

A magnetic field gradient is required to exert a force at a distance in the separation process. From the definition, magnetic force acting on a point like magnetic dipole m will be

$$F_m = (m.\nabla)B \tag{2-3}$$

In case of dilute suspension of nanoparticles in pure water, it can be approximated that the overall response of the particles plus water system $B = \mu_0 H$, so that equation 2-2 becomes:

$$F_m = \frac{V_m \Delta\chi}{\mu_0} (B.\nabla)B \tag{2-4}$$

where, F_m is the magnetic force, χ is the magnetic susceptibility of magnetic particles, V_m is the volume of the magnetic particles, μ_0 is the permeability of free space, and B is magnetic flux density. In general, magnetic force exerted on magnetic particles by magnetic field can be used to capture particles.

Both ferro- or ferrimagnetic materials can be described using a number of basic parameters derived from the magnetization curve where magnetization M or flux

density B is plotted against the magnetic field strength H [63, 64]. Figure 2-3 shows a typical curve, where magnetization always falls behind the applied magnetic field and produces a hysteresis loop because of magnetic domains inside the material [4]. From the magnetization curve, one can easily find the saturation magnetization M_s or the maximum value of M; residual magnetization M_r at zero applied field strength; and the coercivity H_c or the external field required to reduce the magnetization back to zero. A material is called a soft magnet if it can be magnetized readily in a weak field of around 10 Oe (1 Oe=1000/4π Am^{-1}) [63]. On the other hand, some magnetic materials can have very strong coercive fields and require large external fields applied to the opposite direction in order to be demagnetized. Such materials are known as hard magnets.
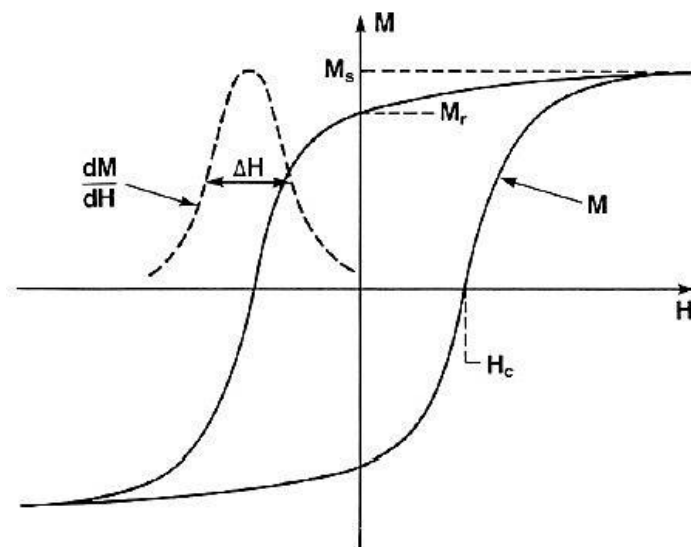
Figure 2-3 The typical magnetization curve of a ferro- or ferromagnetic material [4].

2.3 Superparamagnetic nanoparticles

Magnetism is highly volume and temperature dependent because this property arises from the collective interaction of atomic magnetic dipoles [63, 64, 4]. When the size of a ferro- or ferrimagnet decreases to a certain critical value r_c, the particles change from a state with multiple magnetic domains to one with a single domain. As shown in Figure 2-4 (a), if the size continues to decrease to a value r_0, the thermal energy becomes comparable with that required for spin to flip directions, leading to the randomization of the magnetic dipoles in a short period of time. Such small particles do not have permanent magnetic moments in the absence of an external field but can respond to an external magnetic field. They are referred to as superparamagnetic particles. In superparamagnetic particles, thermal fluctuations are strong enough to spontaneously demagnetize a previously saturated assembly; therefore these particles have zero coercivity and have no hysteresis (Figure 2-4-(b)).

The critical radius r_c for a spherical particle with the stability defined by the flipping probability of the magnetic moment of < 10% over one second can be estimated using the following equation [63]:

$$r_c = (6k_B T/K_u)^{1/3} \hspace{3cm} \text{[2-5]}$$

where k_B is Boltzmann constant, T is temperature, and K_u is the crystalline magnetoanisotropy. Depending on K_u, the critical radii of nanoparticles can be 3–4 nm for very hard magnets and over 20 nm for soft magnets.

(a)

(b)
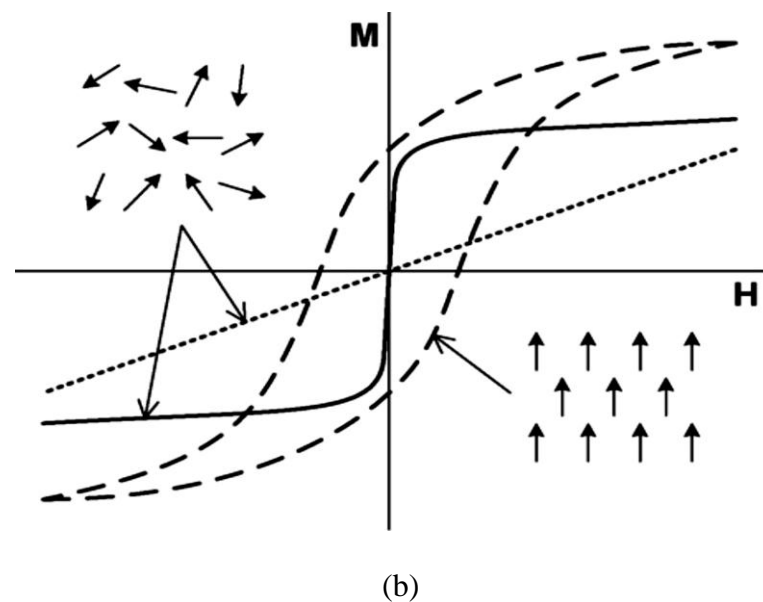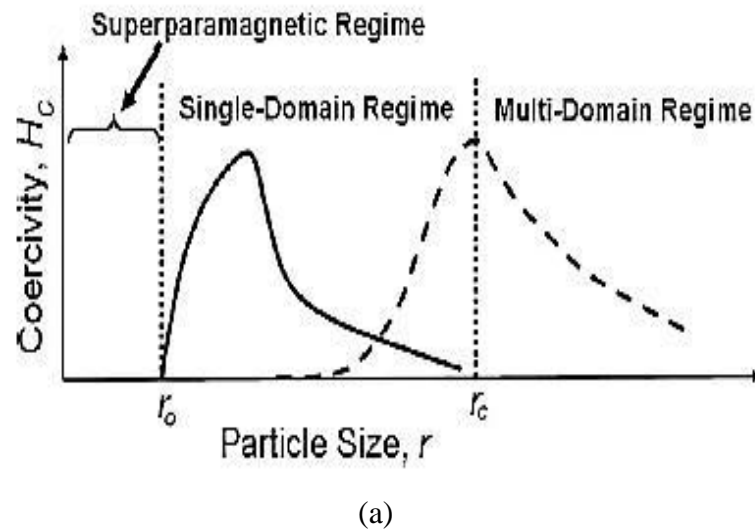
Figure 2-4 (a) Schematic illustrating the dependence of magnetic coercivity on particle size, (b) Magnetization characteristics of superparamagnetic (solid line), paramagnetic (dotted line) and ferromagnetic (dashed line) particles [4].

Superparamagnetic nanoparticles have found widespread use in many traditional areas including magnetic data storage, ferrofluids technology, magnetorheological polishing, and energy storage; they also hold great potential for many other applications related to biomedical research [4]. To this end, superparamagnetic colloids have been exploited for labelling and separation of DNAs, proteins, bacteria, and various biological species,

as well as applied to magnetic resonance imaging (MRI), guided drug delivery, and hyperthermia treatment of cancer [64, 65]. Table 2-1 includes some properties of superparamagnetic particles.

Table-2-1 Selected properties of major superparamagnetic nanoparticles [4].

Composition	Diameter (nm)	Saturation magnetization (Am^{-1}) (bulk)	Curie temperature (T_C) /Neel temperature $(T_N)(^\circ K)$	Data source
Fe	3.0–9.3	1.7×10^6 (0 K)	1043 (T_C)	[63, 66]
Co	2.0–12	1.4×10^6 (0 K)	1394 (T_C)	[63, 66]
Ni	5.0–13	5.1×10^5 (0 K)	631 (T_C)	[66, 67]
FePt	3.0–17	1.1×10^6 (0 K)	750 (T_C)	[63, 68, 69]
CoPt	7.0	0.8×10^6 (0 K)	840 (T_C)	[63, 69]
γ-Fe_2O_3	3.0–25	4.5–4.9×10^5 (300 K)	848 (T_C)	[63, 65]
Fe_3O_4	8.0–30	4.8–5.2×10^5 (300 K)	858 (T_C)	[63, 65, 66] [70]
CoO	~8	1.4×10^6 (0 K)	291 (T_N)	[63, 69]
$CoFe_2O_4$	2.0–12	4.8×10^5 (0 K)	793 (T_C)	[63, 66, 71, 72]

2.3.1 Properties of superparamagnetic nanoparticles

Superparamagnetism is characterized by zero intrinsic coercivity and no residual magnetism. Superparamagnetism is the phenomenon by which magnetic materials exhibit behavior similar to paramagnetism at temperatures below Curie temperature.

Generally, coupling forces in magnetic materials cause the magnetic moments of neighboring atoms to align, resulting in very large internal magnetic field. At

temperatures above Curie temperature, the thermal energy is sufficient to overcome coupling forces, causing the atomic magnetic moments to fluctuate randomly. Because there is no longer any magnetic order, the internal magnetic field no longer exists and the material exhibits paramagnetic behavior. Superparamagnetism occurs when the material is composed of very small crystallites (1-10 nm). In this case, even though the temperature is below Curie temperature and the thermal energy is not sufficient to overcome coupling forces between neighboring atoms, thermal energy is sufficient to change the direction of magnetization of the entire crystallite. The resulting fluctuations in the direction of magnetization cause the magnetic field to average to zero. The susceptibility of magnetic fluid changes with temperature according to Curie-Weiss Law:

$$\chi = \frac{C}{T\text{-}T_C} \tag{2-6}$$

where, χ is the magnetic susceptibility, C is a material-specific Curie constant, T is absolute temperature (°K), T_c is the Curie temperature (°K).

2.3.2 Synthesis of superparamagnetic nanoparticles

Numerous chemical methods can be used to synthesize magnetic nanoparticles for various applications: microemulsions [73], sol-gel syntheses [74], sonochemical reactions [75], hydrothermal reactions [76], hydrolysis and thermolysis of precursors [77], flow injection syntheses [78], and electrospray syntheses [79]. The synthesis of superparamagnetic nanoparticles is a complex process because of their colloidal nature. The synthesis approach is based on homogenous neucleation and subsequent particle growth as depicted in Figure 2-5. The first main chemical challenge consists of defining experimental conditions, leading to a monodisperse population of magnetic grains of suitable size. The second critical point is to select a reproducible process that can be

scaled up without any complex purification procedure, such as ultracentrifugation [80], size-exclusion chromatography [81], magnetic filtration [82] or flow field gradient [83]. The above mentioned methods have been used to prepare particles with homogeneous composition and narrow size distribution. However, the most common method for production of magnetite nanoparticles is the chemical co-precipitation technique of iron salts [84-86].
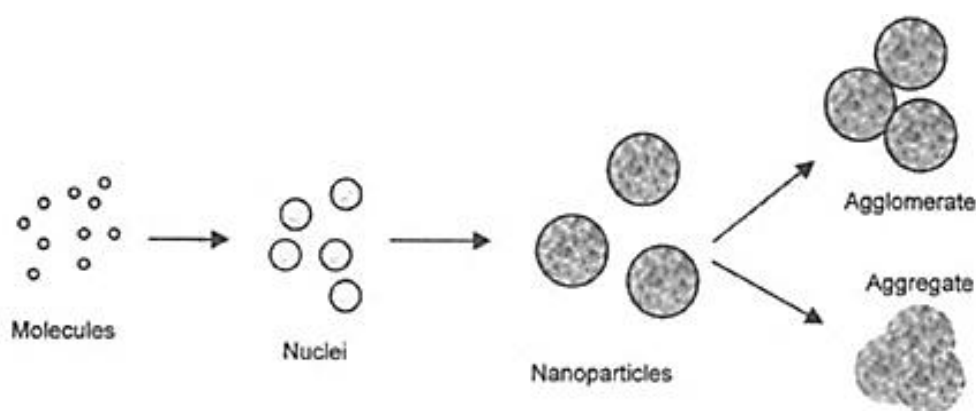
Figure 2-5 Mechanism of nanoparticle production using liquid phase/colloidal methods [87].

The co-precipitation technique is probably the simplest and most efficient chemical pathway to obtain magnetic particles by which large amount of magnetic particles can be synthesized. Iron oxides (either Fe_3O_4 or γ-Fe_2O_3) are usually prepared by adding stoichiometric mixture of ferrous and ferric salts in aqueous medium. The chemical reaction of Fe_3O_4 formation may be written as equation 2-7.

$$Fe^{2+} + 2Fe^{3+} + 8OH^- = Fe_3O_4 + 4H_2O \qquad [2\text{-}7]$$
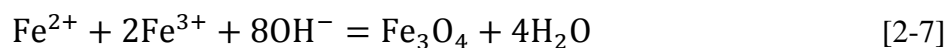
According to the thermodynamics of this reaction, complete precipitation of Fe_3O_4 should be expected at a pH between 8 and 14, with a stoichiometric ratio of 2:1

23

(Fe^{3+}/Fe^{2+}) in a non-oxidizing environment. However, magnetite (Fe_3O_4) is not very stable and is sensitive to oxidation. Magnetite is transformed into maghemite (γ-Fe_2O_3) in the presence of oxygen.

$$Fe_3O_4 + 2H^+ = \gamma\text{-}Fe_2O_3 + Fe^{2+} + H_2O \qquad [2\text{-}8]$$
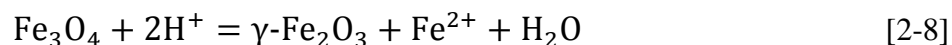
2.3.3 Surface modification of magnetic nanoparticles

Once the nanoparticles are produced and purified to a satisfactory level it is often necessary to introduce surface modifications. Surface modifications can be for the purposes of (a) passivating very reactive nanoparticle, (b) stabilizing very aggregative nanoparticle in a medium (which may be a solvent or a polymer melt) where the nanoparticles are to be dispersed, (c) functionalizing the nanoparticle for further applications or (d) promoting the assembly of nanoparticles (Figure 2-6). Most commonly used surface modification methods include grafting thiolated surfactants or polymers, adsorption of charged surfactants, charged ligands or polymer brushes, attachment of biological molecules such as DNA, peptides, proteins, antigens, streptavidin or coating a continuous polymer film on nanoparticles [87].

(a)   (b)   (c)
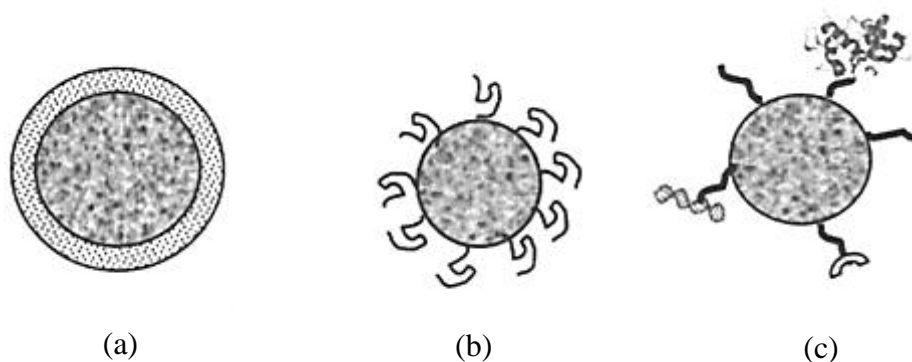
Figure 2-6 Different approaches to surface modifications, (a) surface treatment to attain thermodynamic stability in dispersion, (b) surface adsorption of a surfactant or a block copolymer, (c) surface modification to make the nanoparticle functional [87].

2.3.3.1 Surface functionalization with monomeric stabilizer

2.3.3.1.1 Coated with carboxylates

Functional groups, including carboxylates, phosphates, and sulfates, are known to bind to the surface of magnetites [65]. Furthermore, this stabilization can be tailored for dispersibility into oil/hydrocarbon carrier fluids or aqueous media. The surface of magnetite nanoparticles can be stabilized in aqueous dispersion by the adsorption of citric acid [88]. Bee et al. have investigated the effect of concentration of citrate ions on the size of magnetic particles [89]. Krishnamurti and Huang have studied the influence of citrate on kinetics of Fe^{2+} oxidation and the resulting hydrolytic products of Fe^{3+} [90]. Liu and Huang have observed that increasing concentrations of citric acid causes significant decrease in the crystallinity of the iron oxides formed during the synthesis [91]. Other coating molecules, such as gluconic acid, dimercaptosuccinic acid [92] and phosphorylcholine [93] can be used for stabilization of iron oxide in aqueous medium.

2.3.3.1.2 Coated with phosphates

Several researchers have studied the possibility of using alkanesulphonic and alkanephosphonic acid surfactants as efficient binding ligands on the surface of Fe_2O_3 nanoparticles and as stabilizers for particle dispersion in organic solvents [94, 95]. Yee et al. proposed two possible bonding schemes for the phosphonate ions on Fe^{3+}, i.e., one oxygen or two oxygen atoms of the phosphonate group binding onto the surface [96]. Sahoo et al. have reported the surface derivatization of magnetite by oleic acid, lauric acid, dodecylphosphonic acid, hexadecylphosphonic acid, and dihexadecyl phosphate [97]. Recently, superparamagnetic nanosized particles have been prepared by controlled coprecipitation of Fe^{2+} and Fe^{3+} in the presence of highly hydrophilic poly(vinylalcohol phosphate) (PVAP). The impacts of the polymer concentration on the particle size, size distribution, colloidal stability, and magnetic property have been studied. The aqueous

suspension of magnetite, prepared using 1% PVAP solution, has been found to be stable for 4 weeks at pH 5-8 [98]. The acceptable biocompatibility of phosphonate and phosphate ligands may advance toward the use of encapsulated magnetic nanoparticles in medical applications, such as magnetic resonance imaging, and other biophysical purposes [99].

2.3.3.2 Surface functionalization with inorganic materials

Iron oxide nanoparticles can be coated with silica, gold or gadolinium (III). These coatings not only provide stability to the nanoparticles in solution but also help in binding various biological ligands to the nanoparticle surface. These nanoparticles have an inner iron oxide core with an outer metallic shell of inorganic materials.

2.3.3.2.1 Coated with silica

Silica has been exploited as a coating material for magnetic nanoparticles [100-102]. Usually, an inert silica coating on the surface of magnetite nanoparticles prevents their aggregation in liquid, improves their chemical stability, and provides better protection against toxicity. This coating stabilizes the magnetite nanoparticles in two different ways [103]. One is by shielding the magnetic dipole interaction with the silica shell. On the other hand, the silica nanoparticles are negatively charged. Therefore, silica coating enhances the coulomb repulsion of the magnetic nanoparticles. The first method relies on the well-known Stöber process, in which silica was formed insitu through the hydrolysis and condensation of a sol-gel precursor, such as tetraethyl orthosilicate (TEOS) [103-105]. The second method is based on the deposition of silica from silicic acid solution [106, 107]. The third method is an emulsion method, in which micelles or inverse micelles are used to confine and control the silica coating. This method might require greater effort to separate the core-shell nanoparticles from large amount of

surfactants associated with the emulsion system [108, 109]. Yang et al. have used the emulsion method for the preparation of monodisperse silica-coated iron oxide superparamagnetic nanoparticles and further entrapment of biological macromolecules in the pore of the nanoparticles [110]. Recently, Tartaj et al. have prepared submicronic silicacoated magnetic sphere aerosol by the pyrolysis method [111].

2.3.3.2.2 Coated with gold

Gold is another inorganic coating material which is highly adequate to implement functionality to magnetic nanoparticles as well as to improve their stability in aqueous dispersions. Some protocols exist in the literature to obtain magnetic nanoparticles coated with gold [112]. Lin et al. have synthesized core-shell-structured Fe/Au nanoparticles by a reverse-micelle approach [113]. Water soluble gold-coated magnetite nanoparticles with diameters of about 60 nm were synthesized by the reduction of Au (III) onto the surface via iterative hydroxylamine seeding [114].

2.3.3.3 Surface functionalization with polymer stabilizers

Several approaches have been developed to coat iron oxide nanoparticles, including in situ coatings and post-synthesis coatings. In the first approach, nanoparticles are coated during the synthesis. In literature, the most common coatings are dextran, carboxymethylated dextran, starch, arabinogalactan, glycosaminoglycan, sulfonated styrene-divinylbenzene, polyethylene glycol (PEG), polyvinyl alcohol (PVA), poloxamers, and polyoxamines, poly (N-isopropylacrylamide) or PNIPAM.

2.3.3.3.1 Coated with dextran and polyethylene glycol (PEG)

Dextran is a polysaccharide composed exclusively of α-D-glucopyranosyl units with various degrees of chain length and branching. Dextran has been used often as a polymer coating mostly because of its biocompatibility [115-118]. Molday and

Mackenzie were the first who reported the formation of magnetite in the presence of dextran 40000 [118]. In that study, dextran was functionalized after iron oxide stabilization by oxidation to create more hydroxyl groups to allow for the binding of the amino groups of proteins. Pardoe et al. have reported detailed magnetic and structural properties on iron oxide formed in the presence of dextran (40000 g/mol) [119]. The results of the analysis suggested that the presence of polymer limits the particle size compared to particles prepared without the polymer. Recently, Bautista et al. described surface modification of pure superparamagnetic iron oxide nanoparticles with dextran prepared by laser pyrolysis and the co-precipitation method [120].

PEG is a hydrophilic, water-soluble, biocompatible polymer. Several investigations have reported the use of PEG to increase biocompatibility of the iron oxide dispersions and blood circulation times [121-124]. Various methods of coating were developed to prepare small (60-100 nm) and ultrasmall (20-35 nm) particles without size-separation processes.

2.3.3.3.2 Coated with polyvenylalchohol (PVA)

PVA is a hydrophilic, biocompatible polymer. PVA coating onto the particle surface prevents their agglomeration, giving rise to monodisperse particles [125, 126]. Lee et al. have modified the surface of nanoparticles with PVA by precipitation of iron salts in PVA aqueous solution to form stable dispersion [127]. These investigators suggest that PVA irreversibly binds to the surface of magnetite which was characterized using FTIR absorbance shifts. Recently, Chastellain et al. have synthesized PVA coated iron oxide nanoparticles according to a well-known method [128]. The colloidal stability of the final polymer-coated product as well as the resulting particle size distribution were determined for different iron/polymer ratios. As it is known, PVA is a unique synthetic

polymer that can transform into a polymer gel that is a class of macromolecular network with unique properties. Albornoz et al. have reported the synthesis of aqueous ferrofluid and the preparation of a magnetic gel with PVA and glutaraldehyde (GTA) [129]. The magnetic gel was dried to generate a biocompatible film.

2.3.3.3.3 Coated with alginate

Alginate is an electrolytic polysaccharide with many carboxyl groups. Researchers have thus speculated that the COO^- of alginate and iron ion would interact and the electrostatic repulsion may make the superparamagnetic iron oxide nanoparticles (SPIONs)$^-$ alginate stable. Recently, several investigations dealing with the preparation of iron oxide nanoparticles with alginate have been developed [130-132]. The standard chemical synthesis consists of three steps: (a) gelation of alginate and ferrous ions, (b) in situ precipitation of ferrous hydroxide by the alkaline treatment of alginate and (c) oxidation of ferrous hydroxide with an oxidizing agent, such as O_2 or H_2O_2. Some researchers have developed a new modified two-step co-precipitation method [131]. The results revealed that typical iron oxide nanoparticles had a core diameter of 5-10 nm and that SPIONs-alginate had a hydrodynamic diameter of 193.8-483.2 nm.

2.3.3.3.4 Coated with chitosan

Chitosan is an alkaline, nontoxic, hydrophilic, biocompatible, and biodegradable polymer. Nowadays, the preparations of magnetic nanoparticles encapsulated in chitosan are of great interest [133, 134]. Kim et al. have synthesized SPIONs by a sonochemical method [135]. From these particles, they synthesized ferrofluids for use as MRI contrast agents by coating them with oleic acid as a surfactant and then dispersing them in chitosan, which is a suitable carrier for bioapplications. Microspheres composed of superparamagnetic iron oxide nanoparticles and chitosan

were developed as a novel MRI detectable embolic material. Lee et al. have prepared spherical superparamagnetic nanoparticles by sonochemistry and embedded them in chitosan to synthesize ferrofluids [136]. The synthesized microspheres showed strong enhancement of MR image contrast similar to the ferrofluid in Vitro.

2.3.3.3.5 Coated with thermosensitive polymer

N-isopropylacrylamide (NIPAM) is a commonly used monomer in the preparation of thermosensitive polymer coated magnetic particles. Magnetic particles coated with thermosensitive polymer shows reversible adsorption and desorption cycle sensitive to temperature. The thermosensitive magnetic particles can adsorb proteins when the temperature is higher than the lower critical solution temperature (LCST), and reversely release protein when the temperature is lower than LCST. Some research works showed magnetic particles coated with thermosensitive polymer have the potential in the separation and purification of enzyme and proteins [137, 138]. Some recent works include synthesis of magnetic nanoparticles immobilized inside PNIPAM microgels [139, 140]. These microgels based on poly-(*N*-isopropyl acrylamide), (PNIPAM), are very promising materials for biomedical applications such as drug delivery applications, because they could respond to thermal stimulus, e.g., local hyperthermia produced by a tumor tissue, delivering drugs locally and only when needed [140, 141].

Different polymers that have also been used are polymethacrylic acid [142], poly(ethyleneoxide)-*b*-poly(methacrylic acid) [143], poly(acrylic acid) (PAA) [144], poly(lactic acid) [145], poly(ε-caprolactone) [146], sulfonatedstyrene-divinylbenzene or arabinogalactan [147]. PAA coatings increase the stability and biocompatibility of the particles and also help in bio adhesion.

2.3.3.3.6 Coated with cyclodextrin

CDs are cyclic oligosaccharides consisting of 6, 7, and 8 D-glucopyranose units joined by α-1, 4-glycosidic linkages, respectively designated as α, β, and γ-CDs (Figure 2-7). With the unique structures, CDs have a hydrophobic cavity and a hydrophilic surface, which endows CDs the ability to connect polymer chains to form inclusion complexes via the host-guest interaction [148]. Since all of the primary and secondary hydroxyl groups of CDs are on the outside of this toroidal shaped molecule, the cavity is relatively non-polar, thus allowing CDs to form inclusion complexes with a variety of polar and non-polar guest molecules. It is apparent that size and geometry of a guest molecule in relation to that of the cyclodextrin cavity are important factors in inclusion complex formation.
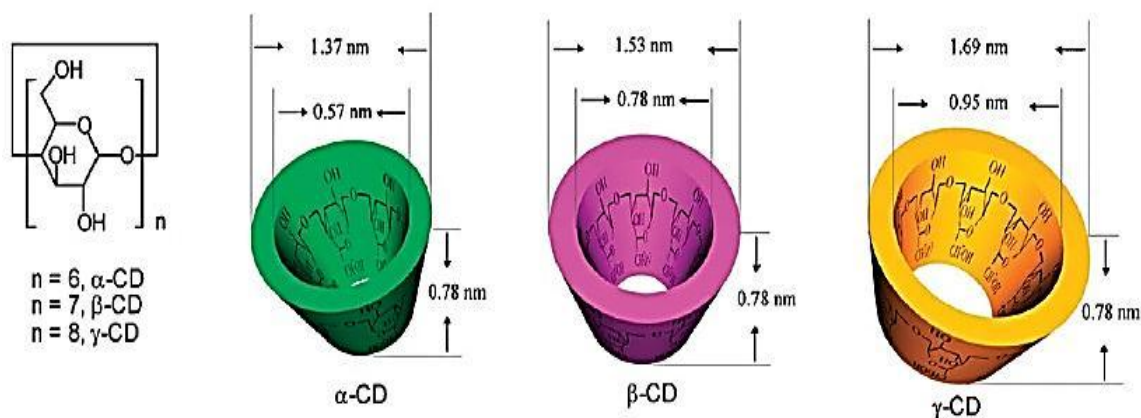
Figure 2-7 Molecular structures of CDs [149].

Various applications and preparation methods of cyclodextrin modified magnetic nanoparticles are summarized in the following Table 2-2.

Table 2-2 List of some applications and preparation methods of cyclodextrin modified magnetic nanoparticles.

Particles	Method of synthesis	Application	Reference
γ-CD stabilized FePt particle	Co-precipitation of iron salt and platinum acethylacetonate, Pt(acac)$_2$ in the presence of oleic acid and oleylamine followed by stirring with γ-CD solution	Catalytic activity	[27]
Fe$_3$O$_4$ nanoparticles coated with CD and fluronic polymer (F-127)	Co-precipitation of iron salts in presence of β-CD and F-127 solution	Hyperthermia, magnetic resonance imaging (MRI) and drug delivery applications	[28]
β-CD fabricated Fe$_3$O$_4$ magnetic nanoparticles	Co-precipitation method followed by carbodiimide activation method	Removal of copper ions from waste water	[150]
Folic acid and β-CD coated Fe$_3$O$_4$ magnetic nanoparticles	Hydrolysis and condensation of Iron(III) allylacetylacetonate followed by reaction with 3-chloropropyldimethylethoxysilane (CPDMES) and β-CD solution	Hyperthermia, drug encapsulation and drug release	[29]
CD-functionalized Fe$_3$O$_4$/aminopropyl triethoxysilane (APTES) nanoparticle	Co-precipitation of iron salts followed by stirring with APTES and solution of β-CD derivative later on	Drug carrier and bio-separation	[151]
α-CD stabilized oleic acid capped iron oxide nanoparticles	Thermal decomposition of iron pentacarbonyl in presence of oleic acid followed by stirring with α-CD solution	Biological and environmental applications	[152]
β-CD based inclusion complex CoFe$_2$O$_4$ magnetic nanoparticle	Stirring of CoFe$_2$O$_4$ magnetic nanoparticles with β-CD solution	Catalyst for chemiluminescence (CL) system	[153]

Table 2-2 (continued)

2-hydroxypropyl-β-cyclodextrin (HPCD) coated gum arabic-modified magnetic nanoparticles (GAMNP)	Co-precipitation of ferrous and ferric salts followed by carbodiimide activation	Targeted delivery of all-trans-retinoic acid-(ATRA)	[30]
FePt core-shell magnetic nanoparticles stabilized by γ–CD	Stirring of $Fe(CO)_5$ and $Pt(acac)_2$ solution in presence of oleic acid and oleylamine followed by mixing with γ–CD solution	Catalysis for aqueous hydrogenation reaction	[154]
Fe_3O_4- NPE$_n$(polyethylene Glycol (n) nonylphenyl ether)-α-CD	Co-precipitation of ferrous and ferric salts in presence of $NH_3•H_2O$ and α-CD solution followed by stirring with NPE$_n$ solution	Magnetic separation, drug delivery	[155]
HP-β-CD coated magnetic nanoparticle	Co-precipitation followed by stirring of magnetic particles with HP-β-CD solution and $NH_3•H_2O$ solution	Drug delivery	[156]
Fe_3O_4/β-CD magnetic nanoparticle	Stirring of magnetite monodomain particles with tetramethylammonium hydroxide ($N(CH_3)_4OH$) solution and β-CD solution	Hyperthermia	[157]
Fe_3O_4/oleic acid (OA)/oleylamine(OAm)/ β-CD Nanoparticle	Stirring of Fe(acetylacetonate) in presence of OA, OAm β-CD solution	Drug delivery	[158]
γ-Fe_2O_3/γ -CD magnetic nanoparticle	Stirring of ferrous chloride solution with γ-CD and NaOH	Contrast agent in MRI and iron career in human body	[159]
Fe_3O_4/polyethylene glycol nonylphenyl ether/CD magnetic nanoparticle	Stirring of ferrous and ferric salts with surfactant and CD solution	Magnetic carrier and biomedical application	[160]
Multiwalled carbon nanotubes/iron oxides/β-CD (MWCNTs/iron oxide/β -CD)	Co-precipitation of iron ferrous and ferric salts in presence of MWCTs followed by plasma induction and stirring with β-CD solution	Removal of metal ions and organic pollutants	[161]

Table 2-2 (continued)

Fe$_3$O$_4$-β-CD complex	Stirring of ferric chloride solution and ferrous chloride solution in presence of β-CD solution	-	[162]
β-cyclodextrin (CD)-citrate-gum arabic modified magnetic nanoparticles (GAMNPs)	Co-precipitation of ferrous chloride and ferric chloride salts followed by sonication with GA solution and carbodiimide activation reaction with β-CD solution	Inclusion and release of hydrophobic drug, Ketoprofen	[163]
Fe$_3$O$_4$/SiO$_2$/β-CD magnetic nanoparticle	Solvothermal reduction method followed by stirring with tetraethyl orthosilicate (TEOS), ammonia and water, finally stirring with β-CD solution, NaOH and 3-glycidyloxypropyltrimethoxysilane (GTMS), ammonia solution	Extraction of biphenolic pollutants (bisphenol A (BPA) and diethylstilbestrol (DES))	[164]
Fe$_3$O$_4$/ β-CD magnetic nanoparticle	Stirring of ferric chloride solution with β-CD solution, in presence of ammonia solution	-	[165]
β-CD polymer/Fe$_3$O$_4$ nanoparticles	Co-precipitation followed by stirring with carboxymethyl-β-CD in presence of epichlorohydrin	Drug carrier and magnetic separator	[166]
Fe$_3$O$_4$/β-CD magnetic nanorods	Stirring of Fe(acetate) and β-CD in de-ionized water	-	[167]
Fe$_3$O$_4$/β-CD magnetic nanoparticle	Co-precipitation of ferrous chloride and ferric chloride solution followed by stirring with β-CD solution	Biomedical applications	[168]

2.4 Separation of chiral amino acids

Compounds where chirality is caused by the presence of asymmetric carbon atoms are the dominating type of pharmaceutical, biochemical and biological interest. Consequently, they are the subject of principal analytical interest also. Determination of the enantiomeric composition of chiral substances has become important in recent years because chirality is a central factor in biological phenomena. Chiral amino acids have two enantiomers (non-superimposable mirror images), which can be defined as D-/L- (by configuration), R-/S- (by configuration) and +/- (by optical activity). Sighting with the hydrogen atom away from the viewer, if the groups (COOH, R, NH_2 and H) are arranged clockwise around the carbon atom, then it is the D-form. Otherwise arrangement is the L-form. Because of the different behavior of the enantiomers of amino acids under chiral environment, several analytical methods and techniques have been developed for separation of chiral amino acid enantiomers.

The earliest experiment on acid hydrolysis of proteins was performed by Braconnot in 1820 in which concentrated acid was used to hydrolyze gelatine, wool and muscle fiber. In 1972, Moore and Stein were awarded the Nobel Prize for developing an automated instrument for separation of amino acids on an ion-exchange resin and quantification of them using ninhydrin [169]. In the past, the "gold standard" for studying chiral separations fell within the realm of chromatography (e.g., high performance liquid chromatography (HPLC), capillary electrophoresis and to some extent gas chromatography) and numerous publications have demonstrated the chiral separation of countless drug molecules using the above methods. However, several broad-ranging analytical techniques such as circular dichroism, crystallography, NMR, and fluorescence spectroscopy have demonstrated their distinctive ability for studying chiral interactions as well [170-172].

More recently, HPLC has been configured for amino acid analysis. Some methods use post column derivatization in which the amino acids are separated on an ion-exchange column followed by derivatization with ninhydrin, fluroscamine, or O-phthaldehyde [173]. Another approach has been to derivatize amino acid prior to separation on a reversed phase HPLC column. Examples of these techniques are dansyl [174], phenylthiocarbamyl (PTC) [175], 9-fluorenylmethyl chloroformate (Fmoc) [176, 177] derivatives of amino acids. The basis of enantioselective chromatography is the transient formation of noncovalent diastereomeric complexes between chiral solute and chiral stationary phase (CSP). In HPLC, chiral stationary phase based on α-cyclodextrin was also used for enantioseparation of amino acids and Armstong et al. achieved very good resolution of 22 chiral compounds [178]. Tao et al. achieved chiral recognition of D- and L-amino acids and mixtures of enantiomers were quantified in the gas phase, using the kinetics of competitive unimolecular fragmentations of trimeric Cu (II)-bound complexes [179]. Hofstetter et al. reported the production of highly stereoselective antibodies to D- and L-α-amino acids, respectively [180]. Use of chiral additives and metal chelate additives are also very attractive to separate enantiomers.

In capillary electrophoresis (CE), achievement of chiral separation of compounds was very good too. So far, more than 200 papers dealing with chiral separation of amino acids and peptides by CE have been published and a variety of chiral CE modes and approaches have been developed, such as capillary zone electrophoresis (CZE) with cyclodextrin (CD-CZE), cyclodextrin modified micellar electrokinetic chromatography (CD-MEKC), gel filled chiral CE, chiral capillary electro chromatography (CEC), diastereomeric separation and so on. In addition, numerous reviews on CE have been presented highlighting continuous new developments of chiral separations of various

compounds [181, 182]. Chankvetadze has published an interesting book on capillary electrophoresis in chiral analysis [183].

Enantiomers behave differently only in a chiral environment. Therefore, to differentiate a pair of enantiomers with mass spectrometry, the target enantiomers are ionized in the presence of a chiral selector (also called reference chiral compound, chiral reagent, resolving agent, etc.) to form diastereomeric complex ions. Yao et al. described how chiral recognition of 19 common amino acids was achieved by investigating the collision-induced dissociation spectra of protonated trimers that were formed from the electrospray ionization of amino acids in the presence of different chiral selectors [184].

Some other methods have recently been developed for enantiomeric separation of amino acids like electrokinetic chromatography [185], high-field asymmetric waveform ion mobility spectrometry (FAIMS) coupled to mass spectrometric detection [186] etc. Following tables (Tables 2-3, 2-4, 2-5, 2-6 and 2-7) broadly summarize enantioseparation and chiral recognition of amino acids by conventional methods.

Table 2-3 Separation of chiral amino acids using Chromatography.

System used	Chiral amino acid separated	Packing material and stationary phase	Mobile phase	Reference
Liquid chromatography (LC)	D-/L-Leu, D-/L-Phe, D-/L-Tyr	Darco G-60	Mobile phase-water, developer-acetone/ ethylacetate	[187]
Liquid chromatography (LC) using ion-exchange resins	Tyr, Glu, Asp, Ser, Thr, Gly, Val, Pro, Met, Ile, Leu, His, Phe, Arg	Dowex 1-X8 (a strongly basic resin) and Dowex 50-X4 columns	Acetic acid / 4 N hydrochloric acid (HCl)	[188]
Gas-liquid chromatography (GLC)	N-acetyl esters of α-Ala, Val, Thr, Ser, Ile, Cys, Nva, Leu, Nle, Met, Gly, β-Ala, Pro, Asp, Glu, Tyr, hydroxyPro	Chromosorb W coated with polyethylene glycol, Carbowax 1540	Carrier gas-argon	[189]
GLC	N-trifluoroacetyl (TFA)- isopropyl esters of D-/L-Ala, D-/L-Ile, D-/L-Leu, D-/L-Val, D-/L-Nva, D-/L-Nle	N-TFA-L-α-amino-n-butyryl- L-α-amino- n-butyric acid cyclohexyl ester	Carrier gas-helium	[190]
Gas chromatography (GC) with glass capillary	D-/L –Lys, D-/L-Tyr, D-/L-Phe, D-/L-Glu, D-/L-Asp, D-/L-Met	Glass capillary coated with N-TFA-L-phenylalanyl-L aspartic acid bis(cyclohexy1) ester (phe-asp)	Carrier gas-hydrogen	[191]
High performance liquid chromatography (HPLC)	Dansyl derivatives of Lys, Met, Phe, Pro, Tyr,Val, Leu, Ile, Glu ,Gly, Trp, Cys, Ala, Asp, Ser, Arg, His, Thr	Li Chrosorb SI 60 (diameter 5 µm)	Benzene-pyridine-acetic acid-methanol	[192]
Liquid-solid chromatography	N-acetyl tert-butyl esters of D-/L-Leu, D-/L-Val, D-/L-Nle, D-/L-Nva, D-/L-Ala, D-/L-Ile, D-/L-Phe, D-/L-Gly, D-/L-Pro and D-/L-O-tert butyl-Ser, D-/L-O-acetyl-Tyr	(N-formyl -L-valylamino) propyl (FVA) silica gel	Diethyl ether, methylene chloride or chloroform in n-hexane	[193]
Reversed phase chromatography	D-/L- Ala, D-/L-Val, D-/L-Nva, D-/L- Tyr, D-/L-Phe, D-/L-Trp, D-/L-Nle, D-/L-Asn, D-/L-Glu, D-/L-Asp, D-/L-Ile, D/L-Leu	Trimethylsilyl-treated Develosil C8 column	Acetonitrile/ solution of N-(p-toluenesulfonyl)-L-phenylalanine-Cu (II)(TosPhe-Cu(II))	[194]
LC	Dansyl derivatives of D-/L-Arg, D-/L-Met, D-/L-Nle, D-/L-Nva, D-/L-Phe, D-/L-Ser, D-/L-Thr	Cyclobond I column (chiral β-cyclodextrin molecules chemically bonded to silica gel)	Methanol-water	[195]

Table 2-3 (continued)

HPLC	D-/L-Glu, D-/L-Asp, D-/L-Ser, D-/L-Thr, D-/L-Nva, D-/L-Val,D-/L-Nle, D-/L-Leu, D-/L-Phe, D-/L-Trp	β-CD, 6-O-phenylcarbamoylated β-CD , and 6-O-propylcarbamoylated β-CD	Phosphate buffer(pH 6.5)/methanol	[196]
LC	D-/L-Trp	Silica immobilized bovine serum albumin (BSA)	Phosphate buffer (pH 7.4)	[197]
HPLC	Dansyl, N-(3,5-dinitrobenzoyl) (DNB), N-(2,4-dinitrophenyl) (DNP), N-benzoyl and β-naphthoyl derivatives of D-/L-Val, D-/L-Ser, D-/L-Trp, D-/L-Ala, D-/L-Glu	Ergot alkaloid-based chiral stationary phase -(1-allyl-(5*R*,8*S*,10*R*)-terguride bonded on silica gel	Phosphate buffer (pH 3.0) /acetonitrile	[198]
Reversed phase-HPLC	Phenylthiocarbamoylated (PTC) derivatives of D-/L-Asp, D-/L-Glu, D-/L-Ser, D-/L-Gly, D-/L-Asn, D-/L-Gln, D-/L-Thr, D-/L-Arg, D-/L-Tyr, D-/L-Val, D-/L-Met, D-/L-Leu, D-/L-Ile, D-/L-Trp, D-/L-Ala, D-/L-His, D-/L -Ser, D-/L -Phe	Phenylcarbamoylated β-cyclodextrin bonded on steel column	Ammonium acetate (pH 6.5) containing butanesulfonate with methanol	[199]
LC	Ala, Asn, Asp, Glu, Leu, Met, Phe, Trp, m-Tyr, Val, Cys	Teicoplanin chiral stationary phase	Methanol-water	[200]
HPLC	D-/L-phosphoTyr, D-/L-Trp, D-/L-Phe, D-/L-Tyr, D-/L-p-aminoPhe	Monoclonal antibody based CSP	Phosphate-buffered saline (pH 7.4)	[180]
Superficial fluid chromatography (SFC)	N(O)-pentafluoropropionyl 1-propyl esters of D-/L-Ala, D-/L-Nva, D-/L-Ile, D-/L-Leu, D-/L-Nle, D-/L-Met, D-/L-Phe, D-/L-Glu, D-/L-Tyr	Fused-silica column of permabond L-Chirasil-Val	Carrier gas- helium	[201]
HPLC	Fmoc-D-/L-Leu, Fmoc-D-/L-Phe, DNB-D-/L-Phe, DNB- D-/L-Glu, D-/L-β-Phe	Ion-exchanger-type CSPs based on zwitterionic selectors	Formic acid and diethylamine in methanol	[202]

Table 2-4 Separation of chiral amino acids using Capillary Electrophoresis.

System used	Chiral amino acid separated	Buffer solution/ electrolyte used(BGE)/ mobile phase and additive	Chiral / non-chiral selector used	Reference
Capillary electrophoresis (CE)	Dansyl derivatives of D-/L-Arg, D-/L-Trp, D-/L-Val, D-/L-Glu, D-/L-Asp, D-/L-Met	2.5 mM Copper (II) sulphate/5.0 mM aspartame/10 mM ammonium acetate	Copper (II) sulphate and aspartame	[203]
Capillary zone electrophoresis (CZE)	D-/L-Trp, D-/L-Thr, D-/L-Phe, D-/L-Tyr	Tris or citrate (10 mM, pH 2.2) as carrier electrolyte with 10 mM 18C6H$_4$	18-crown-6 tetracarboxylic acid (l8C6H$_4$)	[204]
CZE	DNB derivatives of D-/L-Phe	Phosphate buffer with different concentration of 1-(1-naphthy1) ethylcarbamoylated β-cyclodextrins (NEC-β-CDs)	1-(1-naphthy1)ethylcarbamoylated / β -cyclodextrins (NEC-β-CD)	[205]
Cyclodextrin-modified micellar capillary electrophoresis (CD-MCE)	Dansyl (DNS) derivatives of D-/L-Phe, D-/L-Val, D-/L-Thr, D-/L-Ile, D-/L-Leu, D-/L-Met	150mM sodium dodecyl sulphate (SDS)/60mM γ-cyclodextrin (γ-CD)/ 10% acetonitrile/ 250mM borate buffer solution	γ-CD	[206]
CE	Carboxybenzyl derivatives of D-/L-Trp, D-/L-Phe, D-/L-Tyr, D-/L-Leu, D-/L-Asp, D-/L-Asn	4 mM heptakis(6-amino-6-deoxy)-β-cyclodextrin/50 mM phosphate buffer/pH 5.8	Heptakis(6-amino-6-deoxy)-β-cyclodextrin	[207]
CE	Cyanobenz[*f*] isoindole(CBI) derivatized D-/L-Tyr, D-/L-Thr, D-/L-Asn, D-/L-Phe, D-/L-His, D-/L-Glu, D-/L-Met, D-/L-Ala, D-/L-Arg, D-/L-Asp, D-/L-Ile	2 wt % sulfated-β-CD (S-β-CD)/ 25 mM phosphate buffer (pH 2)	S-β-cyclodextrin	[208]
High-speed capillary electrophoresis (HSCE)	Fluorescein isothiocyanate (FITC) labeled D-/L-Leu, D-/L-Asp and mixed FITC labeled Arg, Phe, Gly, Glu, Asp	5 mM borate buffer (pH 9.2)/ 8 mM β-CD/12 mM Sodium tauracholate (STC)	β-CD and sodium tauracholate (STC)	[209]
CE (using PEG-functionalized microchannels) -laser-induced fluorescence (LIF)	Fluorescein isothiocyanate labeled(FITC) D-/L-Asp, D-/L-Glu, D-/L-Asn, D-/L-Gln, D-/L-Leu, D-/L-His, D-/L-Ser, D-/L-Phe, D-/L-Trp	10mM Tris-HCl buffer (pH 8.3)/1mM β-CD	β-CD	[210]

Table 2-4 (continued)

Cyclodextrin modified micellar electrokinetic chromatography- laser-induced fluorescence (CD-MEKC)-LIF	Naphthalene- 2,3-dicar-boxaldehyde labeled D-/L-Thr, D-/L-Asp, D-/L-Tyr, D-/L-Phe, D-/L-Ser, D-/L-Leu, D-/L-Ile, D-/L-Val, D-/L-Met	10 mM β-CD or γ-CD/ 50 mM SDS/ 100 mM borate buffer (pH 9)	β-CD or γ-CD	[211]
Electrokinetic chromatography (EKC)	3, 5-dinitrobenzoylated isopropyl esters of D-/L-Ala, D-/L-Leu, D-/L-Val, D-/L-Phe	N-dodecanoy L-valinate, L-alaninate, and L-threoninate in borate-phosphate buffer	Sodium N-dodecanoyl-L-amino acidate surfactants	[212]
Micellar electrokinetic capillary chromatography (MECC)	FITC labeled Gly, Phe, Ser, Asn, Asp	75 mM SDS/ 10mM disodium hydrogen phosphate / 6mM $Na_2B_4O_7$ (pH 9.2)	SDS	[213]
Micellar electrokinetic chromatography (MEKC)	Dansyl derivatives of D-/L-Leu, D-/L-Phe, D-/L-Val, D-/L-Glu, D-/L-Asp	200 mM SDS/ 75 mM β-CD/ 250 mM borate buffer (pH 9.5)	β-CD	[185]
Packed capillary electro chromatography (CEC)	R/S-N-(9-fluorenylmethoxycarbonyl)-Leu (FMOC-Leu) ,R/S-N-(3,5-dinitrobenzyloxycarbonyl)-Leu (DNZ-Leu)	Mobile phase-acetonitrile/50 mM acetic acid and methanol/50 mM acetic acid	Tert-butyl carbamoyl quinine	[214]
Ligand exchange-capillary electro chromatography (LE-CEC)	Dns-D-/L-Asp, D-/L-Glu, D-/L-Leu, D-/L-Met, D-/L-Nle, D-/L-Nva, D-/L-Phe, D-/L-Ser,	pH 5.5, acetonitrile/ 0.50 mM copper (II)acetate-50 mM ammonium acetate	L-phenylalaninamide	[215]
MEKC	Phenylthiohydantoin (PTH) derivatives of D-/L-Val, D-/L-Nva, D-/L-Tyr	50 mM poly-LV (poly-L-leucylvalinate)/ 275mM boric acid/ 30mM sodium-dihydrogenphosphate /10mM triethylamine	Polysodium-undecanoyl -L-leucylvalinate (poly-L-SULV)	[216]

Table 2-4 (continued)

MEKC	Dns D-/L-Leu	50 mM phosphate/ 25 mM borate buffer (pH 9)/24 mM poly sodium *N*-undecanoyl leucylvalinate (p-SULV)	Diastereomers of poly sodium N-undecanoyl leucylvalinate (p-SULV)	[217]
MEKC in 3D microfluidic/ nanofluidic device	Fluorescein isothiocyanate (FITC) labeled D-/L-Asp and D-/L-Ser	Sodium borate buffer/ sodium taurocholate hydrate (STC)/β-CD/ methanol	β-CD	[218]

Table 2-5 Separation of chiral amino acids using Membrane Separation.

System used	Chiral amino acid separated	Membrane material/membrane phase	Chiral /non-chiral selector	References
Membrane separation	D-/L-Tyr, D-/L-Trp	Poly(L-glutamate) with amphiphilic side chains of (n-nonylphenoxy)oligo (oxyethylene) (NONx-PLG)	NONx-PLG	[219]
Membrane separation	D-/L-Trp, D-/L-Phe, D-/L-Ala, D-/L-Arg, D-/L-Glu	Molecularly imprinted polymeric membranes, bearing tetrapeptide derivative (H-Asp-(OcHex)-Ile-Asp(OcHex)-Glu (OBzl)-CH$_2$-)	Tetrapeptide derivative (H-Asp-(OcHex)-Ile-Asp(OcHex)-Glu(OBzl)-CH$_2$-)	[220]
Membrane separation	D-/L-Ascorbic acid	Optically active polyelectrolyte multilayers (PEMU)	D-poly(lysine), poly(glutamic acid), poly(N-(S)-2-methylbutyl-4-vinyl pyridininum iodide, poly(styrene sulfonate)	[221]
Membrane separation using supported liquid membrane (SLM)	D-/L-Phe, D-/L-Trp, D-/L-Lys, D-/L-Met, D-/L-Gln, D-/L-Glu, D-/L-Ala, D-/L-Nva, D-/L-Nle, D-/L-Arg, D-/L-Ile, D-/L-Eth	Celgard 2500 film with surfactant(dioleyl-L-glutamate ribitol)-protease (protease from *Aspergillus oryzae*, *Aspergillus melleus* and *Bacillus subtillis*) complex	Protesase- α-cymotripsin	[222]
Membrane separation	D-/L-Phe	Acetylated β-CD-immobilized cellulose dialysis membrane	Acetylated β-CD	[223]

Table 2-6 Chiral recognition and analysis of chiral amino acids using Mass Spectrometry.

System used	Chiral amino acid	Chiral/non-chiral modifier or selector	Carrier gas	References
Electrospray ionization mass spectrometry/ mass spectrometry (ESI-MS/MS)	D-/L-Ala, D-/L-Val, D-/L-Leu, D-/L-Ile, D-/L-Pro, D-/L-Phe, D-/L-Tyr, D-/L-Trp, D-/L-His, D-/L-Met, D-/L-Cys, D-/L-Ser, D-/L-Thr, D-/L-Asp, D-/L-Glu	L/D-N-tert -butoxycarbonylPhe (BPhe), L/D-N-tert -butoxycarbonylPro (BPro) and L/D-N-tert -butoxycarbonyl -O-benzylSer (BSer)	Helium	[184]
ESI-MS/MS	D-/L-Arg, D-/L-Asn, D-/L-Gly, D-/L-Asp, D-/L-Glu, D-/L-Phe, D-/L-Trp, D-/L-Tyr, D-/L-His, D-/L-Lys, D-/L-Met	Chiral melamine derivatives	Nitrogen	[224]
Chiral ion mobility spectrometry (CIMS)	D-/L-Trp, D-/L-Met, D-/L-Thr, D-/LPhe, D-/L-Ser	(S)-(+)-2- butanol	Nitrogen (drift gas)	[225]
High-field asymmetric waveform ion mobility spectrometry mass spectrometry (FAIMS-MS)	D-/L-Trp, D-/L-Arg, D-/L-Phe, D-/L-Val, D-/L-Pro, D-/L-Lys	Metal (Zn^{2+}, Mg^{2+}, Cu^{2+}, Ni^{2+}) and reference amino acid (L-Gly, L-Arg, L-Lys, L-Val, L-Pro, L-Gln, L-Ile) complex	Helium/nitrogen	[186]

Table 2-7 Separation of chiral amino acids using other methods.

System used	Chiral amino acid separated	Chiral /non-chiral selector or additive	References
Liquid-liquid extraction	D-/L-Leu, D-/L-Phe, D-/L-Trp	Lanthanide tris (β-diketonate)	[226]
Micelle-enhanced ultrafiltration (MEUF)	D-/L-Phe, D-/L-Val, D-/L-Leu, D-/L-Ser, D-/L-Ala	Cholesteryl D/L-glutamate	[227]
Enantioseparation using over oxidation pseudo-template technique	D-/L-Ala	Overoxidized polypyrrole colloids imprinted with L-lactate	[228]
\Chiral separation by asymmetric crystallization	D-/L-Glu	L-Arg (additive)	[229]
Enantioselective separation using chiral mesoporous silica	D-/L-Val	Chiral block copolymers of poly(ethylene oxide) and chiral D-Phe (PEO-b-D-Phe)	[230]
Continuous enantioselective liquid-liquid extraction using centrifugal contact separator (CCS)	3,5-dinitrobenzoyl (DNB) D-/L-Leu	Extractant-o-(1-tertbutylcarbamoyl)-11-octadecylsulfinyl-10,11-dihydroquinine (CA)	[231]
Chiral separation using CdSe /ZnS quantum dots	D-/L-Phe, D-/L-Tyr	β-CD	[232]

2.5 Removal of pharmaceuticals and endocrine disrupting compounds (EDCs)

Pharmaceuticals represent an important class of emerging organic micropollutants. Although pharmaceuticals are used in large quantities in modern society, their potential to reach surface waters and their impact on the environment have received great attention during the last few decades. Since the 1980s, investigations have been carried out on the occurrence and fate of different therapeutic classes of pharmaceuticals such as antidepressants, beta-blockers and lipid regulators in the environment [233-236]. The majority of these field investigations focused on the determination of concentration levels of specific compounds in various compartments of the aquatic environment. It is found that human pharmaceuticals enter the environment through incomplete wastewater treatment of drugs either not absorbed by the body or intentionally discarded down the drain. Unused human pharmaceuticals may also enter the environment through landfill leachates. Veterinary pharmaceuticals in animal wastes enter the environment directly through infiltration into groundwater or runoff into surface waters. As a result, presence of detectable concentrations of drugs or of their metabolites have then been reported in wastewater treatment plant (WWTP) effluents and natural waters [234, 235]. These pharmaceutically active compounds, including drugs and their active metabolites, have devastating impact on wildlife and on humans due to their presence in the aquatic environment [235].

Investigation on water pollution from emerging contaminants such as endocrine disrupting chemicals (EDCs), is one of the important aspects of current environmental research due to their potential toxic effects on wildlife and humans [237-239]. These compounds exert their effects by: (i) mimicking or antagonizing the effects of hormones; (ii) altering the pattern of synthesis and the metabolism of hormones; (iii)

modifying hormone receptor levels. Although they may not pose direct acute or chronic threats to human or other living organisms, EDCs indirectly interact with the endocrine systems that control the body's function resulting in excessive amounts or suppression of hormones. This phenomenon is called endocrine disruption, which may involve the appearance of: (i) infertility; (ii) sexual underdevelopment; (iii) altered or reduced sexual behavior; (iv) attention deficit or hyperactivity; (v) altered thyroid or adrenal cortical function; (vi) increased incidents of certain cancers; (vii) birth defects, etc [240]. The majority of EDCs are man-made, organic chemicals being introduced to the environment by anthropogenic inputs. In addition, EDCs can be naturally occurring in the environment, e.g. the female hormones E1 (estrone) and E2 (17β-estradiol) are both excreted by females and are hence ubiquitous in the aquatic environment. Such compounds may not be removed by sewage treatment works (STW) and may even be reactivated through deconjugation during these processes, hence prolonging their residence in the aquatic environment. Steroidal estrogens have been found to persist through many sewage treatment processes, and it is widely recognized that effluent discharges from STW are the main source of EDC inputs to the aquatic environment, such as rivers and streams. Although the concentrations of steroidal EDCs are generally low in aquatic systems, concentrations of up to 19.4 ng/L have been detected in surface waters and levels as high as 5400 ng/L have been found in some STW effluents [241].

Beta-blockers or β-blockers are used in the treatment of high blood pressure (hypertension) and to treat patients after heart attacks to prevent recurrences. Substantial amounts of these pharmaceuticals and their metabolites get into the waste-water after excretion and finally end up in surface water. Ecotoxicological studies show that aquatic organisms are sensitive to these substances [242-245]. Escher et al. demonstrated that most beta-blockers had a specific toxicity towards green algae

(*Desmodesmus subspicatus*) [246]. Thus, development of methods for removal/separation of beta-blockers from waste-water is also very important.

Numerous recent studies have examined the removal of emerging pharmaceuticals, beta-blockers and EDCs from wastewater. Conventional approaches include ozonation, adsorption separation using activated carbon and several other adsorbents, biodegradation using constructed wetlands, adsorption and biodegradation using membrane reactor, photocatalysis and coagulation-flocculation. It was demonstrated that among different treatment methods ozonation and filtration with granular activated carbon were effective in removing some pharmaceuticals. Removal efficiencies by granular activated carbon (GAC) adsorption processes for pharmaceuticals have been evaluated using either bench [247] or pilot-scale systems [248], in addition to surveys at full-scale drinking water treatment plants [249]. Eliminations of pharmaceuticals by GAC adsorbers were generally, although not always, found to be satisfactory. Doses of 10-20 mg/L of powdered activated carbon are expected to result in an advanced removal of a broad spectrum of micro pollutants, but highly polar compounds need higher doses or can only be removed partly [250]. The working capacity of activated carbon greatly decreases in the presence of natural organic matter. However, regeneration of adsorbents is questionable. Removal of pharmaceuticals with modified mesoporous silica materials have also been investigated [251]. Among the others, carbon nanotubes (CNTs) are a relatively new group of adsorbents which are currently the focus of intense research [252, 253].

The potential of ozonation and of advanced oxidation processes (AOPs) like UV/H_2O_2 and O_3/H_2O_2 for partial removing of pharmaceuticals and EDCs in drinking water and waste-water was investigated [254, 255]. Initial results from pilot plants utilizing post-

ozonation revealed removal rates of >95% for many micropollutants [256, 254]. Ozone is a selective oxidant which is particularly reactive toward functional groups with high electron density such as double bonds, activated aromatic systems, nonprotonated secondary and tertiary amines, and reduced sulfur species. Although ozonation results only in a partial oxidation, some studies indicate that the initial attack at the reactive functional groups destroys the biological activity of compounds, as shown for estrogenic or antimicrobial compounds [257, 258]. The major uncertainty of ozonation is related to the formation of oxidation by-products from matrix components and transformation products from micropollutants. Various studies revealed reaction products of micropollutants but their concentration as well as the estrogenic and antimicrobial activity of the products was minor compared to the parent compounds [257, 258].

Another approach for removal of these pharmaceuticals and EDCs includes biodegradation utilizing constructed wetlands. Constructed wetlands (CW) are land-based waste-water treatment systems that consist of shallow ponds, beds, or trenches that contain floating or emergent, rooted wetland vegetation [259]. Removal of contaminants in CWs occurs through a series of complex physical, chemical and microbial interactions, and involves a variety of processes including biodegradation, sorption to bed media, sedimentation, microbial and plant uptake, physical interaction with organic matter and volatilization [260, 261]. A main limitation of these CWs is the large surface area generally required, which limits their application to the sanitation of small populations (<2000 inhabitants) or tertiary treatments. Vertical-flow constructed wetlands (VFCWs) are more efficient because they operate under aerobic conditions and require smaller surface area [262].

Membrane bioreactor (MBR) can be recognized as the next generation of wastewater treatment processes because of its excellent effluent quality, low sludge production, small foot print, and flexibility in future expansion [263]. Consequently, considerable dedicated research efforts have been devoted to the assessment of micropollutant removal using MBR [264, 265]. Previous studies have indicated significant variation in the removal of micropollutants by MBRs, ranging from near complete removal for some compounds (e.g. ibuprofen and bezafibrate) to almost no removal for several others (e.g. carbamazepine and diclofenac) [264-266]. In this process, adsorption and subsequent biodegradation of the micropollutants are the dominant removal processes which are influenced by operational conditions such as hydraulic retention time (HRT), sludge retention time (SRT), biomass concentration, temperature and pH [267]. This results in a rather variable and uncertain removal performance.

In recent years, it has been shown that photocatalysis is a promising technology for the purification of waste-water [268-271]. The mostly investigated photocatalyst for degradation of organic pollutants is TiO_2. TiO_2 is remarkably active, cheap, non-toxic, chemically stable over a wide pH range and is not subject to photocorrosion [269]. The photocatalytic degradation of pollutants by means of irradiated TiO_2 (ultraviolet range, $\lambda \geq 413$ nm) is well documented in the literature. It has been described that oxidation takes place by either indirect oxidation by surface-bound hydroxyl radicals or directly via the valence-band hole [269, 272].

To remove pharmaceuticals, beta-blockers and EDCs from waste-water, several unit operations are used as the treatment process. Chemical coagulation is one of the most used processes as it removes efficiently the amount of high molecular organic material, i.e. humic substances, in water. Coagulation is used as a pre-treatment for processes

such as sand filtration, activated carbon filtration and ozonation. Chemical coagulation has been reported to remove only a small portion of pharmaceuticals [273, 274, 248]. Ternes et al. reported less than 10% removal of diclofenac, bezafibrate and carbamazepine [248]. According to Adams et al., coagulation was ineffective for the removal of sulfamethoxazole [274]. Considering the role of dissolved organic matter (DOM), mainly humic substances in the coagulation process can improve the removal efficiency toward several pharmaceuticals [275].

Separation/ removal of pharmaceuticals, beta-blockers and EDCs from waste-water have been studied using several methods. Detailed characteristics of the methods for removal of pharmaceuticals, beta-blockers and EDCs from waste-water are summarized in the Table 2-8.

Table 2-8 List of methods for removal of pharmaceuticals, beta-blockers and EDCs from wastewater.

Pharmaceutical/ EDC	Type of water	Treatment process	Operating condition	Result	Reference
Diclofenac, carbamazepine (CBZ), clofibric acid	Ground water	Ozonation	Ozone dose 0.5mg/L,	>97% of diclofenac and CBZ, 10-15% of clofibric acid were removed	[248]
		Filtration using granular activated carbon (GAC)	GAC filter height of 160 cm	CBZ showed highest adsorption capacity and was removed at throughput of 70m^3/kg	
Carbamazepine, oxazepam (OZP)	Ground water	Adsorption on to burgen sediment	pH 6.6, solid-to-liquid 1:5	60% removal of CBZ and ~30% removal of oxazepam	[276]
		Adsorption on to dausenausediment	pH 6.5, solid-to-liquid 1:5	~38% removal of CBZ and 60% removal of OZP	
Carbamazepine and naproxen (NAP)	Surface water	Adsorption on amberlite XAD-7 (an acrylic ester resin)	pH 7, 20°C, ionic strength of solution 0.01M	98% removal of CBZ and 97% removal of NAP	[277]
Carbamazepine, clofibric acid, diclofenac, Ibuprofen, ketoprofen	Surface water	Adsorption on mesoporous silica, SBA-15	Acidic media (pH 3-5)	85.2% of CBZ, 88.3% of diclofenac, 93.0% of ibuprofen, 94.3% of ketoprofen, and 49% of clofibric acid were removed	[278]
Carbamazepine, clofibric acid, salycilic acid, naproxen sodium	Aqueous solution	Adsorption on inorganic–organic-intercalated (IO) bentonite	Neutral pH and 25°C	Adsorption capacity were 2.61 μmol/g for CBZ, 2.97 μmol/g for clofibric acid, 5.55 μmol/g for salycilic acid, 3.29 μmol/g for NAP sodium	[279]

Table 2-8 (continued)

Nalidixic acid, norfloxacin	Aqueous solution	Adsorption on canadian river alluvium (CRA) in presence of surfactant	pH 7.1±0.13	Adsorption capacity were 7 mg/g for nalidixic acid and 1.5 mg/g for norfloxacin	[280]
Naproxen, carbamazepine	Drinking water	Adsorption on GAC	GAC preloaded for 16 weeks, C_i=500ng/L, pH 6.44 (±0.24)	88-98% of NAP and 73-84% of CBZ initial concentration were adsorbed	[281]
Naproxen, carbamazepine	Aqueous solution	Adsorption on coal-based Calgon Filtrasorb 400 (F400)	C_i=1000ng/L, T=23± 1°C	Adsorption capacity were 600 ng/mg for NAP, 1000 ng/mg for CBZ	[282]
		Adsorption on coconut shell based PICACTIF TE (CTIF)		Adsorption capacity were 400 ng/mg for NAP, 900 ng/mg for CBZ	
Oxytetracycline (OTC) and carbamazepine	Aqueous solution	Adsorption using multiwalled carbon nanotubes (MWCNTs)	C_e=30mg/L, pH 7.0±0.2, T=23± 1°C	Adsorption capacities were 190.2 mg/g for OTC and 7910 mg/g for carbamazepine (after 200 hours of adsorption)	[253]
Naproxen, diclofenac, carbamazepine	Domestic waster	Biodegradation and adsorption onto the surface of Vertical flow constructed wetland (VFCW)	Hydraulic loading rate 70 mm Day^{-1}	62 ±3% of NAP, 53± 2% of diclofenac, 20± 4% of CBZ were removed	[283]
		Filtration using nonplanted Sand filter (SF)		66 ±7% of NAP, 39 ±22% of diclofenac, 8 ±15% of CBZ were removed	
Ketoprofen, propranolol, sotalol	Municipal wastewater	Ozonation followed by sand filtration	Ozone dose~0.60g O_3 g^{-1} dissolved organic content (DOC)	69±14 % of ketoprofen, >96% of propranolol, >98% of sotalol were removed	[250]

Table 2-8 (continued)

Carbamazepine and sulfamethoxazole	Synthetic wastewater	Powdered activated carbon (PAC) amended membrane bioreactor (MBR) technology	PAC concentration of MBR= 1g/L, C_i=30mg/L, T=25°C	92 ± 15% removal of CBZ and 82 ± 11% removal of sulphamethoxazole were achieved	[284]
Carbamazepine	Municipal wastewater	Adsorption and photocatalytic degradation using hydrogen-titanate nanofiber (NF) and commercial P25 (TiO_2) catalysts	UV lamp (8W), pH 7.5, T= 20±1°C,	60% removal using NF and 30% removal using P25 were obtained	[285]
Carbamazepine, gemfibrozil	River water, lake water, ground water	Filtration using GAC / GAC filtration followed by UV treatment	pH 6.95±0.05	71-93% removal of CBZ and 44-55% removal of gemfibrozil	[286]
				75% removal of CBZ and 82% removal of gemfibrozil	
Carbamazepine, naproxen, diclofenac and ibuprofen	Aqueous solution	Adsorption on tropical horizontal constructed wetlands (HSSF CWs) planted with *Typha angustifolia*	Hydraulic residence time 4 day	Removal efficiencies were 26.7±7% for CBZ, 91.3±5.7% for NAP, 55.4±11.1% for diclofenac, 79.7±11.1% for ibuprofen	[261]
Carbamazepine	Aqueous solution	Oxidation followed by UV irradiation	Low pressure mercury monochromatic lamp (17W), 5mM H_2O_2	35% of CBZ was removed	[287]
Gemfibrozil, carbamazepine, triclosan	Surface water	Nanofiltration (NF)	T=20°C, pressure of 724–779 kPa	44-93% of the pharmaceuticals were removed	[288]

Table 2-8(continued)

Ibuprofen, bezafibrate, diclofenac	Aqueous solution	Chemical coagulation using ferric sulphate	Ferric sulphate dose=350 $\mu mol(Fe)l^{-1}$ at pH 4.5	77% of ibuprofen, 50% of bezafibrate, 36% of diclofenac were removed	[275]
Amoxicillin, atenolol, bezafibrate, ibuprofen	Domestic and industrial waste water	Adsorption on sludge in Sewage Treatment Plant	Influent load=13-494mg/day/ 1000 inhabitants	Removal efficiencies were 75-100%, 10-55%, 15-87%, 38-93%	[289]
Diclofenac, diazepam, naproxen	Domestic waste water	Coagulation-flocculation	25 mg/L FeCl$_3$, T=25°C	70% of diclofenac, 20% of diazepam, 25% of naproxen were removed	[290]
Diazepam, carbamazepine, diclofenac, naproxen, ibuprofen	Domestic waste water	Flotation	C_i(wastewater)=150 mg/L, air:solid=0.01, T=25°C	Removal efficiencies were 50%,20%,40%, 30%, 25%	[290]
Ibuprofen, bezafibrate, tonalide, galaxolide	Surface water	Adsorption, biodegradation and biotransformation by membrane bioreactor (MBR)	Solid retention time (SRT)=55days, Hydraulic retention time (HRT)=4 days	>90% removal was obtained for all the pharmaceuticals	[264]
Aspirin, ibuprofen, ketoprofen, naproxen	Domestic wastewater	Microbial and chemical degradation, biodegradation by activated sludge	SRT=5days, HRT=9hours	>90% of aspirin and ibuprofen, ~45% of ketoprofen and naproxen were removed	[291]
Ibuprofen, ketoprofen, naproxen, diclofenac	Domestic wastewater	Biotransformation-Biodegradation and adsorption by MBR /conventional activated sludge (CAS)	HRT=14hours	Removal efficiencies of MBR /CAS techniques were 99.8/82.5%, 91.9/51.5%, 99.3/85.1%, 87.4/50.1%,	[292]

Table 2-8 (continued)

Carbamazepine, sulphamerazine, sulphamethoxazole	Natural water (lake water and effluent from one a membrane bioreactor)	Adsorption onto ultrafiltration (UF) membrane	T=21°C/4°C	Removal efficiencies for lake water and effluent contaminants are 66 and 81% (CBZ), 77 and 75% (sulphamerazine), 77 and 77% (sulphamethoxazole),	[293]
Clofibric acid, carbamazepine	Ultrapure water	Photocatalysis	TiO_2 in suspension; solar simulator (1kW Xe lamp)	Efficient removal was obtained	[294]
Mentronidazol	De-ionized water	UV photo fenton; UV/H_2O_2 treatment	Low pressure lamp, UV= 0–600 mJ cm^{-2}, C_{H2O2} = 25-50 mg /L, C_0 =6µmol/L, pH (UV) = 6, pH (photo-Fenton) = 3.5	UV provides small degradation compared to UV/H_2O_2. Photo-Fenton gives 20% higher removal than Fenton	[295]
Ibuprofen, naproxen, diclofenac, carbamazepine	Industrial wastewater and domestic sewage	Biodegradation/ Photodegradation by horizontal subsurface flow constructed wetlands (HFCW)	HRT=720 hours	Removal efficiencies are 96±2%, 92±1%, 96±1%, 30±10%	[296]

Table 2-8 (continued)

Naproxen, Ketoprofen, fenoprofen, ibuprofen	Domestic sewage	Combined activated sludge treatment, sand filtration and ozonation	HRT(activate sludge)=9hours, flow rate and retention time in sand are110m/d and 1 hour, ozone concentration and r.t. are 3mg/L and 27 mins	>90% of all the pharmaceuticals were removed	[297]
Carbamazepine, diclofenac	Domestic wastewater	Activated sludge treatment by wastewater treatment plant (WWTP)	SRT upto 100 days	Almost 20% of CBZ and 70% of diclofenac were remove	[298]
Furosemide, clofibricacid, sulfamethoxazole, carbamazepine, warfarin	Aqueous solution	Capsular perstraction using liquid core microcapsule	T=25°C, extraction time 50 mins	Removal efficiencies were 15%,19%, 22%,54 and 80%	[299]
Sulfamethoxazole, ibuprofen, ketoprofen, carbamazepine	Aqueous solution	Biodegradation by submerged MBR	pH 5, HRT=24 hours, MBR temperature=22±2°C	Removal efficiencies were ~90%,~100%, ~90%, ~30%	[300]
Paracetamol, Ketoprofen, naproxen, ibuprofen	Synthetic wastewater	Biodegradation by submerged MBR technique	HRT=24 hours, MBR temperature= 20±1°C	Removal efficiencies were 95.1±3.4%, 70.5±0.8%, 40.1±2.8%, 96.7±0.7%,	[301]
Diclofenac	Doubly distilled water	Oxidation using H_2O_2 and UV irradiation treatment	Low pressure lamp (17W, 254 nm), CH_2O_2 = 0.1-1.0 mol/L, pH 7	100% removal of diclofenac with a complete release of chlorine was observed	[302]
Carbamazepine, ibuprofen, naproxen, propranolol	Sewage waste water	Ozonation	O_3 dose=10/15 mg/L	Removal efficiencies were >98%, >62%,>50%, >72%	[254]

Table 2-8(continued)

Clofibric acid	Aqueous solution	H_2O_2/UV treatment	Low pressure lamp (17W, 254 nm), $CH_2O_2 = 1.0$ mol/L, pH 5	Almost complete removal in 60 min	[303]
Carbamazepine	Doubly distilled water	H_2O_2/UV treatment	Low pressure lamp (254 nm) $CH_2O_2 = 5.0$ mol/L, pH 5	100% removal in 4 min was achieved	[287]
Clofibric acid, ibuprofen, diclofenac	River water	Ozonation and advanced oxidation	O_3 (5mg/L) and H_2O_2(1.8 mg/L)	Removal efficiencies were >95%	[304]
Ketoprofen, naproxen, ibuprofen, diclofenac, carbamazepine, propranolol	Domestic wastewater	Biological treatment, sand filtration, chlorination	Daily influent flow rate~15,000m^3/day	Removal efficiencies were 53%, 81%, 87%, 60%, 93%,44%	[305]
Diclofenac, ketoprofen, metoprolol carbamazepine	Municipal waste water	Anaerobic/anoxic/aerobic-membrane bioreactor process	T=25°C, HRT upto 5 hours, sludge retention time=20days	Removal efficiencies of the combined processes were ~85%,80%,~85% and 20%	[306]
Amoxicilin	Aqueous solution	Ozonation	CO_3=0.16 mmol/L; pH 2.5–5.0	Efficient removal and some by product was observed	[307]
Sulfadimethoxine, sulfamerazine, sulfamethazine	Distilled, deionized water and river water	UV irradiation	Low pressure lamp (254 nm), UV dose 3 J/cm^2,T=20°C, pH 7.5	50-80% removal was achieved	[308]
Paracetamol	Distilled water	H_2O_2/UV treatment	Low pressure lamp (17W, 254 nm), $CH_2O_2 = 5$ and 20 mmol/L, pH 2.0–7.0	Complete removal with mineralization between 21-40%	[309]

Table 2-8 (continued)

Ibuprofen, salycilic acid, triclosan	Sewage effluent	Biodegradation using MBR system	HRT=1-2 day, SRT= 2days	Removal efficiencies were~100%,~100%,~90%	[310]
Triclosan, naproxen, ibuprofen, carbamazepine	Drinking water	Adsorption on activated carbon, carbonaceous resin	Activated carbon concentration 1mg/L, resin concentration 1mg/L	Removal efficiencies of activated carbon/carbonaceous resin were 99.5%/>99.8%, 46.6%/31.2%, 23.3%/28.7%, 69.9%/38.9%	[311]
Atenolol, atrazine, carbamazepine	River water	Photocatalytic reactor membrane system	UV-TiO_2-H_2O_2 (20ppm)	Removal efficiencies were 70%,>95%, >95%	[312]
Norfloxacin, ibuprofen, naproxen, clofibric acid	Domestic waste water	Adsorption and biodegradation on activated sludge	Average flow rate=20,000m^3/day, HRT= 35 hours	Removal efficiencies were >70%, 99%, 94%,61%	[313]
Carbamazepine	Drinking water	Ozonation	pH 7.5; CO_3 = 1.5-2.0mg/L	High efficiency in removal after filtration and coagulation/flocculation	[314]
Atenolol, naproxen, triclosan	Wastewater effluent	Biological degradation under anoxic condition on constructed wetlands	HRT= 6 hours, flow rate=18,000 m3/day	Removal efficiencies were ~100%, ~90%, 20-80%	[315]
Triclosan, naproxen, diclofenac, ibuprofen	Raw and finished drinking water	Chlorination/ozonation/UV irradiation	Free chlorine dose 3.5 mg/L, ozone dose 2.5 mg/L, UV at 40mJ/cm2	Removal efficiencies of chlorination/ozonation/UV irradiation were >70%/>70%/30-70% (triclosan),>70%/>70%/<30% (naproxen), >70%/>70%/30-70% (diclofenac), 30-70%/>70%/<30% (ibuprofen)	[316]

Table 2-8 (continued)

Atrazine and some phenylurea herbicides	Ground water	Ozonation and oxidation	pH 7.8, ratio of H_2O_2:O_3= 3.7g/g	80% removal of atrazine and phenylurea herbicides	[317]
		Fenton treatment (Fe2+/H_2O_2)	pH 5.5, C H_2O_2= 10mg/L, C Fe_{2+}=5.1 mg/L	75% removal of atrazine and 94% removal of phenylurea herbicides	
Carbamazepine	Aqueous solution	Ozonation	Ratio of O_3:CBZ=10, CO_3= 1mg/L	Complete removal of CBZ	[318]
Carbadox, sulfachlorpyridazine, sulfadimethoxine, sulfamerazine, sulfamethazine, sulfathiazol, trimethoprim	Deionized and river water	Ozonation	CO_3= 0.3 mg/L, pH 7.5	95% removal of all compounds	[308]
Nonylphenol	Aqueous solution	Adsorption on coal-based Calgon Filtrasorb 400 (F400)	C_i=1000ng/L, T=23± 1°C	Adsorption capacity of 600 ng/mg	[282]
Bisphenol A (BPA)	Distilled water	Ozonation	T=20°C, contact time =1-120 min, CO_3 = 1.5mg/L	100% removal was achieved	[319]
Bisphenol A	Aqueous solution	Ozonation	CO_3 = 7.516μmol/L	Slower removal rate	[320]
Bisphenol A	Doubly distilled water	Photocatalysis	200 W Hg-Xe lamp, TiO_2 in suspension	100% mineralization of BPA in 20 hours	[321]
Nonylphenol	Drinking water	Adsorption on GAC	GAC preloaded for 16 weeks, C_i=500ng/L	11-58% of the initial capacity removal was obtained	[281]

Table 2-8 (continued)

Bisphenol A	River water, lake water, ground water	Filtration using GAC /GAC filtration followed by UV treatment	pH 6.95±0.05	80-99% removal of BPA was obtained	[286]
Bisphenol A	Distilled water	Photocatalysis	Black blue lamp (15 W), TiO_2 immobilized in PTFE	98% removal in 1hour treatment	[322]
Bisphenol A	Deionized water, model natural drinking water and river water	UV/H_2O_2 treatment	Medium pressure and low pressure UV lamp, $CH_2O_2 = 200$ mg/L, pH 6.0–8.0	Efficient removal was achieved by the combined treatment	[323]
Bisphenol A	Milli Q/deionized water	UV irradiation/ UV irradiation and oxidation using H_2O_2	Low pressure lamp (15W, 254 nm), $CH_2O_2 = 0$ to 50 mg/L, pH 5.3–4.3	Only UV irradiation was not enough to degrade BPA, UV/H_2O_2 treatment gave a better removal of estrogenic activity	[324]
Bisphenol A, nonylphenol, nonylphenol ethoxylate, nonylphenoxy acetic acid	Surface water	Adsorption, biodegradation and biotransformation by membrane bioreactor (MBR)	Solid retention time=55day, Hydraulic retention time=4 day	>90% removal was achieved	[264]
Nonylphenol octylphenol, bisphenol A	Domestic wastewater	Aerobic biodegradation by activated sludge	SRT=5days, HRT=9hours	Removal efficiencies were 61-75%, 32-65% and >92%	[291]

Table 2-8 (continued)

Nonylphenol, octylphenol, bisphenol A	Domestic sewage	Combined activated sludge treatment, sand filtration and ozonation	HRT(activate sludge)=9hours, flow rate and retention time in sand are110m/d and 1 hour, ozone concentration and r.t. are 3mg/L and 27 mins	Removal efficiency was >90% for the EDCs	[297]
Bisphenol A	Aqueous solution	Biodegradation by submerged MBR	pH 5, HRT=24 hours, MBR temperature=22±1°C	~100% removal of BPA was achieved	[300]
Bisphenol A, Nonylphenol, t-octylphenol	Synthetic wastewater	Biodegradation by submerged MBR technique	HRT=24 hours, MBR temperature=20±1°C	Removal efficiencies were 90.4±3.1%, 99.3±0.2%, 94.5±1.1%	[301]
Bisphenol A, nonylphenol	Raw waste water samples	Activated sludge treatment, microfiltration and reverse osmosis	SRT=13 days, HRT=24 hours	Removal efficiency was ~100%	[301]
Bisphenol A, Nonylphenol	Municipal waste water	Anaerobic/anoxic/aerobic-membrane bioreactor process	T=25°C, HRT upto 5 hours, sludge retention time=20days	Removal efficiency was ~100%	[306]
4-tert-octylphenol	Sewage effluent	Biodegradation using MBR system	HRT=1-2 day, SRT= 2days	Almost 90% of the EDC was removed	[310]

2.6 Adsorption and desorption

Adsorption is the adhesion of atoms, ions, biomolecules or molecules of gas, liquid, or dissolved solids to a surface. It is a surface phenomenon where the adsorbate will form a film on the adsorbent's surface. Adsorption capacity is directly proportional to the availability of surface area of solid for adsorption. There are two mechanisms for adsorption to take place. One is physisorption, where in this process; adsorbate becomes bonded to the adsorbent by weak van der Waals forces. As the bonding forces are not strong, this process can be reversed by heating. The next mechanism is chemisorption, where the adsorbate is bonded to the absorbent by strong chemical binding forces. To understand adsorption more precisely the adsorption equilibrium and the parameters affecting adsorption should be investigated. Desorption is a phenomenon whereby a substance is released from or through a surface. However, desorption is also important for the recovery of biomolecules from the surface of the particles. Therefore, suitable adsorption and desorption parameters should be developed.

In this study, the solid adsorbent is surface functionalized magnetic nanoparticles (MNPs) while the adsorbates are chiral amino acids, pharmaceuticals endocrine disrupting compound and the beta-blocker. In this particular closed adsorption system, the adsorbate solution and surface functionalized magnetic nanoparticles are mixed together till the solution's solute concentration is at equilibrium with the adsorbed solute concentration. To understand adsorption more precisely adsorption equilibrium and the parameters affecting adsorption should be investigated. After completion of the adsorption process, desorption of the biomolecules should be studied under different conditions.

2.6.1 Adsorption isotherm

Adsorption isotherm describes the amount of adsorbate on the adsorbent surface (adsorption capacity) as a function of equilibrium adsorbate concentration in solution at constant temperature. The quantity of adsorbate adsorbed on the adsorbent is normalized by the mass of the adsorbent to allow comparison of different materials.

2.6.1.1 Adsorption isotherm models

2.6.1.1.1 Langmuir model

Adsorption equilibriums of chemicals on magnetic particles' surface can be described by Langmuir model [325]. The Langmuir isotherm was theoretically derived, based on a number of assumptions: adsorption takes place on fixed homogenous absorption sites of equal energy forming a monolayer surface coverage, there are no interactions between adjacent species adsorbed, the adsorption capacity of the species to be adsorbed is directly proportional to the concentration of the species. The Langmuir model can be described by equation 2-9:

$$Q_e = \frac{Q_m C_e}{k_L + C_e} \qquad \text{[2-9]}$$

where, C_e is equilibrium concentration, Q_e is adsorbate surface concentration , Q_m is maximum monolayer adsorbate adsorption capacity, k_L is Langmuir constant, signifying the affinity between adsorbent and adsorbate. The above Langmuir adsorption isotherm model works well for cases where there is negligible intermolecular interaction between adsorbed solute particles and where only one monolayer of solute can be potentially adsorbed. This model can be thought of as a limiting law just like the analogy for ideal gas equation. To establish the validity of the assumption that independent interaction sites of equivalent affinity are present on the adsorbent surface, several linear transformations of equation 2-9 can be employed as follows:

$$\frac{C_e}{Q_e} = \frac{1}{Q_m k_L} + \frac{C_e}{Q_m}$$

[2-10]

Several more sophisticated models to account for deviation from Langmuir adsorption behavior had also been developed. Freundlich isotherm model which was proposed by Herbert Max Finlay Freundlich is an example of an adsorption isotherm that was formulated to account for case that does not follow the Langmuir adsorption behavior.

2.6.1.1.2 Freundlich model

Another commonly used model to explain adsorption isotherm of chemicals/ biomolecules on magnetic particles' surface is Freundlich isotherm model [326]. It is derived by assuming a heterogeneous surface with a non-uniform distribution of heat of adsorption over the surface and it also takes into account the repulsive interactions between adsorbed solute particles. Freundlich Isotherm is purely empirical and nonlinear. It is given in the following equation:

$$Q_e = k_F C_e^{\left(\frac{1}{n}\right)}$$

[2-11]

$$\text{or, } \ln Q_e = \ln k_F + \frac{1}{n} \ln C_e$$

[2-12]

where, C_e *is* equilibrium adsorbate concentration in solution, Q_e is adsorption capacity of adsorbent and k_F, n are empirical constants for each adsorbent-adsorbate pair. The empirical constants, k_F and n are temperature dependent. As the temperature increases, the constants k_F and n changes, the adsorption rate decreases as higher adsorbate concentration in solution are required to saturate the surface. The empirical constants are determined experimentally via a linear plot of $\ln Q_e$ versus $\ln C_e$.

2.6.1.1.3 Langmuir-Freundlich model

Some researchers combined Langmuir and Freundlich isotherm to describe the adsorption isotherms:

$$Q_e = \frac{Q_{mLF} k_d^* C_e^{(\frac{1}{n})}}{1 + k_d^* C_e^{(\frac{1}{n})}} \qquad\qquad [2\text{-}13]$$

where k_d^* is the apparent dissociation constant that includes contributions from ligand binding to monomer, monomer-dimer, and more highly associated forms of biomolecules; Q_{mLF} is the maximum binding capacity; and n is the Langmuir-Freundlich coefficient. The Langmuir-Freundlich model was analyzed by some researchers and it was found that the energy distribution function corresponds to a symmetrical quasi-Gaussian function [327, 328]. At low concentrations, the model reduces to the Freundlich model and in the case of a homogeneous surface; it reduces to the Langmuir model. Because of the presence of more than two adjustable parameters in Langmuir-Frendlich equation, experimental data are fitted applying nonlinear least-squares analysis.

2.6.2 Adsorption kinetics

The adsorption of biomolecules from aqueous solutions onto solid surface of particles can be considered as a process consisted of several steps: 1) diffusion of solute molecules from bulk solution to the surface of solid particles, 2) attachment of target molecules to active sites on the surface, 3) rearrangement of biomolecules at the surface after adsorption.

It is also a well-recognized fact that the process of adsorption is a two-regime process [329]. At the initial stage, the solid surface is bare and the kinetics of adsorption is governed by the diffusion of the molecules from the bulk solution to the surface. The

mass transport can be interpreted as a Fickian diffusion as the following equation [330]:

$$Q_t = \frac{2}{\pi} C_i \sqrt{(Dt)} \qquad\qquad [2\text{-}14]$$

where, Q_t is the adsorbed amount of target at different time, t. C_i is the initial concentration of target. D is the diffusion constant (cm^2/s). In the later stage, a barrier of adsorbed molecules exists, and the molecules arriving from solution have to diffuse across this barrier. This penetration is slow and can be presented as exponential time dependence for the later stages:

$$Q_t = Q_e[1\text{-}e^{\left(\frac{t}{T}\right)}] \qquad\qquad [2\text{-}15]$$

where Q_e is the adsorbed amount at equilibrium (mg/g) and $1/T$ is the penetration rate constant (mg/g.s).

Recently, some works investigated adsorption kinetics of organic dyes and hazardous materials on modified iron oxide magnetic nanoparticles with the help two kinetic models, namely the Lagergren pseudo-first-order and pseudo-second-order model. The Lagergren rate equation is one of the most widely used adsorption rate equations for the adsorption of solute from a liquid solution. The pseudo-first-order kinetic model is expressed by the following equation [331]:

$$\frac{dQ}{dt} = k_1(Q_e - Q_t) \qquad\qquad [2\text{-}16]$$

Integrating this equation for the boundary conditions $t = 0$ to $t = t$ and $Q = 0$ to $Q = Q_t$, gives:

$$ln(Q_e - Q_t) = lnQ_e - k_1t \qquad\qquad [2\text{-}17]$$

where Q_e and Q_t refer to the amount of target molecule adsorbed (mg/g) at equilibrium and at any time, t (min), respectively, and k_1 is the equilibrium rate constant of pseudo-first-order sorption (1/min). Another kinetic model is pseudo-second-order model, which is expressed by [332]:

$$\frac{dQ}{dt} = k_2(Q_e - Q_t)^2 \qquad [2\text{-}18]$$

Integrating this equation for the boundary conditions $t = 0$ to $t = t$ and $Q = 0$ to $Q = Q_t$, gives,

$$\frac{t}{Q_t} = \frac{1}{k_2 Q_e^2} + \frac{1}{Q_e} t \qquad [2\text{-}19]$$

where k_2 is the equilibrium rate constant of pseudo-second-order adsorption (g/mg min). All these published work provide useful information to study the adsorption of chemical and biomolecules on nano-sized magnetic particles.

2.7 Desorption study

To check the possibility of regeneration and recyclability of the magnetic nanoparticles, it is very important to carry out desorption studies. Generally, desorption condition of the sorbate is dependent on the condition at which the sorbate was adsorbed. Thus, suitable desorbing agents should be selected to facilitate desorption of the solute. For desorption of proteins, sodium dihydrogen phosphate solution, disodium hydrogen phosphate solution, sodium thiocyanate solution at different pH are used as desorbing agent [333, 334]. For desorption of metals from magnetic nanoparticles, acidic solution (citric acid/ acetic acid solution) is used as effective desorbing agent [150]. For desorption of organic molecules, dyes where inclusion complexation is predominant, alchohol solution such as methanol/ethanol solution is generally used [335, 336].

2.8 Scope of the Thesis

The aim of this project is to synthesis cyclodextrin derivatives coated magnetic nano particles and to utilize the particles in chiral separation and separation of pharmaceutically active compound, endocrine disruptors and beta-blockers. Although nano particles have diverse applications in the field of bioscience and biotechnology, only limited work has been published on the preparation of cyclodextrin derivatives coated magnetic nanoparticles and their use as a tool for separation of chiral biomolecules and environmental pollutants. Based on the literature review the scopes of the present project are:

1. Synthesis and characterization of silica and cyclodextrin derivative coated magnetic particle:

Magnetic nanoparticles are synthesized by chemical co-precipitation method using $FeCl_3$ and $FeCl_2$ with ammonia under nitrogen environment in a ratio of 2:1. These magnetic nanoparticles undergo subsequent coating of silica and carboxymethyl-β-cyclodextrin under different reaction environment. Characterization of the chemical, physical and magnetic properties of the as-synthesized magnetic nanoparticles are carried out using FTIR spectroscopy, TEM, XPS, BET method and VSM.

2. Application of silica and cyclodextrin derivative coated magnetic nanoparticle for adsorption of single amino acid enantiomers:

Tryptophan, phenylalanine and tyrosine are three important chiral amino acids which have various applications. Initially, adsorptions of single enantiomers (D-/L-Trp, D-/L-Phe, D-/L-Tyr) are done at neutral condition utilizing the silica and carboxymethyl-β-cyclodextrin coated magnetic nanoparticles. Furthermore, adsorption studies of each of

the enantiomers are carried out in different conditions (different pH, temperature) to summarize the effect of these parameters. This study also helps in obtaining the optimum condition for maximum adsorption. Furthermore, kinetic studies are done to observe the effect of contact time on the adsorption process. Mechanism for single amino acid adsorption on the nanoparticles surface is also explored using FTIR spectroscopy. The condition where adsorption capacity difference between the enantiomer is maximum is determined from the detailed adsorption study. After that, desorption of single amino acid enantiomers is carried out using methanol as desorbing agent.

3. Chiral separation of racemic amino acids using silica and cyclodextrin derivative coated magnetic nanoparticle:

Chiral separation of the amino acids on the nano adsorbents form their racemic mixture is also achieved in this project. Because of the different behaviour of the enantiomers, it is very important to study separation of enantiomers from their racemic mixture. Selective adsorption capacity of the particles from the racemic mixture of the amino acids and enantiomeric excess between the enantiomers are determined using high performance liquid chromatography technique. Enantioselective mechanism is also reported using several analytical techniques such as FTIR, XPS etc. Inclusion complex formation of the particles is also investigated and stability constant (K), Gibbs free energy change ($-\Delta G^0$) of the inclusion complexation process of the enantiomers (L-/D-Trp, L-/D-Phe and L-/D-Tyr) with CMCD is accounted. Furthermore, desorption efficiency of the adsorbed amino acid enantiomers are also checked using methanol as desorbing agent.

4. Synthesis, characterization and application of amino-cyclodextrin coated magnetic particle for removal of pharmaceuticals and endocrine disruptors from aqueous solution:

Magnetic nanoparticles coated with thiodiglycolic acid (TDGA) are also synthesized in this project by chemical co-precipitation method using $FeCl_3$ and $FeCl_2$ in presence of TDGA with ammonia solution under nitrogen environment in a ratio of 2:1. These magnetic nanoparticles are then coated with amino-cyclodextrin (β-CDen). These nanoparticles are characterized using several analytical techniques for example FTIR spectroscopy, TEM, XPS, TGA and VSM etc.

The as-synthesized particles are utilized for detailed adsorption study of two pharmaceuticals, carbamazepine and naproxen and one endocrine disrupting compound bisphenol A. Carbamazepine and naproxen are generally used for treatment of epilepsy and depression. Presence of these pharmaceuticals and EDC in waste-water could be cause of chronic environment pollution. Removal of these drugs from aqueous solution is then scrutinized using the thiodiglycolic acid and amino-cyclodextrin coated magnetic nanoparticle in batch adsorption mode. Equilibrium study and effect of different parameters on the adsorption process are carried out in details. Kinetic studies of the adsorption of the three compounds are carried out as well. Also, inclusion complex formation of the pharmaceuticals and endocrine disrupting chemical with amino-cyclodextrin are explored using FTIR spectroscopy. Desorption study of the chemicals are also done to evaluate regeneration possibility of the magnetic nanoparticles.

5. Adsorption separation of beta-blocker, propranolol using silica and cyclodextrin derivative functionalized magnetic nanoparticles:

Beta-blockers are one class of pharmaceuticals that have been widely detected in effluent of sewage treatment plants and surface water in the range of ng/L to µg/L [337-342]. Propranolol is a beta-blocker which is generally used in the treatment of hypertension and cardiac arrhythmia. Propranolol is considered to be highly persistent and bioaccumulative in the environment and can cause harmful effect to aquatic environment. Thus, separation/ removal of propranolol is very important. In the later part of this project, adsorption behaviour of beta-blocker, propranolol using silica and cyclodextrin derivative coated magnetic nanoparticles is studied in systematic manner. Effect of different operating conditions (solution pH, initial sorbate concentration) is reported using the coated nanomagnetic particles. Binding constant of propranolol with CMCD is also determined using flurometric titrations. Mechanism for adsorption of propranolol on the magnetic nanoparticles surface is then studied with FTIR, XPS spectroscopy etc. Finally, desorption study of propranolol form the nanoparticles' surface is carried out using methanol solution.

Chapter 3: Materials and Methods

3.1 Materials

Chemicals used for experimental purposes are listed in Table 3-1. All the chemicals were used as received without further treatment. For synthesis purpose and for preparation of buffer solutions ultrapure water and de-ionized water were used.

The physical-chemical properties of tryptophan, phenylalanine, tyrosine, carbamazepine, naproxen, bisphenol A and propranolol are listed in Table 3-2 and Table 3-3, respectively.

Table 3-1 Lists of chemical materials

Name	Chemical formula	Grade	Supplier company
Iron (II) chloride tetrahydrate (98%)	$FeCl_2 \cdot 4H_2O$	GR	Alfa-Aesar
Iron (III) chloride hexahydrate (98%)	$FeCl_3 \cdot 6H_2O$	GR	Alfa-Aesar
Ammonium hydroxide (25%)	NH_4OH	GR	Merck
Citric acid (99%)	$C_6H_8O_7$	GR	Alfa-Aesar
Tetraethyl orthosilicate (99%)	$SiC_8H_{20}O_4$	GR	Fluka
β-cyclodextrin hydrate (99%)	$C_{42}H_{70}O_{35} \cdot H_2O$	GR	Sinopharm Chemical
Sodium dihydrogen phosphate monohydrate (99%)	$NaH_2PO_4.H_2O$	GR	Merck
Di-sodium hydrogen phosphate (99%)	Na_2HPO_4	GR	Merck
Acetic acid, glacial (99.7%)	CH_3COOH	GR	Alfa-Aesar
Sodium acetate (99%)	CH_3COONa	GR	Merck
D- and L-tryptophan (99%)	$C_{11}H_{12}N_2O_2$	GR	Alfa-Aesar
D- and L-phenylalanine (99%)	$C_6H_5CH_2CH(NH_2)COOH$	GR	Alfa-Aesar
D- and L-tyrosine (99%)	$C_9H_{11}NO_3$	GR	Alfa-Aesar
DL-tryptophan (99%)	$C_{11}H_{12}N_2O_2$	GR	Alfa-Aesar
DL-phenylalanine (99%)	$C_6H_5CH_2CH(NH_2)COOH$	GR	Alfa-Aesar
DL-tyrosine (99%)	$C_9H_{11}NO_3$	GR	Alfa-Aesar
Carbamazepine (99.5%)	$C_{15}H_{12}N_2O$	GR	Sigma
Naproxen (99%)	$C_{14}H_{14}O_3$	GR	Alfa-Aesar
Bisphenol A (99%)	$C_{15}H_{16}O_2$	GR	Sigma-Aldrich

Table 3-1 (continued)

Propranolol hydrochloride (≥99%)	$C_{16}H_{21}NO_2 \cdot HCl$	GR	Sigma-Aldrich
Cyanamide (99%)	CH_2N_2	GR	Alfa-Aesar
2-propanol (99.9%)	C_3H_8O	GR	Fisher Scientific
Acetone (99.5%)	$(CH_3)_2CO$	GR	Merck
Methanol (99.5%)	CH_3OH	GR	Merck
Ethanol (99.5%)	C_2H_5OH	GR	Merck
P-toluenesulfonyl chloride (99%)	$C_7H_7O_2SCl$	GR	Lancaster
Thiodiglycolic acid (98%)	$C_4H_6O_4S$	GR	Sigma-Aldrich
Copper (II) sulphate pentahydrate	$Cu(II)SO_4.5H_2O$	GR	Hayashi Pure Chemical Ind. Ltd.
N-hydroxybenzotriazole (HOBt)	$C_6H_5N_3O$	GR	Sigma-Aldrich
Pyridine	C_5H_5N	GR	Sigma
Diethyl ether (≥99.7%)	$(C_2H_5)_2O$	GR	Sigma-Aldrich
N-methylpyrolidinone (NMP)	C_5H_9NO	GR	Fluka
N,N-dimethyl formamide (DMF)	C_3H_7NO	GR	Merck

Table-3-2 Physical properties of aromatic amino acids [53].

Amino acid	Molecular mass $(gmol^{-1})$	Isoelectric point	Volume (Å^3)
Tryptophan	204.23	5.89	227.8
Phenylalanine	165.19	5.48	189.9
Tyrosine	181.19	5.66	193.6

Table-3-3 Physical-chemical properties of the pharmaceuticals, EDC and beta-blocker [54, 282].

Property	Carbamazepine	Naproxen	Bisphenol A	Propranolol hydrochloride
Melting point	189-192°C	154-156°C	158-159°C	163-165°C
Boiling point	411°C	403.9°C	220°C	434.9°C
Solubility in water	17.7mg/L	15.9 gm/L	129 mg/L	150mg/L
Solvent solubility	Soluble in alchohol and in acetone	Soluble in methanol, slightly soluble in acetone	Soluble in acetone, methanol, toluene	Soluble in ethanol, methanol
Molecular weight	236.3	230.3	228.3	295.8
Chemical formula	$C_{15}H_{12}N_2O$	$C_{14}H_{14}O_3$	$C_{15}H_{16}O_2$	$C_{16}H_{21}NO_2 \cdot HCl$
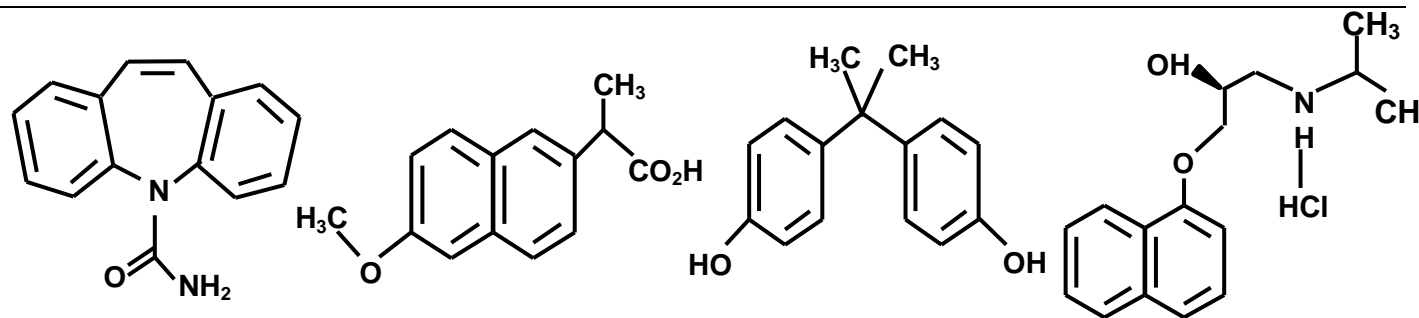
3.2 Methods

3.2.1 Synthesis of bare magnetic nanoparticles (bare MNPs)

Nanosized magnetic particles were synthesized by chemical co-precipitation method under alkaline condition and molar ratio between Fe^{2+} salt and Fe^{3+} salt was maintained at 1:2 [343]. In order to synthesize 1 g of Fe_3O_4 particle, 0.86 g of $FeCl_2 \cdot 4H_2O$ and 2.35 g of $FeCl_3 \cdot 6H_2O$ were dissolved in 40 mL ultrapure water under N_2 atmosphere with vigorous stirring at speed of 1000 rpm. As the solution was heated to 80°C, 5 mL of NH_4OH solution was added and the reaction was continued for another 30 mins. The resulting suspension was cooled down to room temperature and washed with ultrapure water. The product of bare magnetic nanoparticles (bare MNPs) was isolated from the solvent by magnetic decantation. The washing-decantation procedure was repeated five times to eliminate any unreacted chemicals and dried by freeze-dryer (Martin Christ freeze-dryer) for 24 hrs. Yield was 1.005 g. The following chemical reaction occurred -

$$FeCl_2. 4H_2O + 2\ FeCl_3. 6H_2O + 8NH_4OH = Fe_3O_4(s) +\ 8\ NH_4Cl + 20H_2O \qquad [3\text{-}1]$$
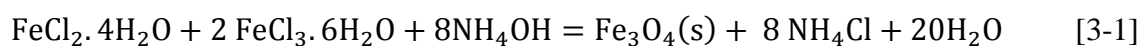
3.2.2 Silica coated magnetic nanoparticles (Fe$_3$O$_4$/SiO$_2$ MNPs)

The procedure of silica coating follows a modified method described by Chen et al. [344]. Prior to coat the magnetic particle with silica, modification of nanoparticle surface with negatively charged citrate groups was done. A solution of the magnetic nanoparticles was prepared by mixing 1 g dry bare magnetic nanoparticles in 200 mL (0.3M) of citric acid solution and the resulting solution was sonicated for 1 hr followed by mechanical stirring for 12 hrs at 400 rpm at room temperature. Subsequently, the obtained citric acid modified nanoparticles (CMPs) were washed several times with distilled water, isolated with help of a magnet and dried at 60 °C in vacuum for 2 hrs. And the weight of the dry product was 1.1 g.

Furthermore, 1g of CMP was mixed with 40 mL deionized (DI) water and 200 mL of 2-propanol and sonication for 15 mins was carried out to maintain proper dispersion. Under continuous mechanical stirring, 20 mL of ammonia solution (25%) and 1.5 mL tetraethyl orthosilicate (TEOS) were added. The reaction was allowed to proceed at room temperature at 650 rpm for 6 hrs. The silica coated core shell magnetic nanoparticles (Fe_3O_4/SiO_2 MNPs) were isolated by magnetic decantation to remove the unbound silica particles and dried in vacuum after being washed with de-ionized water, 2-propanol and acetone (weight of dry product: 1.5 gm).

3.2.3 Synthesis of carboxymethyl-β-cyclodextrin (CMCD)

A derivative of β-cyclodextrin, carboxymethyl-β-cyclodextrin was synthesized according to the method proposed by Prabaharan and Jayakumar with slight modification [345]. In a typical procedure, 20 g β-CD and 18.6 g sodium hydroxide (NaOH) were dissolved in 74 mL de-ionized water. Separately, solution of monochloroacetic acid (16.3%) was prepared in 54 mL de-ionized water and then mixed with the previous solution. The reaction mixture was heated to 50°C and the reaction was continued for 5 hrs under stirring with a magnetic bar. Subsequently, the reaction mixture was cooled down to room temperature and the solution was neutralized (pH 6~7) by adding dilute hydrochloric acid. Evaporation was done to obtain precipitate of unwanted salt (NaCl) and it was removed by vacuum filtration. Then the obtained solution without Cl^- was poured to superfluous methanol solvent and it produced white precipitation. The solid precipitation was filtered and dried under vacuum to give carboxymethylated β-CD (CMCD, 12 g). IR (KBr): v (cm^{-1}): 3140–3680 (–OH), 2923 (–CH), 1704 (C=O), 960–1200 (C–C, C–O–C).

3.2.4 Coating of CMCD on Fe$_3$O$_4$/SiO$_2$ MNPs

Grafting of CMCD on Fe$_3$O$_4$/SiO$_2$ MNPs was done via modified carbodiimide activation method [346]. 1 g of dry Fe$_3$O$_4$/SiO$_2$ MNPs was mixed with 20 mL of sodium phosphate buffer (0.03M, pH~6) and sonicated for 15 mins. Then 125 mg of cyanamide was dissolved separately in 5 mL of the same buffer solution and added to the previous mixture. Further sonication was done for 15 mins and finally 25 mL of CMCD solution (75 mg/mL in same buffer solution) was added and the reaction was continued for 2 hrs. The final product of CMCD coated magnetic silica nanoparticles (Fe$_3$O$_4$/SiO$_2$/CMCD MNPs) were washed several times with sodium phosphate buffer. Weight of wet particles was 1.3 g. Some of the synthesized particles were dried in oven at 60°C and used for characterization while the rest were used for adsorption studies.

The step-by-step reaction procedure to synthesize CMCD modified magnetic silica nanoparticles is shown in Figure 3-1.
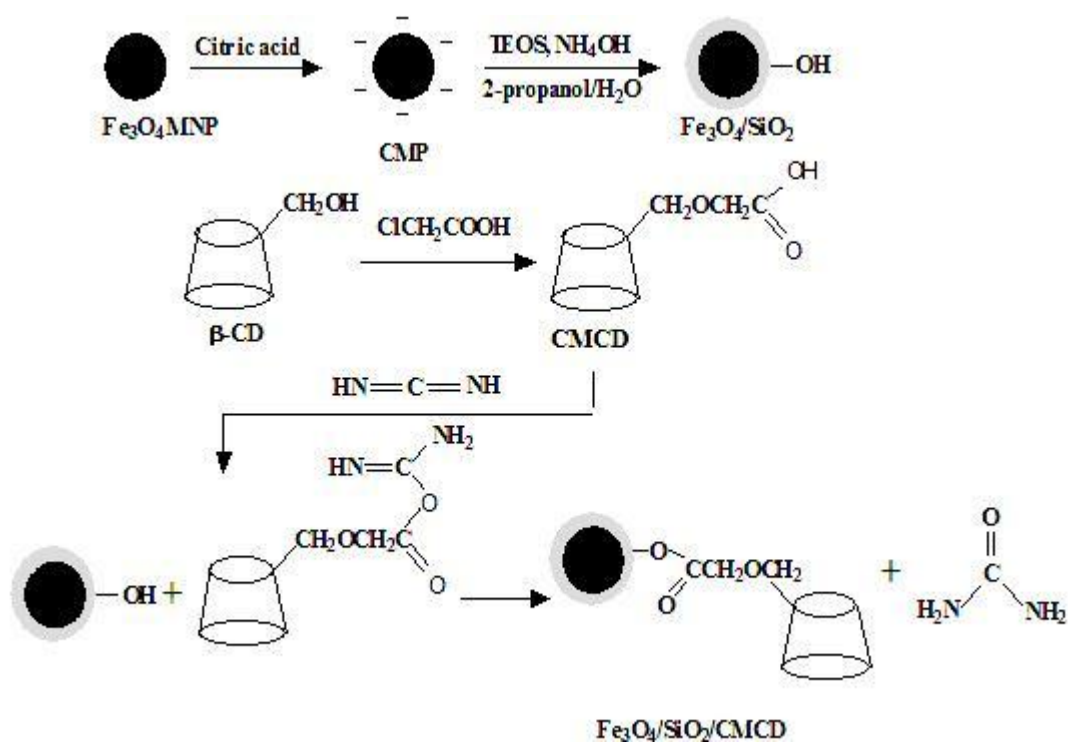
Figure 3-1 Scheme representation of silica and CMCD coating on bare magnetic nanoparticles.

3.2.5 Synthesis of 6-Deoxy-6-(p-toluenesulfonyl)-β-cyclodextrin (Ts-β-CD)

Mono-tosyl-β-cyclodextrin (Ts-β-CD) was synthesized according to the following method. A solution of β-CD (18g, 16mmol) in 100 ml dry pyridine was prepared and 2.5g of p-toluenesulfonyl chloride (12 mmol) was added to this solution. The reaction was carried out at 2-4°C for a period of 8 hrs, and then 2 days at room temperature [347]. After concentrating the solution under vacuum, the mixture was poured into diethyl ether. A white precipitate was collected and purified by repeated crystallization from water. This product was finally washed by acetone and dried under vacuum at 60ºC (weight of dry particles was 4 g). IR (KBr): 3387 (ν, OH), 2927 (ν, C–H), 1636 (δ, OH), 1368 (ν, SO$_2$), 1157 (ν, C–O–C), 1029 (ν, C–O).

3.2.6 Synthesis of 6 deoxy-6-ethylenediamino-β-cyclodextrin (β-CDen)

6-Deoxy-6-ethylenediamino-β-cyclodextrin (β-CDen) (en=-NHCH$_2$CH$_2$NH$_2$) was synthesized following the procedures described by May et al. [348]. Typically, a solution of as-prepared Ts-β-CD (2.0 g, 1.55 × 10^{-3} mol), KI (0.025 g, 0.15 × 10^{-3} mol) and ethylenediamine (5 × 10^{-3} mol) in dry NMP (5 cm^3) was stirred at 70°C in a flask for 6 hrs. The resultant light yellow solution was cooled to room temperature and diluted with ethanol (100 cm^3). The resulting precipitate was collected by vacuum filtration, washed successively with ethanol (100 cm^3) and diethyl ether (50 cm^3) and dried under vacuum to give the crude product. This material was then purified by column chromatography and dried under vacuum over **P$_2$O$_5$** to give β-CDen in yields of 55%. IR (KBr): 3388 (ν, OH), 2927 (ν, C–H), 1656 (δ, OH), 1576(ν, NH$_2$), 1156(ν, C–O–C), 1031 (ν, C–O).

3.2.7 TDGA coated magnetic nanoparticles (TDGA-MNPs)

Magnetite nanoparticles were prepared by chemical co-precipitation method under a nitrogen atmosphere to avoid possible oxidization during reaction [349]. A complete precipitation of Fe$_3$O$_4$ was achieved under alkaline condition, while maintaining a molar ratio of Fe^{2+}: Fe^{3+} = 1: 2 under an inert environment. In a typical synthesis to obtain 1 g Fe$_3$O$_4$ precipitate, 0.86g of FeCl$_2$.4H$_2$O and 2.36g FeCl$_3$.6H$_2$O were dissolved in 40 mL of de-aerated Milli-Q water with vigorous stirring at a speed of 1,000 rpm. As the solution was heated to 80ºC, 100 mg of thiodiglycolic acid (TDGA) was added, followed by 5 mL of NH$_4$OH. Further, TDGA was added to the suspension in five 0.2 gm amounts over 5 min. The experiment was continued for 30 min at 80ºC under constant stirring to ensure complete growth of the nanoparticle crystals. The resulting particles were then washed with Milli-Q water at least five times to remove any unreacted chemicals (weight of wet particles was 1.2 g). TDGA coated magnetic

nanoparticles were synthesized in few batches to get at least 5 g paticles to facilitate further modification and adsorption studies.

3.2.8 β-CDen conjugated magnetic nanoparticles (CDen-MNPs)

Thiodiglycolic acid (TDGA) coated wet magnetic nanoparticles (4 g) were suspended in 50 mL deionized water, and adjusted the pH of the solution to 6.8 after adding β-CDen or β-CDNH$_2$ (1.6 mmol). A mixture of N-(3-dimethyl (aminopropyl)-N'-ethyl carbodiimide hydrochloride (0.96 mmol) and HOBt (N-hydroxybenzotriazole, 0.96 mmol) was dissolved in a 6 mL mixture of H$_2$O and DMF (1:1), and added to the reactant mixture. The reactant mixture was stirred at room temperature for 48 hrs. The CD conjugated powder was isolated from the solvent by magnetic decantation. The washing-decantation procedure was repeated three times to remove excess reactants used for the coating and weight of wet particles was 4.7 g. Some of the synthesized particles were dried for characterization while the rest were used for adsorption studies. Figure 3-2 illustrates the synthetic routes for preparation of β-CDen conjugated magnetic nanoparticles.
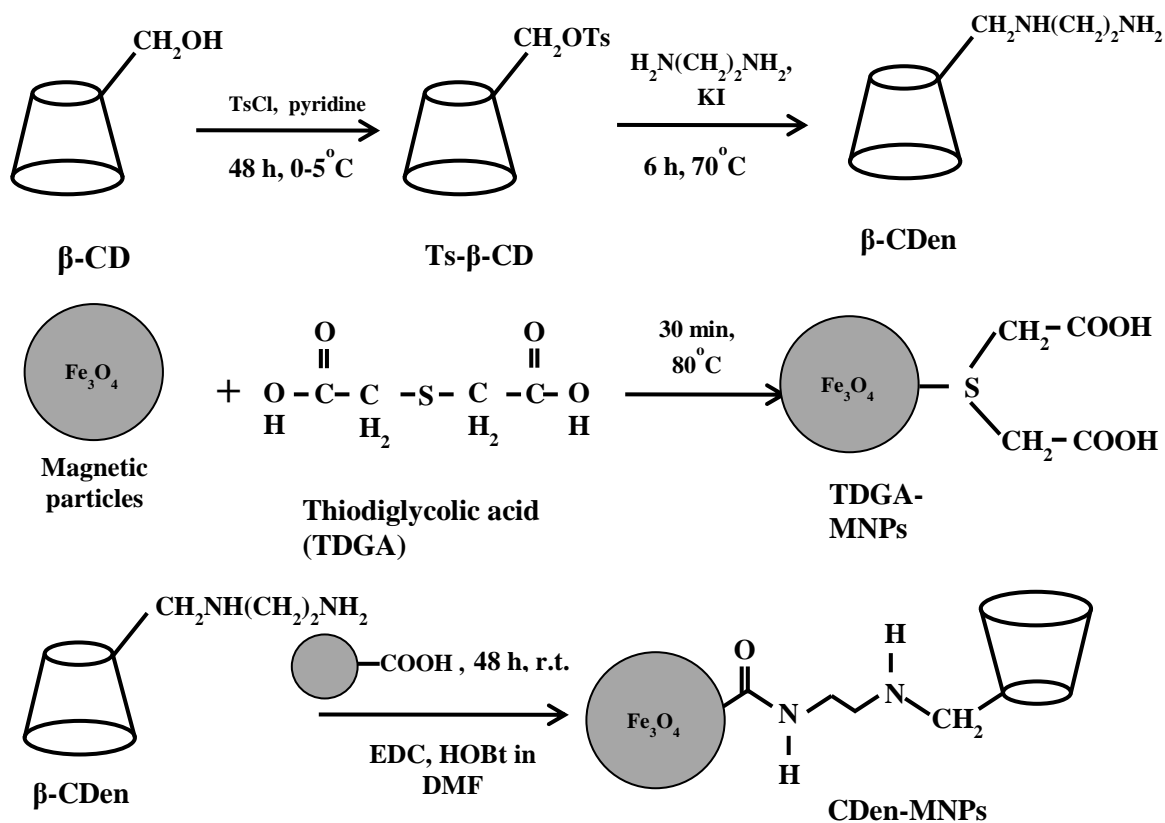
Figure 3-2 Preparation steps for fabricating β-CDen functionalized magnetic nanoparticles.

3.3 Adsorption experiments

3.3.1 Adsorption of chiral aromatic amino acids on Fe_3O_4/SiO_2/CMCD MNPs

Tryptophan, phenylalanine and tyrosine are chiral amino acids with aromatic groups. To examine the effect of pH and effect of temperature on adsorption capacity of silica and CMCD coated magnetic nanoparticle toward the amino acids, detailed adsorption studies were performed at different conditions (pH and temperature).

3.3.1.1 Effect of initial pH

Effect of initial pH was studied in the range of 4-7 at 25°C and ionic strength of 0.03M. Two buffer systems, i.e. 0.03 M sodium acetic acid buffer (pH 4), 0.03 M mono/di

sodium phosphate buffer (pH 5, 5.5, 5.6, 5.9, 6, 7) were used for the experiments. Due to low solubility of tyrosine, it was difficult to obtain tyrosine solution of concentration greater than 2 mM. Hence, to compare adsorption capacities of the synthesized particle toward the aromatic amino acid enantiomers, lower initial concentration range (0.25 mM, 0.5 mM, 1 mM, 1.5 mM, 1.75 mM and 2 mM) of the six amino acid enantiomers (D-/L-Trp, D-/L-Phe, D-/L-Tyr) were prepared. Equilibrium study and comparison of adsorption capacities of coated magnetic nanoparticles toward the chiral amino acid enantiomers were performed by mixing 4 mL of amino acid solution with 50 mg of CMCD coated magnetic nanoparticles. To verify reproducibility of the results, duplicates of each sample were prepared.

Some preliminary kinetic studies for adsorption process were conducted and it was found that equilibrium was reached in less than 24 hrs. The samples were left in a shaker operating at 230 rpm for 24 hrs which was the time to reach adsorption equilibrium. When the particles reached equilibrium, supernatant was separated from the magnetic particles by magnetic decantation method and filtered through 0.45μm syringe filter. The clear solution thus obtained was analyzed by means of a UV–visible spectrophotometer (Model UV- 1800) calibrated at the wavelength of maximum absorbance (λ_{max}) of the specific amino acid enantiomers. Standard solutions of these amino acid enantiomers were prepared and absorbances of those solutions were recorded in the UV-visible spectrophotometer for plotting the standard calibration curves (absorbance against concentration). Tryptophan, phenylalanine and tyrosine show maximum absorbance in the UV spectrum at 280, 258 and 275 nm, respectively. From the calibration curve, final concentrations of the amino acid solutions and adsorption capacities of the particles toward the amino acid enantiomers were calculated.

3.3.1.2 Effect of temperature

After obtaining the optimal condition for adsorption from the effect of initial pH study, effect of temperature on adsorption of amino acid enantiomers was studied at three different temperatures i.e. 25°C, 35°C and 50°C and at optimum pH (where pH corresponds to maximum adsorption capacity of $Fe_3O_4/SiO_2/CMCD$ MNPs toward the enantiomers) and ionic strength of 0.03M. Effect of temperature study was carried out by mixing 4 mL of amino acid solution of different initial concentrations (0.25 mM to 2 mM) and 50 mg of wet magnetic nanoparticles. The sample vials were placed in a water bath with oscillator, and left to oscillate at a speed of 230 rpm for a period of 24 hrs at the desired temperature. Supernatant was collected using magnetic decantation and final concentration was obtained using UV-visible spectrophotometer.

3.3.1.3 Kinetic studies

For the kinetic experiments, the initial amino acid concentrations were 2 mM and the initial solution pH value was 5.9, 5.5 and 5.6 for Trp, Phe and Tyr enantiomers respectively (the solution pH was not controlled during the experiments). These amino acid solutions mixed with 50 mg of magnetic particles were agitated for a contact time varied in the range of 0–24 hrs at a speed of 230 rpm at 25°C. At various time intervals, samples were collected after separation of magnetic adsorbents by magnetic decantation process and the equilibrium concentration of amino acid solutions were determined as mentioned previously.

3.3.1.4 Desorption studies

Desorption of amino acid enantiomers (L-/D- Trp, L-/D-Phe, L-/D-Tyr) from $Fe_3O_4/SiO_2/CMCD$ MNPs was also investigated using methanol as eluent. Adsorption of individual amino acids (2 mM) on the functionalized magnetic nanoparticles was

carried out first. After 24 hrs, amino acid adsorbed on magnetic nanoparticles were separated by magnetic decantation and gently washed with water to remove the unbound amino acids. Desorption was then examined by adding 5 mL of methanol as eluent and shaking was continued at 230 rpm for 24 hrs, $Fe_3O_4/SiO_2/CMCD$ MNPs were collected by magnetic decantation method and the concentration of each amino acid in the supernatant was measured.

3.3.2 Enantioselective separation of chiral aromatic amino acids

3.3.2.1 Adsorption of racemic amino acids

Sorption resolution experiments were carried out to determine the sorption selectivity and capability of $Fe_3O_4/SiO_2/CMCD$ MNPs. To compare enantioselective capacities of the magnetic nanoparticles, initial concentration of the amino acid solutions were maintained same i.e. 2 mM. 4 mL of racemic amino acid solution (DL-Trp, DL-Phe and DL-Tyr) (prepared in mono/disodium phosphate buffer, pH 6) of 2 mM initial concentration and 130 mg of wet magnetic nanoparticles were mixed and the samples were left in a shaker operating at 230 rpm for 24 hrs which is the time to reach adsorption equilibrium. Afterwards, supernatant separated from the magnetic particles by magnetic decantation were collected and filtered through 0.45µm syringe filter and D- and L-amino acid concentrations in the solutions were analyzed by high performance liquid chromatography (HPLC). To verify reproducibility of the results, triplicates of each sample were prepared and each experiment was performed at least twice.

3.3.2.2 Measurement of enantiomeric excess

All the enantiomeric excess and equilibrium concentration of amino acids were quantified on a HPLC-1200 system equipped with a Variable Wavelength Detector system (Agilent Technologies). Instrument control and data acquisition were performed with the HPLC-1200 ChemStation software. Separations were performed on a Phenomenex Chirex column (150 mm×4.6mmI.D.), purchased from Omega Scientific Pte Ltd. The mobile phases were prepared by mixing 2 mM copper sulphate solution with methanol (70:30). All the solutions were filtered through 0.45μm filter. Detection wavelength was set at 258 nm. Flow rate of mobile phase was set at 0.7 mL/min. The test samples (DL-Trp, DL-Phe and DL-Tyr) were dissolved in 0.03 M sodium phosphate buffer with initial concentration of 2 mM and the injected volume was 20 μL and temperature was set at 18°C. The column was equilibrated by washing with copper sulphate and 2-propranol (95:5) at flow rate of 1 mL/min for 1 hr after every run to ensure good performance of the column. All the chiral analyses were performed in triplicate to check accuracy. For the evaluation of enantioseparation, the following parameters were determined: k_1 and k_2 (the retention factors of the eluted enantiomers) were calculated using the formula $(t_1 - t_0)/t_0$ and $(t_2 - t_0)/t_0$ (where t_0 is the time at which the first baseline disturbance by the solvent peak occurred), α (the selectivity factor) was calculated using k_2/k_1, while R_s (the resolution) was evaluated using the formula 1.18 $(t_2 - t_1)/(wh_1 + wh_2)$, where wh_1 and wh_2 are the half peak widths [350]. Sorption selectivity (expressed in enantiomeric excess, *e.e.*) and uptake (Q_e) of $Fe_3O_4/SiO_2/CMCD$ MNPs could be expressed by equation 3-2 and equation 3-3, respectively [351]:

$$e.e = \frac{c_D - c_L}{c_D + c_L} \times 100\% \qquad [3\text{-}2]$$

$$Q_e = \frac{(C_i - C_e) \times V}{w}$$ [3-3]

Where, C_D and C_L denote equilibrium D- and L-amino acid concentrations in the bulk solution (mM), respectively. C_i and C_e represent initial and equilibrium concentrations of aromatic amino acids in the bulk solution (mM), and V and w are the solution volume (mL) and the weight of dry magnetic particles (mg).

3.3.2.3 Flurometric experiments

The flurometric titrations using a series of solutions containing L/D- Trp, L/D- Phe and L/D- Tyr (3×10^{-5} mol/L) and varying amounts of CMCD (0-9.68 $\times 10^{-4}$ mol/L) were carried out in aqueous buffer solution (pH 6) at 25 °C with excitation at 280 nm, 258 nm and 275 nm for Trp, Phe and Tyr enantiomers and observation at 358 nm, 260 nm and 280 nm.

3.3.3 Adsorption of pharmaceuticals and EDCs on CDen MNPs

Carbamazepine, naproxen and bisphenol A are some of the emerging contaminants with aromatic groups. Initially, kinetic studies were done to obtain the time for completion of the adsorption process. Furthermore, detailed adsorption studies of these compounds were carried out at different pH to obtain effect of pH on adsorption capacity of CDen-MNPs towards the pharmaceuticals and EDC.

3.3.3.1 Kinetic studies and effect of pH studies

The kinetics of adsorption process of emerging contaminants (naproxen, carbamazepine and bisphenol A) were investigated in a batch equilibrium mode by adding 100 mg of wet CDen-MNPs into 5 mL of CBZ, NAP and BPA solutions with concentration of 20 ppm. Samples for adsorption experiments were prepared in de-ionized water. The

solution pH was adjusted by 0.01M NaOH or 0.01M HCl. The solutions mixed with wet magnetic particles were agitated for a contact time varied in the range of 0–7 hrs at a speed of 230 rpm at 25°C. At various time intervals, samples were collected after separation of magnetic adsorbents by magnetic decantation and the equilibrium concentration of sorbates were determined as mentioned previously. The residual concentrations of CBZ, NAP and BPA in solutions were determined by Shimadzu UV–visible spectrophotometer (Model 1800) and absorbance values were recorded at 285, 271 and 276 nm, respectively. The amounts of solute adsorbed per unit mass of adsorbent were calculated from the differences between the initial and the final solute concentrations in solution before and after adsorption. Each experiment was repeated twice, and reproducibility was found to be fairly good. The amount of CBZ, NAP and BPA adsorbed onto CDen-MNPs was calculated by a mass balance relationship,

$$Q_e = \frac{(C_i - C_e) \times V}{w} \qquad [3\text{-}4]$$

where V (mL) is the volume, C_i and C_e (ppm) are the initial and equilibrium solution concentration of BPA, NAP or CBZ and w (mg) is the dry mass of the solid.

Effect of pH on adsorption of the PhACs and EDCs were examined over the pH range from 3-11 at 25°C at initial concentration of 20 ppm.

3.3.3.2 Equilibrium studies

Since these pharmaceuticals are present in low concentration in waste-water, adsorption studies were carried out in low concentration range i.e. 5-20 ppm range. The procedure for equilibrium study was basically identical to those of kinetic experiments. The solutions of pharmaceuticals and EDC with different concentrations (5-20 ppm) were mixed with 100 mg of wet CDen-MNPs at pH 7 and 25°C. The solution pH was

adjusted by adding 0.01M NaOH or 0.01M HCl solution. Then the sample solutions were stirred by a horizontal laboratory shaker at 230 rpm and after equilibrium was reached, the MNPs were removed by magnetic decantation from the solution before measurements. The equilibrium concentrations of CBZ, NAP and BPA in solutions were determined by UV–visible spectrophotometer by recording absorbance at 285, 271 and 276 nm, respectively. Adsorption capacities of adsorbent toward the sorbates were obtained from the differences between initial and equilibrium solute concentrations in solution before and after adsorption.

3.3.3.3 Adsorption of a mixture of pharmaceuticals

Adsorption of a mixture of the three selected pharmaceuticals (CBZ, NAP and BPA) was conducted by introducing 100 mg of coated magnetic nanoparticles into 5 mL solution of three pollutants at the same concentration at pH 7 and concentration of 20 ppm. The supernatant was collected by magnetic separation and the supernatant solutions were then filtered (0.45 μm), extracted and analyzed by the Agilent HPLC-1200 series. Analysis with HPLC was carried out using methanol and water (60:40) mobile phase at flow rate of 0.5 mL/min. Column temperature was maintained at 30ºC and detection was done at 286 nm.

3.3.3.4 Desorption of pharmaceuticals and EDC

Desorption of CBZ, NAP and BPA from CDen-MNPs was also investigated using ethanol as eluent. Adsorption of individual PhACs and EDC (20 ppm) on CDen-MNPs was carried out first. After 4 hrs, PhACs or EDC-adsorbed magnetic nanoparticles were separated by magnetic decantation and gently washed with water to remove the unbonded contaminants. Desorption was then examined by adding 5 mL of ethanol as eluent to the either pollutant-sorbed CDen-MNPs. After shaking at 230 rpm for 6 hrs,

CDen-MNPs were collected magnetically and the concentration of each pollutant in the supernatant was measured.

3.3.3.5 Preparation of inclusion complex for investigation by FTIR spectroscopy

The complex of CBZ, NAP and BPA with β-CDen in 1:1 molar ratio was prepared in water. To be more precise, 19.84 mg (0.084 mmol) of CBZ, 19.35 mg (0.084 mmol) of NAP, 19.17 mg (0.084 mmol) of BPA were added to 5 mL de-ionized water in three separate glass vials where 100 mg (0.084mmol) of CDen were added later on. The vials were sealed and the mixture was stirred at 25°C for 2 days. Afterwards, the residue containing inclusion complexes were separated using vacuum filtration and solid samples were obtained by freeze drying. The freeze dried complexes were investigated using FTIR spectroscopy.

3.3.4 Adsorption of beta-blocker, propranolol onto $Fe_3O_4/SiO_2/CMCD$ MNPs

3.3.4.1 Adsorption experiments

The adsorption of beta-blocker, propranolol was investigated using a batch equilibrium mode by adding 60 mg of wet $Fe_3O_4/SiO_2/CMCD$ MNPs into 4 mL of propranolol hydrochloride solutions with different concentrations (10– 50 ppm) at pH 7 and 25°C. Samples for equilibrium adsorption studies were prepared in de-ionized water. The solution pH was adjusted by 0.01M NaOH or 0.01M HCl. After preparation of propranolol solution, samples were stirred by a horizontal laboratory shaker at 230 rpm and after the equilibrium was reached, the MNPs were removed by magnetic decantation from the solution before measurements. Some initial kinetic studies were done and it showed that adsorption reached equilibrium within 1 hr. The residual

concentrations of propranolol hydrochloride in solutions were determined by Shimadzu UV–visible spectrophotometer (Model 1800) and absorbance values were recorded at 289 nm. The amounts of solute adsorbed per unit mass of adsorbent were calculated from the differences between the initial and the final solute concentrations in solution before and after adsorption following equation 3-4.

Effect of pH on adsorption of propranolol was examined over the pH range from 3-11 at initial concentration of 50 ppm.

The procedure for kinetic experiments was basically identical to those of equilibrium tests. The solutions mixed with 60 mg of wet magnetic particles were agitated at a speed of 230 rpm at 25°C. At various time intervals, samples were collected after separation of magnetic adsorbents by magnetic decantation and the equilibrium concentration of sorbate were determined as mentioned previously. The amount of propranolol adsorbed onto Fe_3O_4/SiO_2/CMCD MNPs was calculated by a mass balance relationship following equation 3-4.

3.3.4.2 Flurometric experiments

The flurometric titrations using a series of solutions containing propranolol hydrochloride (4.5×10^{-5} mol/L) and varying amounts of CMCD ($0–4.7\times10^{-4}$ mol/L) were carried out in aqueous buffer solution (pH 7) at 25°C with excitation at 283 nm and observation at 343 nm.

3.3.4.3 Desorption studies

Desorption studies of beta-blocker, propranolol was carried out using 50% methanol solution when adsorption was carried out at pH 7 (sodium phosphate buffer solution). To ensure that equilibrium was achieved for adsorption, shaking was done for 5 hrs and the supernatant was separated from the magnetic particles by help of a magnet. Then

the particles were washed using Milli Q water. Magnetic particles containing propranolol was then mixed with 5 mL of 50% methanol solution. After 6 hrs of incubation at 25°C, the supernatant was collected and analyzed in UV-Visible spectrophotometer at 289 nm.

3.4 Analytical Methods

The analytical methods used in this experiment are described in the following sections.

3.4.1 Fourier-transform Infrared (FTIR) Spectroscopy

Fourier Transform Infrared Spectroscopy is a technique that provides information about the chemical bonding or molecular structure of materials, whether organic or inorganic. Structural information of a molecule can be determined using infrared spectroscopy. The vibrational movements e.g., bending, stretching of the various types of bonds (O-H, C=O etc.) correspond to the absorption of certain wavelengths in the infrared region of electromagnetic radiation. Infrared spectroscopy is used more for qualitative than quantitative purposes. The region of the infrared spectrum obtained is usually from 400 to 4000 cm^{-1}. The region of the spectrum below 1500 cm^{-1} is the fingerprint region, in which the bands for each compound are unique. Hence, it is considered that two molecules are identical if they share the same 'Fingerprint' in this region. The region above 1500 cm^{-1} is called the functional group region, where vibrational modes of the functional groups are observed. The Shimadzu Infra-Red spectrometer (Model no. 400) was used to characterize all the synthesized particles at room temperature. A small portion of samples were grinded with approximately 225/230 mg of potassium bromide powder into a smooth, fine powder. This powder was subjected to high pressure and

compressed into a thin pellet. The pellet was placed into the spectrometer and scanned over a broad wavelength ranging from 4000 to 400 cm^{-1}.

3.4.2 Transmission Electron Microscopy (TEM)

Transmission electron microscopy (TEM) is a technique which involves shining a beam from a light source, through an electromagnetic lens which focuses the electrons into a very thin beam, and then finally through an ultra-thin specimen, interacting with the specimen as it passes through. This result in the formation of an image due to the interaction of the electrons transmitted through the specimen. The image is magnified and focused onto an imaging device, such a layer of photographic film, or can be detected by a sensor such as a CCD camera. Characterization of size and morphology of the samples were carried out using transmission electron microscopy. Dilute sample of magnetic nanoparticles were suspended in ethanol and ultrasonicated. Suspension containing the dispersed magnetic particles was thinly coated on copper grids. The copper grids were left to dry for 24 hrs at room temperature and finally the samples were analyzed using Field Emission TEM (JEOL 2011F) machine (at an acceleration voltage of 200 kV).

3.4.3 X-ray Diffraction (XRD) analysis

X-Ray diffraction of samples was measured using Shimadzu XRD 6000 spectrometer (using Cu Kα λ 1.5418 Å radiations). This is a method to determine arrangement of atoms within a crystal in which a beam of X-ray strikes a crystal and diffracts it in many specific directions. From angles and intensities of those diffracted beams, the mean position of atoms in the crystal can be determined which is a characteristic property of the specific compound. Some valuable information like chemical bond, disorder of the structure can also be determined through this analysis. Even, a

crystallographer can produce a three dimensional structure of density of electrons within the crystal structure.

3.4.4 Vibrating Sample Magnetometer (VSM)

The vibrating sample magnetometer has become a widely used instrument for determining magnetic properties of a large variety of materials: diamagnetics, paramagnetics, ferromagnetics, ferromagnetics and antiferromagnetics as a function of magnetic field and temperature. Wet magnetic particles were freeze-dried (Martin Christ freeze-dryer) for 24 hrs and then used for VSM measurement (Lakeshore, model no.665). A plastic cylinder cell containing the sample was attached on a rod in the applied magnetic field from -15,000 to 15,000 Oe, in which the rod was vibrating in a certain rate. The magnetization curve of the magnetic particles at room temperature was then plotted with the changes of magnetic field strength and its direction.

3.4.5 Brunauer-Emmett-Teller (BET) method

The specific surface area was measured by BET analyzer (Model: Quantachrome NOVA 4200e). The Brunauer-Emmett-Teller (BET) theory explains the physical adsorption of gas molecules on a solid surface, which serves as an important basis for the measurement of the specific surface area of a material. Surface cleaning (degassing) of the dried solid magnetic particles were carried out by placing the sample in a glass cell and heating at 120°C under vacuum for 12 hrs before the measurements. Once clean, small amount of gas molecules were admitted in steps into the sample chamber and then stick to the surface of solid particles, which was carrying out in an external bath maintained by liquid nitrogen. As the equilibrium adsorbate pressure approach saturation, surfaces of magnetic particles become completely occupied by adsorbate.

Knowing the density of the adsorbate, it is easy to calculate the specific area of the magnetic particles.

3.4.6 Zeta Potential analysis

The magnitude of the zeta potential gives an indication of the potential stability of the colloidal system. For example, if the particles have low zeta potential, there is no force to prevent the particles coming together and flocculating, whereas if all particles in the suspension have large negative/positive zeta potential, they will tend to repel each other and there is no tendency to flocculate. The zeta potentials of coated magnetic particles and amino acid solution (Trp, Phe and Tyr) at different pHs were measured using Malvern ZEN2600 Zetasizer Nano ZS analyzer. Samples were prepared by diluting 20 mg wet magnetic particles/amino acids in 100mL of 10^{-3} M NaCl solution at different pH adjusted with diluted HNO_3 or NaOH solution.

3.4.7 Thermogravimetric Analysis (TGA)

TGA is a thermal analysis technique used to measure changes in the weight of a sample as a function of temperature/time. The thermogravimetric analysis was performed on a thermal analysis system (Model: TA 2050). For TGA measurements, 12/15 mg of the dried sample was loaded into the system; weight loss of dried sample was monitored under N_2 from room temperature to 800°C at a rate of 10°C/min.

3.4.8 X-ray Photoelectron Spectroscopy (XPS)

The working principle of X-ray photoelectron spectrophotometer is based on having a primary X-ray beam of precisely known energy impinged on sample atoms, inner shell electrons are then ejected and the energy of the ejected electrons is measured. The difference in the energy of the impinging X-ray and the ejected electrons gives the binding energy of the electron to the atom which is used to identify the element

involved. XPS measurements were made on an Axis Ultra DLD (Kratos) spectrometer with Al mono Kα X-ray source (1486.71 eV photons) at a constant retard ratio of 40. The sample was mounted on the standard sample studs by means of double sided adhesive tape. The core-level signals were obtained at a photoelectron take-off angle 90° (with respect to the sample surface). The X-ray source was run at a reduced power of 75W. The pressure in the analysis chamber was maintained at 5×10^{-8} Torr or lower during each measurement. All binding energies (BEs) were referenced to the C1s neutral carbon peak at 284.6 eV.

3.4.9 Fluorescence

Fluorescence is the phenomenon in which absorption of light of a given wavelength by a fluorescent molecule is followed by the emission of light at longer wavelengths. The distribution of wavelength-dependent intensity that causes fluorescence is known as the excitation spectrum, and the distribution of wavelength-dependent intensity of emitted energy is known as emission spectrum. The fluorescence measurements of amino acids and beta-blocker were carried out with fluorescence spectrometer (Quantamaster, GL-3300 & GL-302 laser systems) with a 10-mm path length sample cuvette. The excitation wavelength was set and emission was scanned in the range specific for the samples. The scan rate was 0.25 nm/min^{-1} with a 10 nm bandpass for both excitation and emission.

Chapter 4: Characterization of silica and carboxymethyl-β-cyclodextrin bonded magnetic nanoparticles

4.1 Introduction

The stabilization of the iron oxide particles is crucial to obtain magnetic colloidal ferrofluid that is stable against aggregation in both biological medium and magnetic field. The stability of magnetic colloidal suspension results from the equilibrium between attractive and repulsive forces. Theoretically, four kinds of forces can contribute to the interparticle potential in the system. van der Waals forces induce strong short-range isotropic attractions. The electrostatic repulsive forces can be partially screened by adding salt to the suspension. The theoretical description of these two forces is known as the Derjaguin-Landau-Verwey-Overbeek (DLVO) theory [352]. For magnetic suspensions, magnetic dipolar forces between two particles must be added. These forces induce anisotropic interactions, which are found to be globally attractive if the anisotropic interparticle potential is integrated over all directions. Finally, steric repulsion forces have to be taken into account for non-naked particles [353]. Stabilization of magnetic particles can be achieved by playing on one or both of the two repulsive forces: electrostatic and steric repulsion [354].

The formation of Fe_3O_4 nanoparticles by co-precipitation of ferrous and ferric cations in alkaline condition is a classical method and widely practiced. Generally, long-chain surfactants such as oleic acid, lauric acid, dodecyl phosphonate, hexadecyl phosphonate, and dihexadecyl phosphate are used to stabilize the nanoparticles and disperse them in organic solvents. In the past few years, much work has been done to fabricate magnetic composite particles by encapsulating magnetite nanoparticles with organic polymers through monomer polymerization or by coating magnetite

nanoparticles with inorganic matrixes such as silica and titanium dioxides through a sol-gel approach [355-357]. The sol-gel approach has been frequently employed for coating magnetite nanoparticles with inorganic matrix, especially silica, and proved to be a robust way to fabricate magnetic nanocomposites, because surface of magnetite has strong affinity toward silica. Furthermore, silica coatings provide magnetite nanoparticles with a chemically inert surface, which is especially important in biological applications [358, 105]. Some works have been done to prepare silica-coated magnetite nanoparticles through a sol-gel approach. Wang et al. synthesized magnetite particles by co-precipitation method and directly coated them with silica in a basic alcohol/water mixture [359]. Aliev et al. synthesized silica-coated magnetite particles through a slow sol-gel process using sodium silicate as the silica source [360]. The above methods could lead to silica coated magnetite particles. However, the structure and morphology of resultant composites could not be well controlled because the magnetite nanoparticles were used directly as seeds without any treatment and they can spontaneously aggregate in the liquid reaction systems. In order to synthesize well-dispersed silica coated magnetite nanoparticles with well-defined structures, surface modification of magnetite nanoparticles is needed to increase their dispersing stability in reaction media. Philips et al. synthesized core-shell silica-coated magnetite particles via sol-gel approach by using surfactant stabilized magnetite nanoparticles as seeds [104]. Through an analogous approach, Lu et al. reported the formation of silica on the surface of magnetite nanoparticles stabilized with oleic acid [105]. Although surfactant stabilized magnetic nanoparticles could be used to prepare silica-coated magnetic nanoparticles via sol-gel approach, the coating process is difficult to control because surfactant molecules are easy to desorb from magnetic nanoparticles by alcohol dissolution. Thus, for coating with silica using modified Stöber method, it is necessary

to render the particles well dispersed in polar solvents. So in this work, citric acid was chosen to modify the magnetic particles which allow formation of a stable aqueous dispersion by reducing the aggregation tendency of magnetite and ultimately will lead to obtain well-dispersed core-shell nanoparticle after coating with silica.

Many nanostructural compounds and composites have been constructed by utilizing cyclodextrin (CD) as the surface modifier. Wang et al. utilized α-CD as an inclusion host to modify the surface of oleic acid-coated magnetite nanoparticles to "pull" them from hydrophobic solvents to aqueous phase [152]. Hou et al. and Xia et al. used a similar inclusion complex mechanism to form spherical magnetite aggregates with controllable size by changing the concentration of β-CD [158, 160]. Moreover, CD was also used to coat magnetite nanoparticles as a surfactant to make the particles more biocompatible [361]. Fan et al. used β-cyclodextrin bonded silica as the sorbent for on-line SPE-HPLC analysis of 4-nitrophenol from water samples [362]. However, little or no work has been done so far using cyclodextrin bonded magnetic nanoparticles to separate chiral biomolecules or beta-blockers to our knowledge. Benefit of using cyclodextrin bonded magnetic silica particles is tributed by the combined properties of the particles such as magnetic properties of Fe_3O_4, biocompatibility of silica shell and chiral recognition properties of cyclodextrin.

In this work, novel nano-adsorbents were prepared using surface modified Fe_3O_4 as the core and silica and cyclodextrin derivatives as the shell. Surface of magnetic silica nanoparticles is modified by grafting with carboxymethyl-β-cyclodextrin (CMCD) via carbodiimide activation. The size, structure, and magnetic properties of the resultant magnetic nanoparticles were characterized by TEM, XRD, and VSM. Moreover,

binding of silica and cyclodextrin derivative to the magnetic nanoparticles was confirmed by FTIR and XPS.

4.2 Results and discussion

4.2.1 Characterization of silica and CMCD coated magnetic nanoparticle

4.2.1.1 FTIR spectroscopy

The FTIR spectra of bare MNPs, CMPs, Fe_3O_4/SiO_2 MNPs and $Fe_3O_4/SiO_2/CMCD$ MNPs are presented in Figure 4-1. It is shown that the characteristic absorption band of Fe–O bonds in the tetrahedral sites of bare magnetic nanoparticles is 586 cm^{-1}. The broad band at 3300-3500 cm^{-1} is due to –OH stretching vibrations. Compared to the bare magnetite nanoparticles (Figure 4-1(a)), two new absorption peaks at 1631 and 1392 cm^{-1} appear in the FTIR spectra of citric acid treated magnetite nanoparticles (Figure 4-1(b)), which are characteristics of the carboxylate [363]. The existence of the characteristic Si-O-Si stretching at 1091 and 1087 cm^{-1} on Fe_3O_4/SiO_2 MNPs (Figure 4-1(c)) and $Fe_3O_4/SiO_2/CMCD$ MNPs (Figure 4-1(d)) respectively, are evidences to confirm the formation of the silica shell [344]. In the spectra of Fe_3O_4/SiO_2 MNPs and $Fe_3O_4/SiO_2/CMCD$ MNPs, other characteristic absorption bands such as Si–OH stretching, Si–O bending and Si–O–Si bending, are shown at 960, 794, 464 cm^{-1} and at 958, 794, and 459 cm^{-1}, respectively [164]. Characteristic Fe-O peak of bare MNPs at 586 cm^{-1} is shifted to 578 and 576 cm^{-1} in the spectrum of Fe_3O_4/SiO_2 MNPs and $Fe_3O_4/SiO_2/CMCD$ MNPs, respectively. Thus, undoubtedly it can be said that the silica shell is linked to the surface of the magnetic nanoparticles by Fe-O-Si chemical bond [344]. In the spectrum for $Fe_3O_4/SiO_2/CMCD$ MNPs (in Figure 4-1(d)), the most important asymmetric and symmetric C-H stretching bands are found at 2854 and 2924 cm^{-1} respectively, which prove successful grafting of CMCD on silica coated magnetic particles and the characteristic peaks of CMCD in the region of 900-1200 cm^{-1} might

have overlapped with the broad and strong peak due to silica coating. The two other main characteristic peaks are observed at 1623 and 1400 cm^{-1} due to bands of COOM (M represents metal ions) groups, which indicate that the COOH groups of CMCD reacted with the surface OH groups of Fe$_3$O$_4$/SiO$_2$ MNPs resulting in the formation of the silica carboxylate [364]. Therefore, the above results indicate that the magnetic particles are successfully coated by silica and CMCD which was further evidenced by XPS. In the spectrum of Fe$_3$O$_4$/SiO$_2$ MNPs, a short band is observed at 3168 cm^{-1} while in the spectrum of Fe$_3$O$_4$/SiO$_2$/CMCD MNPs this band is absent, rather a broad band is seen which indicates the presence of O-H groups (originated from hydroxyl groups of CMCD) on the surface of the particles.
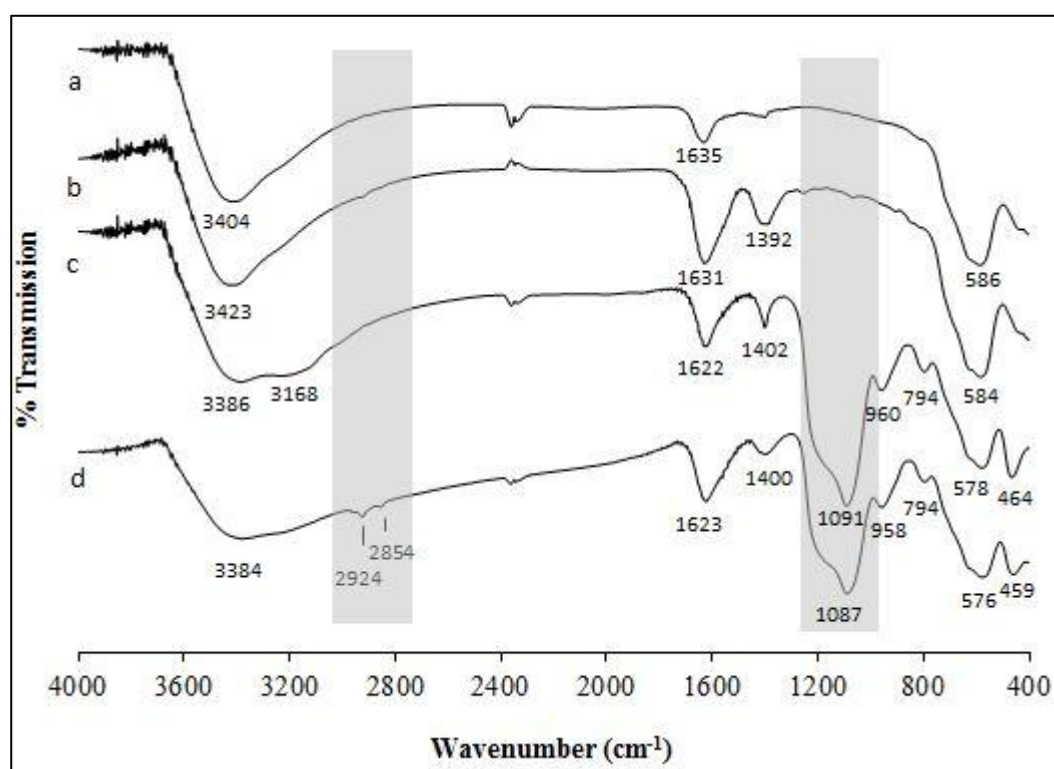
Figure 4-1 FTIR spectra of (a) bare MNPs, (b) CMPs, (c) Fe$_3$O$_4$/SiO$_2$ MNPs, (d) Fe$_3$O$_4$/SiO$_2$/CMCD MNPs.

4.2.1.2 TEM images and surface area measurements

TEM images and size distributions of bare MNPs, CMPs and $Fe_3O_4/SiO_2/CMCD$ MNPs are presented in Figure 4-2. From Figure 4-2(a) and Figure 4-2(b), it is clear that the synthesized bare nanoparticles and CMPs are well dispersed, but also in some areas bigger structures with non-spherical morphology are observed, more likely resulting from aggregation/ coalescence of individual nanoparticles which is also evident from other research works [365]. The average size of bare nanoparticles and CMPs are about 11 nm and 12 nm correspondingly. Figure 4-2(c) depicts the TEM image and corresponding size distribution of $Fe_3O_4/SiO_2/CMCD$ MNPs. Images of bare and coated MNPs were taken using HRTEM machine and afterwards, size of at least 100 particles from different areas were measured and average size of the particles were calculated using following equation:

$$d_i' = \frac{\sum(d_i \times n_i)}{\sum n_i}$$

$\qquad$ where, $\qquad n_i$ = No. of particles within the same size range

$\qquad\qquad\qquad d_i$ = Particle diameter of the same size range

$\qquad\qquad\qquad d_i{}'$ = Average particle size

It can be clearly seen that these magnetite silica nanoparticles are nearly all in core-shell structures with dark core of magnetite and grey porous silica shell. These nanoparticles have also been observed as well-shaped spherical or ellipsoidal. The average diameter of the $Fe_3O_4/SiO_2/CMCD$ MNPs is around 29 nm (thickness of silica layer ~9 nm). However, the thickness of silica shell of the Fe_3O_4/SiO_2 particles can be conveniently adjusted by controlling the addition amount of silica source (TEOS) through the seeded sol-gel approach. No detectable layer due to CMCD can be observed on the surface of magnetite silica nanoparticles.
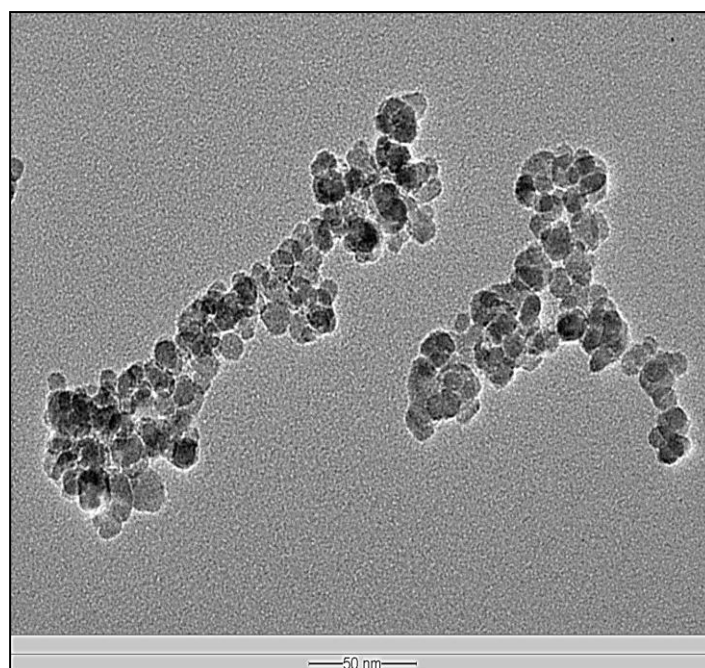
(a)
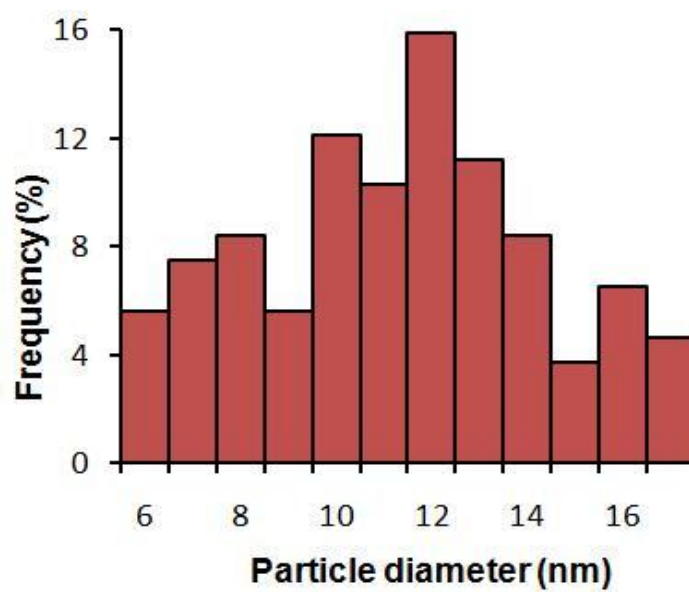
(b)

Figure 4-2 (a) TEM image and (b) size distribution of bare MNPs (scale bar is 50 nm).
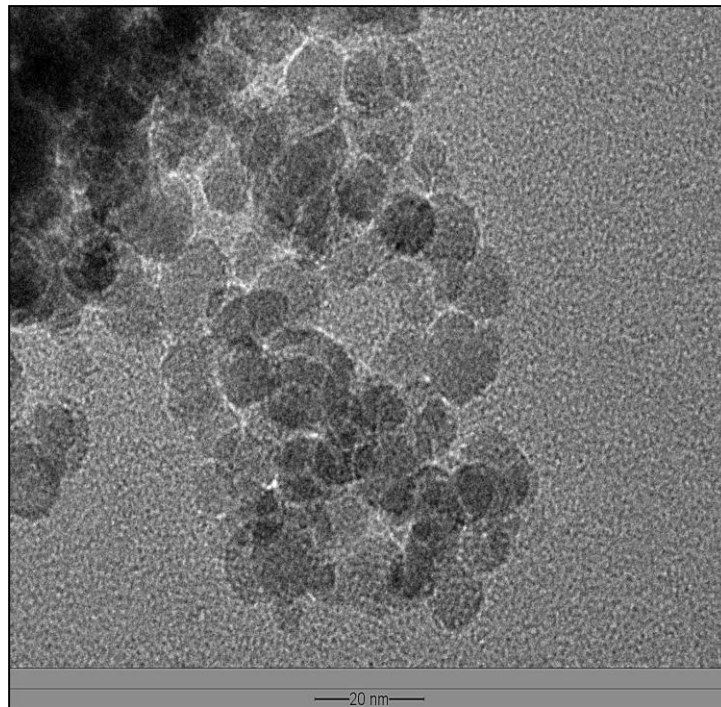
(c)
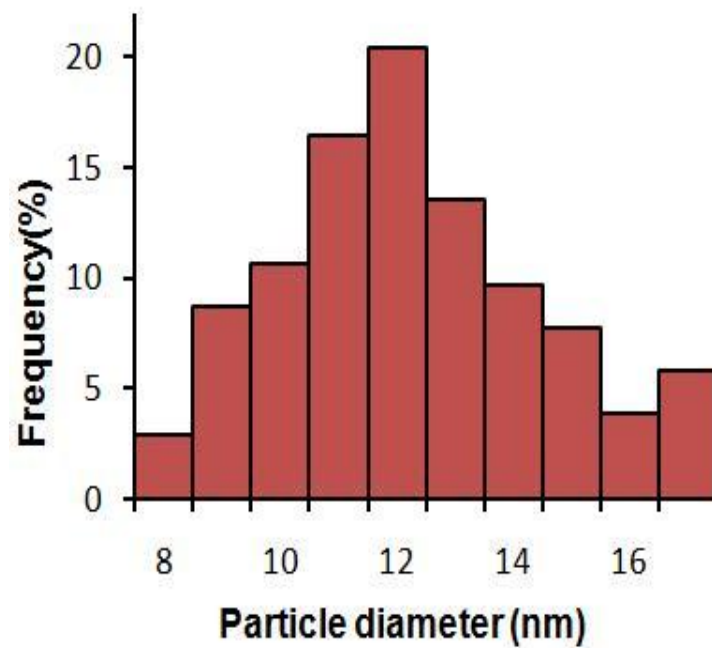
(d)

Figure 4-2 (c) TEM image and (d) size distribution of CMPs (scale bar is 20 nm).
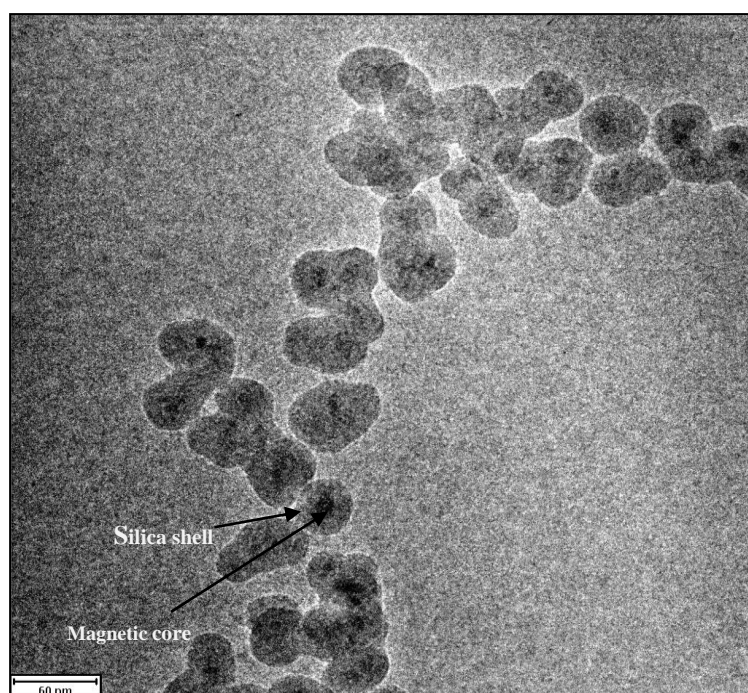
(e)
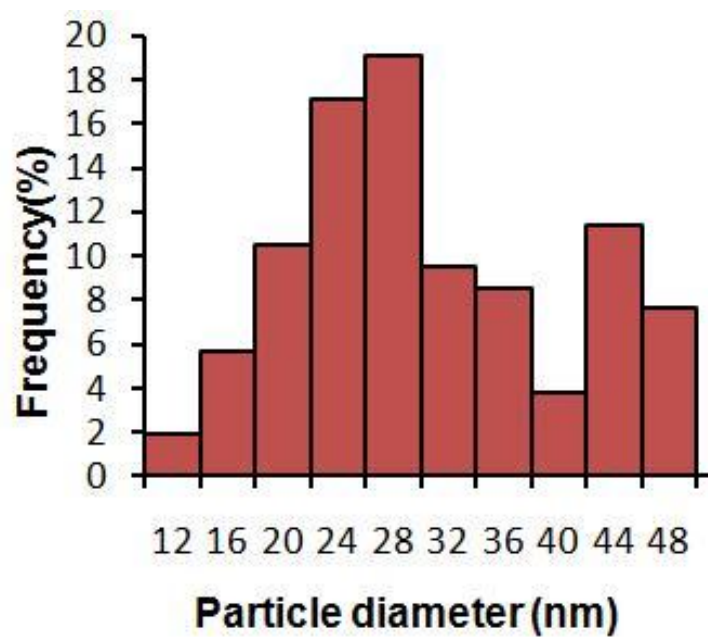
(f)

Figure 4-2 (e) TEM image and (f) size distribution of $Fe_3O_4/SiO_2/CMCD$ MNPs (scale bar is 60 nm).

The specific surface areas of the magnetic nanoparticles' were calculated based on standard Brunauer-Emmett-Teller (BET) method. The BET surface area of bare and $Fe_3O_4/SiO_2/CMCD$ MNPs are 105 and 74 m^2/g, respectively. As compared with bare MNPs, $Fe_3O_4/SiO_2/CMCD$ MNPs exhibit smaller BET surface area. The decrease of surface area could be ascribed to the presence of silica shell and CMCD on the particle surface.

4.2.1.3 X-ray Diffraction analysis

Figure 4-3 shows XRD patterns of the prepared CMPs, Fe_3O_4/SiO_2 MNPs and $Fe_3O_4/SiO_2/CMCD$ core-shell nanoparticles. The XRD patterns of the synthesized particles show five characteristic peaks at $2\theta = 30.22°$, $35.56°$, $43.08°$, $57.48°$, $63.08°$ related to their corresponding indices (220), (311), (400), (511) and (440), respectively. These data describe that resultant nanoparticles are pure Fe_3O_4 with spinel structure [349]. So, the coating process did not induce any phase change of Fe_3O_4. Average crystal size of the nanoparticles is calculated from the most intense peak, corresponding to the indice (311) according to the Debye–Scherrer's formula, [$D = 0.9\lambda/(\beta\cos\theta)$, where β expresses the half width of XRD diffraction lines and λ is the X-ray wavelength (0.154 nm) and θ is the half diffraction angle of 2θ]. For CMPs, the average crystal size is found to be 11.5 nm, slightly less than that measured from the TEM image. After coating with silica and CMCD, intensities of the corresponding diffraction peaks for magnetic nanoparticles shown in Figure 4-3 are reduced because of the layer of silica and CMCD on the particle surface. Also, the presence of mesoporous silica oxide shell is evident from the broader hump in between $2\theta=20°$ to $25°$ [366].
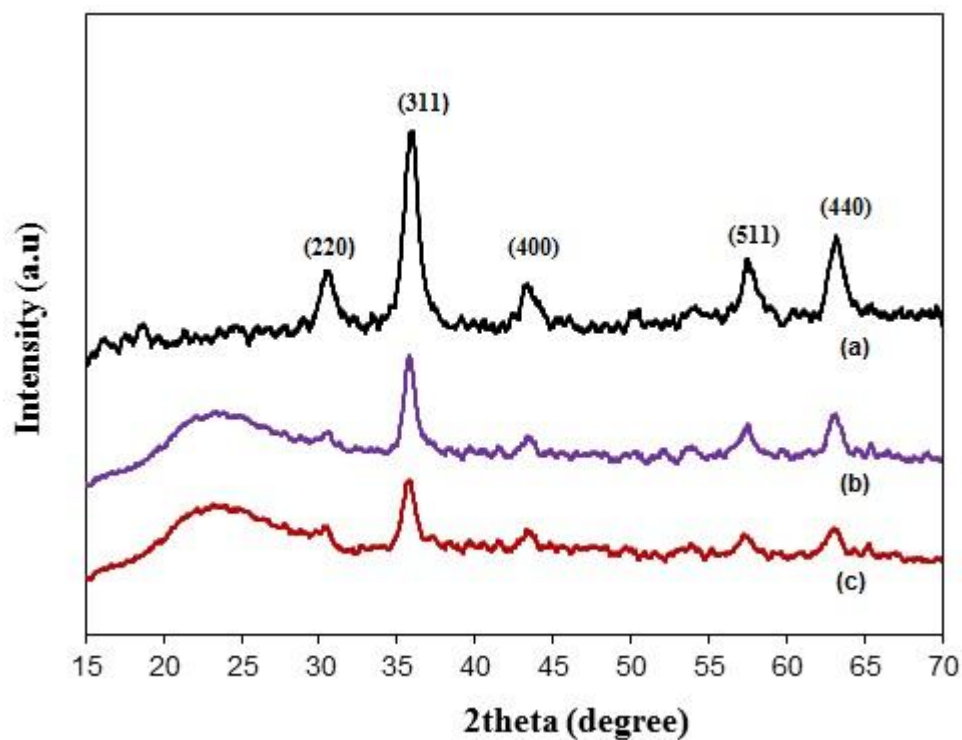
Figure 4-3 XRD patterns of (a) CMPs, (b) Fe_3O_4/SiO_2 MNPs, (c) $Fe_3O_4/SiO_2/CMCD$ MNPs.

4.2.1.4 XPS results

In order to concretely study the combination of magnetic particle cores and silica and CMCD shells of core–shell structured materials, x-ray photoelectron spectra (XPS) of samples are analyzed. Figure 4-4 presents the XPS wide spectra of (a) CMPs, (b) Fe_3O_4/SiO_2 MNPs, (c) $Fe_3O_4/SiO_2/CMCD$ MNPs. The wide scan spectrum shows the Fe2p, O1s, C1s, Si2p peaks of magnetic particles at around 709, 529, 284 and 102 eV.
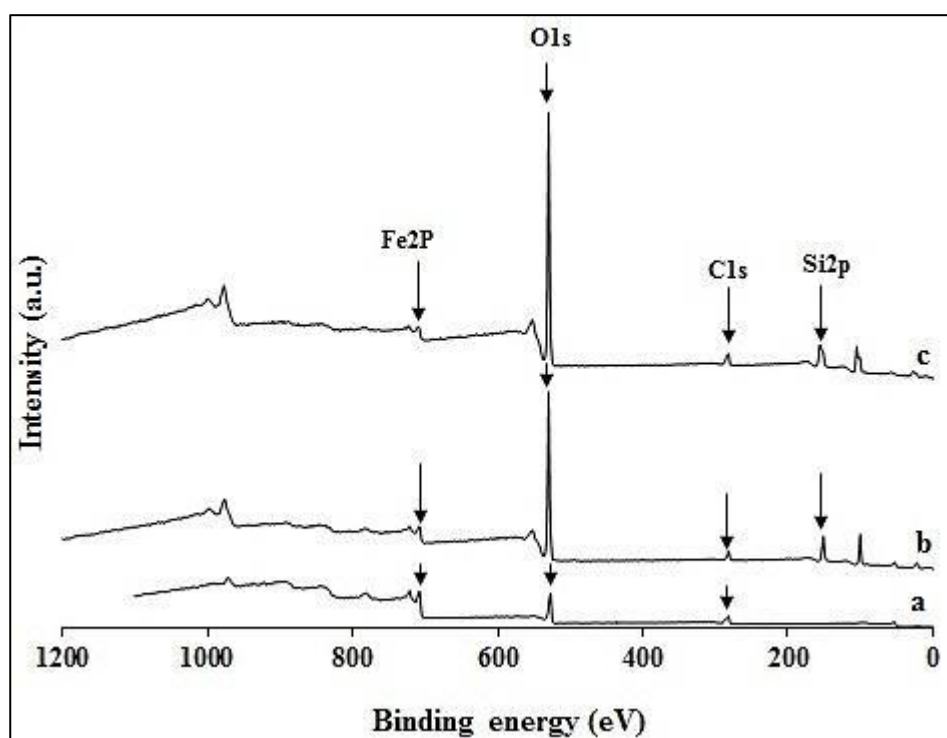
Figure 4-4 XPS wide scan spectra of (a) CMPs, (b) Fe_3O_4/SiO_2 MNPs, (c) $Fe_3O_4/SiO_2/CMCD$ MNPs.

From Figure 4-4(b), the peak of Si2p (100.75eV) can be seen on Fe_3O_4/SiO_2 MNPs core–shell structure materials, which comes from the silica coating. As depicted from Figure 4-5(b), the binding energy of O1s of CMPs is 527.25 eV, which is in agreement with previously reported values [344]. This value is of Fe_3O_4/SiO_2 MNPs is less by 3 eV compared to CMPs (Figure 4-5(b)). The formation of Fe–O–Si bond on the surface of the particles makes the electronic density of O combined with Fe decrease, so the binding energy of O1s for a core–shell particle has a chemical shift of 3 eV.
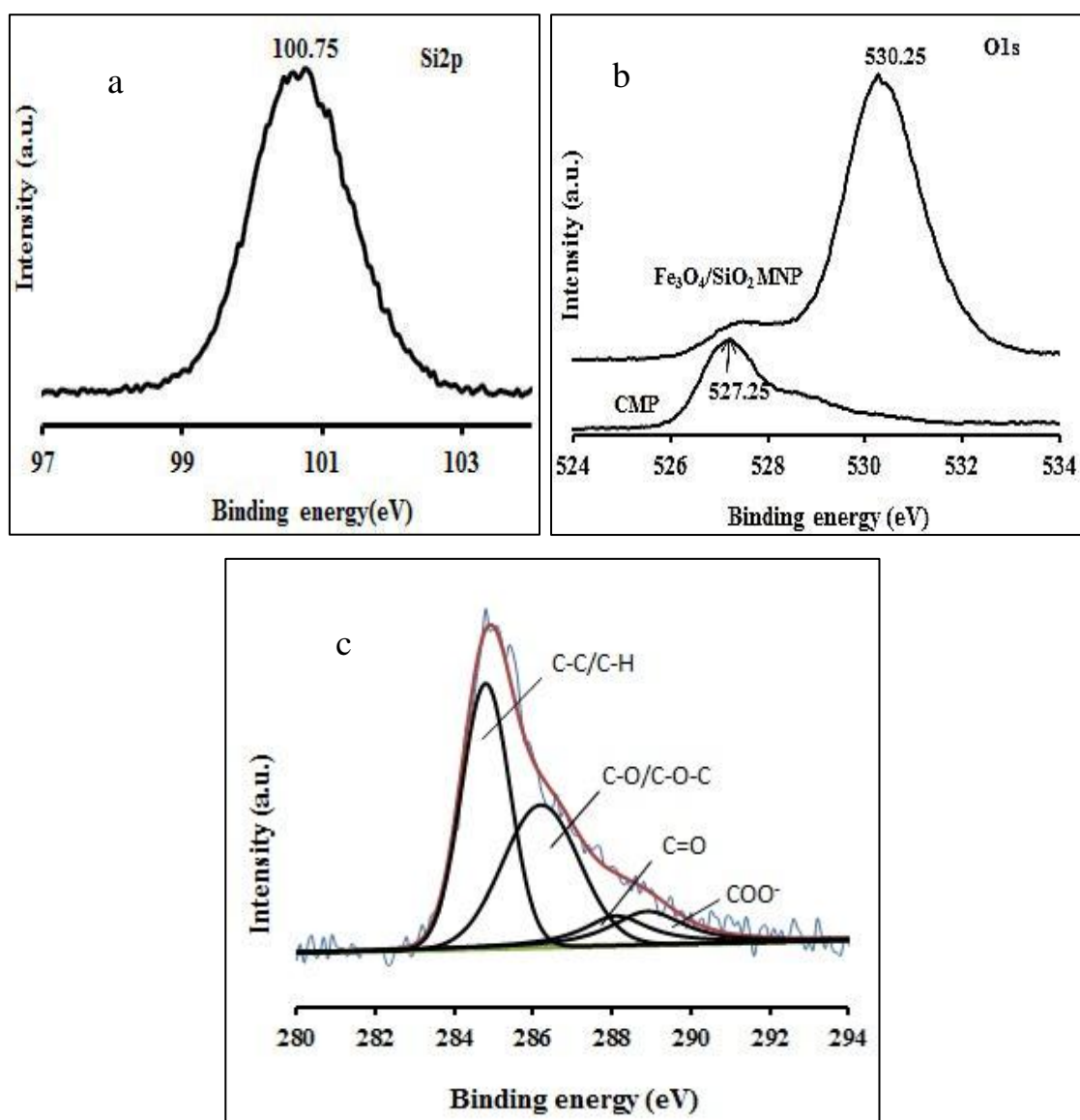
Figure 4-5 XPS wide scan spectra of (a) Si2p of Fe_3O_4/SiO_2 MNPs, (b) O1s of CMPs and Fe_3O_4/SiO_2 MNPs, (c) C1s spectrum of $Fe_3O_4/SiO_2/CMCD$ MNPs.

XPS analysis was also applied to find the chemical binding in the synthesized $Fe_3O_4/SiO_2/CMCD$ MNPs. The C1s deconvoluted spectrum is shown in Figure 4-5 (c). The C1s spectrum can be curve-fitted into four peak components with binding energy of about 284.6, 286, 287.9 and 288.7 eV, attributable to C–C (aromatic)/C–H, C–O/ C–O–C (alcoholic hydroxyl and ether), C=O (carbonyl) and COO^- (carboxyl) species, respectively [164]. The C–O/C–O–C and C=O peaks are the characteristics of CMCD. Moreover, the presence of COO^- peak at 288.7 eV indicates that the COOH functional

groups on CMCD reacted with surface OH groups to from metal carboxylate (COOM). Thus, the modification of magnetic silica surface with CMCD was confirmed.

4.2.1.5 VSM results

The diagram of magnetization verses magnetic field (M-H loop) at 25 °C for bare MNPs and $Fe_3O_4/SiO_2/CMCD$ MNPs are depicted in Figure 4-6. This figure shows almost zero coercivity and no residual magnetism, which proves the superparamagnetic properties of the synthesized magnetic nanoparticles. Superparamagnetic particles do not have permanent magnetic moments in the absence of an external field but can respond to an external magnetic field. The saturation magnetization of bare MNPs was found to be 75.7 emu/g which is much lower than its bulk counter parts (92 emu/g) [367]. It is well known that the energy of magnetic particles in an external field is proportional to their size via the number of magnetic molecules in a single magnetic domain. When this energy becomes comparable to the thermal energy, thermal fluctuations significantly reduce the total magnetic moments at a given field [368]. This phenomenon is more important for the nanoparticles due to their large surface area to volume ratio. Therefore, the smaller saturation magnetization value for the nanoparticles compared to the bulk materials is reasonable. The saturation magnetization of $Fe_3O_4/SiO_2/CMCD$ MNPs was 45 emu/g of particles, which is lower than that of bare magnetic nanoparticles. This might result from binding of silica and CMCD on the particle surface, which might have quenched the magnetic moment [369]. In addition, magnetic molecules on the surface have deficiency of complete coordination and thus increase the surface spin disorientation [368]. This disordered structure in the amorphous materials and at the interface might have caused a decrease in the effective magnetic moment.
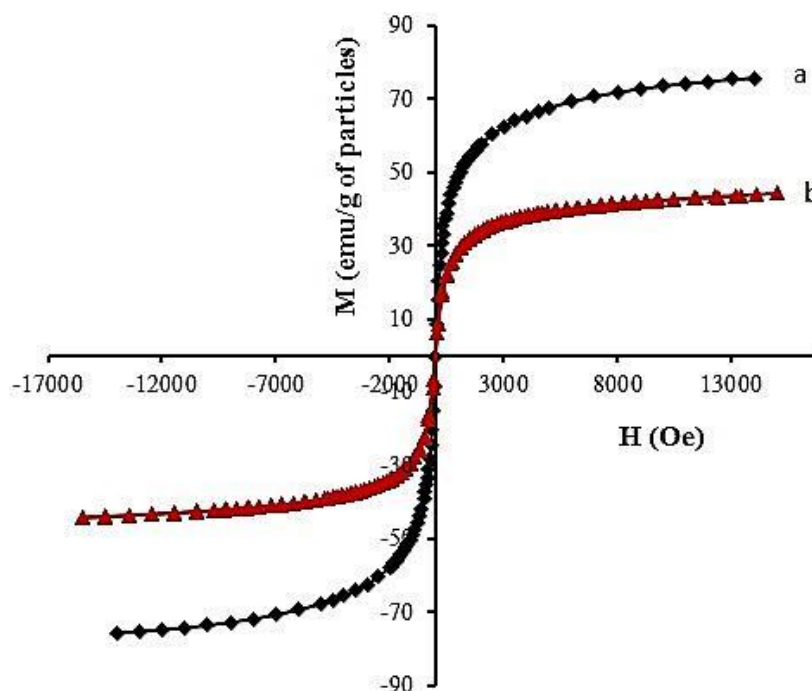
Figure 4-6 Magnetization vs magnetic field curves for (a) bare MNPs and (b) $Fe_3O_4/SiO_2/CMCD$ MNPs obtained by VSM at 25°C.

4.2.1.6 Zeta potential measurement

The magnitude of the zeta potential gives an indication of the potential stability of colloidal system. Measurement of zeta potential of bare and coated magnetic nanoparticles is very important to understand the interaction of the particles with target molecules. In this work, zeta potential of bare, Fe_3O_4/SiO_2 MNPs and $Fe_3O_4/SiO_2/CMCD$ MNPs were first measured in a wide range of pH i.e. pH 2-11. The pH value of isoelectric point (pI) of silica particles synthesized by stöber method was reported as 3 [370]. Figure 4-7 represents the zeta potential of the magnetic particles. As shown in Figure 4-7, the pH value of isoelectric point (pI) of uncoated Fe_3O_4 nanoparticles is about 6.8, consistent with the values reported in literature. After being grafted with silica and CMCD, the pI has been shifted to 2.45 and 2.86, respectively indicating that the grafting of silica and CMCD onto uncoated MNPs is successful. Moreover, magnetic nanoparticles modified with silica and CMCD yields acidic surface

since pI is lower than that of uncoated MNPs and this surface acidity is due to the introduction of several oxygen-containing functional groups [371].
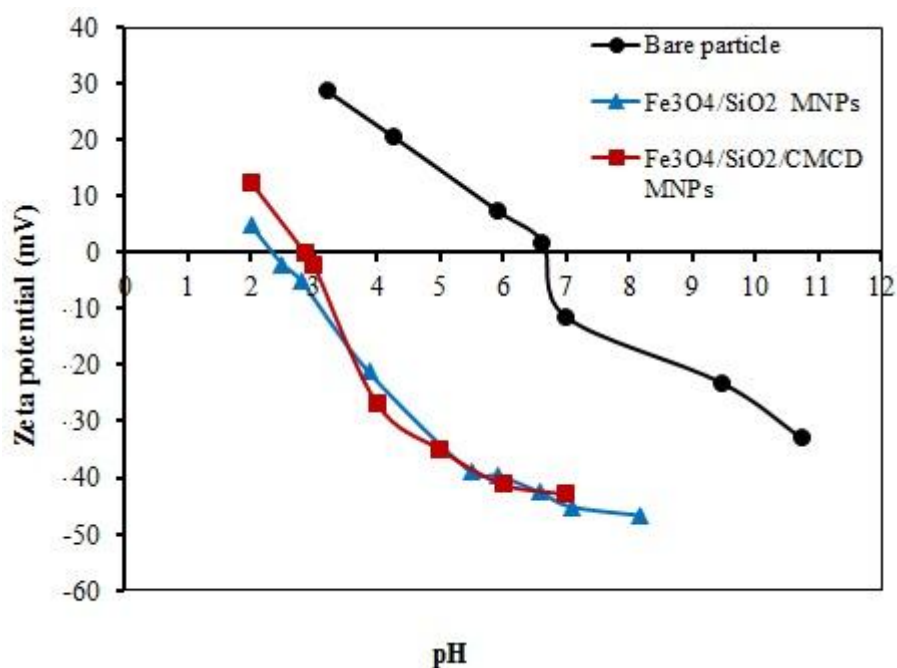
Figure 4-7 Zeta potential of bare MNPs, Fe_3O_4/SiO_2 MNPs and $Fe_3O_4/SiO_2/CMCD$ MNPs (20mg/100mL) in 10^{-3} NaCl solution at different pH.

4.3 Conclusions

Bare iron oxide magnetic nanoparticles were prepared by chemical co-precipitation method and surface of the magnetic particles underwent subsequent modification with silica and CMCD through modified Stöber method and carbodiimide activation method, respectively. The particles were characterized using Transmission Electron Microscopy (TEM), X-ray Diffractometer (XRD) and Vibrating Sample Magnetometer (VSM). The results showed that the $Fe_3O_4/SiO_2/CMCD$ MNPs are of nanometer size with a mean diameter of 29 nm and have superparamagnetic properties. FTIR Spectroscopy, XPS and zeta potential measurements proved the attachment of silica and CMCD on the particle surface. These surface functionalized magnetic nanoparticles can be used as a tool for the separation of chiral amino acids and beta-blocker.

Chapter 5: Adsorption/desorption of chiral aromatic amino acids onto carboxymethyl-β-cyclodextrin bonded Fe₃O₄/SiO₂ core-shell nanoparticles

5.1 Introduction

In Chapter 4, preparation and characterization of silica and carboxymethyl-β-cyclodextrin bonded magnetic nanoparticles have been presented in details. With respect to practical applications and implications, adsorption of chiral amino acids is very much relevant. Chiral amino acids are one of the most important biomolecules because of their relevance in nature and their chemical richness. Enantiomers of chiral amino acids are generally represented as L- or D-enantiomer. It is well known that in nature amino acids occur in L-forms and they play important role in the food and pharmaceutical industries. D-forms were discovered in species of lower animals, mammalian organs and blood [372]. Some of D-amino acids were also detected in various vegetables and fruits. 0.6-3.8% of D-alanine was found in freshly pressed plant juices [373]. In the field of neuroscience, Okuma and Abe found significant amounts of the D-amino acids in the nerve tissues and eyes of crustaceans [374] and Nagata et al. found D-serine in mouse and rat in different regions of brain [375]. Furthermore, D-amino acid was also found in peripheral organs of mice [376]. It has been recognized that enantiomers have identical physical and chemical properties except for optical rotation. Because of these similarities, chiral discrimination of enantiomers is a very challenging task. Therefore analysis of D-/L-amino acids is of increasing importance in biological science.

In 1999, total market for proteinogenic amino acids was 1.5 million tons, revenue of around €3.5billion. Their use in human nutrition and health covers 40% of market;

animal nutrition sector corresponds to 55%. Consumption of high amount of D-tryptophan causes frequent weight gain and subsequent diseases. L-lysine, L-threonine and L-tryptophan are important additives in modern animal feed. L-glutamic acid, L-phenylalanine, L-aspartic acid are used as additives for foodstuffs. Total content of D-phenylalanine and D-tyrosine were significantly greater in patients suffering from chronic renal failure. Thus, in this work, separation of proteinogenic aromatic amino acids was mainly focused because of their use in modern food additives. This part of the work deals with adsorption separation of chiral aromatic amino acid enantiomers (D-/L-tryptophan, D-/L-phenylalanine and D-/L-tyrosine) utilizing surface functionalized magnetic nanoparticles (Fe$_3$O$_4$/SiO$_2$/CMCD MNPs).

This part of the present work is based on study of adsorption of chiral aromatic amino acid enantiomers' on surface functionalized magnetic nanoparticles. Some researchers studied chiral separation of the complexes formed by native and modified CDs with the pharmaceutical molecules and amino acids. Although there are some studies regarding adsorption of amino acids using several adsorbents (i.e. insoluble cyclodextrin polymer [53], β-cyclodextrin bonded silica particles [52], minerals [377], solid surfaces such as steel [378], gold [379], copper [380] etc.), little or no work has been done so far using cyclodextrin bonded magnetic nanoparticles to separate chiral aromatic amino acid enantiomers to our knowledge. In the present work magnetic nanoparticles were used as adsorbent for detailed adsorption study of chiral aromatic amino acid enantiomers at different conditions of pH and temperature. Desorption of the abovementioned enantiomers was also done in the present work.

5.2 Results and discussion

5.2.1 Adsorption of chiral aromatic amino acid enantiomers

5.2.1.1 Equilibrium study of single amino acid enantiomers

Silica and CMCD coated magnetic nanoparticles were utilized for adsorption of chiral amino acid enantiomers namely, D-/L-tryptophan (Trp), D-/L-phenylalanine (Phe) and D-/L-tyrosine (Tyr). Figure 5-1 represents structures of the amino acid enantiomers used in this work. Since there are dissimilarities in structures of the amino acids; it is expected that it will result in difference in adsorption capacities of the particles towards the six enantiomers [381]. As the solubility of tyrosine is very low, equilibrium studies were carried out at different low initial concentrations (0.25 mM - 2 mM) of D- and L-Trp, D- and L-Phe and D- and L-Tyr under neutral condition (pH 7) and the results are shown in Figure 5-2.
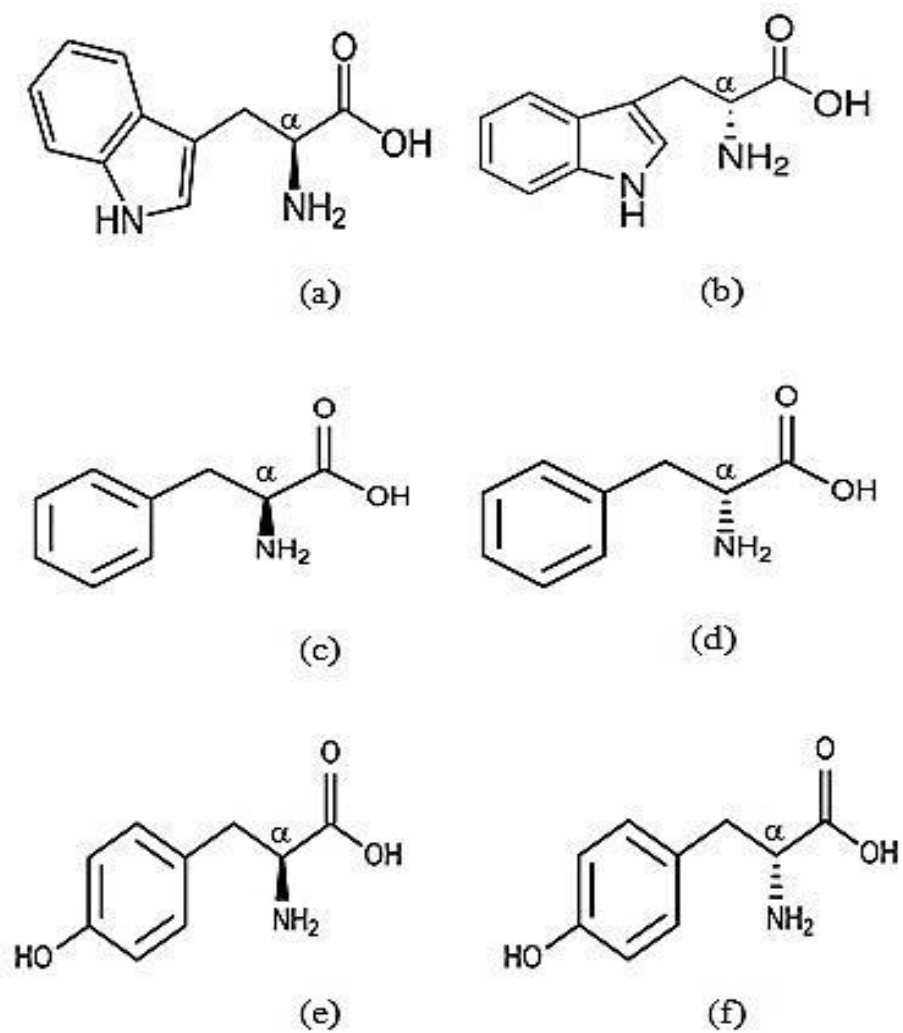
Figure 5-1 Structures of amino acid enantiomers: (a) L-Trp, (b) D-Trp, (c) L-Phe, (d) D-Phe,(e) L-Tyr and (f) D-Tyr.
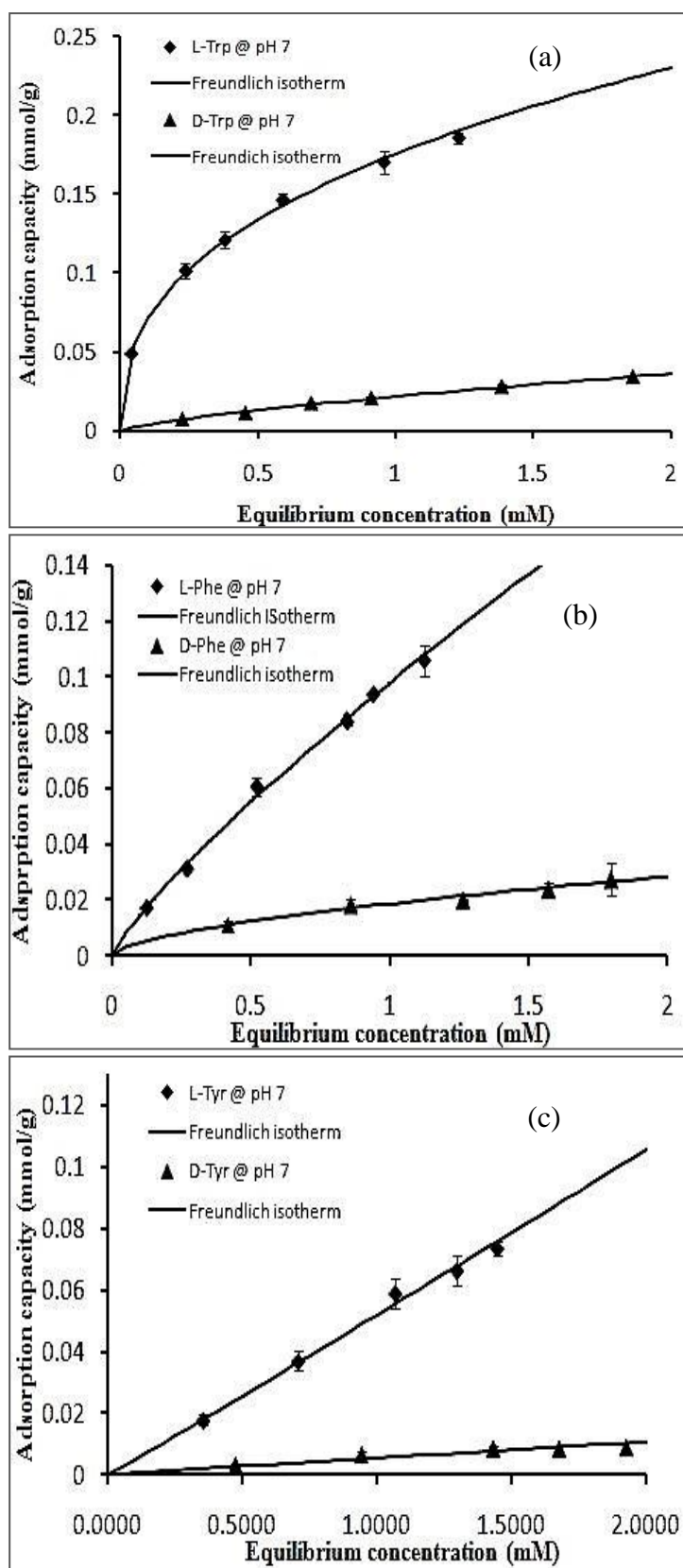
Figure 5-2 Adsorption equilibrium isotherms for: (a) L- and D-Trp, (b) L- and D-Phe, (c) L- and D-Tyr (pH 7 and ionic strength 0.03M).

It can be summarized from Figure 5-2 that maximum equilibrium adsorption capacities of the nano adsorbent were 0.185 mmol/g, 0.034 mmol/g, 0.105 mmol/g, 0.027 mmol/g, 0.073 mmol/g, 0.008 mmol/g for L-Trp, D-Trp, L-Phe, D-Phe, L-Tyr and D-Tyr, respectively at pH 7. The equilibrium adsorption capacities (at maximum equilibrium concentration studied) of $Fe_3O_4/SiO_2/CMCD$ MNPs are higher for the L-enantiomers than the corresponding D-enantiomers.

Based on equilibrium adsorption capacities, it can be stated that $Fe_3O_4/SiO_2/CMCD$ MNPs offer good discrimination (equilibrium discrimination ratio > 1) toward the enantiomers (equilibrium discrimination ratio = equilibrium adsorption capacity for L-amino acid/ equilibrium adsorption capacity for D-amino acid). Armstrong et al. suggested that for chiral recognition of any molecule by β-CD there are a number of prerequisites [381]. For example, to form an inclusion complex, there must be a relatively tight fit between the complexed moiety and β-CD and the chiral center or one substituent of the chiral center must be near and interact with the hydroxyl groups of mouth of the cyclodextrin cavity. Tang et al. showed that difference in structure and hydrophobicity of aromatic amino acid molecules resulted in difference in adsorption on cross-linked β-CD polymer [53]. It can be seen from Figure 5-1 that differences between three dimensional structures of D- and L-enantiomers are in the position of primary amine groups. When these aromatic amino acid enantiomers interact with β-CD, hydrophobic aromatic rings can form inclusion complex to the hydrophobic cavity of β-CD. Hydrophobic interactions are mainly involved in the formation of inclusion complex with cyclodextrin. Furthermore, substituents of the chiral center can interact with hydroxyl groups at the mouth of β-CD and hydrogen bond can be formed. In this case, primary amine group at the chiral center of D-enantiomers might have positioned less favorably for hydrogen bonding, which might have resulted in less adsorption

capacities of the particles toward D-enantiomers. Armstrong et al. studied the inclusion complex formation of Propranolol enantiomers using X-ray crystallography and found that due to less favorable position of the secondary amine group for hydrogen bonding, L-propranolol interacted less with β-cyclodextrin molecule than D-propranolol [381]. Difference in favorability of hydrogen bond formation resulted in selective adsorption between D-/L-enantiomers.

Equilibrium results were better fitted to Freundlich isotherm model. The Freundlich isotherm is expressed using the following equation:

$$Q_e = k_F C_e^{(\frac{1}{n})}$$ [5-1]

Here Q_e is the equilibrium adsorption capacity of the adsorbent (mmol/g), C_e is the equilibrium concentration of the solute being adsorbed (mM), while k_F (L/g) and n are empirical constants dependent on the nature of sorbent and solute and temperature. By taking logarithm of both sides of equation, it can be written as

$$ln\, Q_e = ln\, k_F + \frac{1}{n} ln\, C_e$$ [5-2]

Hence a plot of lnQ_e versus lnC_e should be linear with slope equal to *1/n* and intercept equal to lnk_F.

Parameters of Freundlich model are shown in Table 5-1 and correlation coefficients varying from 0.973 to 0.998 indicate that the adsorption of amino acid enantiomers on the Fe_3O_4/SiO_2/CMCD MNPs was consistent with the Freundlich isotherm equation, which indicates that the adsorption mechanism is a heterogeneous adsorption.

Table 5-1 Parameters of Freundlich equation for adsorption of amino acids at pH 7.

Amino acid	k_F(L/g)	*1/n*	Correlation coefficient, R^2
L-Trp	0.175	0.390	0.998
D-Trp	0.021	0.738	0.993
L-Phe	0.097	0.828	0.997
D-Phe	0.018	0.604	0.973
L-Tyr	0.051	1.022	0.996
D-Tyr	0.005	0.965	0.987

5.2.1.2 Adsorption at different pH

Since Fe_3O_4/SiO_2/CMCD MNPs shows good adsorption capacity towards the single amino acid enantiomers, adsorption characteristics of the magnetic nanoparticles should be explored under different conditions to obtain the optimum condition for maximum adsorption. Furthermore, adsorption studies at different conditions may help to achieve the condition where difference between adsorption capacities toward the D- and L-enantiomers is maximum to facilitate chiral separation of the enantiomers from the racemic mixture. Thus, effect of pH on adsorption of amino acid enantiomers (L-/D-Trp, L-/D-Phe, L-/D-Tyr) on magnetic particles was studied in detail. Isoelectric point (pI) of L-Trp, L-Phe and L-Tyr were determined following the procedure for pI determination of protein molecules [334]. pI of Trp, Phe and Tyr were found to be around 5.9, 5.5 and 5.6, respectively, which are in agreement with values reported in literature and have been shown in Figure 5-3 [382]. The values of zeta potential of Fe_3O_4/SiO_2/CMCD MNPs are 12 mV at pH 2 and -43 mV at pH 7 (Figure 4-7). The larger value of zeta potential may affect the adsorption of amino acids. Thus, solution pH was changed from 4 (below the pI of amino acids) to 5.9/5.5/5.6 (pI of Trp, Phe and Tyr), and finally to 7 (above the pI of amino acids).
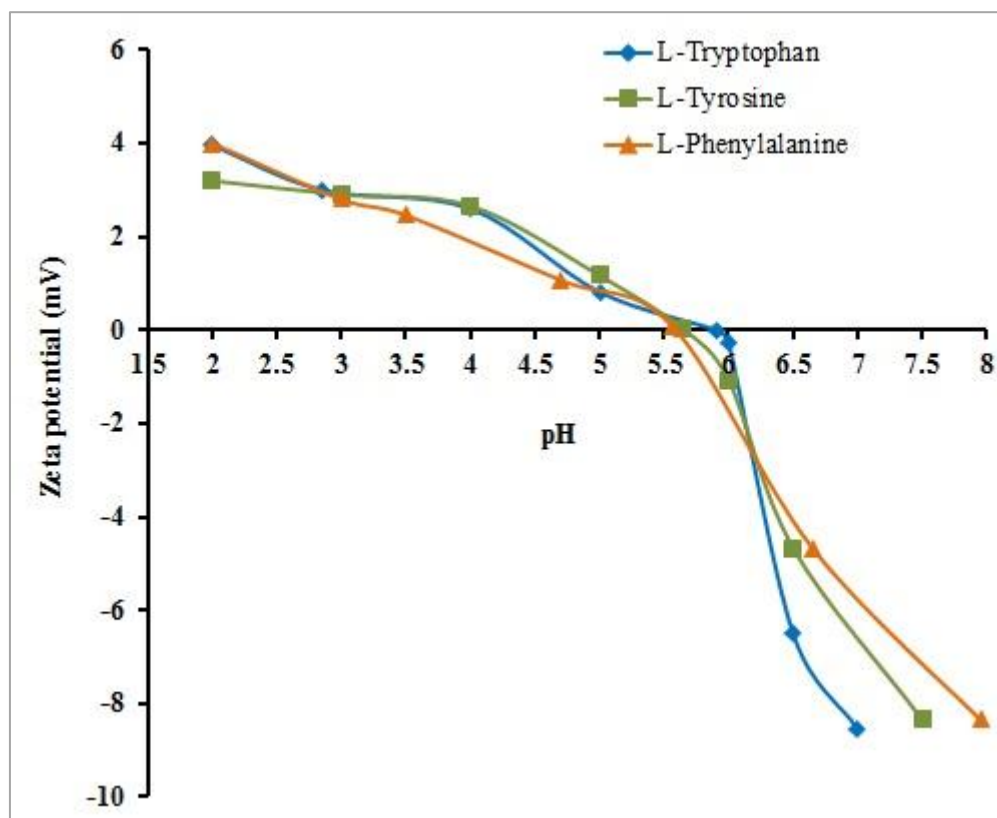
Figure 5-3 Zeta potential of L-Trp, L-Phe and L-Tyr (20mg/100mL) in 10^{-3} M NaCl at different pH.

Adsorption isotherms for the six enantiomers (L- and D-Trp, L- and D-Phe, L- and D-Tyr) at pH 4, 5, 5.9/5.5/5.6 are shown in Figures 5-4, 5-5, 5-6 and corresponding adsorption capacities of the magnetic particles are listed in Table 5-2. Equilibrium results of adsorption studies at different pH were also fitted well to Freundlich isotherm equation and corresponding parameters of Freundlich isotherm equation are listed in Table 5-3. Results of adsorption studies for the six enantiomers at pH 7 are shown in Figure 5-2. It can be observed that pH has some effect on the adsorption of amino acids on the magnetic particle. With the increase of pH from 5.9/5.5/5.6 to 7, adsorption capacities of magnetic particles toward the amino acids decreased significantly. The maximum adsorption of the single amino acid enantiomers occurred at pH 5.9/5.5/5.6 for Trp, Phe and Tyr enantiomers, respectively which is close to isoelectric point of the amino acids. When pH was decreased from 5.9/5.5/5.6 to 4, the adsorbed amount of

amino acid on magnetic particles also decreased. It is known that hydrophobic interaction has major role in amino acid adsorption phenomena [53]. The hydrophobic cavity of CMCD on magnetic nanoparticles offers hydrophobic surface which favours the interaction between coated magnetic particle and amino acid. At the isoelectric point (pI), amino acid molecules had both the NH_3^+ and COO^- groups in the structure (according to the definition of zwitterion) and as the $Fe_3O_4/SiO_2/CMCD$ MNPs were negatively charged at pH 5.9/5.5/5.6, so probably, there were some additional ionic interactions between the amino acids and the nano adsorbents which resulted in maximum adsorption at pI of the amino acids.

Since at pH 4, the magnetic nanoparticles and amino acids were oppositely charged, electrostatic interaction could enhance the adsorption. But, in this case, thermodynamic parameters played major role here, e.g. size, shape and hydrophobicity of the molecule to form inclusion complex [53]. As a result, inclusion complexation was more dominant than electrostatic/ionic interaction and it resulted in better adsorption capacity toward amino acids.
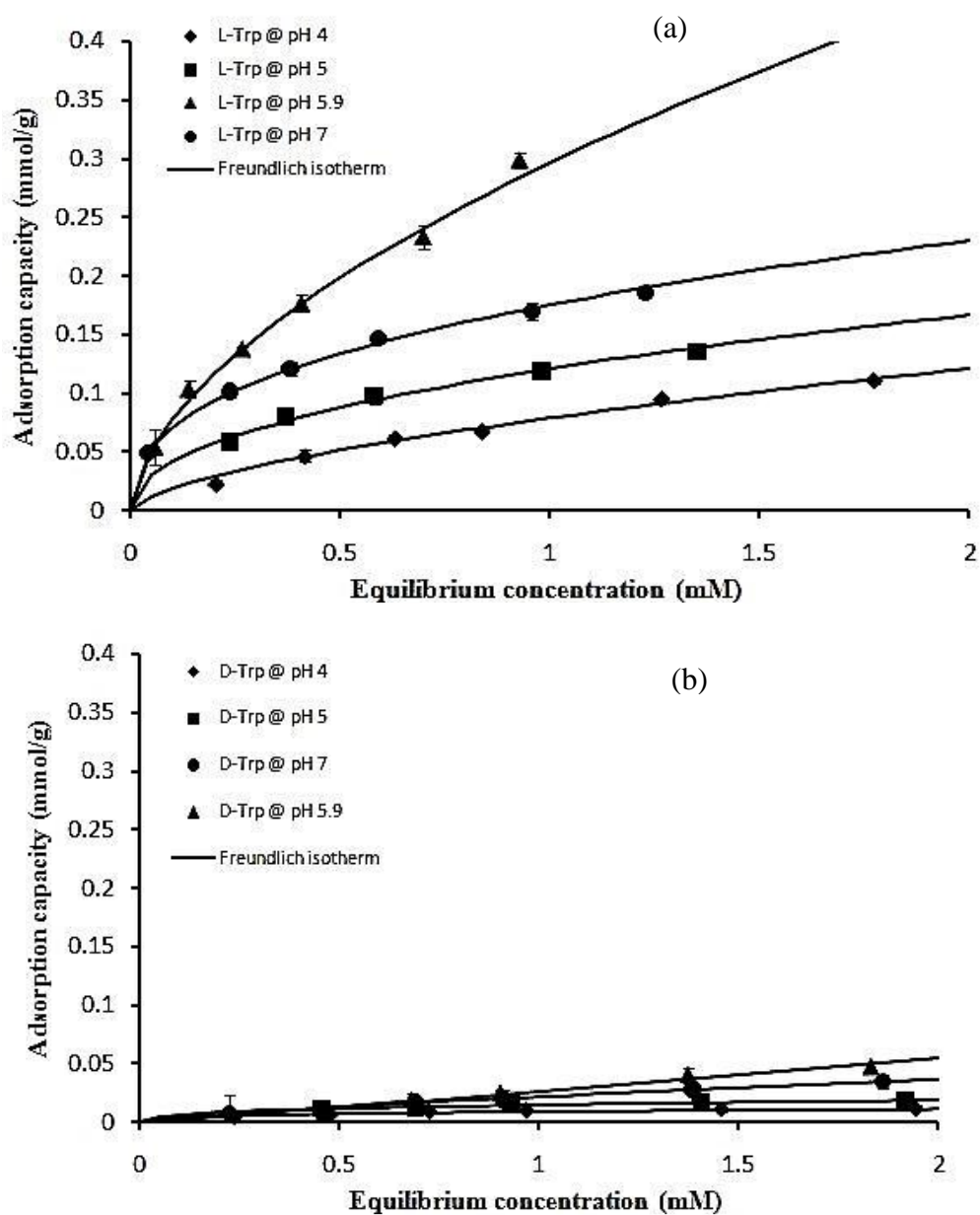
Figure 5-4 Adsorption equilibrium isotherms of (a) L- and (b) D-Trp at pH 4, pH 5, pH 5.9, pH 7 (25°C and ionic strength 0.03M).
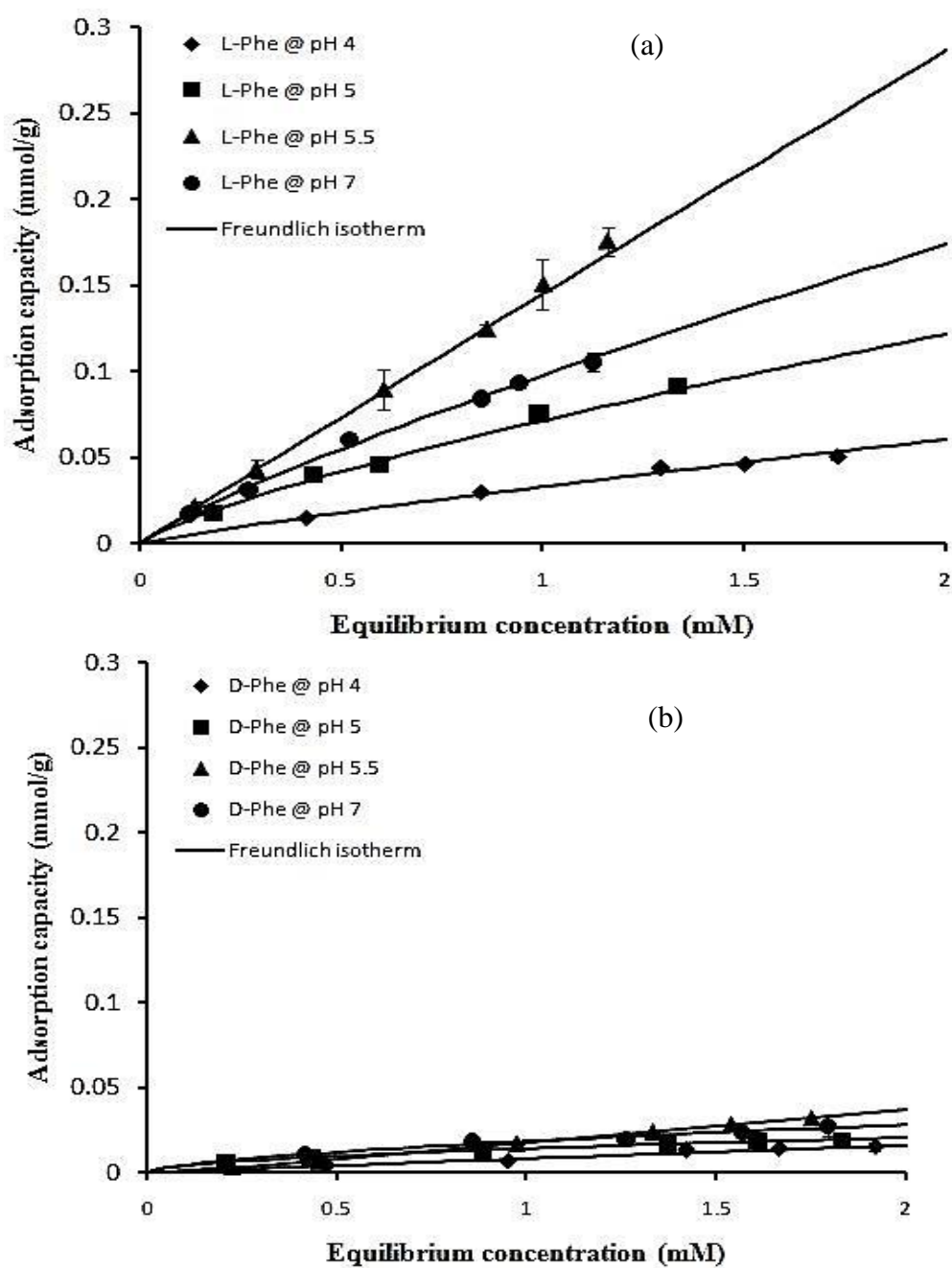
Figure 5-5 Adsorption equilibrium isotherms of (a) L- and (b) D-Phe at pH 4, pH 5, pH 5.5 and pH 7(25°C and ionic strength 0.03M).
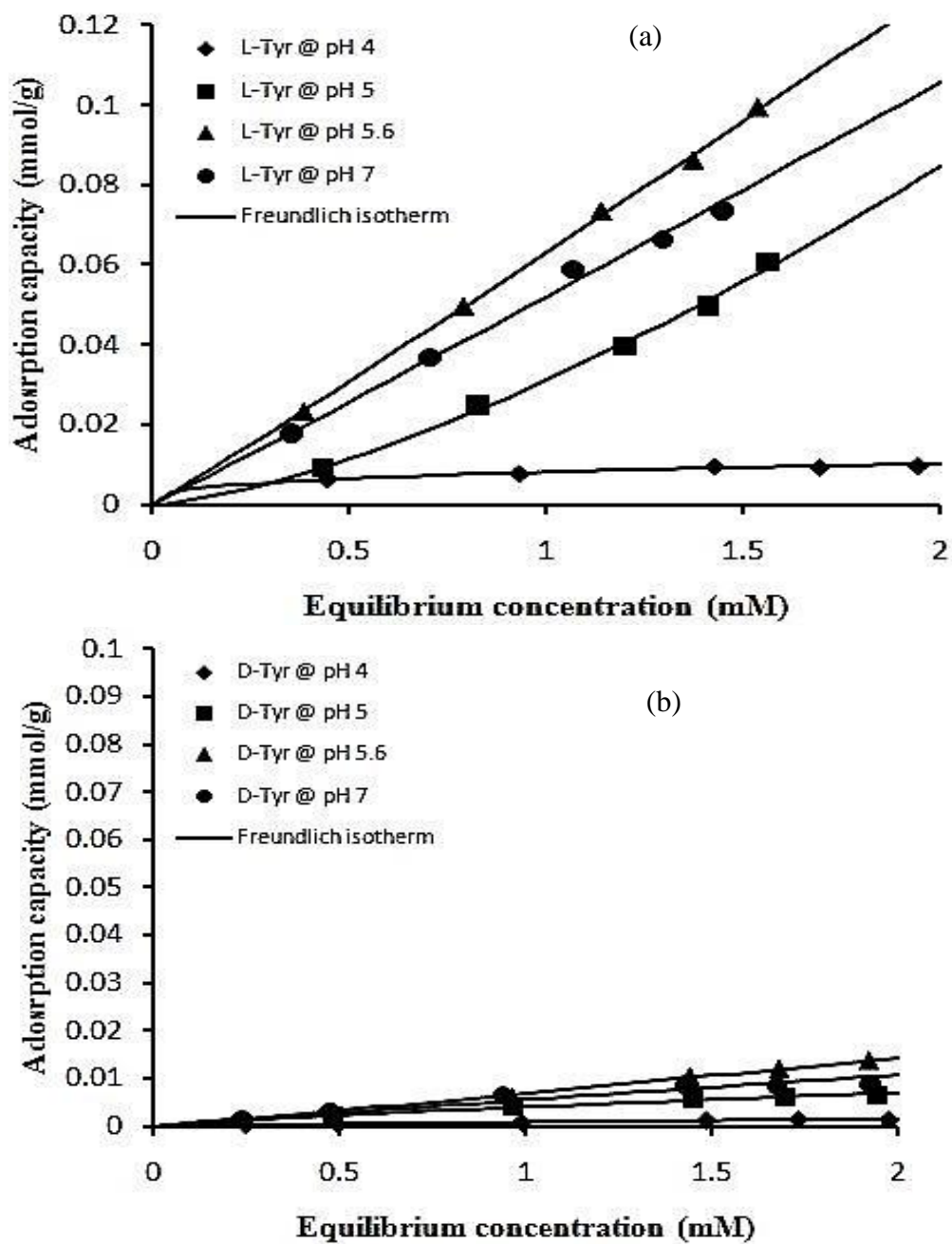
Figure 5-6 Adsorption equilibrium isotherms of (a) L- and (b) D-Tyr at pH 4, pH 5, pH 5.6 and pH 7 (25°C and ionic strength 0.03M).

Table 5-2 Adsorption capacities of magnetic particle towards single enantiomer at different pH.

Amino acid	Adsorption capacity at pH 4 (mmol/g)	Adsorption capacity at pH 5 (mmol/g)	Adsorption capacity at pI* (mmol/g)	Adsorption capacity at pH 7 (mmol/g)
L-Trp	0.110	0.135	0.298	0.185
D-Trp	0.012	0.018	0.046	0.034
L-Phe	0.050	0.091	0.175	0.105
D-Phe	0.015	0.018	0.031	0.027
L-Tyr	0.009	0.060	0.099	0.073
D-Tyr	0.001	0.006	0.013	0.008

(***pI** (isoelectric point) of Trp, Phe and Tyr are 5.9, 5.5 and 5.6, respectively)

Equilibrium results of adsorption studies at different pH are better fitted to Freundlich isotherm model. Parameters of Freundlich model are shown in Table 5-3.

Table 5-3 Parameters of Freundlich isotherm equation at different pH.

Amino acid	pH 4			pH 5			pI		
	k_F	$1/n$	R^2	k_F	$1/n$	R^2	k_F	$1/n$	R^2
L-Trp	0.079	0.614	0.991	0.120	0.463	0.979	0.296	0.579	0.992
D-Trp	0.008	0.320	0.984	0.014	0.342	0.977	0.028	0.857	0.998
L-Phe	0.033	0.871	0.990	0.071	0.768	0.994	0.145	0.980	0.999
D-Phe	0.008	0.965	0.990	0.014	0.532	0.992	0.017	1.117	0.997
L-Tyr	0.008	0.325	0.965	0.031	1.445	0.997	0.063	1.036	0.999
D-Tyr	0.0008	0.908	0.988	0.003	0.813	0.986	0.006	1.072	0.998

As compared, remarkable difference exists between the adsorption capacities of the D- and L-enantiomers of tryptophan, phenylalanine and tyrosine at all the pH (pH 4, pH 5,

pH 5/9/5.5/5.6, pH 7) and this difference becomes more prominent at the pI. Adsorption

capacity differences are 0.251 mmol/g, 0.143 mmol/g and 0.085 mmol/g enantiomers of

tryptophan, phenylalanine and tyrosine, respectively. Based on these results, it can be

mentioned that $Fe_3O_4/SiO_2/CMCD$ MNPs offers good discrimination toward the

enantiomers. Results from effect of pH study are summarized based on difference

between adsorption capacities of L- and D-enantiomer in Figure 5-7.
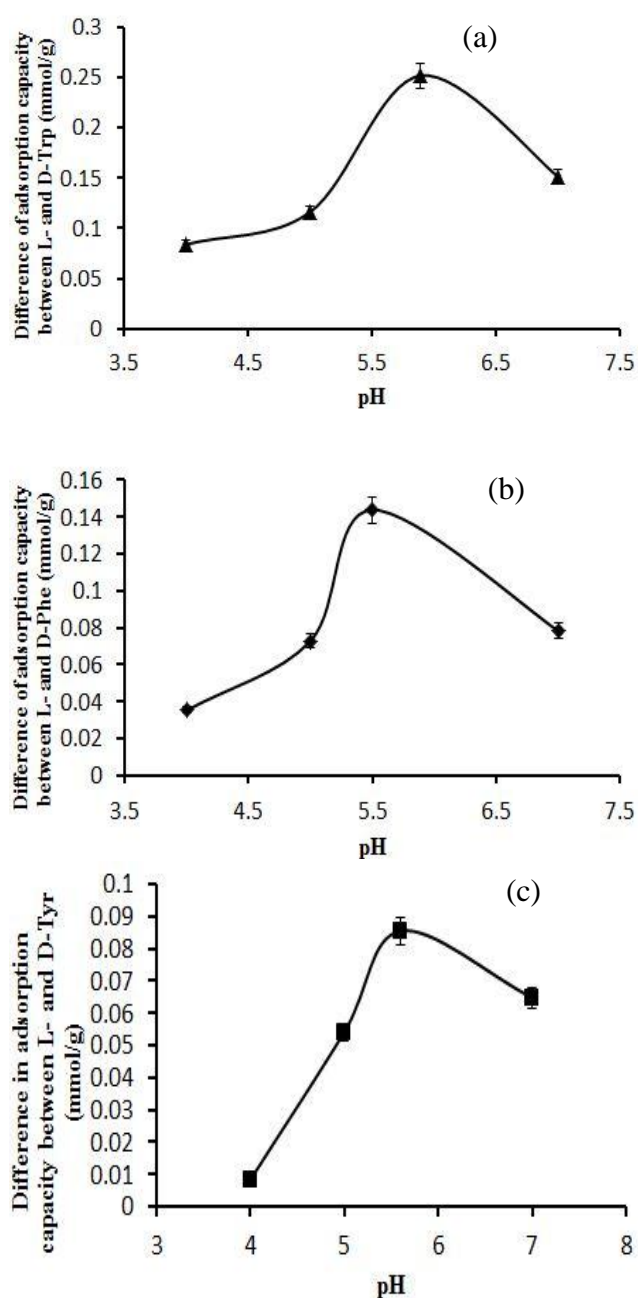
Figure 5-7 Effect of pH on adsorption: (a) D- and L-Trp, (b) D- and L-Phe, (c) D- and L-Tyr. (25°C and ionic strength 0.03M).

5.2.1.3 Adsorption at different temperatures

After obtaining the optimum pH for adsorption of the amino acids, further equilibrium studies were carried out at different temperatures at the isoelectric point of the corresponding enantiomers, which is the optimum pH. The effect of temperature on adsorption of single amino acid enantiomers on $Fe_3O_4/SiO_2/CMCD$ MNPs is shown in Figures 5-8, 5-9 and 5-10 at 25, 35 and 50°C, ionic strength 0.03M. It can be observed that the amount of adsorbed amino acid enantiomer per unit amount of the nanoparticle decreased with increasing temperature. Similar observation was reported in the literature [53]. Noteworthy, adsorption capacities of the nanoparticle toward L-Trp, L-Phe and L-Tyr at 35°C and 50°C were less than those at 25°C. Comparison of adsorption capacities of the nano adsorbents toward the six enantiomers at different temperatures are presented in Table 5-4 and 5-5, respectively. As the temperature increased, higher adsorbate concentration in solution was required to saturate the surface of the nano adsorbents. Thus adsorption capacity decreased. However, equilibrium results of adsorption studies at different temperature were also fitted well to Freundlich isotherm model. Parameters of Freundlich model are shown in Table 5-5.
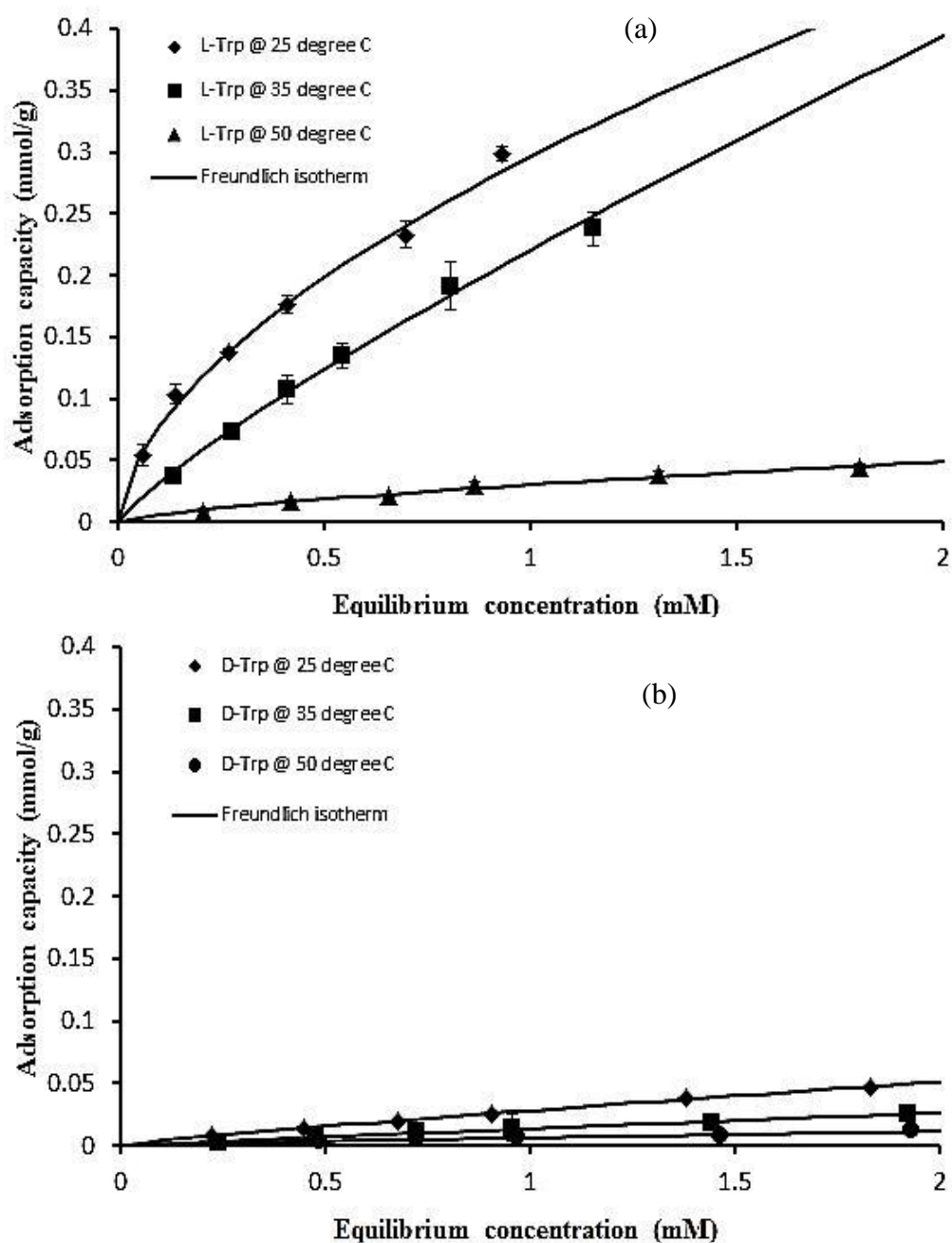
Figure 5-8 Adsorption equilibrium isotherms of (a) L- and D-Trp at 25°C, 35°C and 50°C (pH 5.9 and ionic strength 0.03M).
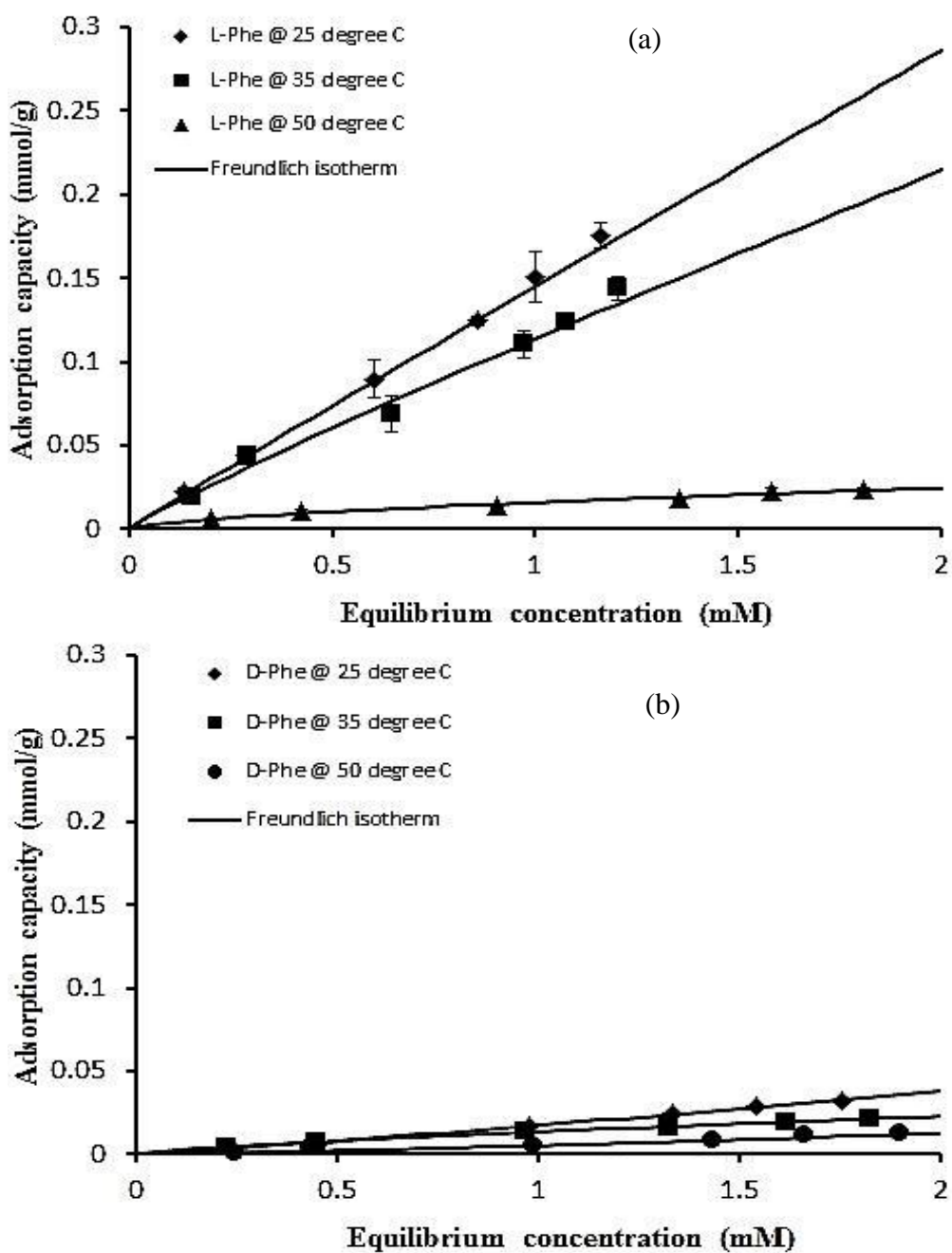
Figure 5-9 Adsorption equilibrium isotherms of (a) L- and (b) D-Phe at 25°C, 35°C and 50°C (pH 5.5 and ionic strength 0.03M).
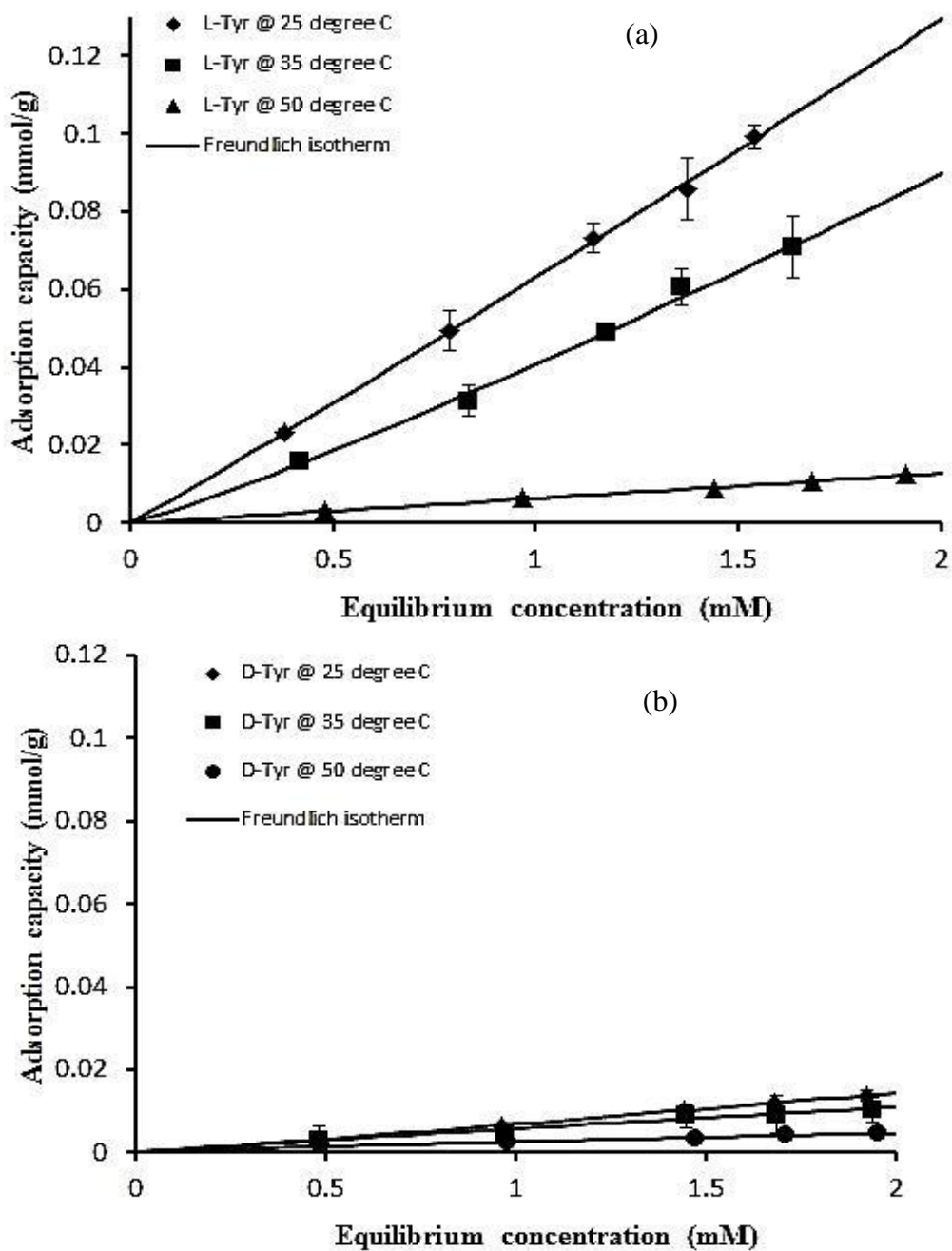
Figure 5-10 Adsorption equilibrium isotherms of (a) L- and (b) D-Tyr at 25°C, 35°C and 50°C (pH 5.6 and ionic strength 0.03M).

Table 5-4 Adsorption capacities of magnetic particle toward single enantiomers at different temperatures.

Amino acid	Adsorption capacity at 25°C (mmol/g)	Adsorption capacity at 35°C (mmol/g)	Adsorption capacity at 50°C (mmol/g)
L-Trp	0.298	0.237	0.044
D-Trp	0.046	0.024	0.011
L-Phe	0.175	0.143	0.023
D-Phe	0.031	0.021	0.012
L-Tyr	0.099	0.070	0.012
D-Tyr	0.013	0.010	0.004

Table 5-5 Parameters of Freundlich isotherm equation at different temperatures.

Amino acid	25°C			35°C			50°C		
	k_F	$1/n$	R^2	k_F	$1/n$	R^2	k_F	$1/n$	R^2
L-Trp	0.296	0.579	0.992	0.220	0.893	0.994	0.030	0.701	0.971
D-Trp	0.028	0.857	0.998	0.013	0.949	0.987	0.006	0.822	0.964
L-Phe	0.145	0.980	0.999	0.113	0.915	0.983	0.015	0.629	0.984
D-Phe	0.017	1.117	0.997	0.013	0.766	0.998	0.005	1.434	0.998
L-Tyr	0.063	1.036	0.999	0.040	1.132	0.995	0.006	1.016	0.997
D-Tyr	0.006	1.072	0.998	0.005	0.944	0.991	0.002	0.842	0.972

Based on the results of effect of pH and effect of temperature study, it can be mentioned that significant difference is observed between the adsorption capacities of the D- and L-enantiomers of tryptophan, phenylalanine and tyrosine at pH close to the isoelectric point of the enantiomers and 25°C. Results from effect of temperature study are summarized in Figure 5-11.
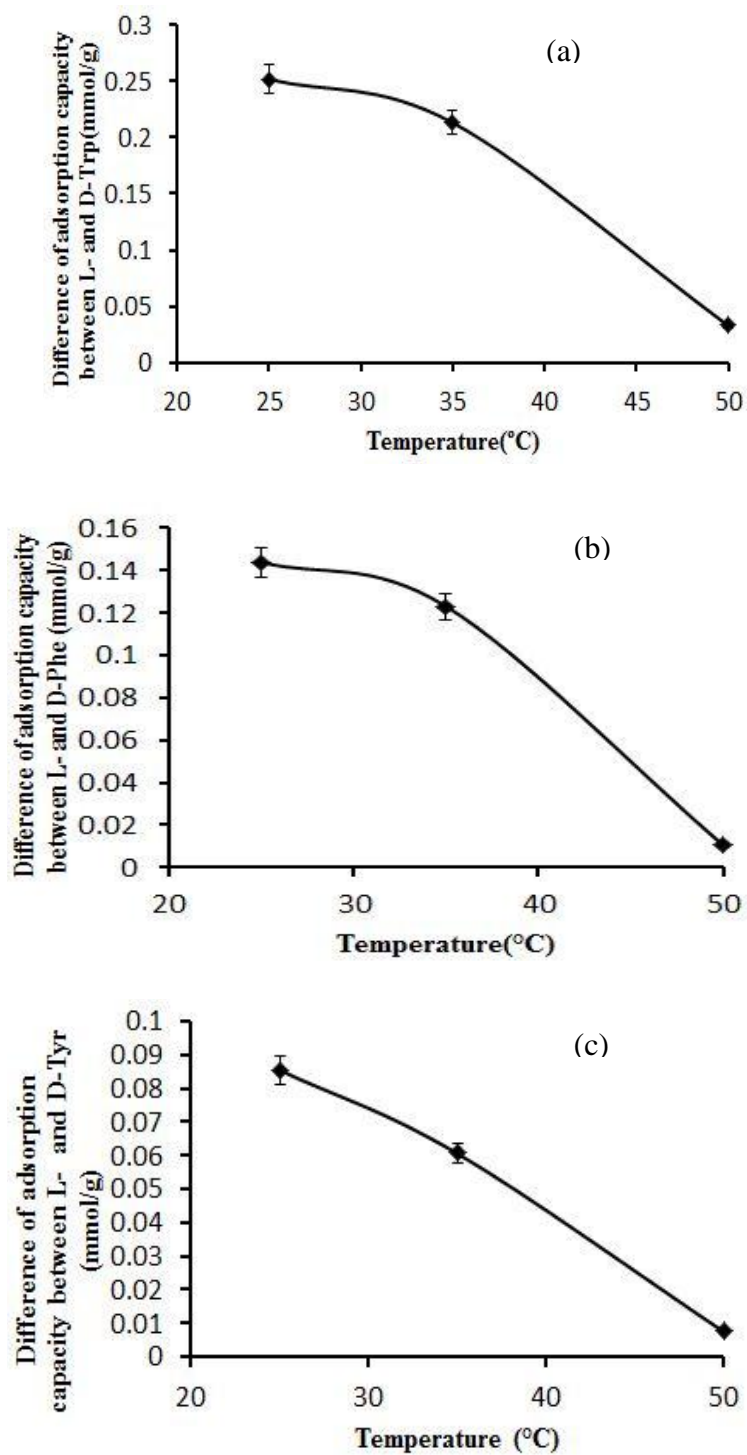
Figure 5-11 Effect of temperature on adsorption: (a) D- and L-Trp, (b) D- and L-Phe, (c) D- and L-Tyr. (ionic strength 0.03M).

5.2.1.4 Comparison of adsorption capacities of different amino acids

Adsorption capacities of the particles for amino acid enantiomers were compared in low concentration range and Figure 5-12 shows the results of equilibrium study for L- and D-Trp, L- and D-Phe and L- and D-Tyr up to concentration of 2 mM. From our results, it can be concluded that adsorption capacities of $Fe_3O_4/SiO_2/CMCD$ MNPs toward amino acids are in the order: L-Trp>L-Phe>L-Tyr and D-Trp>D-Phe>D-Tyr [383]. This is due to the structures and hydrophobicity of amino acid molecules and the CMCD molecule. Tang et al. suggested that molecular volume and hydrophobicity play important roles in interaction among the amino acids and β-CD polymers [53]. Since the cavity volume of β-CD ($[A^{\circ 3}]$, 262) is comparable to that of tryptophan (volume $[A^{\circ 3}]$, 227.8) and tryptophan is most hydrophobic among the three amino acids, interaction between tryptophan and CMCD molecule is the strongest. As it is seen from Figure 5-1, the hydroxyl group in structure of tyrosine molecule decreases the hydrophobicity of the molecule but increases volume of the molecule slightly. So, volume of tyrosine molecule is slightly bigger than that of phenylalanine, but hydrophobicity of phenylalanine is much higher than tyrosine as shown in Table 5-6. Thus the adsorption capacities of $Fe_3O_4/SiO_2/CMCD$ MNPs toward L- and D-phenylalanine are higher than those of L- and D-tyrosine.
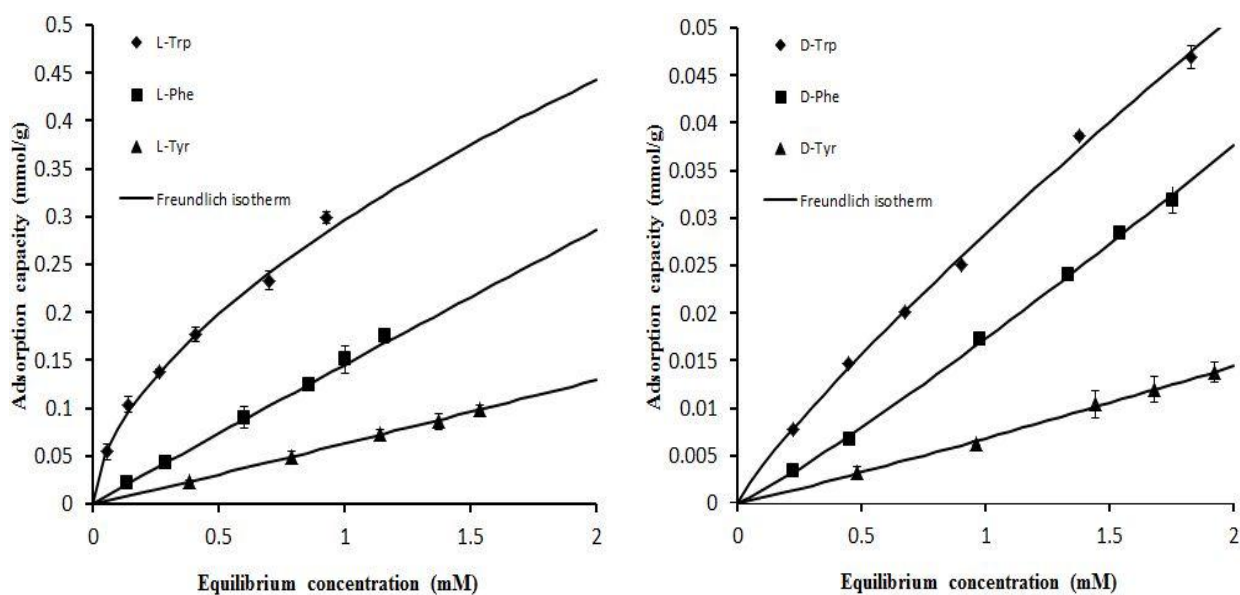
Figure 5-12 Adsorption isotherms for (a) L-Trp, L-Phe, L-Tyr and (b) D-Trp, D-Phe, D-Tyr at initial concentrations of (0.25-2 mM) incubated with 50 mg of $Fe_3O_4/SiO_2/CMCD$ MNPs.

Table 5-6 Physical properties of aromatic amino acids [53].

Amino acid	Volume (Å^3)	Residue non-polar surface area (Å^2)	Estimated hydrophobic effect for residue burial (kcal/mol)	Estimated hydrophobic effect for side chain burial (kcal/mol)
Trp	227.8	37+199	4.11	2.9
Phe	189.9	39+155	3.46	2.3
Tyr	193.6	38+116	2.81	1.6

Maximum adsorption capacities of silica and CMCD coated MNPs ($Fe_3O_4/SiO_2/CMCD$ MNPs) toward the single amino acid enantiomers are: L-Trp-0.298 mmol/g, D-Trp-0.046 mmol/g, L-Phe-0.175 mmol/g, D-Phe- 0.031 mmol/g, L-Tyr- 0.099mmol/g, D-Tyr- 0.013 mmol/g. Some data are found in literature regarding adsorption of amino acids on cross-linked β-cyclodextrin polymer. Maximum adsorption capacities are: L-Trp- 0.256 mmol/g, L-Phe-0.260 mmol/g, L-Tyr-0.017 mmol/g [53]. Comparing adsorption capacities, it can be mentioned that adsorption capacities of

$Fe_3O_4/SiO_2/CMCD$ MNPs are higher than adsorption capacities of cross-linked β-cyclodextrin polymer toward L-Trp and L-Tyr.

5.2.2 Adsorption kinetics

The adsorption kinetics of the L-/D-Trp, L-/D-Phe and L-/D-Tyr onto the $Fe_3O_4/SiO_2/CMCD$ MNPs were carried out at the pI of the enantiomers and 25°C. The main objective of the study was to determine how adsorption capacity of the solid changes with time via studying how the concentration of amino acid solution changes with time. The initial concentration of D- and L-enantiomers provided the necessary driving force to overcome the mass transfer resistance of the enantiomers between the aqueous and solid phases. Figures 5-13, 5-14 and 5-15 show the effect of contact time on adsorption of Trp, Phe and Tyr enantiomers onto $Fe_3O_4/SiO_2/CMCD$ MNPs.
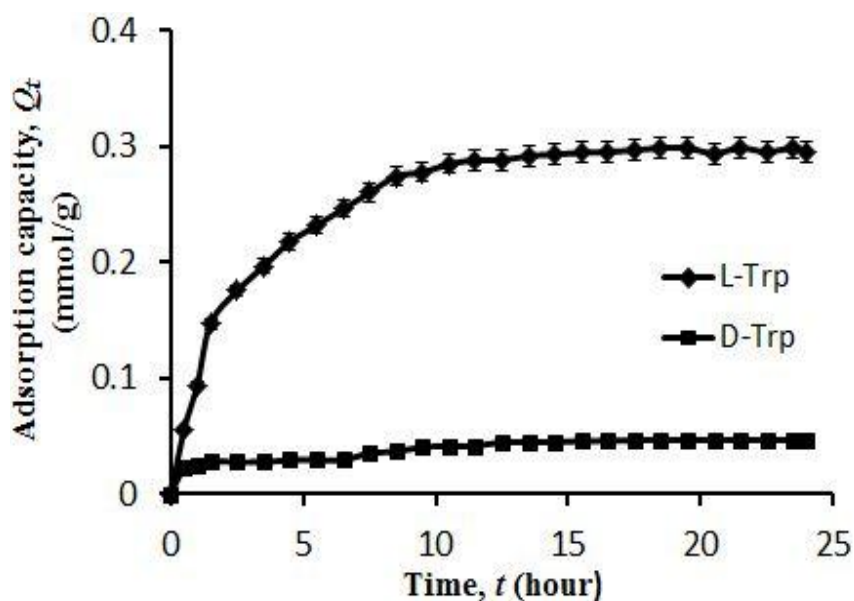
Figure 5-13 Effect of contact time on adsorption of D-/L-Trp on $Fe_3O_4/SiO_2/CMCD$ MNPs.
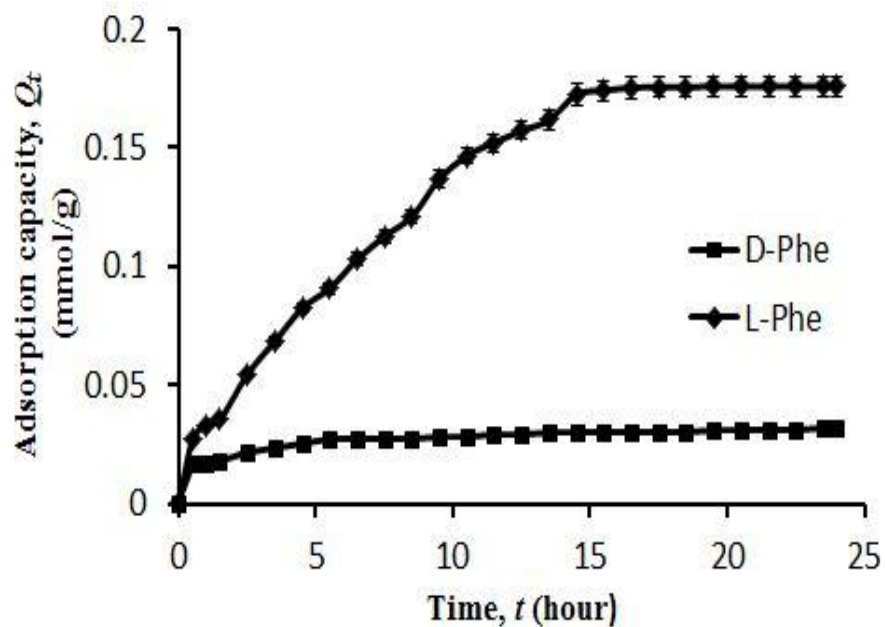
Figure 5-14 Effect of contact time on adsorption of D-/L-Phe on $Fe_3O_4/SiO_2/CMCD$ MNPs.
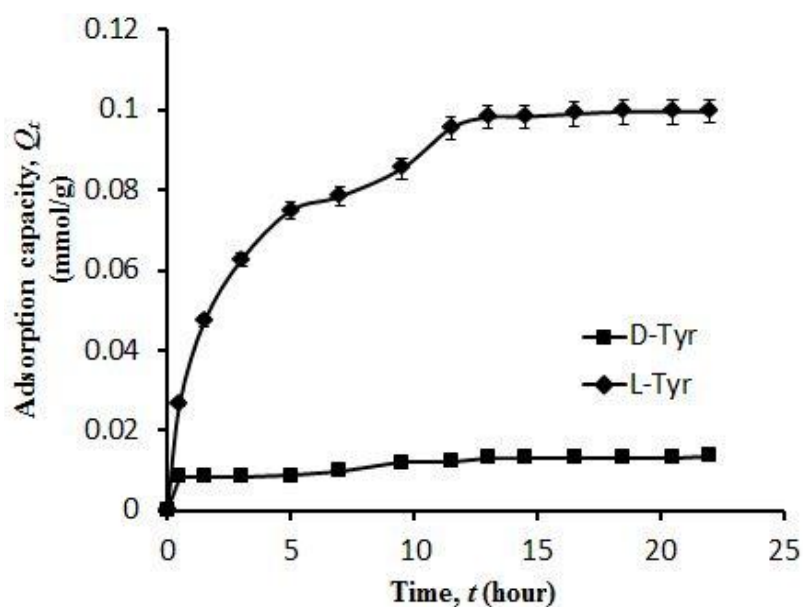
Figure 5-15 Effect of contact time on adsorption of D-/L-Tyr on $Fe_3O_4/SiO_2/CMCD$ MNPs.

It can be observed that equilibrium was reached in approximately 20 hrs for the enantiomers. Within the first 5 hrs of the reaction, 70-80% of the maximum adsorption capacity had been reached.

The Lagergren rate equation is one of the most widely used adsorption rate equations used to describe the adsorption rate of a solute from a solution. It is based on an empirical model, where a rate law is proposed and integrated to predict the time course of concentration. In this study, the adsorption kinetics of the amino acids onto $Fe_3O_4/SiO_2/CMCD$ MNPs was fitted well with Lagergren pseudo-second order model.

Lagergren pseudo-second-order model is expressed by [332]:

$$\frac{dQ}{dt} = k_2(Q_e - Q_t)^2$$

[5-3]

Integrating the equation for the boundary conditions $t = 0$ to $t = t$ and $Q = 0$ to $Q = Q_t$, gives,

$$\frac{t}{Q_t} = \frac{1}{k_2 Q_e^2} + \frac{1}{Q_e} t$$

[5-4]

where k_2 is the equilibrium rate constant of pseudo-second-order adsorption (g/mmol.hour). The slope and intercept of the plot of t/Q_t versus t are used to calculate k_2 and Q_e,cal. The corresponding kinetic parameters from the model are listed in Table 5-7. It is found that the correlation coefficients (R^2) for the pseudo-first-order kinetic model are less than 90% indicating a poor pseudo-first-order fit to the experimental data (data not shown). On the other hand, the correlation coefficient (R^2) for the pseudo-second-order adsorption model has high value (>98%), and the Q_e values (Q_e,cal) calculated from pseudo second-order model are more consistent with the experimental

Q_e values (Q_e, exp). These facts suggest that the adsorption data are well represented by

pseudo-second-order kinetic model.

Table 5-7 Adsorption kinetic parameters for amino acids onto $Fe_3O_4/SiO_2/CMCD$ MNPs.

Amino acid	Lagergren pseudo-second-order model parameters			Experimental value
	k_2 (g/mmol.hour)	Q_e (mmol/g)	R^2	Q_e (mmol/g)
L-Trp	1.745	0.300	0.998	0.298
D-Trp	9.816	0.048	0.982	0.046
L-Phe	0.940	0.183	0.986	0.175
D-Phe	29.71	0.029	0.997	0.031
L-Tyr	4.250	0.110	0.996	0.099
D-Tyr	36.69	0.014	0.988	0.013

5.2.3 Desorption studies

The success of an adsorption process usually depends on the regeneration step of the adsorbent from the economic point of view. Regeneration of the adsorbed solute from the adsorbent is generally accomplished by one of two general methods. One is to change a physical operating condition, namely temperature, of the adsorber, which affects the equilibrium interaction between the adsorbent and the solute. The other is to perform a chemical reaction in the adsorber to change the nature of adsorbed component so that it can be desorbed and removed from the system readily. In general, there are many regeneration techniques such as thermal, steam, acid, base, and solvent regenerations. In this study, methanol was used as desorbing agent. Figure 5-16 shows the result of desorption efficiency of L-Trp, L-Phe and L-Tyr after adding methanol as desorbing agent. Around 90%, 89% and 88% of adsorbed L-Trp, L-Phe and L-Tyr were desorbed using methanol solution, respectively. Furthermore, 80%, 78% and 75% desorption of D-Trp, D-Phe and D-Tyr were achieved using methanol (Figure 5-17). Desorption of D-enantiomers were less than those of L-enantiomers which could be due to less affinity of the D-enantiomers to methanol. Further work should be done to increase the desorption percentage using other solvents like ethanol, IPA (isopropyl alchohol). Complete desorption of the amino acid could be achieved by repeated desorption steps. Some researchers also found that addition of alchohol solution was effective as desorbing agent for desorption of Trp and Phe solution from non-ionic polymeric adsorbent [384]. In this case desorption might have been facilitated by the greater affinity of amino acids in methanol than the adsorbent. It should be noted that desorption equilibrium of enantiomers were achieved within about 20 hrs, similar to the adsorption equilibrium.
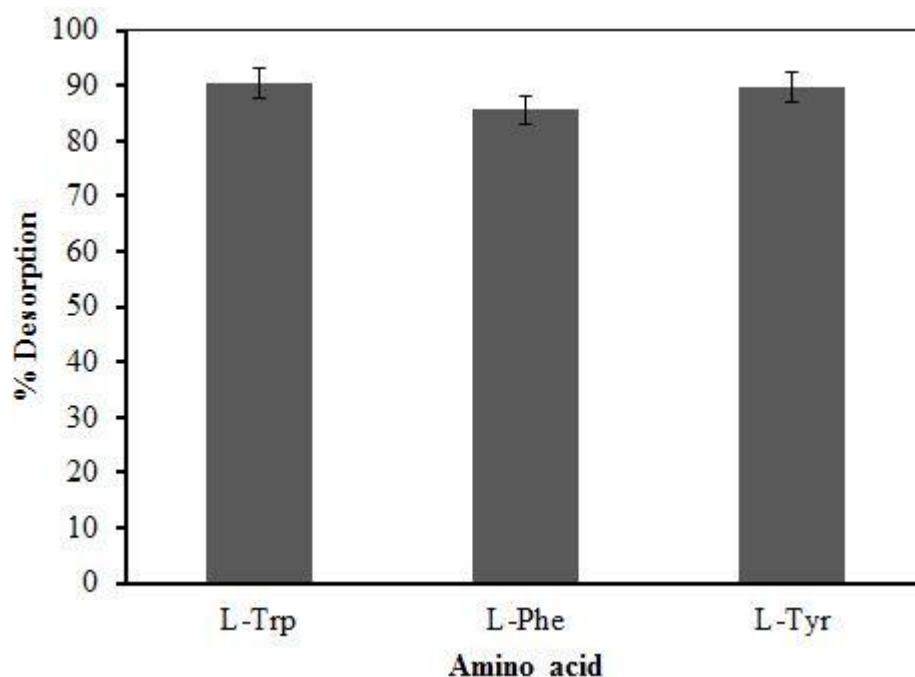
Figure 5-16 Desorption of L-Trp, L-Phe, L-Tyr from $Fe_3O_4/SiO_2/CMCD$ MNPs in methanol. Adsorption condition: $Fe_3O_4/SiO_2/CMCD$ MNPs 50 mg; L-Trp/L-Phe/L-Tyr: 2 mM; pH 6; temperature 25°C, contact time 24 hrs. Desorption condition $Fe_3O_4/SiO_2/CMCD$ MNPs: 50 mg; temperature 25°C, contact time 24 hrs.
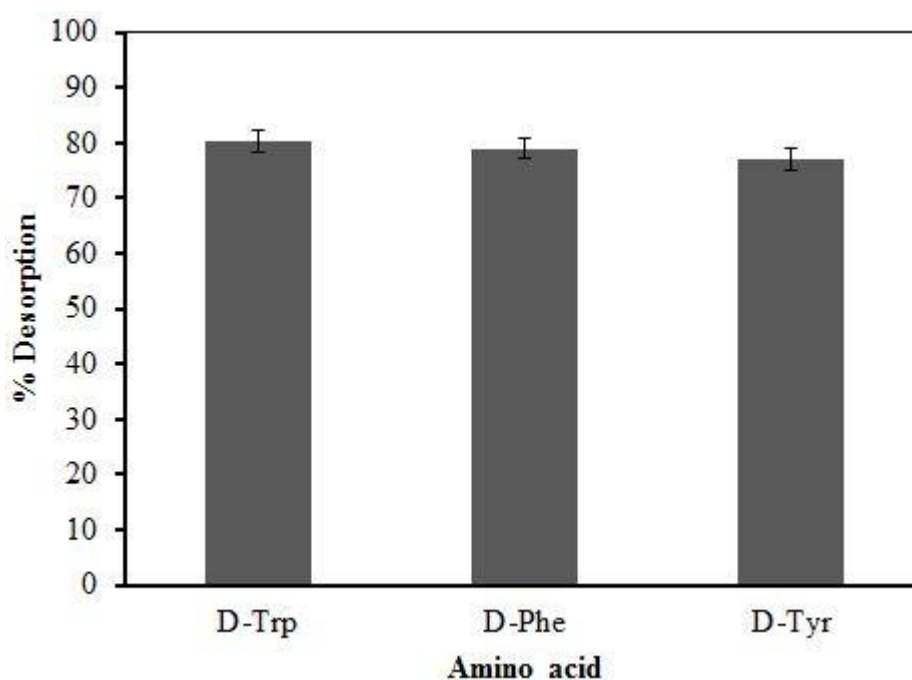
Figure 5-17 Desorption of D-Trp, D-Phe, D-Tyr from $Fe_3O_4/SiO_2/CMCD$ MNPs in methanol. Adsorption condition: $Fe_3O_4/SiO_2/CMCD$ MNPs 50 mg; L-Trp/L-Phe/L-Tyr: 2 mM; pH 6; temperature 25°C, contact time 24 hrs. Desorption condition $Fe_3O_4/SiO_2/CMCD$ MNPs: 50 mg; temperature 25°C, contact time 24 hrs.

5.2.4 Adsorption mechanism

For understanding of the amino acid/magnetic nanoparticle interaction, FTIR data are introduced to gain insight into the adsorption mechanism. Analysis of FTIR spectra depicts direct evidence of functional groups present on the adsorbent surface. Therefore, careful examination of the FTIR spectra of adsorbent surface after adsorption reaction provides information regarding the surface groups that might have participated in the adsorption reaction.
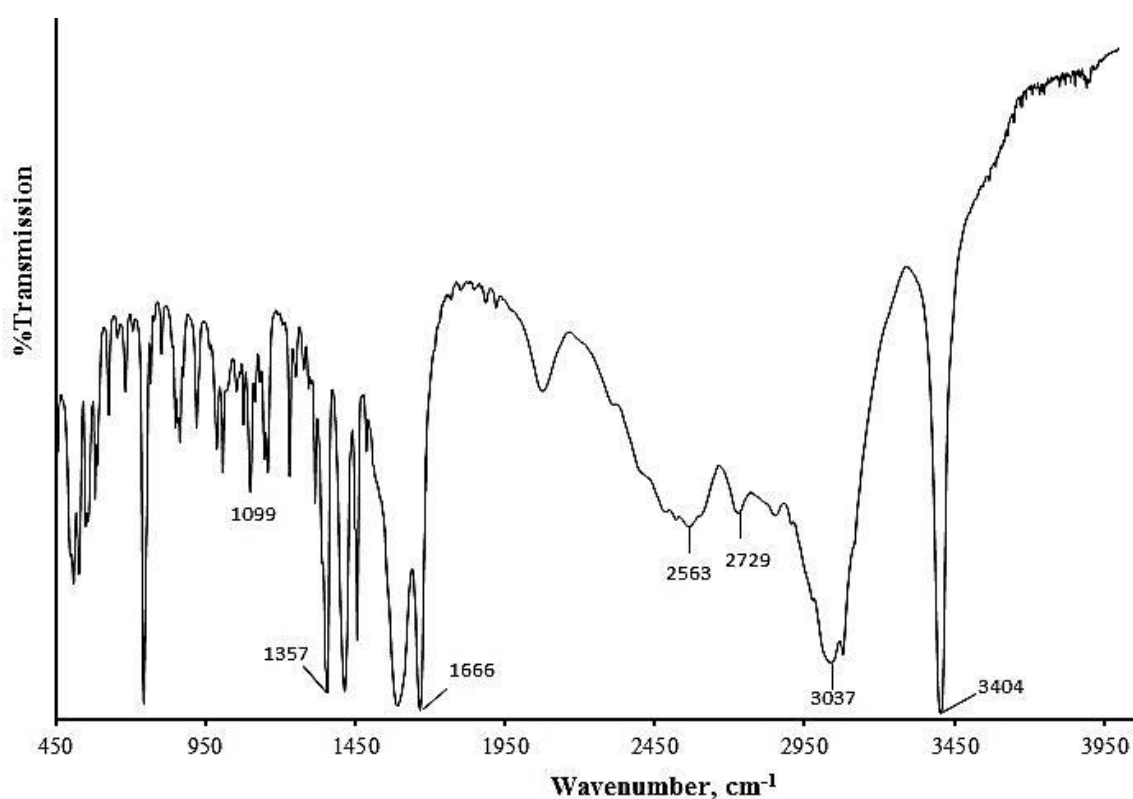
Figure 5-18 FTIR spectra of L-tryptophan.

Figure 4-1(d) and Figure 5-18 depict the FTIR spectra of $Fe_3O_4/SiO_2/CMCD$ MNPs and L-Trp, respectively before adsorption. Since L-Trp and D-Trp are chiral enantiomers; their spectra before adsorption are similar. The spectra of $Fe_3O_4/SiO_2/CMCD$ MNPs after adsorption of L-Trp and D-Trp are shown in Figure 5-19 and Figure 5-20, respectively. In Figure 5-18, the absorption peak with the maximal frequencies is at

3404 cm^{-1} which may be attributed to the N-H stretching vibrations of tryptophan. Other stretching vibrations are observed at 2500-3000 cm^{-1} (O–H of carboxylic acid), 1666 cm^{-1} (C=C), 1357 cm^{-1} (C–N), and 1099 cm^{-1} (C–O) [385]. The shape of the stretching vibration peak at 3404 cm^{-1} in native L-Trp (Figure 5-18) is changed after adsorption and it became more intense for particles that adsorbed with L-Trp than D-Trp. Also the peak at 3037 cm^{-1} in the spectra of L-Trp which can be assigned to the presence of C-H stretching vibrations (from phenyl ring) is red shifted to 3024 cm^{-1} (Figure 5-19) indicating the formation of complex between L-Trp and CMCD. On the other hand, a small peak for C-H group (from phenyl ring) is observed at 3056 cm^{-1} in the FTIR spectra (Figure 5-20) of Fe$_3$O$_4$/SiO$_2$/CMCD MNPs after adsorption of D-Trp, which supports our experimental observation that adsorption of L-Trp on coated magnetic nanoparticles is higher than D-Trp. Again, the peaks at 1666 and 1652cm^{-1} in the spectra of the Trp-CMCD complex (Figure 5-19 and Figure 5-20) could be attributed to C=C stretching vibrations. Last but not the least, Figure 5-19 and Figure 5-20 illustrate that the intensities of native N-H stretching vibrations on L-Trp after formation of complex is changed (in both L-Trp and D-Trp after adsorption on particles), which could be attributed due to the complex formation of the amino groups of the amino acid molecules with the cyclodextrin molecules.
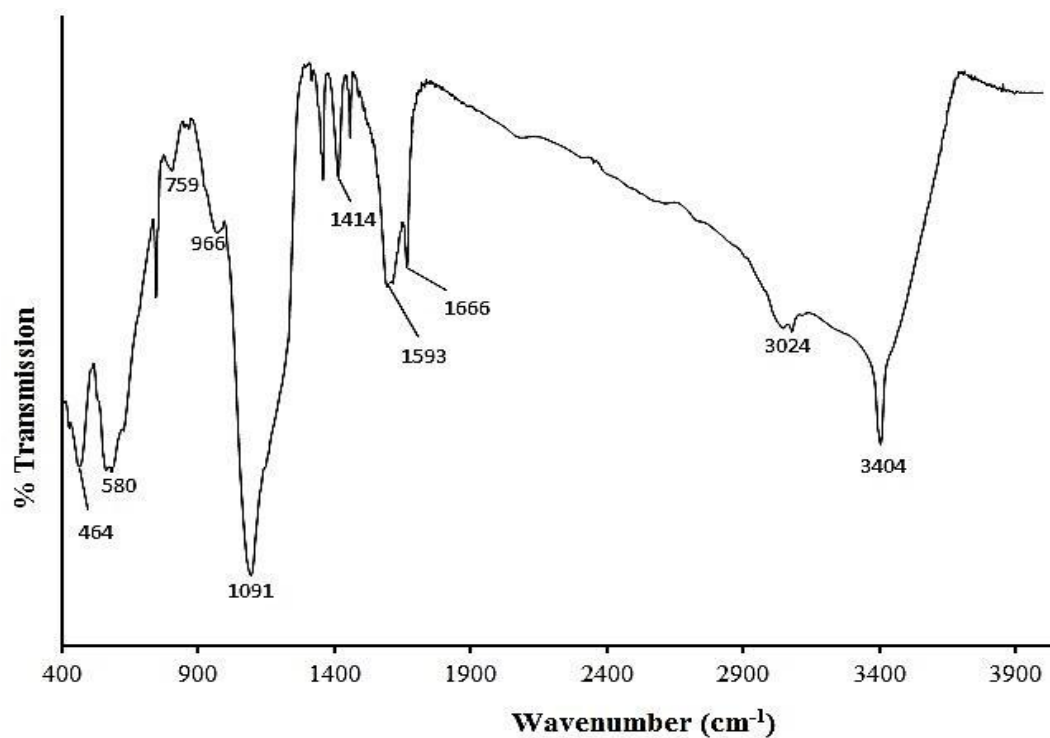
Figure 5-19 FTIR spectra of $Fe_3O_4/SiO_2/CMCD$ MNPs after adsorption of L-tryptophan.
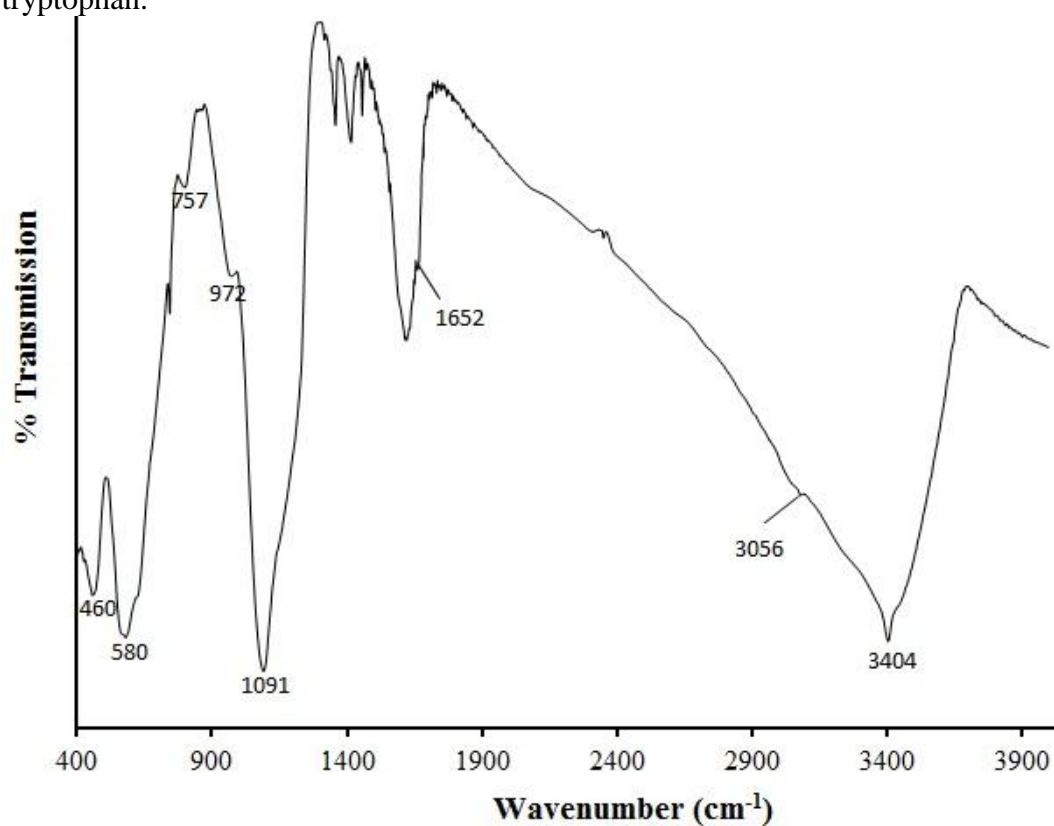
Figure 5-20 FTIR spectra of $Fe_3O_4/SiO_2/CMCD$ MNPs after adsorption of D-tryptophan.

5.3 Conclusions

Adsorptions of D-/L-Trp, D-/L-Phe and D-/L-Tyr were studied on silica and CMCD coated nano-sized magnetic particles at various pH and temperature conditions. Higher adsorption occurred at pH close to the isoelectric point of the amino acids and at 25°C. Maximum difference between adsorption capacities of L- and D-enantiomers were also obtained at the same conditions. Adsorption of amino acid enantiomers reached equilibrium within 20 hrs and kinetics of adsorption followed the pseudo-second-order model. Results of equilibrium study showed that the synthesized particles can preferentially adsorb L-enantiomers of aromatic amino acids than the corresponding D ones. Experimental data of equilibrium adsorption studies were fitted well to Freundlich model. Desorption studies showed that the enantiomers was desorbed using methanol as eluent. Finally, FTIR studies showed that coated nanoparticles bonded to amino acid enantiomers to form complexes. The amino groups of the amino acids might have formed complexes with the CMCD molecules. Since this study shows that $Fe_3O_4/SiO_2/CMCD$ MNPs can selectively adsorb amino acid enantiomers; these particles can be utilized for chiral separation of aromatic amino acids.

Chapter 6: Enantioselective separation of chiral aromatic amino acids with surface functionalized magnetic nanoparticles

6.1 Introduction

Chirality in nature and living systems is of great impact for a variety of active compounds interacting with them. The molecular building blocks of life, such as amino acids and sugars that form peptides, proteins and polysaccharides exist in chiral structures. Thus, in recent years, chiral analysis has received increased attention in many research fields including pharmaceutical, clinical, environmental and food analysis since enantiomers show different physiological activities depending on their configurations [386-389]. Generally, enantiomerically pure compounds are obtained either from available chiral starting materials generated during a reaction by asymmetric catalysis or by chiral resolution of the enantiomers using various separation methods. Asymmetric synthesis is, in principle, the most cost effective method of producing single-isomer products. Although asymmetric synthesis is the ultimate way to obtain the compounds and has been intensively developed [390], it has one limitation: it gives high enantiomeric purity only for exceptionally enantioselective reactions. Resolution of racemates is still considered as a powerful method for production of enantiomerically pure compounds. Various methods can be applied for separation of enantiomers and/or for the determination of enantiomeric composition of chiral compounds. Among others, various chromatographic methods including high performance liquid chromatography (HPLC) [391], gas chromatography (GC) [389], supercritical fluid chromatography (SFC) [392], simulated moving bed (SMB) chromatography [393], various electromigration capillary methods [394], enzymatic or non-enzymatic dynamic kinetic resolutions [395], membrane separation [396],

crystallization [397], methods using molecularly imprinted polymer (MIP)s [230] have been successfully utilized.

Magnetic nanoparticles can be good candidate for enantioselective separation of chiral biomolecules due to their unique size, large surface area, biocompatibility, low toxicity, superparamagnetic properties and well understood surface chemistry. Currently, iron oxide (Fe_3O_4) nanoparticle is one of the most popular materials among them and has been widely used in the fields of biology and medicine such as targeted drug delivery [230], enhanced resolution magnetic resonance, protein and enzyme immobilization [398], bio-separation etc. These superparamagnetic materials possess an advantage of not retaining any magnetization after removal of external magnetic field. But these magnetic nanoparticles suffer from the problem of agglomeration. Considerable interest has been focused on the surface modification of superparamagnetic iron oxide nanoparticles to prevent agglomeration of the particles, increase the stability and provide biocompatibility. Recently, surface functionalized magnetic nanoparticles are found to be good adsorbents for magnetic field induced separation of some chiral enantiomers. Choi et al. demonstrated that magnetic silica nanoparticles tagged to a chiral selector (S-/R- -N-(2,2-dimethyl-5-ethoxydimethylsilylpentanoyl)-proline-3,5-dimethylanilide) could be utilized in magnetic field induced separation of enantiomers of N-(3,5-dinitrobenzoyl)alanine (Ala), valine (Val) and leucine (Leu) N-propylamide [399]. Enantiomeric excess was determined and it varied between 17-80%. In the work, chiral separation was not studied for aromatic amino acid enantiomers. Furthermore, magnetite nanoparticles (MNPs) immobilized with an appropriate chiral catalyst or enzyme was also successfully utilized for asymmetric reactions or enzymatic kinetic resolutions [365, 400]. Novel magnetite nanoparticle supported chiral Ruthenium(II) complexes were prepared that catalyze heterogeneous asymmetric hydrogenation of

aromatic ketones with remarkably high activity and enantioselectivity (e.e. 95-98%) [400]. Furthermore, chiral DMAP (hypernucleophilic' 4-N,N-dimethylaminopyridine) variant immobilized on magnetite nanoparticles was capable of promoting the kinetic resolution of sec-alcohols with synthetically useful selectivity under process-scale friendly conditions (ambient temperature, low catalyst loading, and acetic anhydride as the acylating agent), which allowed the isolation of resolved alcohols with good to excellent enantiomeric excess (e.e 82-99%) [365].

The cyclodextrins (CDs) are a series of cyclic oligosaccharides composed of α(1–4)-linked D-glucopyranose units and these compounds are torus-shaped with a hydrophilic external surface and a hydrophobic internal cavity. Such structural characteristics allow CDs and their derivatives to form stable inclusion complexes with a variety of compounds through host-guest interactions [18]. But due to relative low solubility of natural cyclodextrins in water as well as in organic solvents, their direct use is greatly limited. Several synthetic strategies have been developed to modify natural cyclodextrin to improve their performance as host to specific guest molecules and to increase their solubility in water [401]. Usefulness of cyclodextrin in enantioseparation is attributed by several main advantages over the other adsorbents. The outstanding one of cyclodextrins is their ability to form inclusion complexes. The capability to form inclusion complexes with wide variety of guest molecules make CDs valuable and useful in many research areas such as resolution of enantiomers using HPLC [402], enantioseparation in electrophoresis [403], targeted drug delivery [30, 404, 163], removal of contaminants from aqueous solution [405] etc. Banerjee et al. first synthesized magnetic nanocarriers by grafting cyclodextrin onto gum arabic modified magnetic nanoparticles (GAMNPs) for ketoprofen release study [163]. Cao et al. also fabricated β-CD functionalized Fe_3O_4/amino-silane core-shell nanoparticles layer-by-

layer approach which can act as drug carriers [151]. However, to the best of our knowledge, detailed studies of the adsorption characteristics of aromatic amino acid enantiomers and chiral resolution of amino acids utilizing superparamagnetic Fe_3O_4 nanoparticles bearing cyclodextrin moieties from phosphate buffer solution are very scarce in the literature.

Amino acid enantiomers or their derivatives are frequently found in food stuffs and many drugs as well. Enantiomers of different optical activities might have different interactions with our body since chiral drugs present different activity, toxicity, transport mechanism and metabolic route. Thus, resolution of aromatic amino acid enantiomers is of prime importance. In previous chapter, we have reported adsorption behavior of the chiral aromatic amino acid enantiomers (D-/L-tryptophan (Trp), D-/L-phenylalanine (Phe), D-/L-tyrosine (Tyr)) on magnetic silica nanoparticles bonded to carboxymethyl-β-cyclodextrin (CMCD) from phosphate buffer solution at neutral condition in order to understand the host-guest interaction in-depth. We herein report chiral separation of DL-Trp, DL-Phe and DL-Tyr utilizing cyclodextrin derivative functionalized magnetite silica nanoparticles. Selective adsorption capacity of the particles toward the enantiomers from their racemic mixture was examined using high performance liquid chromatography. Enantioselective mechanism was investigated using several analytical techniques for example FTIR, XPS etc. Finally, inclusion complex formation of the particles was scrutinized and stability constant (K), Gibbs free energy change $(-\Delta G^0)$ of the inclusion complexation of the enantiomers (L-/D-Trp, L-/D-Phe and L-/D-Tyr) with CMCD were determined.

6.2 Results and discussion

6.2.1. Enantioseparation of aromatic amino acids

6.2.1.1 Adsorption separation of single enantiomers and racemic amino acids

Initially, adsorption capacity of the magnetic nanoadsorbent toward single amino acid enantiomers (D-/L-Trp, D-/L-Phe and D-/L-Tyr) was investigated in chapter 5. Thus, in Figure 5-1, three dimensional structures of D- and L-amino acids were presented whereas in Figure 6-1, three dimensional structures of D- and L- amino acid and racemic amino acids are presented. Since chiral resolution is based on the stability difference of CMCD-amino acid complexes, effect of initial amino acid concentration was investigated at pH 6 and all the adsorption data are given in Figure 6-2, where adsorption capacity of $Fe_3O_4/SiO_2/CMCD$ MNPs (mmol/g of solid) are plotted against the equilibrium concentration of amino acids in the bulk solution (mM). Adsorption capability of the $Fe_3O_4/SiO_2/CMCD$ MNPs toward single enantiomers, i.e. D- and L-amino acid varies significantly as the initial amino acid concentration increases. Sorption capacities of the as-synthesized particles are in the order: L-Trp>L-Phe>L-Tyr. Adsorption capacities of the $Fe_3O_4/SiO_2/CMCD$ MNPs are 0.29 mmol/g, 0.04 mmol/g, 0.17 mmol/g, 0.03 mmol/g, 0.09 mmol/g and 0.01 mmol/g toward L-Trp, D-Trp, L-Phe, D-Phe, L-Tyr and D-Tyr, respectively. Noteworthy, differences in the adsorption capacities of these adsorbents toward L- and D-enantiomers of the amino acids are obtained due to the difference in three dimensional structures of L- and D-enantiomers [381].
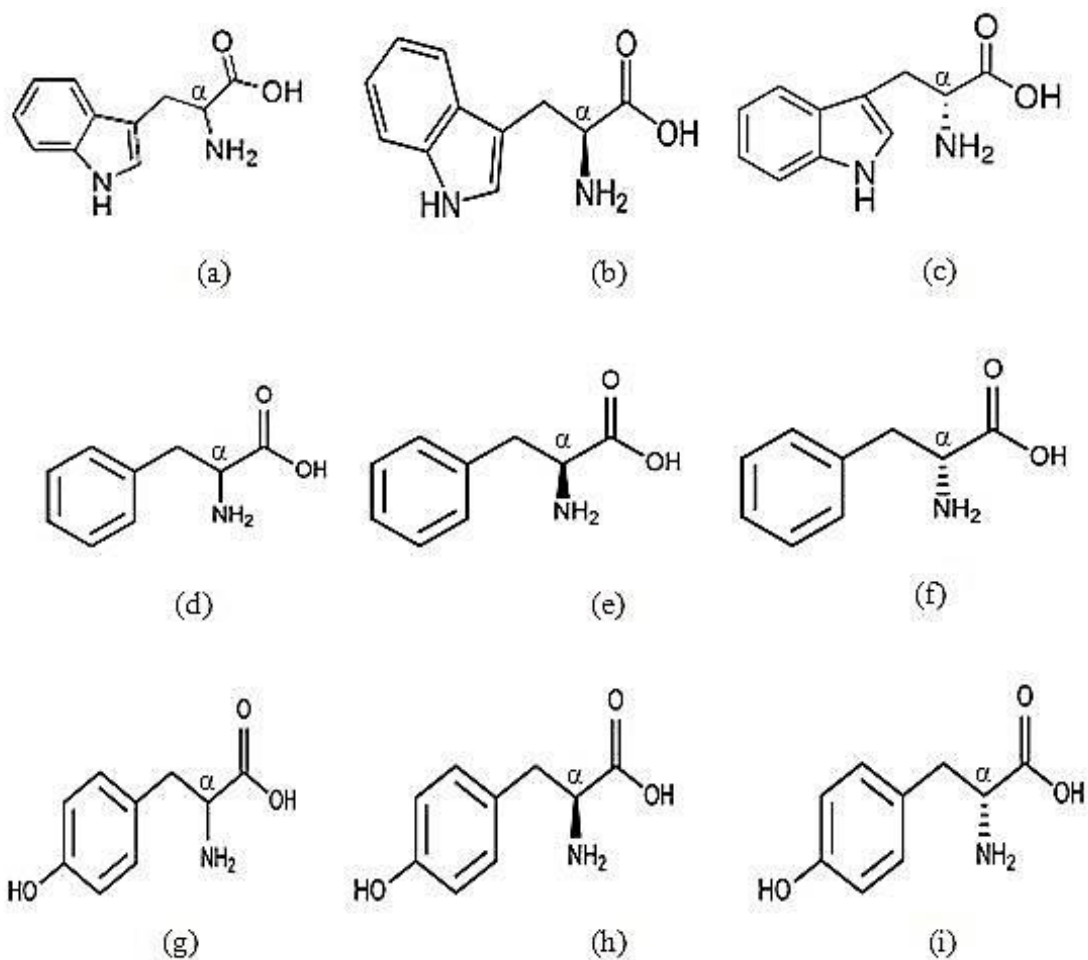
Figure 6-1 Schematic structures of the molecules: (a) DL-Trp, (b) L-Trp, (c) D-Trp, (d) DL-Phe, (e) L-Phe, (f) D-Phe, (g) DL-Tyr, (h) L-Tyr, (i) D-Tyr.
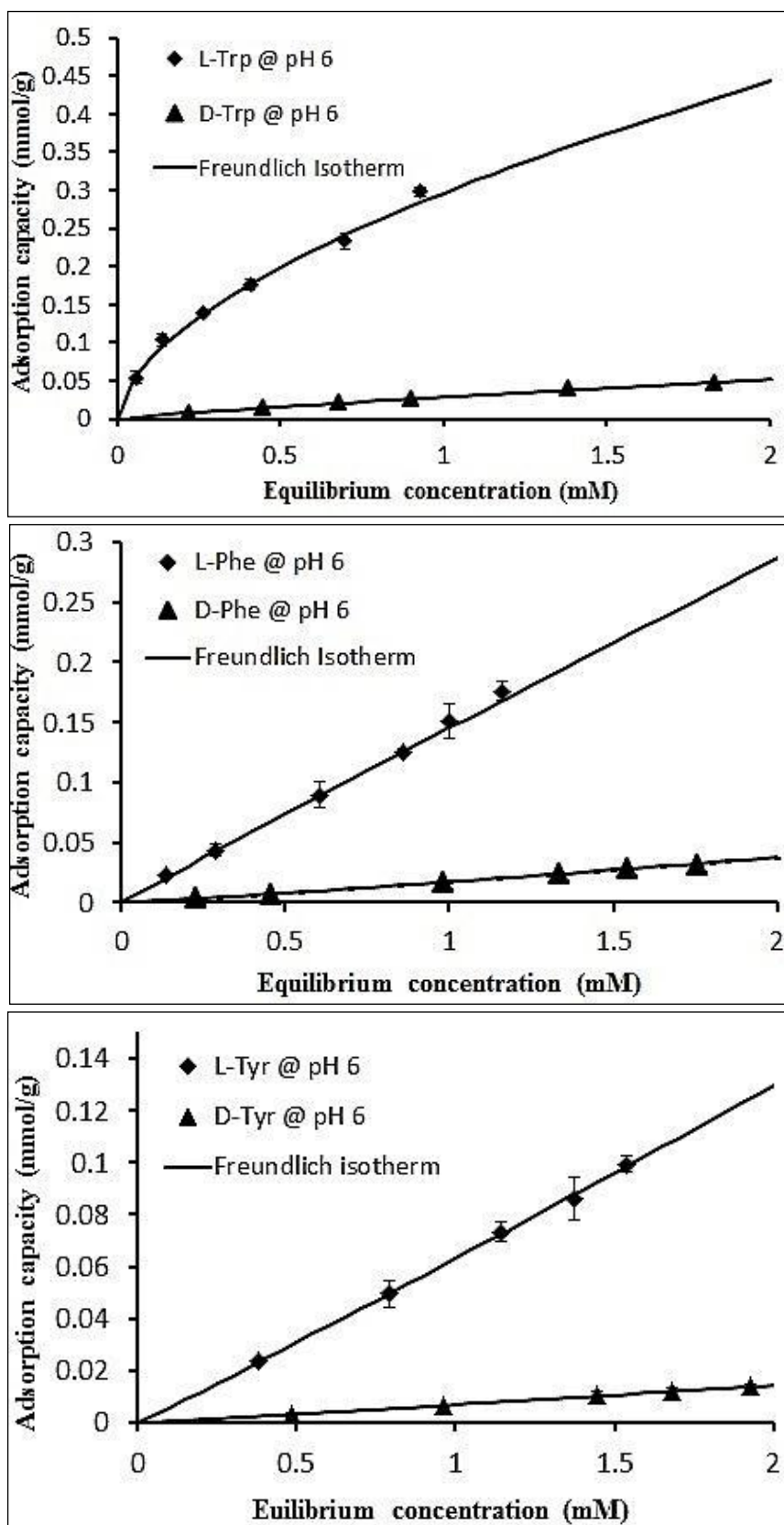
Figure 6-2 Adsorption equilibrium isotherms for: (a) L-Trp, (b) D-Trp, (c) L-Phe, (d) D-Phe, (e) L-Tyr and (f) D-Tyr at pH 6 (25°C and ionic strength 0.03M).

Amino acids are widely used as the analytical samples for the study of derivatized-β-cyclodextrin selectors [406-408]. In this study, the $Fe_3O_4/SiO_2/CMCD$ MNPs were evaluated for enantioseparation of three racemic aromatic amino acids (DL-Trp, DL-Phe and DL-Tyr). The separation results and conditions are summarized in Table 6-1. As shown in Table 6-1, all the aromatic amino acids could be resolved by the $Fe_3O_4/SiO_2/CMCD$ MNPs and significant selectivity and resolution was obtained for separation of the enantiomers by the column. Noteworthy, the enantiomeric excesses of Trp, Phe and Tyr after adsorption onto the modified magnetic nanoparticles were 94%, 73% and 58%, respectively. These good separation results show that the $Fe_3O_4/SiO_2/CMCD$ MNPs substantiate fine chiral recognition abilities towards aromatic amino acid enantiomers. Good inclusion complexation might have occurred by the penetration of benzene ring into cyclodextrin cavity, while its chiral center being close to the hydroxyl groups on the cyclodextrin rims favoring hydrogen bond formation with the carboxylate and amine moieties [408].

As mentioned, enantiomeric excesses of Trp, Phe and Tyr enantiomers after adsorption onto the modified magnetic nanoparticles were 94%, 73% and 58%, respectively. Enantiomeric excess can vary sometimes from 17% to 80% [399]. In this case, hydrophobicity and size/shape of the molecules played role for adsorption of the amino acids. Enantiomeric excess of Trp enantiomers is higher than those of other two aromatic amino acid enantiomers. Molecular volume and hydrophobicity play important roles in interaction among the amino acids and β-CD polymers [53]. Since the cavity volume of β-CD ($[A^{\circ 3}]$, 262) is comparable to that of tryptophan (volume $[A^{\circ 3}]$, 227.8) and tryptophan is most hydrophobic among the three amino acids, interaction between tryptophan and CMCD molecule should be the strongest. As a result, adsorption was higher and enantioselectivity was also higher. As it is seen from Figure 6-1, the

hydroxyl group in structure of tyrosine molecule decreases the hydrophobicity of the molecule but increases volume of the molecule slightly. So, volume of tyrosine molecule is slightly bigger than that of phenylalanine, but hydrophobicity of phenylalanine is much higher than tyrosine as shown in Table 5-6. The larger the hydrophobicity of this group, the better the chiral recognition. As a result, enantiomeric excess of Phe enantiomers was higher than that of Tyr enantiomers.

Furthermore, adsorption capacities of the magnetic particles are 0.208 mmol/g for L-Trp, 0.036 mmol/g for D-Trp, 0.141 mmol/g for L-Phe, 0.026 mmol/g for D-Phe, 0.079 mmol/g for L-Tyr and 0.009 mmol/g for D-Tyr after adsorption of racemic amino acids i.e. DL-Trp, DL-Phe and DL-Tyr. Adsorption capacities of $Fe_3O_4/SiO_2/CMCD$ MNPs toward amino acids are in the order: L-Trp>L-Phe>L-Tyr and D-Trp>D-Phe>D-Tyr. Considering the racemic condition, adsorption capacities of the $Fe_3O_4/SiO_2/CMCD$ MNPs are less than those of single enantiomers. The representative chromatograms of racemic amino acid resolution (2 mM) before and after adsorption are shown in Figure 6-3.1- 6-3.3.

Table 6-1 Enantioseparation of amino acids on $Fe_3O_4/SiO_2/CMCD$ MNPs.

Amino acid	k_1	k_2	α	R_s	e.e (enantiomeric excess)
DL-Trp	20.98	25.97	1.23	2.54	94%
DL-Phe	12.05	17.51	1.45	5.70	73%
DL-Tyr	5.21	6.83	1.31	2.69	58%

Chiral separation results of the racemic amino acids in terms of enantiomeric excess obtained in this study compared with other results reported in literature are shown in Table 6-2.

Table 6-2 Comparison of enantiomeric excess obtained using $Fe_3O_4/SiO_2/CMCD$ MNPs with other chiral selectors reported in literature for chiral separation of amino acids.

Amino acid	Chiral selector	Enantiomeric excess	Reference
DL-Trp	Protesase-α-cymotripsin encapsulated in support liquid membrane (SLM)	>99%	[222]
DL-Trp	Carboxymethyl-β-cyclodextrin (CMCD)	94%	This study
DL-Trp	Chitosan functionalized on cellulose acetate membrane	94% (under concentration gradient), 66% (under hydraulic pressure) and −19% (under electric field driven process)	[409]
DL-Trp	Lanthanide Tris(β-diketonates)	53%	[226]
DL-Trp	Bovine Serum Albumin (BSA) immobilized in membrane by ultrafiltration technique	30.8%	[410]
DL-Trp	α-cyclodextrin	14% (single stage separation), >99% (multistage separation)	[411]
α-DL-Trp	Functional ionic liquid (1-ethyl-3-methylimidazolium prolinate [Emim][l-Pro])	$5.9 \pm 0.3\%$	[412]
DL-Phe	L-Chirasil-Val	100%	[201]
[11C]DL-Phe	Crownpak CR(+)	>98%	[413]
DL-Phe	β-CD glutaraldehyde cross-linked in membrane	>81%	[414]
DL-Phe	Protesase-α-cymotripsin encapsulated in support liquid membrane (SLM)	81%	[222]

(Table 6-2 continued)

DL-Phe	Carboxymethyl-β-cyclodextrin (CMCD)	73%	This study
DL-Phe	Lanthanide Tris(β-diketonates)	62%	[226]
α-DL-Phe	Functional ionic liquid (1-ethyl-3-methylimidazolium prolinate [Emim][l-Pro])	35.8 ± 0.1 %	[412]
β-DL-Phe	Functional ionic liquid (1-ethyl-3-methylimidazolium prolinate [Emim][l-Pro])	0.3± 0.1%	[412]
[11C]DL-Tyr	Crownpak CR(+)	>98%	[413]
DL-Tyr	Nitorcellulose	85%	[415]
DL-Tyr	Carboxymethyl-β-cyclodextrin (CMCD)	58%	This study
α-DL-Tyr	Functional ionic liquid (1-ethyl-3-methylimidazolium prolinate [Emim][l-Pro])	21.9 ± 0.3%	[412]
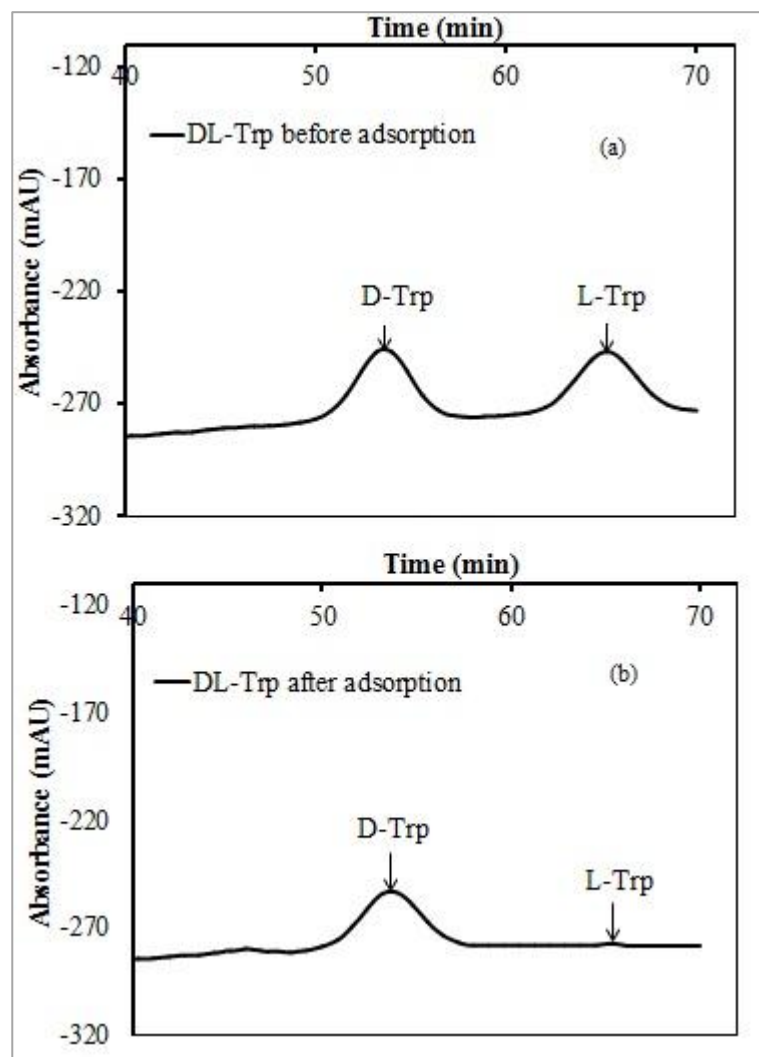
Figure 6-3.1 Chromatogram for HPLC separation of (a) DL-Trp (2 mM) before adsorption, (b) DL-Trp after adsorption onto the modified magnetic nanoparticles. Column Chirex Phenomenx, (150 mm×4.6mmI.D.), maintained at 18°C, mobile phase 2 mM copper sulphate: methanol (70:30).Isocratic elution was carried out as described in the experimental condition at flow rate of 0.7 mL/min. Detection UV 258 nm.
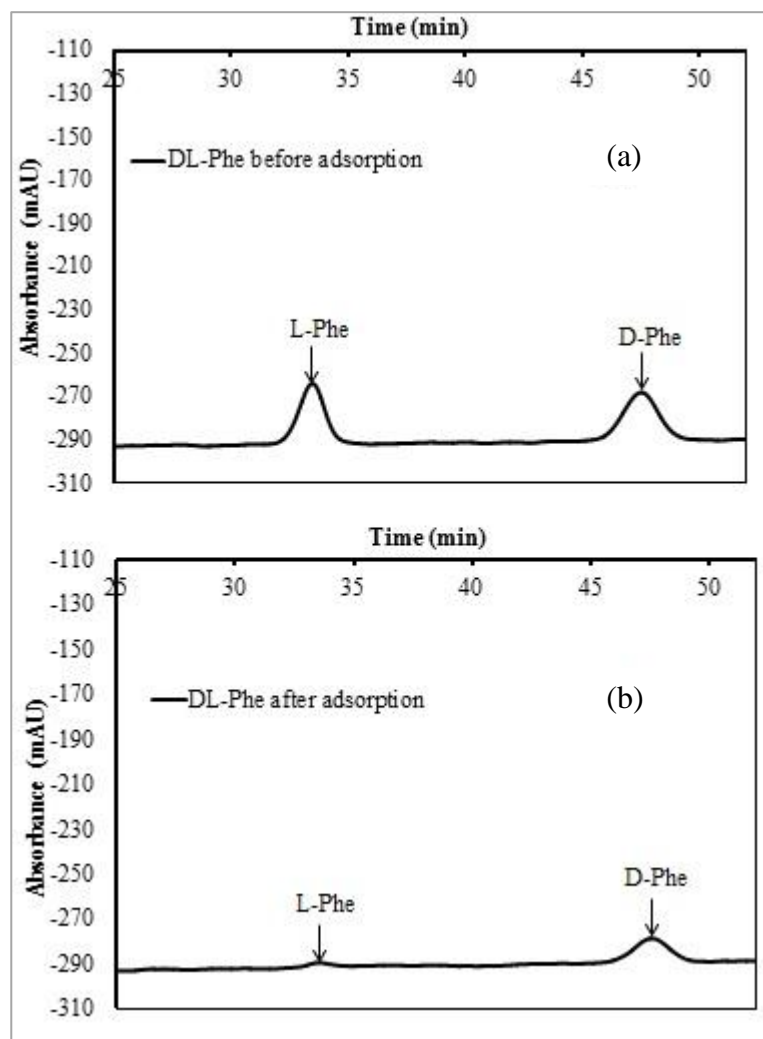
Figure 6-3.2 Chromatogram for HPLC separation of (a) DL-Phe (2mM) before adsorption, (b) DL-Phe after adsorption onto the modified magnetic nanoparticles. Column Chirex Phenomenx, (150 mm×4.6mmI.D.), maintained at 18°C, mobile phase 2 mM copper sulphate: methanol (70:30).Isocratic elution was carried out as described in the experimental condition at flow rate of 0.7 mL/min. Detection UV 258 nm.
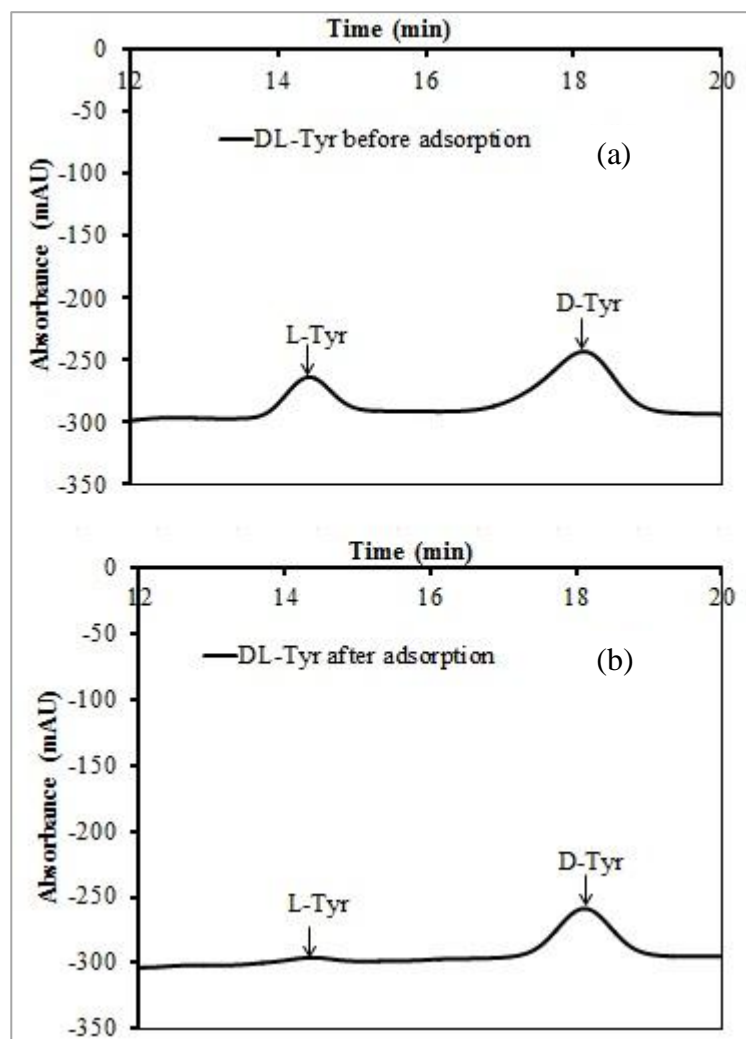
Figure 6-3.3 Chromatogram for HPLC separation of (a) DL-Tyr (2mM) before adsorption, (b) DL-Tyr after adsorption onto the modified magnetic nanoparticles. Column Chirex Phenomenx, (150 mm×4.6mmI.D.), maintained at 18°C, mobile phase 2 mM copper sulphate: methanol (70:30). Isocratic elution was carried out as described in the experimental condition at flow rate of 0.7 mL/min. Detection UV 258 nm.

6.2.1.2 Linearity, limits of detection, reproducibility of the developed method

In order to validate our proposed method for analysis of DL-amino acids, the reproducibility of migration time and peak area were studied. The relationship between D/L-amino acid concentration and UV-absorbance was determined by a series of D- and L-amino acid (Trp, Phe, Tyr) standard solutions. The regression equations and correlation coefficients showed an excellent linear relationship at 0-2 mmol/L for the

analytes. The chromatograms of racemic amino acids as shown in Figure 6-3.1- 6-3.3 clearly indicate that baseline resolution of racemic DL-Trp, DL-Phe and DL-Tyr can be achieved in 68 min, 50 min and 20 min. Determination of final concentration of the separated amino acids was done by the calibration equation with correlation coefficient in the range of 0.996–0.999 as shown in Table 6-3. This establishes that for a given sample of DL-amino acid, precise number of moles can be calculated from the integrated peak areas. Table 6-3 gives the analytical parameters of this method. In the range of 0.01–2 mmol/L good linearities were found for D-Trp, L- Trp, D-Phe, L-Phe, D-Tyr, L-Tyr. The RSDs of the peak areas for calibration curves were between 2.95% and 4.78% for the tested amino acids.

Table 6-3 Analytical parameters for determination of amino acid concentration by HPLC.

Amino acid	Calibration range (mmol/L)	Limit of Detection (LOD), mM	Calibration equation	Correlation coefficient (R^2)	Repeatability, RSD (%)
L-Trp	0.01-2 mmol/L	0.032	y = 0.0001x - 0.0202	0.998	3.19%
D-Trp	0.01-2 mmol/L	0.043	y = 0.0003x + 0.0372	0.997	4.87%
L-Phe	0.01-2 mmol/L	0.048	y = 1121x − 35.333	0.997	2.98%
D-Phe	0.01-2 mmol/L	0.027	y = 1194.5x +6.833	0.999	2.95%
L-Tyr	0.01-2 mmol/L	0.135	y = 0.0015x +0.0408	0.997	3.91%
D-Tyr	0.01-2 mmol/L	0.158	y = 0.0006x - 0.0185	0.996	3.46%

*RSD-Relative Standard Deviation
y- concentration of amino acid enantiomer
x- integrated peak area of the eluted enantiomer

6.2.1.3 Investigations on the mechanism of sorption resolution by XPS and FTIR spectroscopy

To explore the enantioselectivity mechanism of CMCD and silica modified magnetic nanoparticles for aromatic amino acids enantiomers, analysis of FTIR spectra of the modified Fe_3O_4 nanoparticles after adsorption of racemic DL-Trp, DL-Phe and DL-Tyr solution and in absence of the amino acids were performed. As shown in Figure 6-4, an obvious shift from 1635cm^{-1}(CMCD, OH in-plane bending vibration absorption) to 1627 cm^{-1} could be observed after adsorption of DL-Trp solution, which is ascribed to the inclusion complexation of CMCD and guest molecules. As for DL-Trp, peaks at 3047 cm^{-1}(carboxylic acid OH stretching absorption), 1662 cm^{-1}, 1583 cm^{-1}, and 1456 cm^{-1}(benzene's structure skeleton vibration) disappeared after adsorption on CMCD modified Fe_3O_4 nanoparticles. This latter result provides evidence that indole group of DL-Trp entered hydrophobic cavity of CMCD. As shown in Figure 6-4, obvious shifts from 1635 cm^{-1} (CMCD, OH in-plane bending vibration absorption) to 1630 cm^{-1} and 1634 cm^{-1} could be observed after adsorption of DL-Phe and DL-Tyr solution, respectively. As for DL-Phe, peaks at 3064 cm^{-1} (carboxylic acid OH stretching absorption), 1620 cm^{-1}, 1585 cm^{-1}, and 1444 cm^{-1} (benzene's structure skeleton vibration) and for DL-Tyr peaks at 3039 cm^{-1}, 1627cm^{-1}, 1589 cm^{-1}, and 1454 cm^{-1} disappeared after mixing with CMCD modified Fe_3O_4 nanoparticles. All these results provide evidence that phenyl group of DL-Phe and phenol group of DL-Tyr also penetrated into the hydrophobic cavity of CMCD. Thus, hydrophobic portion of these aromatic amino acids interacted with the hydrophobic cavity of CMCD. No change in the Si-O-Si stretching vibration after adsorption of racemic amino acid solution proves that amino acid molecules had interactions only with CMCD on the magnetic nanoparticles' surface.
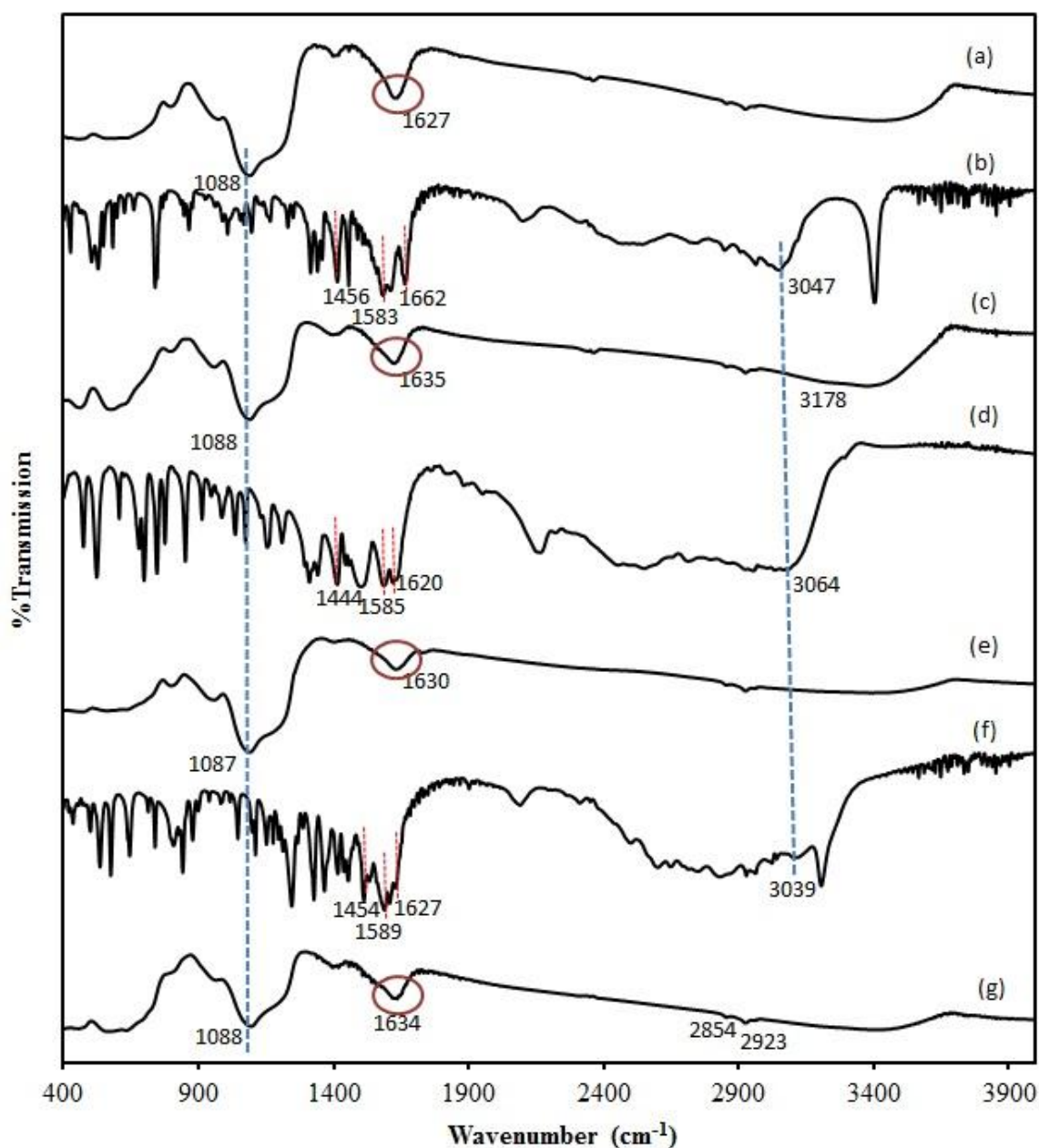
Figure 6-4 FTIR spectra of (a) DL-Trp after adsorption, (b) DL-Trp, (c) Fe₃O₄/SiO₂/CMCD MNPs, (d) DL-Phe, (e) DL-Phe after adsorption, (f) DL-Tyr, (g) DL-Tyr after adsorption.

Furthermore, to ascertain the adsorption site of chiral amino acids on magnetic nanoparticles surface, electronic structure of tryptophan, phenylalanine and tyrosine before and after adsorption were investigated by XPS. Phenylalanine, tyrosine, and tryptophan contain large rigid aromatic groups on the side chain, known as phenyl,

phenol, and indole groups, respectively. Schematic structures of these compounds are shown in Figure 6-1. Tryptophan has two nitrogen atoms, one in the amino group and one in the indole side chain. Phenylalanine and tyrosine each has one nitrogen atom in structure and the presence of hydroxyl group at the benzene ring makes structure of tyrosine different than that of phenylalanine. For better understanding, carbon atom at the chiral centre which is also bonded to the amino group is labelled as C_α, while the carboxylic carbon atom is not labelled. Oxygen atoms are present as carbonyl oxygen and hydroxyl oxygen atoms. XPS analyses results for N1s, C1s and O1s spectra are presented in Table 6-4. The most fascinating XPS spectra of these molecules are those of N1s. In the DL-Trp molecule, there are two nitrogen atoms but three peaks can be deconvoluted from experimental N1s spectra, at 399.2, 399.7, and 400.7 eV in Figure 6-5.1 (a) , which is in agreement with literature [416, 351]. The highest binding energy peak corresponds to the N atom in the pyrrole ring of Trp for bonding N-C (pyrrole) [416]. The other two peaks at lower binding energy are related to the nitrogen for bonds N-H and $N-C_\alpha$. After adsorption of DL-Trp on magnetic nanoparticles, these nitrogen molecules' binding energy shifted to higher eV and most importantly, the binding energy shift of nitrogen atom at N-C(pyrrole) (1.25eV) and N-H (1.75eV) are higher than the binding energy change of nitrogen atom at the $N-C_\alpha$ (0.4 eV). Thus it can be interpreted that the nitrogen atom at the side chain interacted with the secondary hydroxyl group of cyclodextrin cavity and nitrogen atom at the pyrrole ring interacted with the hydrophobic cavity. The N1s XPS spectrums of DL-Phe and DL-Tyr show two peaks due to N-H and $N-C_\alpha$ bonding (Figure 6-5.2, 6-5.3 and Table 6-4). Shifting of nitrogen atom at N-H bonding of DL-Phe and DL-Tyr after adsorption to higher eV also describes that the amino group at the chiral centre interacted well with the hydroxyl group of cyclodextrin rim. Because of the favorability of hydrogen bond formation, the

electron density of nitrogen atom is greatly reduced. As a result, the BE of N 1s increases considerably.

On the other hand, O1s spectra of $Fe_3O_4/SiO_2/CMCD$ MNPs shows two oxygen peaks at 530.3 eV and 532.8 eV due to presence of C=O group and hydroxyl oxygen, respectively which originates from the presence of CMCD on the magnetic nanoparticles surface. Molecular dimensions and functional structure of cyclodextrin molecule are depicted in Figure 6-6(a) and 6-6(b), respectively. As a consequence of the $4C_1$ conformation of the glucopyranose units, all secondary hydroxyl groups are situated on one of the two edges of the cyclodextrin ring, whereas all the primary ones are placed on the other edge. After adsorption of DL-Trp, DL-Phe and DL-Tyr on the magnetic nanoparticles surface, binding energies of hydroxyl oxygen slightly shifted to higher energy which also represent that interaction with secondary hydroxyl group of cyclodextrin rim on the magnetic nanoparticles took place (data shown in Table 6-4). Apart from this, there's no major binding energy shift of C1s spectra of $Fe_3O_4/SiO_2/CMCD$ MNPs before and after adsorption.
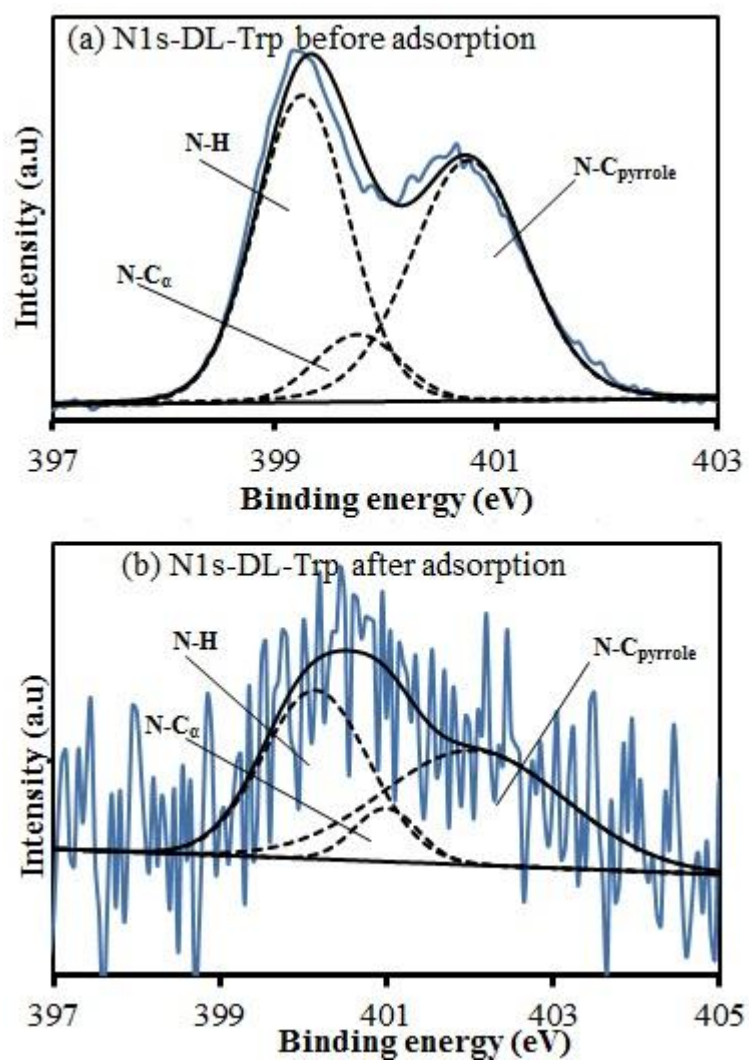
Figure 6-5.1 XPS N1s spectra of (a) DL-Trp, (b) DL-Trp after adsorption.
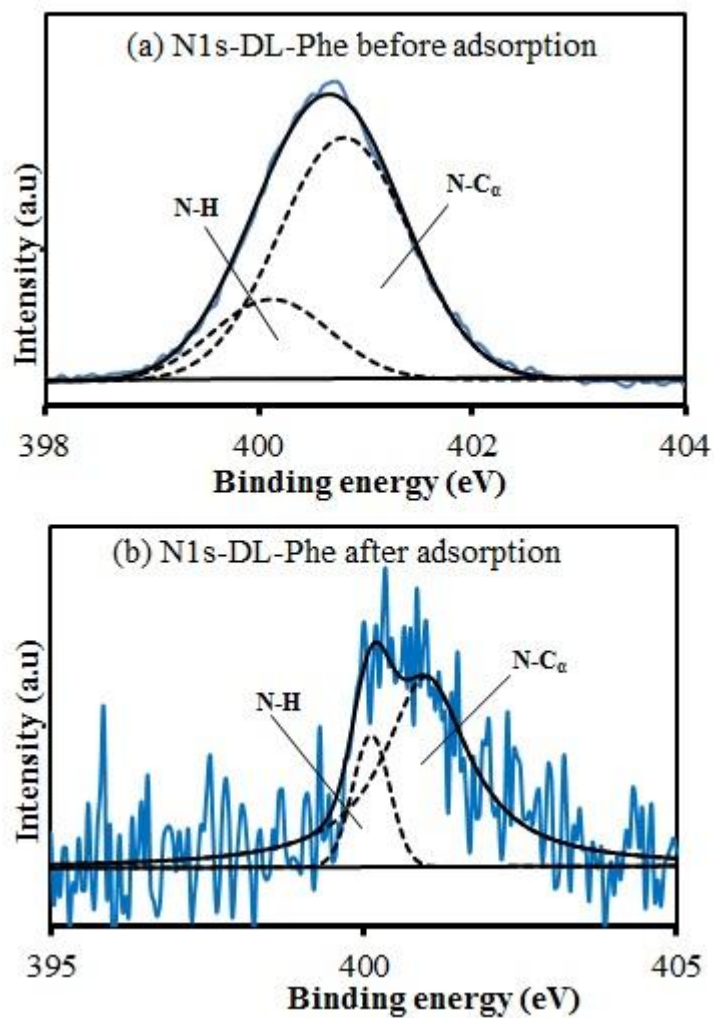
Figure 6-5.2 XPS N1s spectra of (a) DL-Phe, (b) DL-Phe after adsorption.
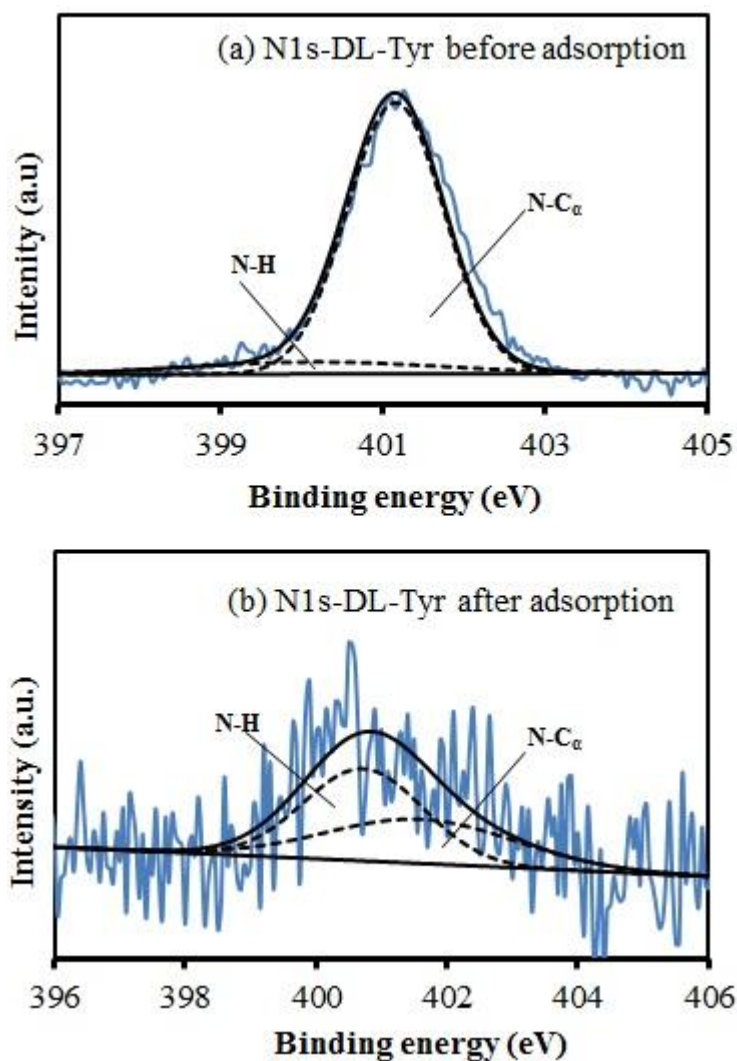
Figure 6-5.3 XPS N1s spectra of (a) DL-Tyr, (b) DL-Tyr after adsorption.

Initially, analysis was done with single enantiomers (Chapter 5) and then interaction point was investigated by analyzing the racemic mixture before and after adsorption. FTIR analysis showed that the hydrophobic portion penetrated into hydrophobic cavity. And XPS analyses further showed that amino group interacted with the secondary hydroxyl group. The magnetic nanoparticles selectively adsorbed L-enantiomers of the amino acids from their racemic mixture which could be due to favorability of hydrogen bond formation between secondary hydroxyl groups of cyclodextrin molecule and amino group of L-enantiomers compared to that of D-enantiomers [381]. As depicted

from Figure 6-1, differences between three dimensional structures of D- and L-enantiomers are in the position of primary amine group. In this case, primary amine group at the chiral center of the D-enantiomers might have positioned less favorably for hydrogen bonding, which might have resulted in less adsorption capacities of D-enantiomers followed by subsequent chiral separation of DL-amino acid. Structure of beta cyclodextrin and simplified adsorption mechanism of L-Trp and D-Trp onto $Fe_3O_4/SiO_2/CMCD$ MNPs are depicted in Figure 6-6.

Table 6-4 XPS data analyses for adsorption of racemic amino acids.

Element	Binding energy (eV)						
	Fe_3O_4/SiO_2 /CMCD MNPs	DL-Trp	DL-Trp (after adsorption)	DL-Phe	DL-Phe (after adsorption)	DL-Tyr	DL-Tyr (after adsorption)
N1s	-	399.2 (N-H) 399.7(N- Cα) 400.7(N-Cpyrole)	400.95(N-H) 400.1(N- Cα) 401.95(N-Cpyrole)	400.1 (N-H) 400.8 (N-Cα)	400.3 (N-H) 401(N- Cα)	400.15(N-H) 401.1(N-Cα)	400.7(N-H) 401.45(N-Cα)
C1s	284.6 (C-C/C-H) 286 (C-O/C-O-C) 287.9 (C=O) 288.7(COO⁻)	284.6(C-C) 285.5(C-C) 286.1(C-Cα) 288.6(COOH)	284.6(C-C) 286.2(C-C) 287.8(C-Cα) 288.9(COOH)	284.2 (C-C) 285.7(C-Cα) 287.5(COOH)	284.6(C-C) 285.3(C-Cα) 286.8(C-O/C-O-C) 288.6(COOH)	284.6(C-C) 286.2(C-Cα) 288.6(COOH)	284.2(C-C) 285.7(C-Cα) 287.5(C-O/C-O-C) 288.2(COOH)
O1s	530.3(C=O) 532.8 (-OH)	530.7(C=O) 531.65(-OH)	531(C=O) 533.6(-OH)	530.2(C=O) 531.05(-OH)	530.5(C=O) 533.1(-OH)	530.5(C=O) 531.7(-OH)	530.2(C=O) 532.9(-OH)

(a)

(b)

(c)

(d)
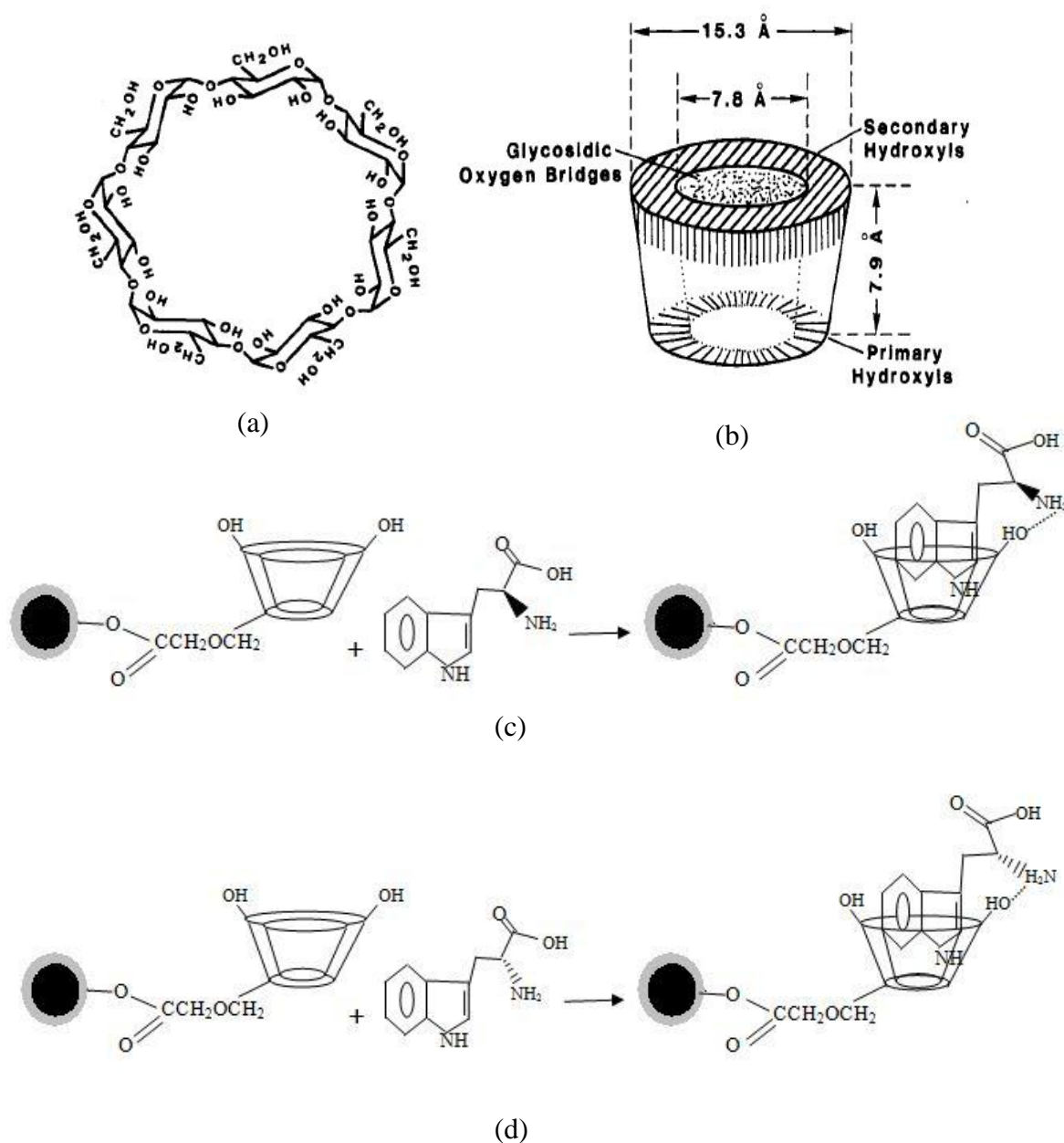
Figure 6-6 (a) Structure of β- cyclodextrin, (b) molecular dimensions and functional structural scheme of β-cyclodextrin, (c) simplified schematic showing adsorption mechanism of L-Trp onto $Fe_3O_4/SiO_2/CMCD$ MNPs, (d) simplified schematic showing adsorption mechanism of D-Trp onto $Fe_3O_4/SiO_2/CMCD$ MNPs.

6.2.2 Flurometric titrations

At the optimum experimental conditions, fluorescence intensity of inclusion complexes in aqueous solution was measured and corresponding fluorescence spectral changes upon addition of different concentrations of CMCD to the L-Trp solution are shown in Figure 6-7(a). In the titration experiments using fluorescence spectrometry,

fluorescence intensity of D-Trp, L- and D-Phe and L- and D-Tyr also gradually changed with increasing concentration of CMCD (data not shown). When concentration of CMCD was increased, fluorescence maximum of L-Trp-CMCD was slightly blue shifted with a gradual increase in fluorescence. This behavior could be attributed to the enhanced dissolution of the guest molecule, through the hydrophobic interaction between guest molecule and non-polar cavity of CMCD. As a result, fluorescence intensity increased as CMCD concentration was increased. Similar changes were observed while studying inclusion complex formation of amino acid with native β-CD [417].

It is also crucial to determine the stoichiometric ratio of inclusion complex formation. Employing the conventional double reciprocal method, stoichiometry and inclusion constant for the host guest combination from analysis of sequential changes of fluorescence intensity is determined at various host concentrations using the following equation [418, 419]:

$$\frac{1}{F\text{-}F_0} = \frac{1}{(F_\infty\text{-}F_0)K[CD]_0} + \frac{1}{(F_\infty\text{-}F_0)} \qquad \text{[6-1]}$$

Where, F is the determined fluorescence intensity of the amino acid solution at each CMCD concentration. F_0 and F_∞ are the fluorescence intensity in the absence of CMCD and when all the amino acid molecules were included, respectively. K is the stability constant for inclusion complex formation and $[CD]_0$ denotes the concentration of CMCD solution. K can be calculated from a plot of $1/(F\text{-}F_0)$ vs. $1/[CD]_0$. Figure 6-7 (b) shows the double reciprocal plots of $1/(F\text{-}F_0)$ versus $1/[CD]_0$ for L-Trp inclusion complexation with CMCD at pH 6. The plot exhibits good linearity (the linear regression coefficient $R^2 = 0.996$). This verifies the formation of inclusion complexes

with a stoichiometry of 1:1 between L-Trp and CMCD. It is also observed that the other enantiomers (D-Trp, L-Phe, D-Phe, L-Tyr and D-Tyr) formed inclusion complexes with CMCD with same stoichiometry (1:1). The inclusion complex stability constant (K) of CMCD with L-Trp is estimated to be 1000 M^{-1}. The stability constant (K) was measured form curve fitting method while Gibbs free energy changes (-$\Delta G°$) for the inclusion complexation of CMCD with L-/D-enantiomers were determined from the equation: $\Delta G° = -RT \ln K$ (K=stability constant) [420]. The stability constants along with free energy changes (-ΔG^o) between CMCD and the amino acid enantiomers obtained are listed in Table 6-5.
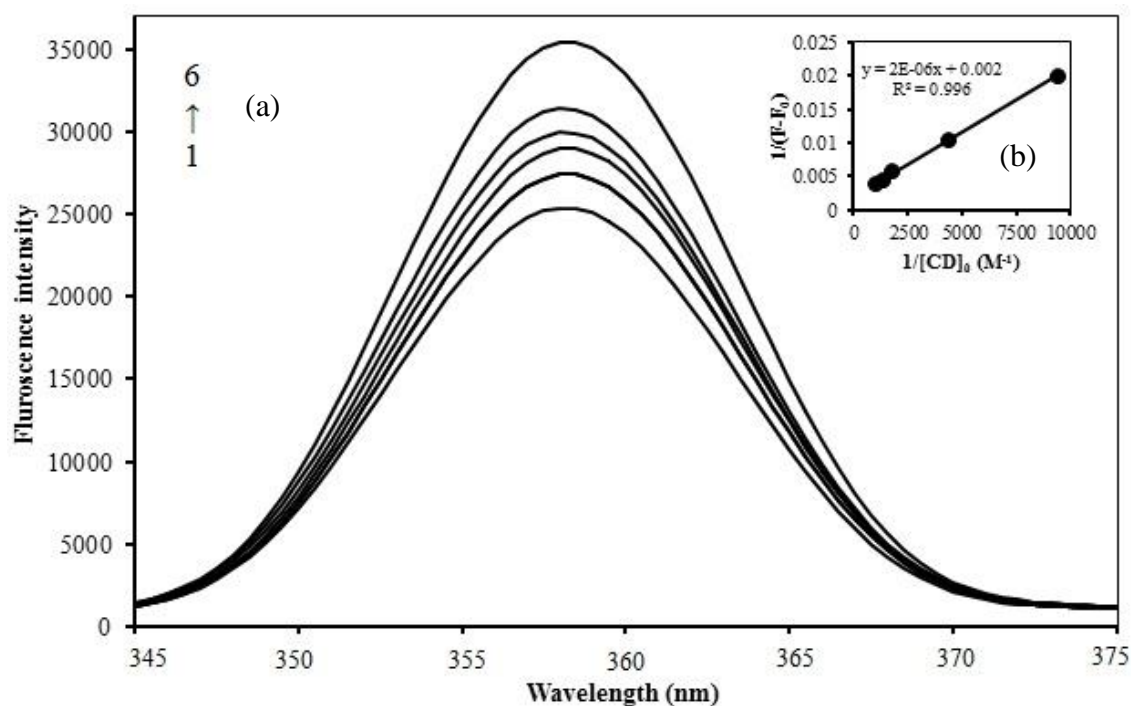
Figure 6-7 (a) Fluorescence spectrum of L-tryptophan upon addition of CMCD of various concentrations at 25°C; [L-tryptophan]=3×10^{-5} mol/L, concentration of CMCD: (1) 0, (2) 1.06x10^{-4} mol/L, (3) 2.27x10^{-4} mol/L, (4) 5.69x10^{-4} mol/L, (5) 7.26x10^{-4} mol/L, (6) 9.68 x10^{-4} mol/L (from 1 to 6), (b) double reciprocal plot for L-Trp inclusion complexes with CMCD.

Table 6-5 The Stability Constants (K) and the Gibbs Free Energy Changes ($-\Delta G^o$) for the inclusion complexation of L-and D-Trp, L-and D-Phe and L- and D-Tyr with CMCD in 0.03 mol/L phosphate buffer Solution (pH 6) at 25°C, determined by flurometric titrations.

Host	Guest	K (stability constant), M^{-1}	Log K	$-\Delta G^o$ (kJ/mol)
CMCD	L-Trp	1000	3	17.11
	D-Trp	650	2.69	16.05
	L-Phe	600	2.77	15.80
	D-Phe	450	2.65	15.12
	L-Tyr	300	2.47	14.09
	D-Tyr	250	2.39	13.63

One of the most important features of inclusion complexation is the simultaneous operation of several weak interactions between the guest and host, which have been proved by the extensive studies on molecular recognition by cyclodextrins [420]. In the present case, hydrogen-bonding and hydrophobic interactions of the hydrophobic part and functional sidearm attached to the edge of cyclodextrin cavity are considered to be jointly responsible for the inclusion complexation. As can be seen from the Table 6-5, stability constant for inclusion complex formation is higher for Trp enantiomers than the other enantiomers, which might have resulted in better adsorption capacities of the nanoparticles toward the Trp enantiomers. And the values of stability constants for L-enantiomers are higher than those of D-enantiomers which also confirm our previous observations regarding higher adsorption capacities of the magnetic particles toward L-enantiomers. Finally the negative values of Gibb's free energy change show the spontaneous nature of inclusion complex formation.

6.3 Conclusions

In short, silica and carboxymethyl-β-cyclodextrin functionalized Fe_3O_4 magnetic nanoparticles were utilized for enantioselective separation of racemic aromatic amino acid solution. The as-synthesized magnetic nanoparticles preferentially adsorbed L-enantiomers of Trp, Phe and Tyr than the D-enantiomers and offered significant enantiomeric excess in aqueous system. XPS and FTIR spectroscopy were applied to investigate the enantioselective mechanism and it was found that hydrophobic portion of amino acid penetrated completely into the cyclodextrin cavity and the amino group of the amino acid molecules formed hydrogen bond. Apparently, hydrophobicities of the amino acids influenced the interaction with cyclodextrin molecules to different degrees and thus resulted in different enantiomeric excesses. Flurometric studies also supported the observation of higher binding of CMCD to L-enantiomer compared to D-enantiomers. The proposed method offers promising synthesis of adsorbents, rapid analysis, high enantiomeric excess and reliable quantitative assay. Thus, the as-synthesized CMCD functionalized magnetic nanoparticles with all significant properties would have great potentials in chiral separation technologies.

Chapter 7: Adsorptive removal of emerging contaminants from aqueous solutions using superparamagnetic Fe₃O₄ nanoparticles bearing aminated β-cyclodextrin

7.1 Introduction

Over the last decade, environmental pollution by pharmaceutically active compounds (PhACs) and endocrine disrupting chemicals (EDCs) in different water sources and industrial effluents aroused the public concern [421, 282]. Pharmaceuticals are class of emerging environmental contaminants that are increasingly being used in human and veterinary medicine [363]. EDCs are anthropogenic chemicals with the potential to elicit negative effects on the endocrine systems of humans and wildlife. Their occurrence is most often a result of municipal waste-water discharge, as these compounds are not completely removed in sewage treatment plants [422]. Wide range of PhACs and EDCs were found ubiquitously up to μgL^{-1} level in aqueous environment, soil, waste-water, surface water, sediments, groundwater and even drinking water [278, 423]. Due to the adverse effects on living creatures and persistency of these emerging contaminants in environment, removal of these contaminants is of great importance.

Several treatment techniques for the removal of PhACs and EDCs from environmental matrices have been investigated, including coagulation-flocculation, adsorption, chlorination, electrochemical oxidation, ozonation, and photocatalytic oxidation [253,424-428]. Among these methods, adsorption has become one of the most promising techniques, due to its convenience, efficiency and economy. Moreover, adsorption to remove pollutants without disturbing quality of water or leaving behind any toxic degraded products has competed with electrochemical, biochemical or

photochemical degradation processes. So far, removal of PhACs and EDCs have been achieved by adsorption using activated carbons [282, 427], carbon nanomaterials [429], zeolites [423], minerals [430], hybrid particles [431, 432], inorganic-organic modified bentonite [279], mesoporous silica based materials [433] etc. However, these types of adsorbents suffer from separation inconvenience though some have high adsorption capacities. Therefore, efforts are still needed to carry out investigation for new promising adsorbents with high capacity and recognition and ease of separation.
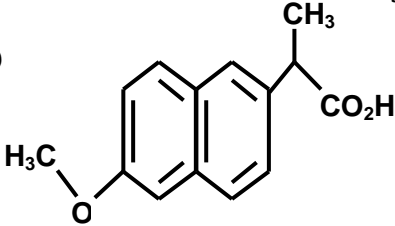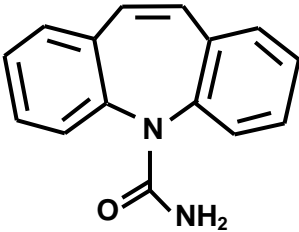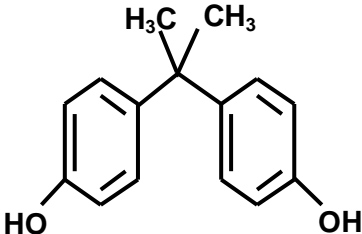
Recently, functionalized magnetic nanocomposites have received many attentions for use in adsorption of both organic and inorganic pollutants [150, 434, 435]. Magnetic nanoadsorbents can bind with non-magnetic target molecules via some intermediates forming complex which can be easily separated and recovered from multiphase systems, opening the door for sorbent regeneration, safe disposal of waste and/or recovery of loaded species. For effective removal of toxic contaminants from waste-water, functional magnetic nanomaterials are synthesized by anchoring immobilized polymer, inorganic or organic molecules to surface. For example, Guo et al. prepared magnetic molecularly imprinted polymers based on kaolinite/Fe_3O_4 for selective adsorption and separation of BPA [436]. Ispas et al. developed biomagnetic capsule platform with immobilized enzyme as an environmentally benign method incorporating both sensing and removal capabilities for BPA [437]. However, to the best of our knowledge, detailed studies of adsorption characteristics of pharmaceuticals and EDCs from aqueous solution onto superparamagnetic Fe_3O_4 nanoparticles bearing cyclodextrin moieties are very scarce in literature.

β-cyclodextrin (β-CD) is a cyclic oligosaccharide consisting of 7 D-glucopyranose units joined together by α (1–4) linkage forming a torus-shaped ring structure with a hydrophilic exterior and a hydrophobic cavity. They can form inclusion complexes with

a wide variety of compounds in their hydrophobic cavity [18]. While some research have been done using cyclodextrin functionalized magnetic nanoparticles for drug delivery [163, 151] and biomolecule purification [438], very little attention has been paid to their explicit application to remove PhACs and EDCs from waste-water.

The aim of this study was to investigate the adsorption characteristics for removal of PhACs and EDCs from aqueous solutions using β-CDen (en: -NHCH$_2$CH$_2$NH$_2$) functionalized Fe$_3$O$_4$ nanospheres (CDen-MNPs), in which β-CDen provides the ability to adsorb organic pollutants through inclusive host-guest interactions, while Fe$_3$O$_4$ nanoparticles serve as magnetic separators. Two PhACs- carbamazepine (CBZ) and naproxen (NAP) and one EDC- Bisphenol A (BPA) were chosen as model contaminants as they are ubiquitous in waste-water effluent, surface water and groundwater [282]. CBZ is a basic therapeutic agent for treatment of epilepsy, trigeminal neuralgia, bipolar affective disorder and acute mania [253]. NAP is a nonsteroidal anti-inflammatory drug which has been shown to be persistent in environment [439]. BPA is one of the endocrine disrupters which can affect reproductive behavior of both human and animals [440]. BPA is commonly found in aquatic and terrestrial environments because of its widespread use as an intermediate compound in preparation of epoxy resins and polycarbonates [441]. Physicochemical properties of CBZ, NAP and BPA are presented in Table 7-1. In this study, influence of several parameters such as initial pH, contact time were investigated on adsorptive removal of CBZ, NAP and BPA from aqueous solutions. Adsorption behaviors of CDen-MNPs with these emerging contaminants were studied using both equilibrium and kinetic viewpoints. Finally, desorption of pharmaceuticals and EDC was studied with ethanol to assure regeneration possibility of the magnetic particles.

Table 7-1 Physicochemical properties of the three target compounds.

Compound	Molecular structure	LogK_{ow}	Log$D$	pK_a	Water solubility (mg/L at 25°C)
Naproxen (MW=230.3)		3.18[a]	3.15 (pH 3), 0.33 (pH 7)	4.15[a]	15.9[a]
Carbamazepine (MW=236.3)		2.45[a]	2.45 (pH 3), 2.45 (pH 7)	13.9[a]	17.7[a]
Bisphenol-A (MW=228.3)		3.30[b]	3.32 (pH 3), 3.32 (pH 7)	9.6[b], 10.2[b]	129[c]

[a] Data from reference [282]

[b] Data from reference [442]

[c] Data from reference [443]

7.2 Results and discussions

7.2.1 Characterization of as-synthesized magnetic nanoparticles

In this study, β-CDen (en = -NHCH$_2$CH$_2$NH$_2$) was grafted on the surface of magnetic nanoparticles via layer-by-layer method. Initially, Fe$_3$O$_4$ nanoparticle surface was functionalized with thiodiglycolic acid (TDGA) which provides carboxylic acid (-COOH) functional groups for linking amino containing CD molecules. The thiol group (-SH) present in TDGA was combined with magnetic particles as sulfur has great

affinity for iron. β-CDen was grafted on the surface of TDGA coated magnetic nanoparticles through amide (-NH-CO-) bond formation. HOBt and EDC were added in the reaction mixture to promote the amide bond formation between carboxylic acid groups on the magnetic particle surface and amino group on cyclodextrin. Figure 7-1 illustrates the synthetic routes for preparation of β-CDen conjugated magnetic nanoparticles. When CDen-MNPs were added into solution containing PhACs and EDCs, immobilized β-CDen adsorbed the micropollutant through inclusion and hydrophobic interactions. The pollutant-adsorbed particles were then separated from solution by applying an external magnetic field.
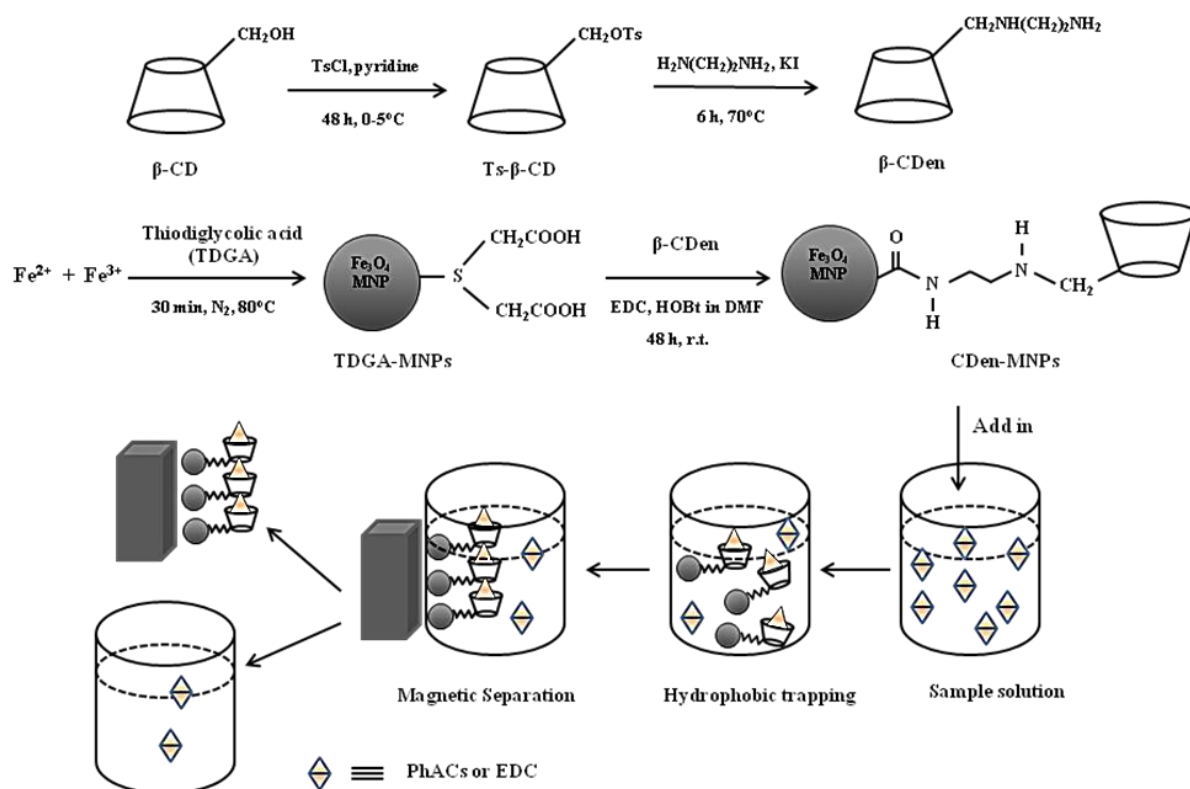
Figure 7-1 Schematic illustration of the fabrication of the β-CDen modified magnetic nanoadsorbent and mechanism for separation of PhACs and EDCs.

7.2.1.1 FTIR analysis

The reaction pathway for grafting β-CDen on the surface of TDGA-MNPs was verified by FT-IR studies. Figure 7-2 shows IR spectra of TDGA-MNPs, CDen-MNPs and β-CDen in the range of 400-4000 cm^{-1} wave number. It is shown that the characteristics adsorption band of Fe–O bonds in the tetrahedral sites of TDGA-MNPs is 586 cm^{-1}. Strong absorption band at 3427 cm^{-1} is due to O-H stretching vibration. However, the TDGA coating over the surface of TDGA-MNPs can be confirmed with the bands at 1633 cm^{-1} from carbonyl C=O stretching present in TDGA. The above characteristic bands can be observed with a little shift after the modification with β-CDen. In the spectrum for CDen-MNPs, the characteristics peaks at 1030, 1080 and 1153 cm^{-1} can be observed due to immobilized β-CDen on the surface. The peak at 1030 cm^{-1} is due to α-1,4-bond skeleton vibration of β-CDen and the peak at 1080 and 1153 cm^{-1} correspond to the antisymmetric glycosidic v_a(C–O–C) vibrations and the coupled v(C–C/C–O) stretch vibration, respectively. Thus, the comparison between FTIR spectra of TDGA and β-CDen coated magnetite nanoparticles gives evidence for successful grafting of β-CDen on the magnetite surface which is further supported by XPS and thermal analysis.
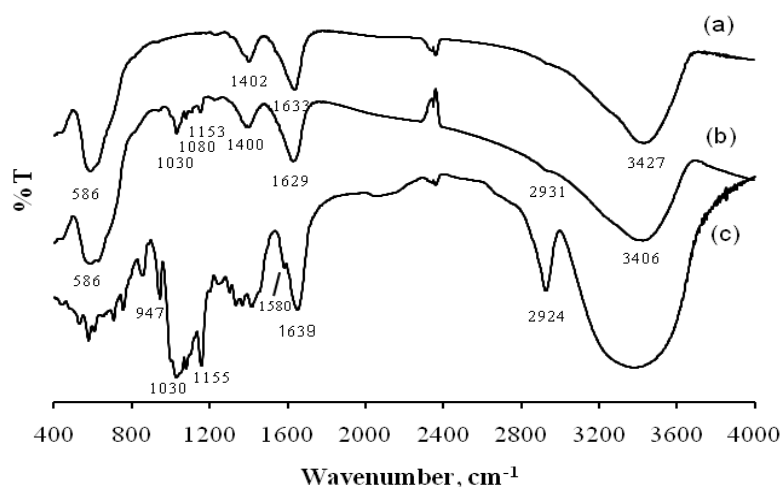
Figure 7-2 FTIR spectra of (a) TDGA modified magnetic nanoparticles (TDGA-MNPs), (b) β-CDen conjugated magnetic nanoparticles (CDen-MNPs) and (c) β-CDen.

7.2.1.2 TEM images

High Resolution TEM (HRTEM) was applied to characterize the size and morphology of the nano-magnetic nanoparticles. Typical TEM image of CDen–MNPs is shown in Figure 7-3. It shows that magnetic nanoparticles bonded with β-CDen are sphere-like shaped or ellipsoidal particles with nano-size. The mean diameter calculated from the TEM image was estimated as 11.5 nm.
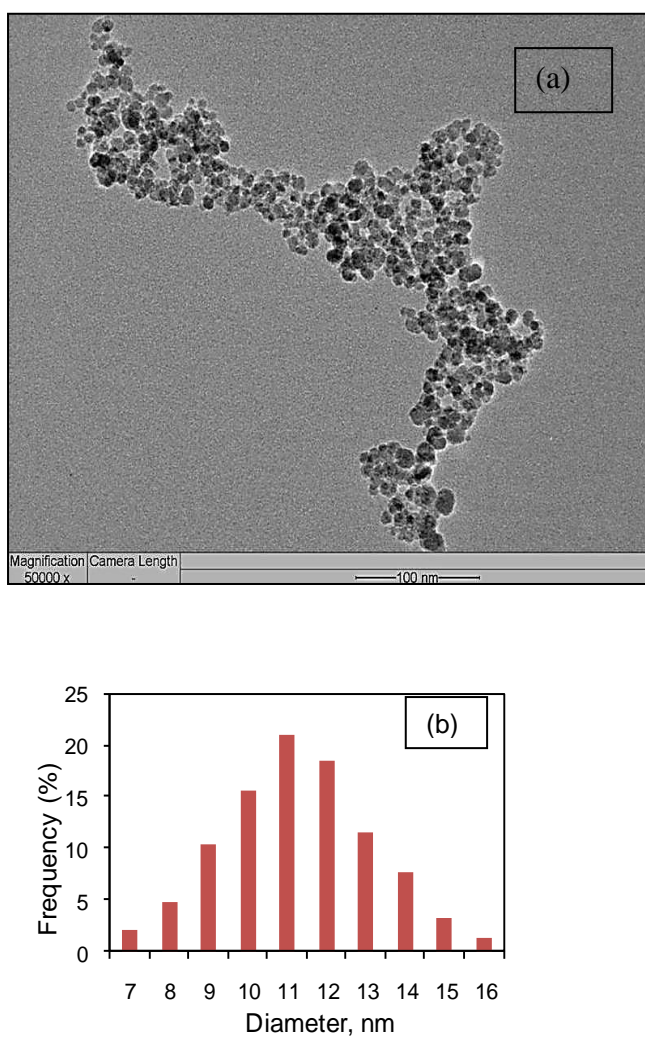
Figure 7-3 (a) TEM image and (b) particle size distribution of CDen-MNPs. (Scale bar is 100 nm).

7.2.1.3 XRD analysis

The crystal structures of uncoated MNPs, TDGA-MNPs and CDen–MNPs were characterized by X-ray diffraction (XRD) as shown in Figure 7-4. The six characteristic peaks at 2θ = 30.5°, 35.9°, 43.4°, 53.4° 57°, and 63.1° are related to their corresponding indices (220), (311), (400), (422), (511), and (440), respectively. For all the samples, absence of the peaks (110) (2θ = 21.22°) and (104) (2θ = 33.15°) indicates that both goethite (α-FeOOH) and hematite (α-Fe_2O_3) did not form in the as-synthesized samples since the two compounds present characteristic diffraction peak of (110) and (104), respectively [151, 444]. This revealed that the resultant nanoparticles were pure Fe_3O_4 with a spinel structure and the grafting of β-CDen onto TDGA-MNPs did not result in the phase change of Fe_3O_4. The crystal size of CDen-MNPs can be evaluated from XRD pattern by using Scherrer's equation, [$D= (0.9\lambda/\beta cos\theta)$]; where D is the average crystalline diameter, 0.9 is the Scherrer constant, λ is the X-ray wavelength, β is the angular line width of half-maximum intensity and θ is the Bragg's angle in degree. Here, the (311) peak of the highest intensity was used to evaluate crystal size of the magnetic particles and the average crystal size of CDen-MNPs was calculated to be 10.4 nm which is slightly less than that observed from the TEM images.
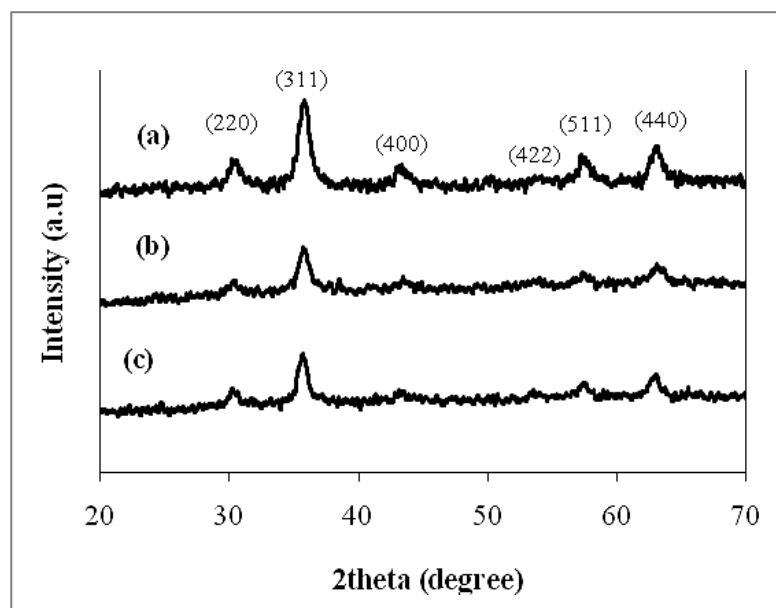
Figure 7-4 XRD patterns of (a) uncoated MNPs, (b) TDGA modified magnetic nanoparticles (TDGA-MNPs), (c) β-CDen modified magnetic nanoparticles (CDen–MNPs).

7.2.1.4 X-ray photoelectron spectroscopy (XPS) analysis

XPS analysis was applied to find the chemical binding in the as-synthesized TDGA-MNPs and CDen-MNPs. Wide scan spectra of TDGA and β-CDen bonded magnetic nanoparticles are shown in Figure 7-5. The binding energy of S2p of both samples is 161.3 eV, which indicates the deposition of thiodiglycolic acid on magnetic surface. The appearance of nitrogen (N1s) bands implies the grafting of β-CDen on the surface of TDGA modified magnetic nanoparticles. The C1s deconvoluted spectra are also shown in Figure 7-5. The C 1s core-level spectrum of TDGA-MNPs can be curve-fitted into three peak components with binding energies at about 284.6, 285.7 and 288.7 eV, attributable to the C–C, C–S and O–C=O species, respectively. For CDen-MNPs, the C1s spectrum can be curve-fitted into five peak components with binding energy of about 284.6, 285.7, 286, 288.2 and 288.7 eV, attributable to C–C, C–S and C–O/C–O–C (alcoholic hydroxyl and ether), O=C–N, and O–C=O (carboxyl) species, respectively [164]. The C-S peak confirms the deposition of thiodiglycolic acid on the magnetic

184

surface. The <u>C</u>–O/<u>C</u>–O–<u>C</u> peaks are the characteristic of β-CDen. Moreover, the peak for O=<u>C</u>-N at 288.2 eV indicates that β-CDen reacted with the free COOH functional groups on TDGA-MNPs through amide bond formation. Thus, the modification of magnetite surface with β-CDen was confirmed.
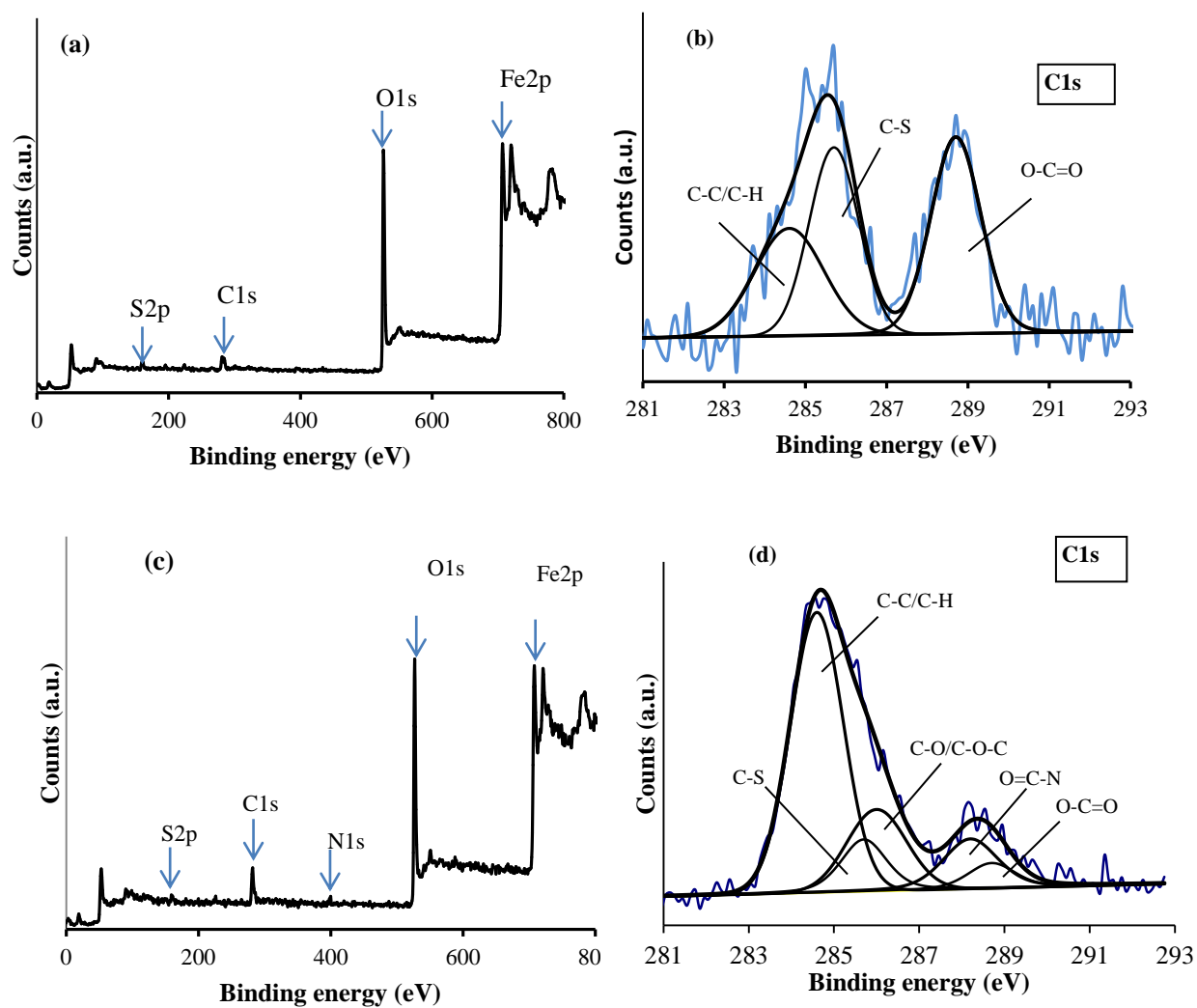
Figure 7-5 XPS wide scan and C1s deconvoluted spectra for TDGA-MNPs (a-b) and for CDen-MNPs (c-d).

7.2.1.5 Thermogravimetric (TGA) analysis

The amount of β-CDen grafted on the surface of magnetic nanoparticles was estimated from the thermogravimetric analyses of uncoated, TDGA coated, and β-CDen coated nanoparticles. As shown in Figure 7-6, the TGA curve of uncoated MNPs shows weight loss of 2.2 % over the temperature range 30–200°C which might be due to the loss of residual water in the sample. The total weight loss over the full temperature range is estimated to be 3.3% due to the loss of adsorbed water as well as dehydration of the surface –OH groups. The TGA curves for TDGA-MNPs exhibits two steps of weight loss, contributed from the loss of residual water in the sample in 30–200°C and the loss of TDGA (~3.5%) in the range of 200–450 ^{o}C. From the TGA curve for CDen-MNPs, a drastic drop of 9.5% can be seen in the range 190–430°C and it is contributed from the thermal decomposition of thiodiglycolic acid and β-CDen moieties. Below 200 ^{o}C, the rate of weight loss is relatively slow owing to the loss of residual water adhering to the sample surface and adsorbed in the β-CD cavities. So far, the TGA curves also confirm successful grafting of β-CDen molecules on the surface of nanoparticles. From these data, the amount of β-CDen grafted onto the surface of CDen-MNPs was estimated to be 0.050 mmol g^{-1}.
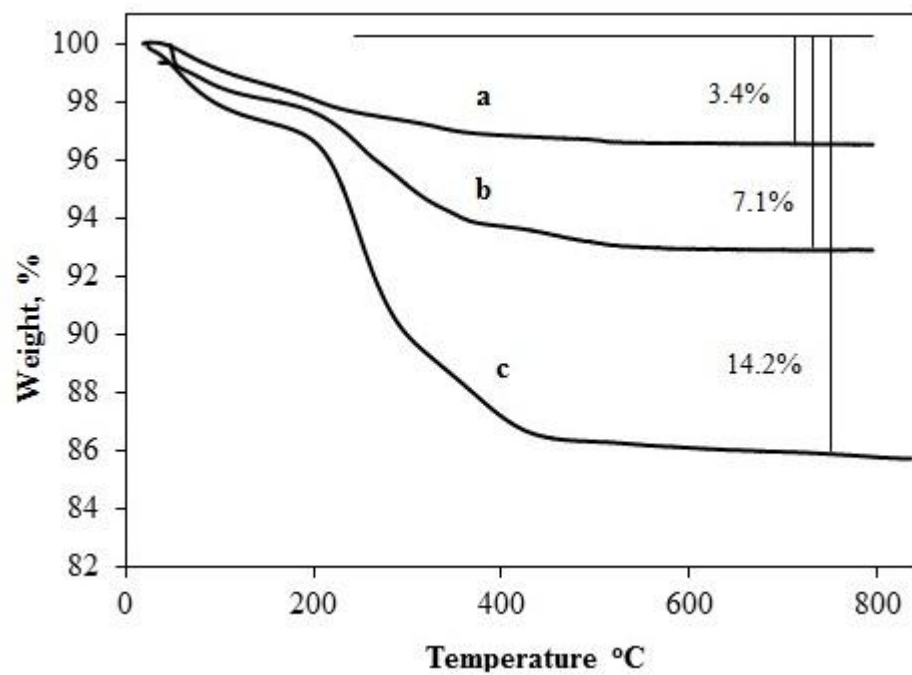
Figure 7-6 TGA curves of (a) uncoated Fe_3O_4 nanoparticles (MNPs), (b) TDGA modified magnetic nanoparticles (TDGA-MNPs), and (c) β-CDen modified magnetic nanoparticles (CDen–MNPs).

7.2.1.6 VSM analysis

The magnetization curve for the uncoated Fe_3O_4 nanoparticles and CDen-MNPs at room temperature is shown in Figure 7-7. The magnetic hysteresis loop of the sample indicates no remanence and reveals its superparamagnetic nature, which is beneficial to their dispersibility and redispersibility in the solution. Superparamagnetism is the responsiveness to an applied magnetic field without retaining any magnetism after removal of the applied magnetic field. The saturated magnetization of samples is quite high, which guarantees quick response of these nanoparticles to external magnetic fields. However, the saturated magnetization obtained for CDen-MNPs (57.1 emu/g) at same field was lower than that of uncoated Fe_3O_4 (75 emu/g). This is mainly attributed to the existence of non-magnetic materials (TDGA and β-CDen layer) on the surface of nanoparticles. Thus both the superparamagnetic property and high magnetization of the as-prepared nanoparticles are ideal for practical applications.
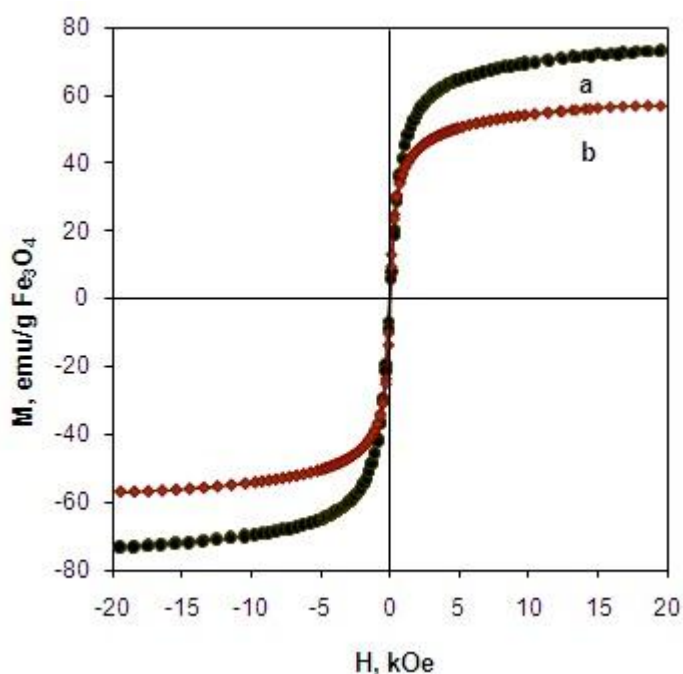
Figure 7-7 Magnetization curve for (a) unmodified MNPs, (b) β-CDen modified magnetic nanoparticles (CDen–MNPs).

7.3 Adsorption study

7.3.1 Effect of initial pH

Effect of pH on removal of PhACs and EDCs by CDen-MNPs were explored in this work, because solution pH was known to affect properties of both adsorbents and adsorbates. Figure 7-8 shows adsorption capacities of magnetic nanoadsorbents toward CBZ, NAP and BPA at different pH. For CBZ, adsorption capacity of nanoadsorbent was not affected by solution pH in the tested pH range (pH 3 to 11). But, when solution pH increased from 3 to 11, adsorption capacity of acidic pharmaceutical, NAP reduced gradually. For BPA, adsorption capacity of the sorbent decreased as pH was increased from 9 to 11. Adsorption of contaminants onto CDen-MNPs can be controlled by both non-electrostatic and electrostatic interaction. CBZ, NAP and BPA were present in either neutral or ionized forms, depending upon solution pH. Speciation of chemicals can be determined by the Henderson–Hassel Balch equations [54].

For an acid, the Henderson–Hassel Balch equation is,

$$pH = pK_a + \log\left(\frac{[A^-]}{[HA]}\right) \hspace{3cm} [7\text{-}1]$$

For a base, the equation is,

$$pH = pK_a + \log\left(\frac{[B]}{[BH^+]}\right) \hspace{3cm} [7\text{-}2]$$

where, pK_a is acid dissociation constant of weak acid BH^+. Ratio of conjugated acid and base can be calculated using solution pH and pKa value for the compound. In the case of CBZ ($pK_a = 13.9$), it exists as a neutral compound in tested pH range (Figure 7-9). Thus its binding onto CDen-MNPs is solely attributable to nonelectrostatic interaction involving hydrogen bonding, hydrophobic and van der Waals interactions. For acidic pharmaceutical, NAP where the pK_a values is 4.15 (Table 7-1), the chemical

is neutral (HA) at pH $\leq$ 3 and anion (A⁻) at pH > 6. Thus, adsorption of NAP onto CDen-MNPs is highest at pH 3 due to favourable hydrophobic interaction between adsorbent and the neutral adsorbate. As pH increased from 3 to 11, less favourable interaction occurred between ionized NAP molecules and hydrophobic cyclodextrin molecule, hence, adsorption capacity of CDen-MNPs toward NAP decreased.

It can be also seen that when pH value of solution was lower than 9, adsorption of BPA by CDen-MNPs was not influenced by pH values while increase in pH above 9 resulted in a gradually decreased adsorption. It was reported that interaction forces between BPA and cyclodextrin molecules are hydrogen bonding, van der Waals force and hydrophobic interaction [445]. However, a decreasing trend at a higher pH ranging from 8 to 11 was also observed when insoluble cross-linked cyclodextrin polymers were used as adsorbents [446]. The result could be elucidated by the pK_a value of BPA ranging from 9.6 to 10.2 [443], implying that ionization of BPA occurred at around pH 9–11 to form the phenolate and bisphenolate anions as shown in Figure 7-9. Its hydrophobic character would be lowered greatly on the formation of anion. The phenolate anions have fewer tendencies to be included in the hydrophobic cavity of cyclodextrin; hence adsorption capacity of CDen-MNPs was reduced.
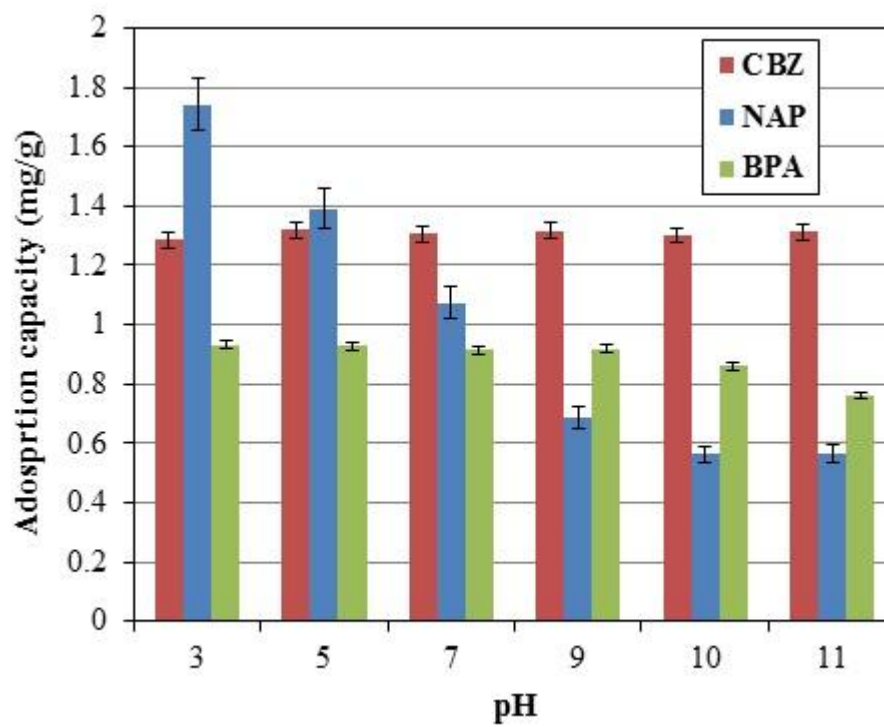
Figure 7-8 Effect of pH on adsorption capacity of CBZ, NAP and BPA. Experimental conditions: $[CBZ]_0$, $[BPA]_0$ and $[NAP]_0$: 20 ppm; volume of solution: 5 mL; contact time: 4 hrs; temperature: 25°C.
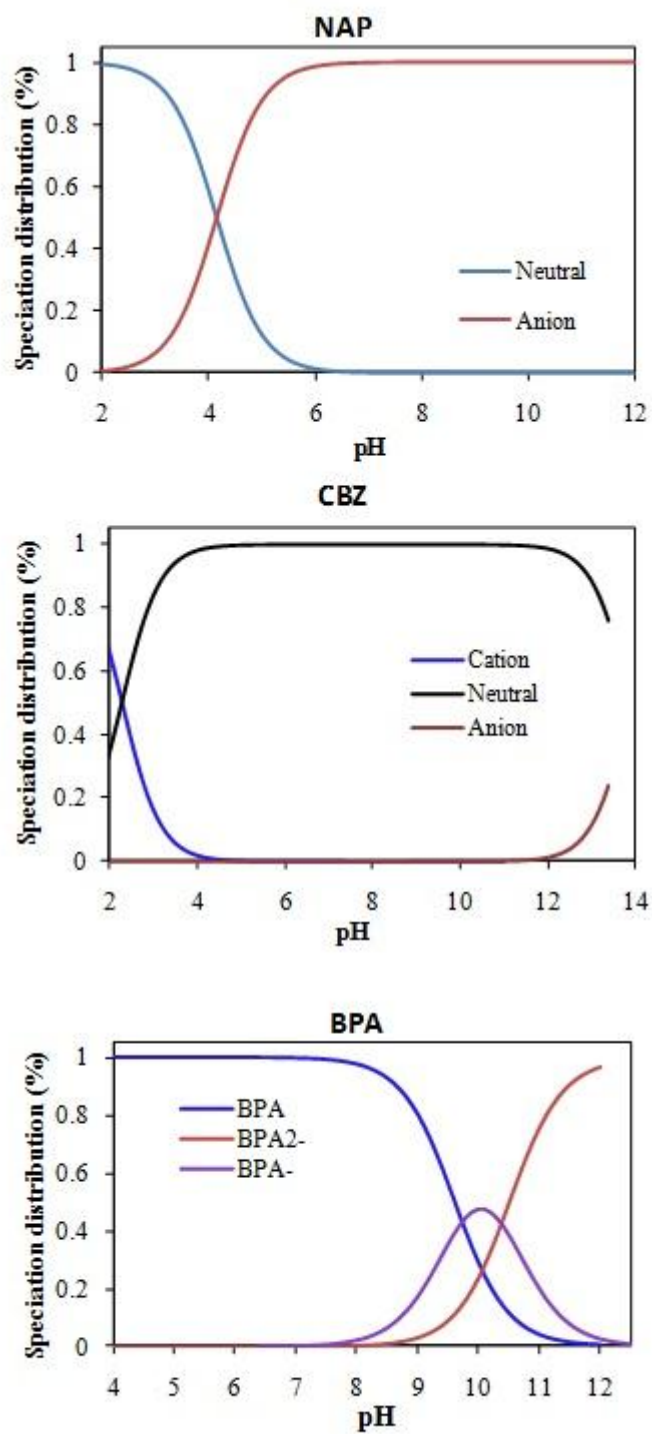
Figure 7-9 The species distribution diagrams of NAP, CBZ and BPA.

7.3.2 Effect of contact time and adsorption kinetics

For effective designation and representation of the on-going adsorption process, study

of kinetics of the adsorption process was carried out. Figure 7-10(a) shows the influence

of contact time on adsorption of CBZ, NAP and BPA. High adsorption rate was observed at the initial stage due to rapid attachment of adsorbates to the surface of adsorbents. In case of BPA, above 95% of the equilibrium adsorption value occurred in the first 40 min. And, in case of NAP, more than 95% of equilibrium value occurred in the first 60 min. And thereafter rate of adsorption of CBZ was found to be slow and the equilibrium was reached and remained constant at nearly 2 hrs contact time. One possible reason for difference in rate of adsorption of CBZ, NAP and BPA onto magnetic nanoparticles could be different size of molecules with respect to cavity size of β-CD. The size of targeted contaminant is important because molecular diameter in a size range similar to molecular size of adsorbent is one important factor that determines the progression of adsorption of a given adsorbent. Xiao et al. found that molecular sizes and structures of three pharmaceuticals, namely levofloxacin, aspirin and acetaminophen influenced sorption rates on cyclodextrin based polymer [447]. Among three organic molecules studied here, diameter of BPA molecule is the smallest (3.83Å) [443], thus the adsorption of BPA onto CDen-MNPs reached equilibrium very fast. Since size of the CBZ molecule (7.60 Å) and NAP molecule (7.60 Å) are comparable to the cavity size of β-CD (7.8 Å) [311], it took more time to reach adsorption equilibrium for these two pharmaceuticals. However, adsorption of NAP onto these nanoadsorbents was faster than that of CBZ. This could be related to their molecular structures which might affect their inclusion into cavity of β-CDen. Noteworthy, the naphthalene moiety of NAP is of the planar structure, whereas the benzene rings in the carbamazepine structure are nonplanar. In this study, shaking time of 4 hrs was used in all further adsorption experiments to ensure equilibrium.

The data of adsorption kinetics of CBZ, NAP and BPA onto CDen-MNPS were examined with Lagergren pseudo-second-order model. The Lagergren rate equation is

one of the most widely used adsorption rate equations for adsorption of solute from a liquid solution. Pseudo-second-order kinetic model is expressed by the following equation [331]:

$$\frac{t}{Q_t} = \frac{1}{k_2 Q_e^2} + \frac{1}{Q_e} t \qquad\qquad [7\text{-}3]$$

Where k_2 is equilibrium rate constant of pseudo-second-order adsorption (g/(mg.min)). Slope and intercept of the plot of t/Q_t versus t were used to calculate the second-order rate constant, k_2 (Figure 7-10 (b)). Correlation coefficient (R^2) for pseudo-second-order adsorption model has high value (>99%), and Q_e values ($Q_{e,cal}$) calculated from pseudo-second-order model are more consistent with the experimental Q_e values ($Q_{e,exp}$). These facts suggest that adsorption data are well represented by pseudo-second-order kinetic model and overall rate of the adsorption process appears to be controlled by the chemical interactions. Pseudo-second-order adsorption of some selected pharmaceuticals and EDCs have also been reported for many adsorbents such as mesoporous silica SBA-15 [278], magnetic molecularly polymers (MMIPs) based on kaolinite/Fe_3O_4 composites [436] and multiwalled carbon nanotube [253]. Parameters of pseudo-second-order rate model for adsorption of CBZ, NAP and BPA on the nanoadsorbents are presented in Table 7-2.
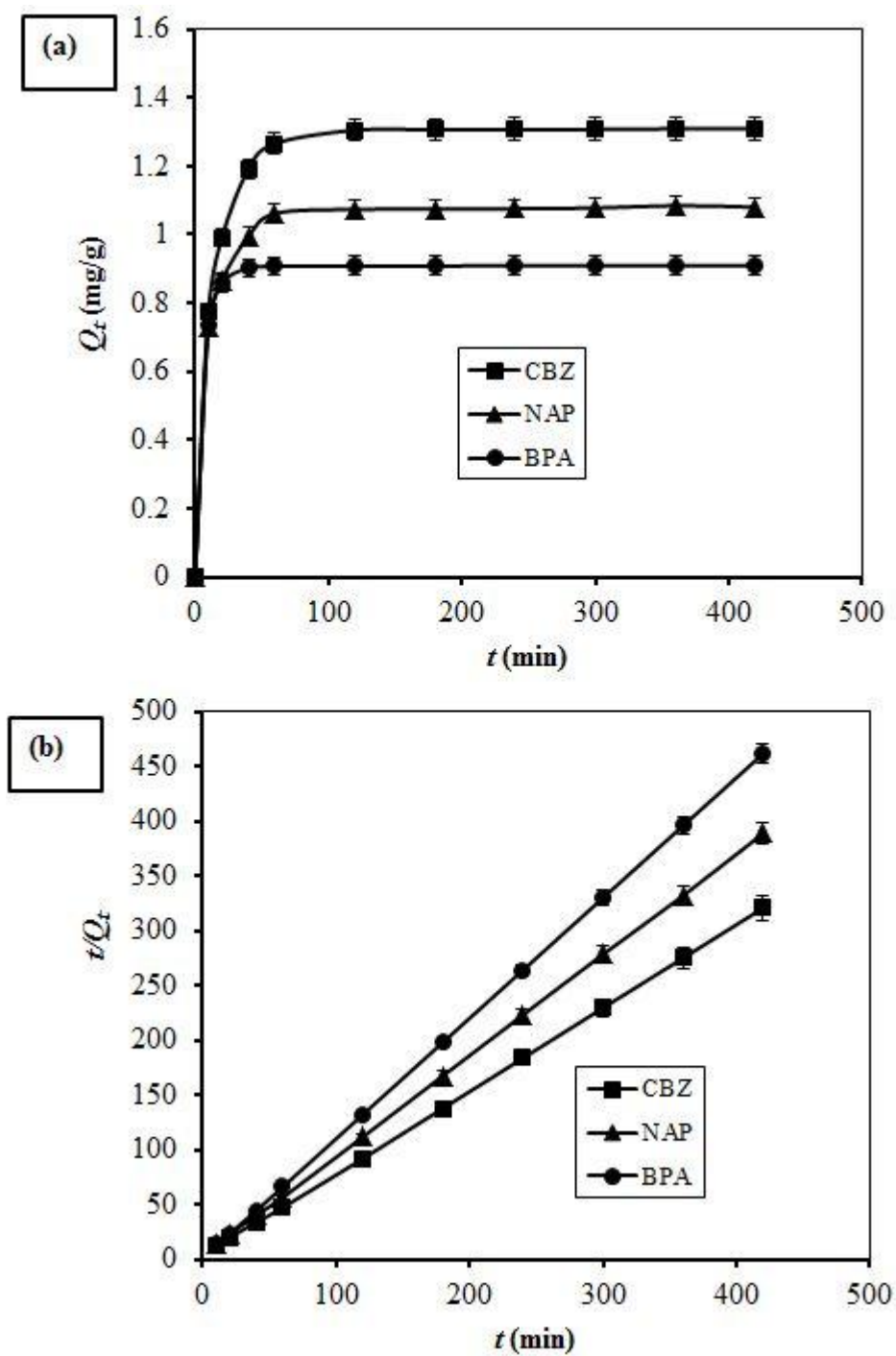
Figure 7-10 (a) Effect of contact time on adsorption capacities of CBZ, NAP and BPA at pH 7 and 25°C; (b) Linear plot of pseudo-second-order kinetic model for CBZ, NAP and BPA adsorption.

Table 7-2 Adsorption kinetic parameters of CBZ, NAP and BPA onto CDen-MNPs at 25°C and pH 7.

Pharmaceutical / EDC	Initial conc. C_i (ppm)	Lagergren pseudo-second-order model parameters			
		k_2, g/(mg. min)	Q_e^b, mg/g	R^2	Q_e^a, mg/g
CBZ	20	0.160	1.328	0.999	1.31
NAP	20	0.260	1.090	0.999	1.07
BPA	20	1.051	0.912	0.999	0.90

[a] experimental

[b] calculated

7.3.3 Isotherm test and role of physicochemical properties of pollutants

The equilibrium isotherms for the adsorption of CBZ, NAP and BPA in single solute system by TDGA-MNPs and CDen-MNPs at pH 7 and 25°C are shown in Figure 7-11. From various isotherm equations that may be used to analyze adsorption data in aqueous phase, the Langmuir-the theoretical equilibrium isotherm and the Freundlich-the empirical equilibrium isotherm are the most common models. The Langmuir equation can be expressed as [325]:

$$\frac{C_e}{Q_e} = \frac{1}{Q_m k_L} + \frac{C_e}{Q_m}$$

[7-4]

where Q_e is amount of adsorbed material at equilibrium (mg/g), C_e the equilibrium concentration in solution (ppm), Q_m the maximum capacity of adsorbent (mg/g), and k_L is the "affinity parameter" or Langmuir constant (L/mg).

On the other hand, Freundlich isotherm gives an empirical expression encompassing surface heterogeneity and exponential distribution of active sites and their energies. The linear form of Freundlich equation, which is an empirical equation derived to model heterogeneous adsorption, can be represented as follows [326]:

$$ln\, Q_e = ln\, k_F + \frac{1}{n} ln\, C_e \qquad\qquad [7\text{-}5]$$

Where, Q_e and C_e are defined as above, k_F is Freundlich constant (L/g), and n is heterogeneity factor. The adsorption isotherm parameters for PhACs and EDC are represented in Table 7-3.
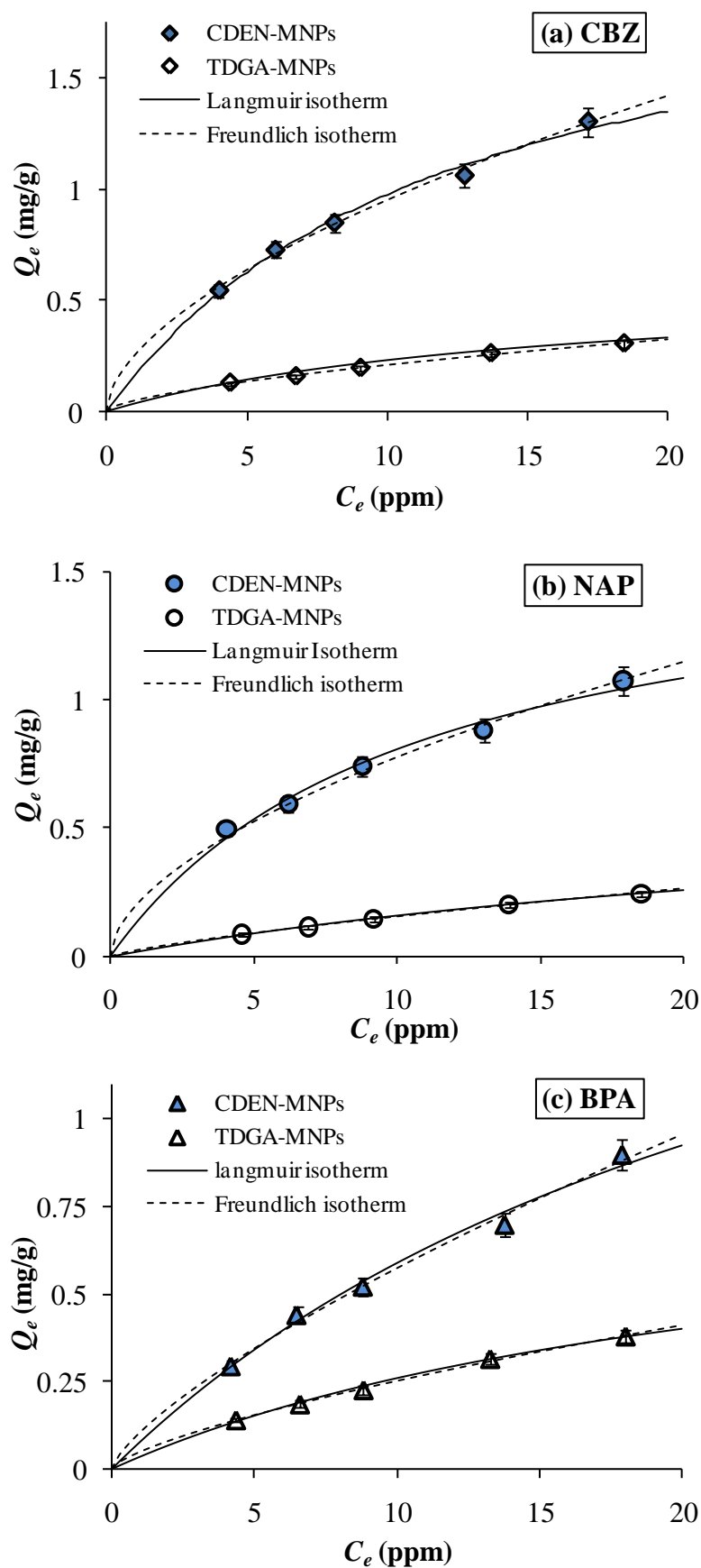
Figure 7-11 The adsorption isotherm of (a) CBZ, (b) NAP and (c) BPA on CDen-MNPs and TDGA-MNPs at pH 7 and 25°C.

Table 7-3 Adsorption isotherm parameters for NAP, CBZ and BPA onto CDen-MNPs and TDGA-MNPs at 25ºC and pH 7.

Isotherm Models	Parameters	NAP		CBZ		BPA	
		CDen-MNPs	TDGA-MNPs	CDen-MNPs	TDGA-MNPs	CDen-MNPs	TDGA-MNPs
Langmuir	Q_m (mg/g)	1.656	0.677	2.186	0.593	2.162	0.872
	k_L (L/mg)	0.095	0.030	0.080	0.063	0.037	0.042
	R^2	0.975	0.972	0.980	0.964	0.926	0.967
Freundlich	*(1/n)*	0.564	0.765	0.579	0.632	0.736	0.707
	k_F (L/g)	0.212	0.026	0.249	0.048	0.105	0.049
	R^2	0.998	0.995	0.995	0.995	0.993	0.998

As can be seen from Figure 7-11, maximum adsorption capacities of TDGA-MNPs towards CBZ, NAP and BPA are 0.307, 0.244 and 0.378 mg/g, respectively at 25°C and pH 7, whereas those using CDen-MNPs are 1.304, 1.074 and 0.899 mg/g, respectively at the same experimental conditions. Thus, CDen-MNPs could adsorb CBZ, NAP and BPA more than twice than that by TGDA coated magnetic nanoparticles indicating that modification of magnetite surface with β-CDen which had hydrophobic cavity had enhanced adsorption capacities. However, all the experimental data were fitted well with Freundlich isotherm model than Langmuir model ($R^2 > 0.99$). Thus, the adsorption process is governed by heterogeneous adsorption.

The isotherms in Figure 7-11 show that in the investigated concentration range, absorbabilities of the three target compounds on CDen-MNPs decreased as their hydrophobicity, which can be expressed as their octanol–water partition coefficients ($\log K_{ow}$) increased (Table 7-1). It was reported that $\log K_{ow}$ is an important factor in

evaluation of adsorption capacity for a given micropollutant; and a micropollutant with a higher $\log K_{ow}$ value should have higher sorption affinity on CDen-MNPs [282]. Considering the $\log K_{ow}$ values, the absorbabilities of these pollutants on CDen-MNPs would have been in the order of BPA > NAP > CBZ instead of CBZ > NAP > BPA. The relatively lower adsorption affinity of NAP compared to CBZ found in this study could be mainly attributed to dissociation of acidic naproxen at pH values. This result is in agreement with the observation reported by Yu et al. [282]. Adsorption capacity of nano-adsorbent bearing cyclodextrin moieties toward CBZ, NAP and BPA is based on two factors, namely, the hydrophobicity (conditioned by the value of octanol water partition coefficient, K_{ow}) and ionization of the molecules (determined by values of pH and pK_a). Both parameters K_{ow} and pK_a are taken into account for calculation of $\log D$. $\log D$ is a pH-dependent modified octanol water partition coefficient and is relevant for solutes that are partly dissociated or protonated. It can be calculated using following equations. For acidic molecules $\log D$ is determined as:

$$\log D = \log K_{ow} - \log(1 + 10^{(pH-pKa)})\qquad\text{[7-6]}$$

Whereas for basic molecules $\log D$ is:

$$\log D = \log K_{ow} - \log(1 + 10^{(pKa-pH)})\qquad\text{[7-7]}$$

The modified $\log D$ value for NAP decreases from 3.15 at pH 3 to 0.33 at pH 7 while $\log D$ values for CBZ, and BPA are constant at pH 3-7 (Table 7-1) based on above equation [443, 54]. According to the modified hydrophobicity values, BPA is most hydrophobic at pH 7 and hydrophobicity of CBZ is higher than that of NAP. The chemical structure of CDen-MNPs (Figure 7-1) suggests that presence of ionizable groups on the surface is very limited. Thus, hydrophobic interaction between β-CDen

and target molecules should be dominating. As a result, higher adsorption capacities of CDen-MNPs toward more hydrophobic CBZ than that of NAP are justified. However, hydrophobicity would not explain the lowest adsorption affinity of BPA on CDen-MNPs, though BPA is a neutral compound at pH 7. There might be other interactions between CDen and BPA molecules. Yu et al. also observed that nonylphenol-an endocrine disrupter was least absorbable among naproxen, carbamazepine and nonylphenol on activated carbon, though nonylphenol has high $\log K_{ow}$ value [282]. To elucidate the underlying mechanisms for BPA adsorption results in relation to the other two compounds in this study, FTIR spectra were obtained for β-CDen and solid complex residues containing inclusion complexes of CBZ/β-CDen, NAP/β-CDen and BPA/β-CDen (see section 7.3.6).

7.3.4 Adsorption of a mixture of pharmaceuticals and EDCs

As the emerging contaminants usually occur in the environment as a mixture, the investigation of adsorption of a mixture of these contaminants is necessary as a succeeding step for further application. Figure 7-12 represents the results for adsorption results of a mixture of two pharmaceuticals and one EDC onto CDen-MNPs as a function of initial concentration. At pH 7, adsorption capacities of the adsorbent were higher for CBZ than those of NAP and BPA. In other word, adsorption capacities of CDen- MNPs toward CBZ, NAP and BPA are in the same order as obtained in single adsorption study. At initial concentration of 20 ppm for each component, adsorption capacity of the CDen-MNPs toward CBZ, NAP and BPA were 0.51, 0.45 and 0.34 mg/g, respectively. It can be interpreted that there exist some kind of binding or interactions among CBZ, NAP and BPA and CDen-MNPs which induce adsorption of the three compounds at the same time on surfaces of these magnetic adsorbents. At pH 7, there should be more favourable interaction among neutral CBZ and the adsorbents

bearing pendant hydrophobic β-CDen moieties than those of NAP and BPA. Considering the mixed condition, adsorption capacities of CDen-MNPs were somewhat smaller than that of individual cases.
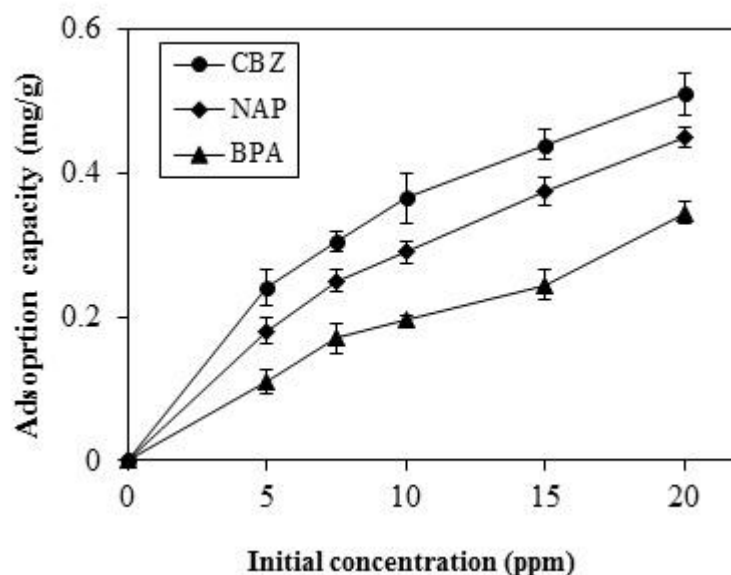
Figure 7-12 Adsorption of a mixture of CBZ, NAP and BPA onto CDen-MNPs as a function of initial concentration. (Contact time, 4 hrs; temperature, 25°C; pH 7).

7.3.5 Desorption study

Desorption study was done in this work to explore the regeneration and reusability of modified magnetic nanoparticles. Desorption of the CBZ, NAP and BPA was demonstrated using ethanol as desorbing agent. It was found that desorption efficiency achieved was around 80% 75% and 89% for CBZ, NAP and BPA using ethanol as eluent. Alcohol solution was used by researchers to desorb organic pollutants from other cyclodextrin-based adsorbents. For example, Aoki et al. also found that 4-nonylphenol ethoxylates (NPEs) was successfully released from chitosan bearing cyclodextrin beads using 50% ethanol solution [445].
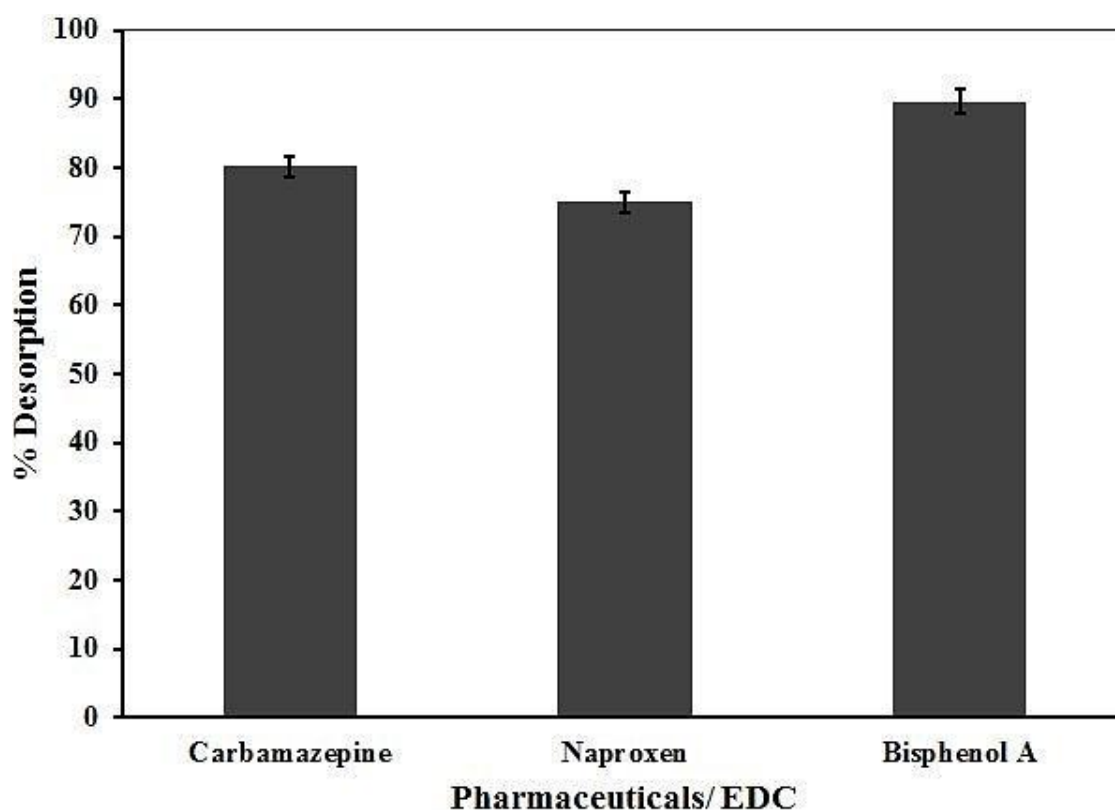
Figure 7-13 Desorption of CBZ, NAP and BPA from CDen–MNPs in ethanol. Adsorption conditions: CDen–MNPs: 100 mg; CBZ, NAP and BPA concentration: 20 ppm; temperature: 25°C; pH: 7; contact time: 4 hrs. Desorption conditions: CDen–MNPs: 100 mg; temperature: 25°C; contact time: 6 hrs.

7.3.6 Interaction of pharmaceuticals/EDC and β-CDen

Inclusion complexes among the pharmaceuticals and β-CDen were investigated with FTIR spectroscopy to gain insight of the interaction among the molecules. FTIR spectra obtained for β-CDen and solid complex residues containing inclusion complexes of CBZ/β-CDen, NAP/β-CDen and BPA/β-CDen are shown in Figure 7-14. To be more accurate, discussion in this section would focus on FTIR bands in two regions: 900-1750 cm^{-1} and 2800-3250 cm^{-1}. It is very interesting to note that, presence of CBZ, NAP and BPA does not cause significant shifts of the FTIR bands in the residues containing complexes of CBZ/β-CDen, NAP/β-CDen and BPA/β-CDen in the range of wavenumber 900-1750 cm^{-1} as compared to bands in native CBZ/NAP/BPA (Figure 7-

14, Table 7-4). It can be interpreted that not much strong interaction exists between CBZ, NAP and BPA and C–C, C–O–C, OH groups of β-CDen. Firstly, the νC–O of residues increases of about 1–6 cm^{-1} as compared to that of native CBZ/NAP/BPA. These shifts may be associated with the intramolecular hydrogen bonds formed between these groups of β-CDen in the presence of CBZ, NAP and BPA [448]. Bonenfant et al. also observed that FTIR spectra of nonylphenol ethoxylates/ β-CD and nonylphenol/β-CD inclusion complex residues shows small differences with native β-CD in the wavenumber region of 800-1400 cm^{-1} [448]. Hence, it can be suggested that hydrogen bonding is less dominant in formation of inclusion complex.

In the spectra, bands observed in the region 2800-3250 cm^{-1} are associated with asymmetric and symmetric ν CH$_2$ stretching vibrations (ν CH$_2$) and bands identified in the region 900-1750 cm^{-1} are assigned to C–O, C–C, C–O–C stretching, and O–H in planar angular deformation vibrations (νC–O, νC–C, νC–O–C, and (δO–H) of complexes [448]. Figure 7-14 shows νCH$_2$ stretching of β-CDen at 2924 cm^{-1} increased 4 cm^{-1}, 4 cm^{-1} and 8 cm^{-1} for the residues of CBZ/β-CDen, NAP/β-CDen and BPA/ β-CDen which indicates van der Waals interaction took place between β-CDen and BPA than those of CBZ and NAP (Figure 7-14, Table 7-4). Van der Waals interaction is considered to be weak compared to hydrogen bonding or electrostatic interaction and as a result of this weak van der Waals interaction between BPA and β-CDen, adsorption capacities of the magnetic particles toward BPA was less. According to Alvira et al., van der Waals interactions are considered to contribute to the formation of inclusion complexes with β-CD [449]. Mimeault and Bonenfant have shown that the strengthening of the van der Waals interactions in the alkyl chains causes shifts of νCH$_2$ in the inclusion complexes [450].
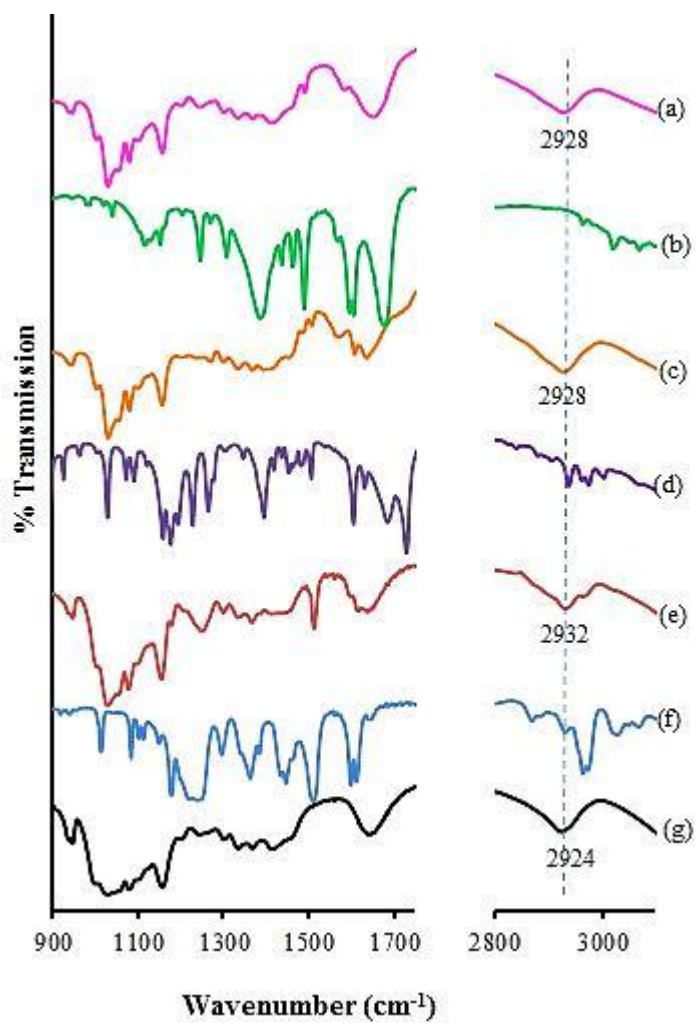
Figure 7-14 FTIR spectra of (a) CBZ/β-CDen inclusion complex, (b) CBZ, (c) NAP/β-CDen inclusion complex, (d) NAP, (e) BPA/β-CDen inclusion complex, (f) BPA, (g) β-CDen.

Table 7-4 Maximum wavenumber of FTIR bands of CBZ, CBZ/β-CDen inclusion complex, NAP, NAP/β-CDen inclusion complex, BPA, BPA/β-CDen inclusion complex and β-CDen.

Mode	Wavenumber (cm^{-1})						
	CBZ	CBZ/ β-CDen	NAP	NAP/ β-CDen	BPA	BPA/ β-CDen	β-CDen
ν CH$_2$	3020		3002		3029		
	2983	2928		2928		2932	2924
δ O-H		1335	1346	1335		1335	1335
ν C-O	1154	1156	1158	1159	1150	1156	1158
ν C-C		1079		1081		1079	1082
ν C-O-C		1028		1028		1030	1028

7.4 Conclusions

In summary, β-CDen (en: -NHCH$_2$CH$_2$NH$_2$) functionalized Fe$_3$O$_4$ nanospheres (CDen-MNPs) were successfully synthesized, in which β-CDen had the ability to adsorb pharmaceutically active compounds (PhACs) and endocrine disrupter (EDCs) through inclusive host-guest interactions, while the Fe$_3$O$_4$ nanoparticles served as magnetic separators. Successful grafting of β-CDen onto magnetic particles was ascertained from the results of FTIR, TGA and XPS analyses. Analyses by TEM and VSM indicated that the as-synthesized nanoparticles were superparamagnetic with mean diameter of 11.5 nm. The solution pH and physicochemical properties of each pollutant greatly affected the adsorption process on CDen-MNPs. Absorbabilities of these pollutants on CDen-MNPs were found in the order of CBZ > NAP > BPA. The kinetics and equilibrium of pharmaceutical and EDC adsorption were best described using pseudo-second-order equation and Freundlich isotherm model, respectively. Desorption studies

showed that ethanol solution can be used as desorbing agent with multiple desorbing steps. Our results indicate that these as-synthesized magnetic nanoadsorbents would have great potentials in removal of pharmaceuticals and endocrine disrupting chemicals from waste-water.

Chapter 8: Adsorption/desorption of beta-blocker propranolol from aqueous solution by surface functionalized magnetic nanoparticles

8.1 Introduction
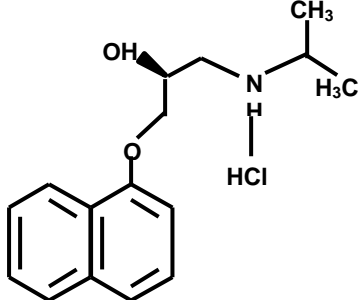
In the recent decades, pharmaceutical compounds received immense concern as emerging micropollutants for contamination of aquatic environments [236]. Among the pharmaceuticals, beta-blockers (sometimes written as β-blockers) or beta-adrenergic blocking agents constitute a class of drugs used for various indications. As beta adrenergic receptor antagonists, they are widely used to treat a variety of cardiovascular diseases by diminishing the effects of epinephrine (adrenaline) and other stress hormones on the β-adrenergic receptor in the body, primarily in the heart [451]. Nonetheless, with low retention in human body and not completely eliminated by the conventional waste-water treatment process, these beta blockers have been widely detected in effluent of sewage treatment plants and surface water in the range of ng/L to μg/L [337-340, 452, 341, 342, 453, 454]. Some published data show that beta-blockers are likely to cause harmful effects on aquatic organisms, such as fish, algae, and invertebrates even at low concentrations [455]. Propranolol, a beta-adrenergic blocking agent, is widely used in the treatment of cardiovascular diseases (hypertension, cardiac arrhythmia). Propranolol is available in generic form as propranolol hydrochloride; some of the properties of propranolol hydrochloride are presented in Table 8-1. It is considered to be of low volatility, highly persistent [456, 457], and bioaccumulative [458]. Moreover, it was found that propranolol had the highest acute and chronic toxicity within the class of the beta-blockers [459]. So development of more effective technologies to remove propranolol from aqueous environment is of prime importance.

Among the other methods, photo degradation has been utilized by many researchers as a way of removal of beta-blockers from aqueous solution [460, 461]. But photo degradation is accompanied by many disadvantages such as high energy consumption, generation of secondary products, complicated reaction pathways. Compared to other methods, adsorption has become one of the most promising techniques for removal of pharmaceuticals from aqueous solution, due to its convenience, less/ no energy consumption, efficacy etc. Adsorption has been used for the removal of pharmaceuticals from wastewaters, primarily focusing on the use of activated carbon as the adsorbent [427]. Efficiency of pharmaceutical removal have also been examined using mesoporous silica based materials [278], inorganic-organic modified bentonite [279] etc. However high cost of manufacturing and regeneration of these adsorbents limit the application to some extent. Hence, development of alternative adsorbents which are effective, abundant and affordable is a research hot spot now. Recently, many studies have focused on use of superparamagnetic nanoparticles as alternative adsorbents for sorption separation/ removal of organic and inorganic contaminants [434] etc. These superparamagnetic materials possess an advantage that they do not retain any magnetization after removal of external magnetic field.   In addition, it is desired that the magnetic nanoparticles remain nonaggregated and are stable against oxidation from the point of these technological and medical applications. Because the nanoparticle surface can influence its behavior in the biological environment, suitable coating is very necessary to prevent such limitations [344]. If considered as surface modifying agent, silica particles are not toxic and are also highly biocompatible. They are regularly used as food additives and components of vitamin supplements. In addition, amorphous silica particles have surfaces decorated with hydroxyl groups which not only render them intrinsically hydrophilic but also provide platform for

further surface functionalization. On the other hand, cyclodextrins (CDs) are torus shaped cyclic oligosaccharides consisting of α-(1, 4) linked D-glucopyranose units. The most common cyclodextrins are α, β and γ-cyclodextrin, which contain six, seven and eight glucose units, respectively. A characteristic feature of cyclodextrin is the presence of an internal hydrophobic cavity with a remarkable capacity to form inclusion complexes whose stability constants depend on the polarity, size and shape of the guest molecule included [25]. Studies have been reported for adsorption of beta-blocker propranolol onto other adsorbent such as modified attapulgites [58], cyclodextrin polymer [60]. However to the best of our knowledge, reports about silica and cyclodextrin coated magnetic nanoparticles used in separation of beta-blocker are rather limited.

The primary objectives of this study were to investigate the sorption behavior of propranolol onto silica and carboxymethyl-β-cyclodextrin modified magnetic nanoparticles to evaluate their feasibility for removing propranolol from aqueous solution in ppm concentrations. Factors affecting adsorption of propranolol onto the nanoadsorbents were systemically investigated and the sorption kinetics and sorption isotherms for propranolol were studied in detail. Adsorption mechanism was explored in details using XPS and FTIR spectroscopy as well. Finally, desorption study and possibility of regeneration of the magnetic nanoparticles were evaluated.

Table 8-1 Physicochemical properties of propranolol.

Compound	Molecular structure	MW (g/mol)	LogK_{ow}	pK_a	Log$D$ at pH 3, 7 and 9	Water solubility (mg/L at 25°C)
Propranolol hydrochloride		295.8	3.48[a]	9.42[a]	-2.94[a] 1.06[a] 2.92[a]	150

[a] Data from reference [54]

8.2 Results and discussion

8.2.1 Adsorption of propranolol

8.2.1.1 Effect of initial pH

The sorption of propranolol onto $Fe_3O_4/SiO_2/CMCD$ MNPs as a function of initial solution pH was also investigated in the pH range of 3–11 (Figure 8-1). $Fe_3O_4/SiO_2/CMCD$ MNPs were synthesized according to the procedures described in section 3.2.1-3.2.4 and Figure 3-1 shows the schematic representation of the reaction pathway. As can be seen in Figure 8-1, sorption capacities of propranolol onto the nanoadsorbent increased with increasing pH. In the case of propranolol (pK_a = 9.42), it exists as a positively charged molecule in the tested pH below its pK_a and it exists as negatively charged molecule above its pK_a (Figure 8-2) [58]. In the prepared sample, propranolol was present in either cation or anion form, depending upon the solution pH.
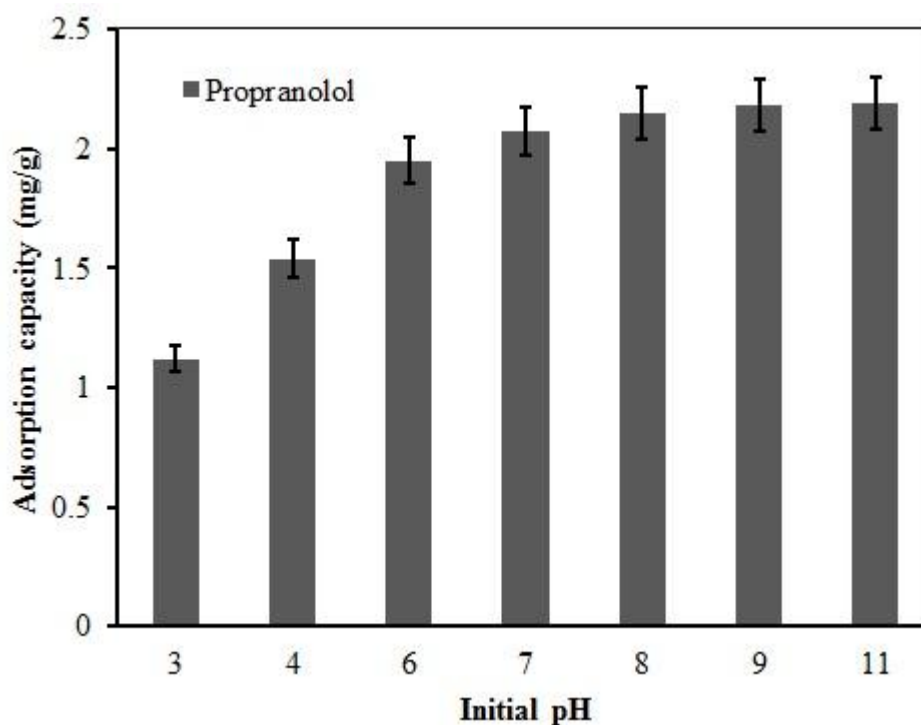
Figure 8-1 Effect of pH on the sorption of propranolol onto the four sorbents (T = 25°C, C_0 = 50 ppm, sorbent dosage = 60 mg/4 mL)
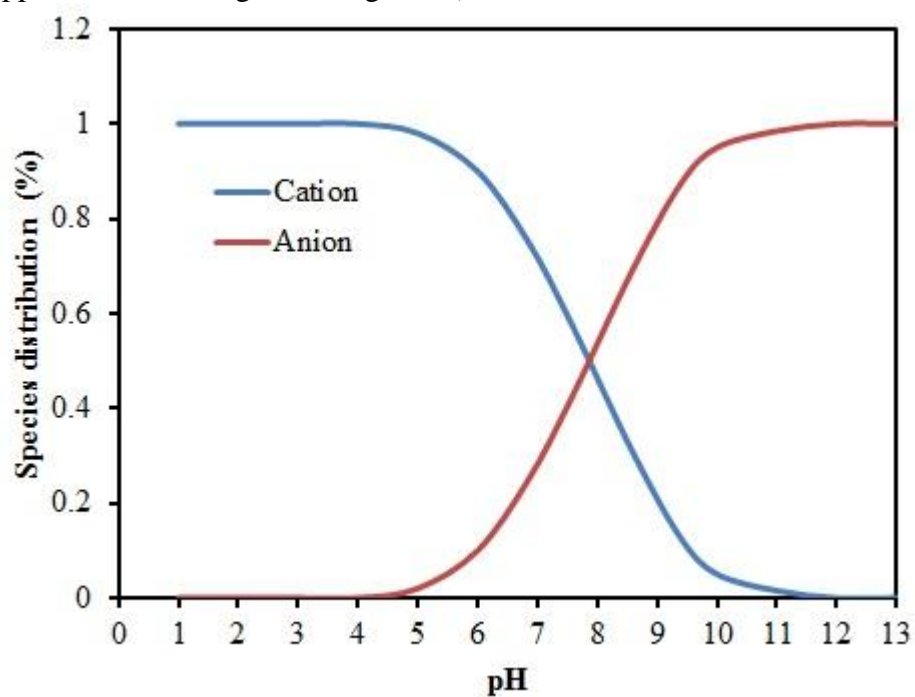
Figure 8-2 Species distribution of propranolol.

It was reported that interaction forces between propranolol and cyclodextrin molecules are hydrogen bonding and hydrophobic interaction [60]. Adsorption capacity of the nano-adsorbent bearing cyclodextrin moieties toward the beta-blocker, propranolol is

based on two factors, namely, the hydrophobicity of the drug (conditioned by the value of the octanol water partition coefficient, K_{ow}) and the ionization of the molecule (determined by the values of pH and pK_a). Both parameters K_{ow} and pK_a can be taken into account for the calculation of log$D$. Log$D$ is a pH-dependent modified octanol water partition coefficient and is relevant for solutes that are partly dissociated or protonated [57]. It can be calculated using equations 8-1 and 8-2. For acidic molecules log$D$ is determined as:

$$\log D = \log K_{ow} - \log(1 + 10^{(pH-pKa)})$$ [8-1]

Whereas for basic molecules log$D$ is:

$$\log D = \log K_{ow} - \log(1 + 10^{(pKa-pH)})$$ [8-2]

The modified log$D$ value of propranolol at pH 3, 7 and 9 are found as -2.94, 1.06, 2.92 [54]. According to the modified hydrophobicity values, hydrophobicity of propranolol increases from pH 3 to pH 9. Noteworthy, the chemical structure of $Fe_3O_4/SiO_2/CMCD$ MNPs (Figure 3-1) suggests that the presence of ionizable groups on the surface is very limited. Thus, hydrophobic interaction between CMCD and propranolol molecules should be dominating. As a result, higher adsorption capacities of $Fe_3O_4/SiO_2/CMCD$ MNPs toward propranolol at higher solution pH are justified.

8.2.1.2 Effect of contact time and adsorption kinetics

To investigate the effect of contact time on the ongoing adsorption process, detailed kinetic studies were carried out for adsorption of propranolol onto $Fe_3O_4/SiO_2/CMCD$ MNPs. Adsorption of propranolol was investigated in the initial concentration of 50 ppm, pH 7 at temperature 25°C. Figure 8-3 shows the influence of contact time on the adsorption of propranolol. It can be seen that adsorption was increased instantly at initial stage due to rapid attachment of the adsorbates to the surface of the adsorbents.

In the case of propranolol, around 96% of the equilibrium adsorption value occurred in the first 40 min. And thereafter equilibrium was reached within 1 hr contact time. Gazpio et al. also observed that maximum adsorption capacity of cyclodextrin polymer toward propranolol was obtained after 20 min stirring time [60]. It is well known that cyclodextrin molecules show specific adsorption characteristics which can be explained by inclusion complex formation. As it is said before, inclusion complexation is a complicated process that depends on different properties of the guest molecule, such as polarity, size and ability to closely fit within the cavity, together with various interactions involving van der Waals, dispersive forces, dipole–dipole interactions, electrostatic forces and hydrogen bonding. The formation constant for the inclusion complexes of naphthalene with β-CD at 25 °C is 676 M^{-1} [60]. This high binding constant for inclusion complexation of β-CD and naphthalene ring might have resulted in fast adsorption saturation through inclusion complex formation between β-CD and propranolol.

The data of adsorption kinetics of propranolol onto $Fe_3O_4/SiO_2/CMCD$ MNPs were examined with Lagergren pseudo-second-order model. The Lagergren rate equation is one of the most widely used adsorption rate equations for adsorption of solute from a liquid solution. Pseudo-second-order kinetic model is expressed by the following equation [331]:

$$\frac{t}{Q_t} = \frac{1}{k_2 Q_e^2} + \frac{1}{Q_e} t \qquad \text{[8-3]}$$

where, k_2 is the equilibrium rate constant of pseudo second- order adsorption (g/mg.min). Slope and intercept of the plot of t/Q_t versus t were used to calculate the second-order rate constant, k_2. It was found that the correlation coefficient (R^2) for pseudo-first-order kinetic model has low value (< 90%) for propranolol adsorption and

a very large difference exists between $Q_{e,cal}$ and $Q_{e,exp}$, indicating a poor pseudo-first-order fit to the experimental data (data not shown). On the other hand, the correlation coefficient (R^2) for pseudo-second-order adsorption model has high value (>99%), and Q_e values calculated ($Q_{e,cal}$) from pseudo-second-order model are more consistent with the experimental Q_e values ($Q_{e,exp}$) than those calculated from pseudo-first-order model (Table 8-2). These facts suggest that the adsorption data are well represented by pseudo-second-order kinetic model. The pseudo-second-order adsorption of propranolol was also reported for other adsorbents such as modified attapulgites [58].

Table 8-2 Adsorption kinetic parameters of propranolol onto Fe_3O_4/SiO_2/CMCD MNPs at 25°C and pH 7.

Pollutant	Initial conc. C_i (ppm)	Lagergren pseudo-second-order model parameters			
		k_2, g/(mg. min)	Q_e^b, mg/g	R^2	Q_e^a, mg/g
Propranolol	50	0.307	2.094	0.999	2.078

[a] experimental
[b] calculated
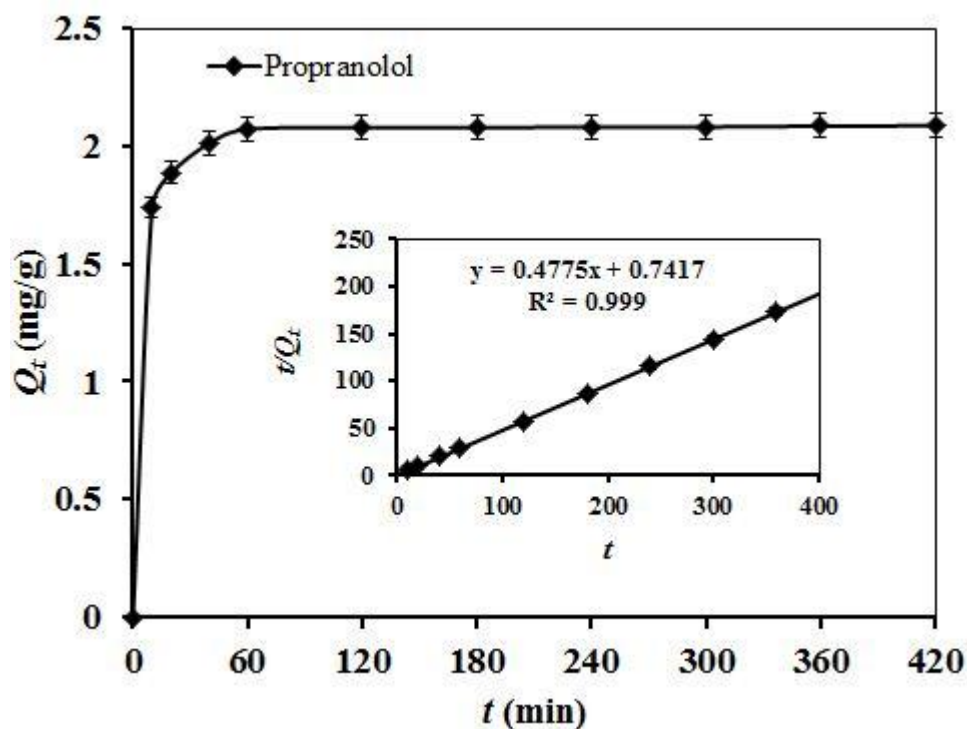
Figure 8-3 Effect of contact time on adsorption capacity of propranolol at pH 7 and 25°C and fitting for pseudo-second-order kinetics model (inset Figure 8-3).

8.2.1.3 Adsorption isotherm

The equilibrium isotherms for the adsorption of propranolol in single solute system by both $Fe_3O_4/SiO_2/CMCD$ MNPs and bare MNPs at pH 7 and 25°C are shown in Figure 8-4. From the various isotherm equations that are used to analyze adsorption data in aqueous phase, the Langmuir-the theoretical equilibrium isotherm and the Freundlich-the empirical equilibrium isotherm are the most common models. The Langmuir model was originally developed to represent physisorption on a set of well-defined localized adsorption sites having the same adsorption energy, independent of the surface coverage and with no interaction between adsorbed molecules. The Langmuir equation can be expressed as [325]:

$$\frac{C_e}{Q_e} = \frac{1}{Q_m k_L} + \frac{C_e}{Q_m} \qquad\qquad [8\text{-}4]$$

Where, Q_e is the amount of adsorbed material at equilibrium (mg/g), C_e the equilibrium concentration in solution (ppm), Q_m the maximum capacity of adsorbent (mg/g), and k_L is the "affinity parameter" or Langmuir constant (L/mg).

On the other hand, the Freundlich isotherm, one of the more widely employed mathematical descriptions, usually fits the experimental data over wide range of concentrations. This isotherm gives an empirical expression encompassing the surface heterogeneity and the exponential distribution of active sites and their energies. The linear form of Freundlich equation, which is an empirical equation derived to model the heterogeneous adsorption, can be represented as follows [326]:

$$ln\,Q_e = ln\,k_F + \frac{1}{n}ln\,C_e \qquad\qquad [8\text{-}5]$$

where Q_e and C_e are defined as above, k_F is Freundlich constant (L/g), and n is the heterogeneity factor. The values of k_F and $1/n$ are determined from the slope and intercept of the linear plot of $ln Q_e$ versus $ln C_e$. The isotherm plots are shown in Figure 8-4 and 8-5 and isotherm parameters for propranolol adsorption are represented in Table 8-3.
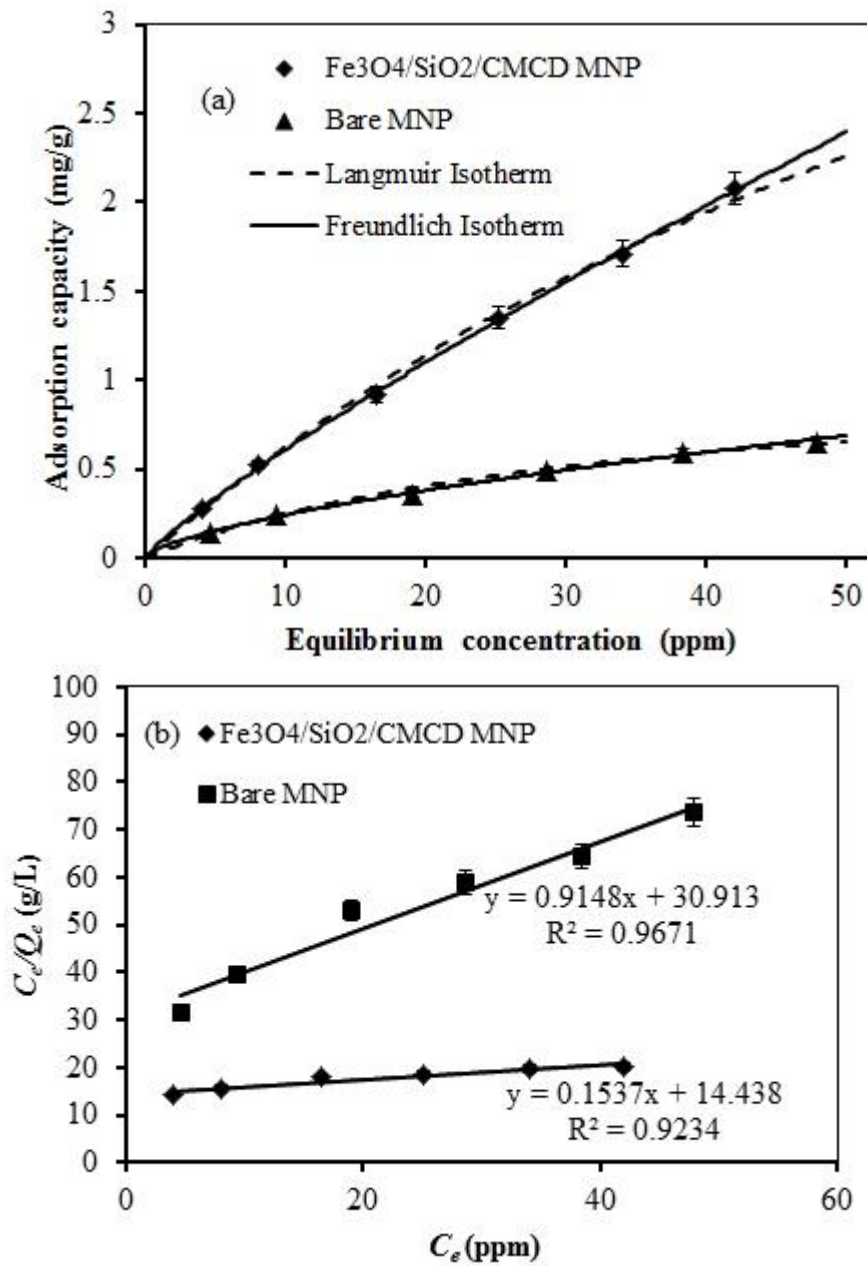
Figure 8-4 (a) Sorption isotherm of propranolol onto $Fe_3O_4/SiO_2/CMCD$ MNPs and bare MNPs (T = 25°C, sorbent dosage = 60 mg/4 mL), (b) Langmuir isotherm plots.
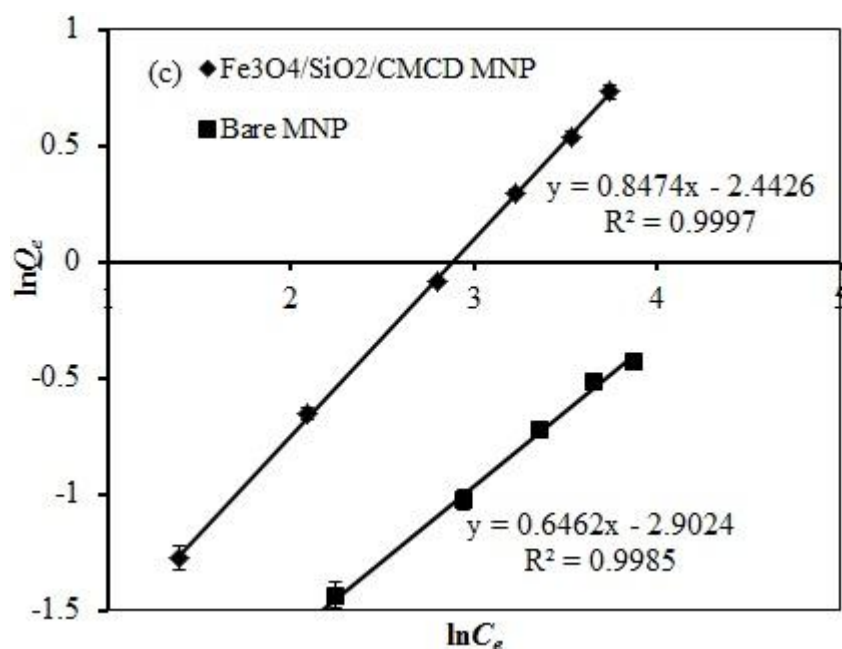
Figure 8-5 Freundlich isotherm plots for propranolol adsorption onto $Fe_3O_4/SiO_2/CMCD$ MNPs and bare MNPs (T = 25°C, sorbent dosage = 60 mg/4 mL).

As can be seen from Table 8-3, maximum adsorption capacity of $Fe_3O_4/SiO_2/CMCD$ MNPs toward propranolol is 2.078 mg/g at 25°C and pH 7, whereas that using bare MNPs is 0.652 mg/g, at the same experimental conditions. Thus, $Fe_3O_4/SiO_2/CMCD$ MNPs had adsorbed propranolol more than three times than that by bare magnetic nanoparticles indicating that the modification of magnetite surface with CMCD which had hydrophobic cavity enhanced the adsorption capacities. However, all the experimental data were fitted well to Freundlich isotherm model than Langmuir model ($R^2 > 0.99$). Thus, the adsorption process is governed by heterogeneous adsorption.

Table 8-3 Adsorption isotherm parameters for propranolol onto $Fe_3O_4/SiO_2/CMCD$ MNPs and bare MNPs at 25ºC and pH 7.

Isotherm Models	Parameters	Propranolol	
		Fe_3O_4/SiO_2 /CMCD MNPs	Bare MNPs
Langmuir	Q_m (mg/g)	6.506	1.093
	k_L (L/mg)	0.010	0.029
	R^2	0.923	0.967
Freundlich	*(1/n)*	0.847	0.646
	k_F (L/g)	0.086	0.054
	R^2	0.999	0.998

8.2.2 Investigation of adsorption mechanism with FTIR and XPS spectroscopy

To investigate the adsorption mechanism of $Fe_3O_4/SiO_2/CMCD$ MNPs toward propranolol, analysis of FTIR spectrum of the modified nanoparticles after adsorption of propranolol and in absence of propranolol were performed. The FTIR spectra of $Fe_3O_4/SiO_2/CMCD$ MNPs, propranolol and $Fe_3O_4/SiO_2/CMCD$ MNPs after sorption of propranolol are shown in Figure 8-6. As depicted in Figure 8-6 an obvious shift from 1635 cm^{-1} (CMCD, OH in-plane bending vibration absorption) to 1627 cm^{-1} could be observed after adsorption of propranolol solution, which is ascribed to the inclusion complex formation between cyclodextrin derivative and guest molecule. This result provides evidence that propranolol entered hydrophobic cavity of CMCD. In the native propranolol, functional groups are found as follows: peaks at about 2962 and 2831 cm^{-1} (characteristic of the aliphatic C–H stretching vibration), and peaks at about 1581–1450 cm^{-1} (attributed to the benzene ring skeletal vibration). The peaks at 1581–1450 cm^{-1} all disappeared after adsorption onto $Fe_3O_4/SiO_2/CMCD$ MNPs, which shows the

interaction of propranolol with the cyclodextrin cavity occurred on the modified magnetic nanoparticles' surface. Besides, the bands at 3236 and 3344 cm^{-1} are found due to presence of hydroxyl groups on the particle surface. The bands at about 3236 cm^{-1} on the $Fe_3O_4/SiO_2/CMCD$ MNPs broaden to some extent probably due to OH groups of propranolol. Notably, the vibration of backbone of the silicate structure (at 1088 cm^{-1}) of $Fe_3O_4/SiO_2/CMCD$ MNPs before and after propranolol sorption remain same, which further shows that the interaction occurred mainly in between propranolol and cyclodextrin cavity.
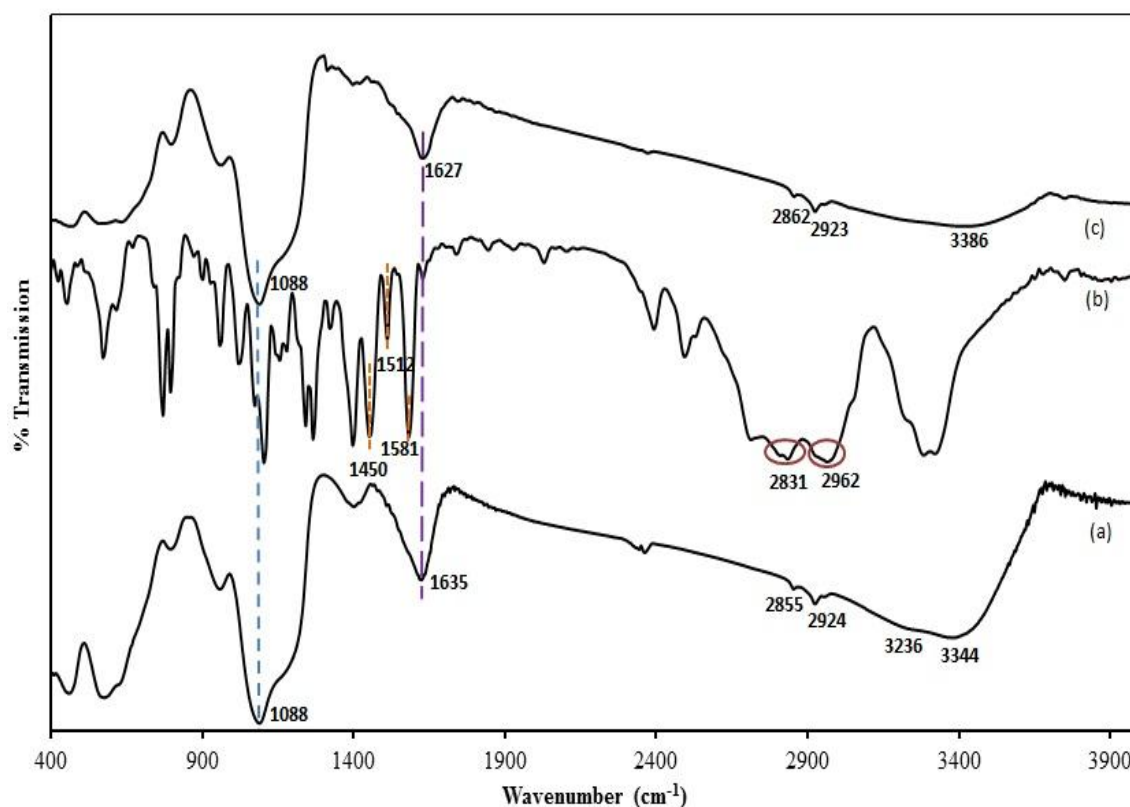
Figure 8-6 FTIR spectra of (a) $Fe_3O_4/SiO_2/CMCD$ MNPs before adsorption, (b) propranolol, (c) $Fe_3O_4/SiO_2/CMCD$ MNPs after adsorption of propranolol.

To further scrutinize the adsorption mechanism of propranolol on magnetic nanoparticles, XPS analyses were carried out on propranolol and $Fe_3O_4/SiO_2/CMCD$ MNPs after adsorption of propranolol and the corresponding results are shown in the Figure 8-7 and Table 8-4. There are major changes in the N1s spectra of propranolol

before and after the adsorption onto $Fe_3O_4/SiO_2/CMCD$ MNPs, which indicates that the amino group of propranolol took part in adsorption and complex formation. Clearly, the spectrum of propranolol exhibits two N1s peaks at 398.4 and 400.5 eV which could be attributed due to N-H and N-C functional groups. After adsorption of propranolol onto $Fe_3O_4/SiO_2/CMCD$ MNPs, the spectrum shows that peak at 398.4 eV in propranolol is shifted to 401.2 eV and peak at 400.5 eV in native propranolol is shifted to 402.3 eV. Binding energy (BE) of the peaks shifted to higher eV after adsorption compared to that of native propranolol molecule. The significant change in BE of N1s indicates that propranolol-magnetic nanoparticle complex formation occurred. Because of the favorability of amide bond formation, free electron density of nitrogen atom is greatly reduced. As a result, the BE of N1s increased considerably. Furthermore, O1s spectra of $Fe_3O_4/SiO_2/CMCD$ MNPs depicts two oxygen peaks at 530.3 eV and 532.8 eV due to presence of C=O and C-O-H/C-O-C group, respectively which originates from presence of CMCD on nanoparticles' surface. After adsorption of propranolol on magnetic nanoparticles' surface, binding energy of C-O-H/C-O-C group shifted to higher eV which represents that interaction with the secondary hydroxyl group of cyclodextrin outer rim on the magnetic nanoparticles took place (data shown in Table 8-4). Apart from these, there are no major changes in C 1s spectra.

Thus, from FTIR and XPS analysis, it can be estimated that the hydrophobic part of propranolol penetrated into the hydrophobic cavity of CMCD and nitrogen molecule was involved into hydrogen bond formation. Structure of beta cyclodextrin and adsorption mechanism are depicted in Figure 8-8.

Table 8-4 XPS data analyses for adsorption of propranolol.

Element	Binding energy (eV)		
	$Fe_3O_4/SiO_2/CMCD$ MNPs	Propranolol	$Fe_3O_4/SiO_2/CMCD$ MNPs after adsorption of propranolol
N1s	-	398.4 (N-H)	401.2 (N-H)
		400.5 (N-C)	402.3 (N-C)
C1s	284.6 (C-C/C-H)	284.6(C-C/C-N)	284.8(C-C/C-N)
	286 (C-O/C-O-C)	286.2 (C-O/ C-O-C)	286.3(C-O/C-O-C)
	287.9 (C=O)		288.1(C=O)
	288.7(COO$^-$)		288.9(COO$^-$)
O1s	530.3(C=O)		530.75(C=O)
	532.8(C-O-H/C-O-C)	532(C-O-H/ C-O-C)	533.6(C-O-H/C-O-C)
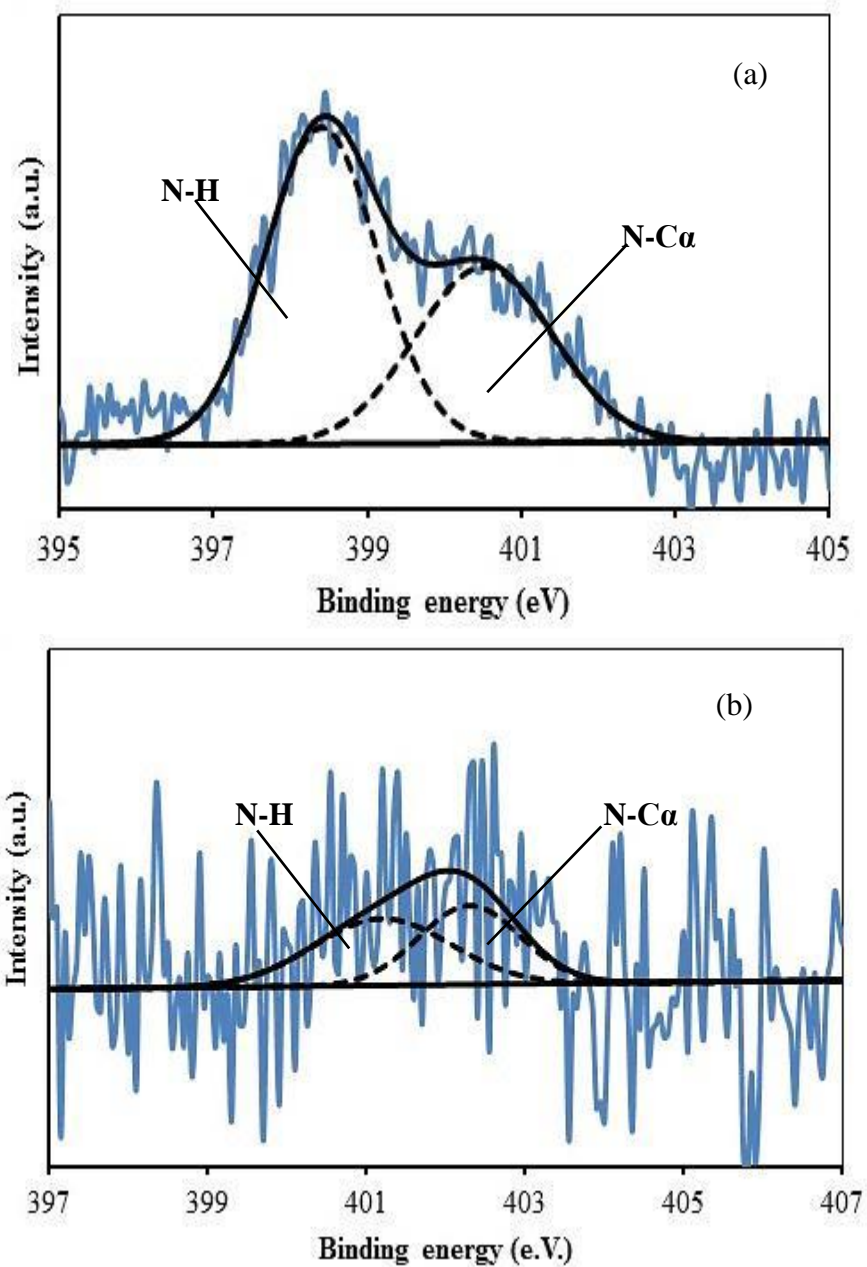
Figure 8-7 XPS spectra of (a) propranolol before adsorption, (b) $Fe_3O_4/SiO_2/CMCD$ MNPs after adsorption of propranolol.
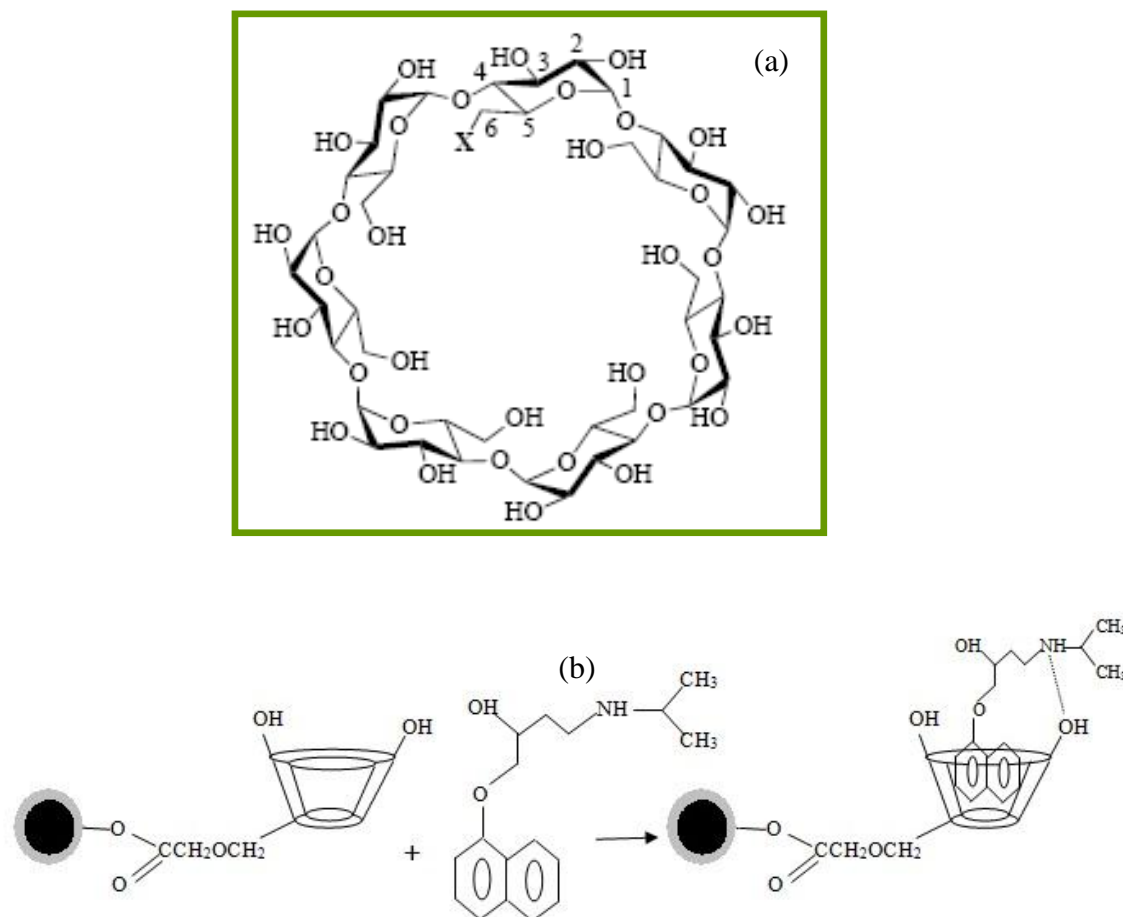
Figure 8-8 (a) Structure of beta cyclodextrin, (b) simplified schematic showing adsorption mechanism of propranolol onto $Fe_3O_4/SiO_2/CMCD$ MNPs.

8.2.3 Spectroflurometry measurements and binding constant of CMCD/propranolol

Fluorescence spectra of propranolol in pH 7 buffer containing various concentrations of CMCD are presented in Figure 8-9 (a). The fluorescence intensity of propranolol increased with increasing CMCD concentration with slight blue shift of fluorescence maximum. The change of fluorescence spectra is due to the interaction between propranolol and CMCD, implying the formation of propranolol-CMCD inclusion complex. Because cyclodextrin's non-polar cavity can offer hydrophobic environment for guest molecules, the fluorescence intensity would enhance when propranolol is included into the cyclodextrin's cavity. The revolving freedom of propranolol

decreases, resulting in an increase in fluorescence quantum yield of propranolol molecules.

Inclusion constant (K) is an important parameter, which represents the inclusion interaction. The inclusion constants of complexes are estimated according to the double-reciprocal method. It can be obtained by the following equation [418, 419].

$$\frac{1}{F-F_0} = \frac{1}{(F_\infty - F_0)K[CD]_0} + \frac{1}{(F_\infty - F_0)} \qquad \text{[8-6]}$$

where, F is the determined fluorescence intensity of the propranolol solution at specific CMCD concentration. F_o and F_∞ are the fluorescence intensity in the absence of CMCD and when all the propranolol molecules were included, respectively. K is the inclusion constant and $[CD]_0$ denotes the concentration of CMCD solution. K can be calculated from a plot of $1/(F-F_0)$ vs. $1/[CD]_0$. Figure 8-9 (b) shows the double reciprocal plots of $1/(F-F_0)$ versus $1/[CD]_0$ for propranolol inclusion complexation with CMCD at pH 7. The plot exhibits good linearity (the regression coefficient $R^2 \sim 0.993$). This verifies the formation of inclusion complexes with a stoichiometry of 1:1 between propranolol and CMCD. The inclusion constant, K of CMCD with propranolol is estimated to be 3850 M^{-1}. This high value indicates great affinity of propranolol to CMCD and thus representing non-covalent interaction.
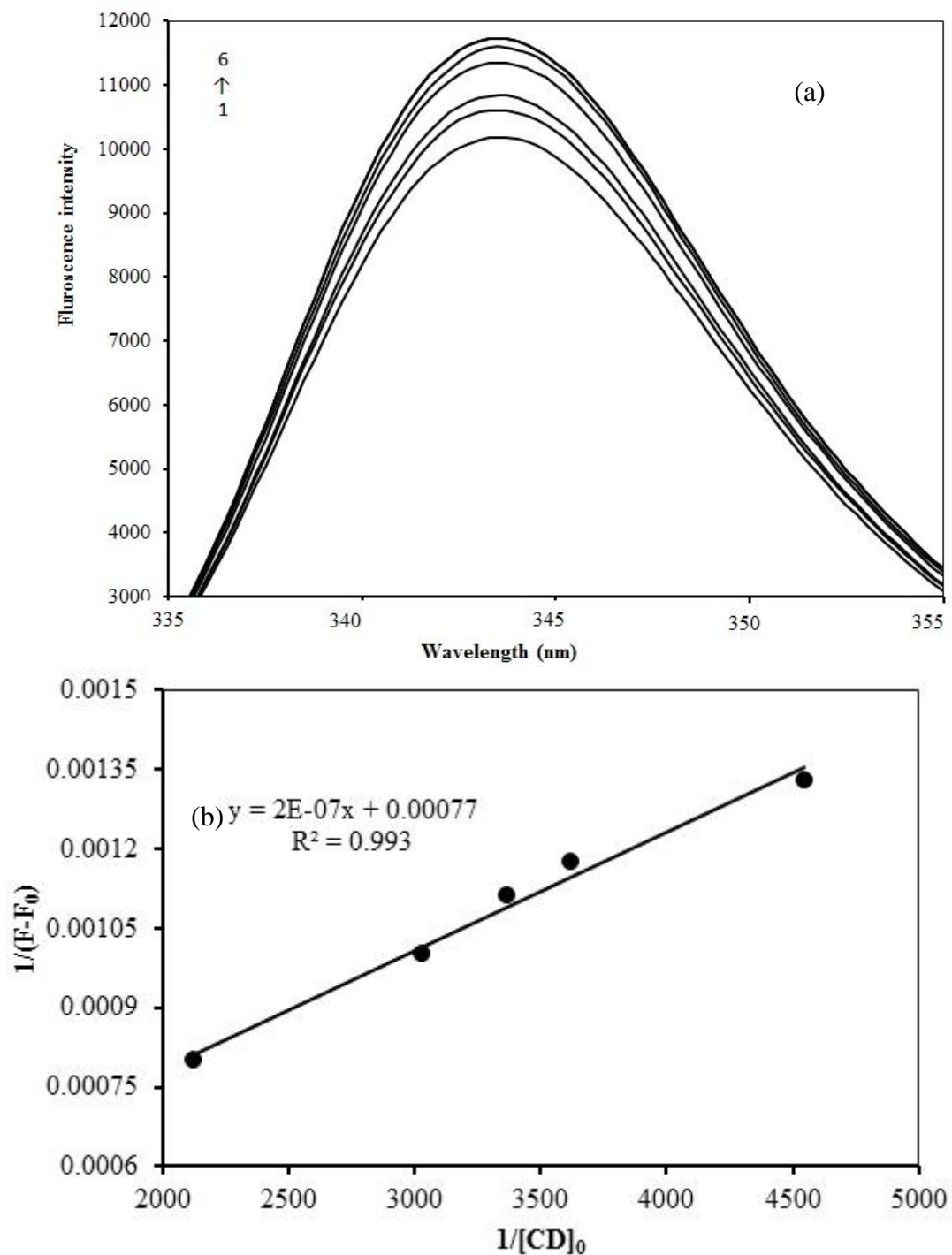
Figure 8-9 (a) Emission (λ_{max} = 343 nm) spectra of propranolol (4.5x 10^{-5} mol/L, pH=7.0) solution at various CMCD concentrations (from 0 to 4.7 x 10^{-4} mol/L), (b) double reciprocal plot for propranolol inclusion complexes with CMCD.

8.2.4 Desorption studies

The success of an adsorption process usually depends on the regeneration step of the adsorbent. Generally desorption of the adsorbed solute from adsorbent is accomplished by two methods: (1) by changing a physical operating condition, namely temperature, of the adsorber, which affects the equilibrium interaction between the adsorbent and the solute, (2) by performing a chemical reaction using some chemical reagent with higher affinity toward the adsorbed species so that it can be desorbed and removed from the system readily. There are a number of regeneration techniques such as thermal, steam, acid, base, and solvent regenerations. In this study, acetonitrile and methanol were used as desorbing agents for propranolol. Among these, methanol solution was found as effective desorbing agent.

Desorption of propranolol from nanomagnetic particles was carried out separately by 10%, 30% and 50% methanol solutions at equilibrium and 25°C. Figure 8-10 shows the result of desorption studies of propranolol after adding 50% methanol solution at equilibrium with respect to solid loading. Around 94% desorption of propranolol was achieved using 50% methanol solution when 14.47 mg of solid adsorbent was added.
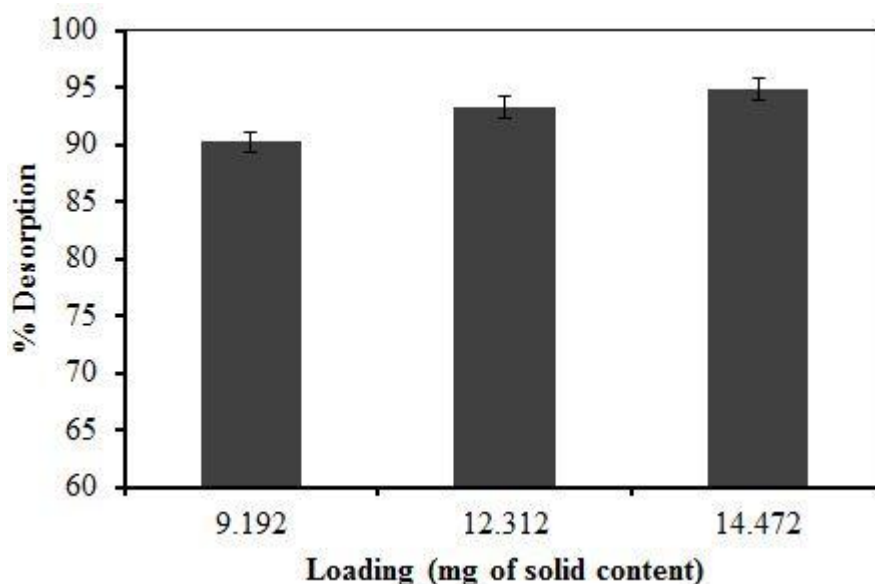
Figure 8-10 Desorption of propranolol from $Fe_3O_4/SiO_2/CMCD$ MNPs as a function of loading of adsorbent. Adsorption condition: propranolol 50 ppm; pH 7; temperature 25°C, contact time 5 hrs. Desorption condition $Fe_3O_4/SiO_2/CMCD$ MNPs; 50% methanol solution, temperature 25°C, contact time 6 hrs.

8.3 Conclusions

In summary, silica and carboxymethyl-β-cyclodextrin functionalized Fe_3O_4 magnetic nanoparticles were utilized for adsorptive removal of propranolol. Results from effect of pH study showed that adsorption capacities of the particles increased as solution pH was increased and the behavior was dominated by hydrophobic interaction between propranolol and the nanoadsorbents. Adsorption capacities of as synthesized particles were compared to bare nanoparticles and it was found that adsorption capacity of cyclodextrin derivative functionalized particles was three times higher than that of bare magnetic nanoparticles. Kinetic studies showed that the adsorption process was very fast, adsorption equilibrium reached within 1 hr and kinetic data followed pseudo second order model. All the adsorption equilibrium data were fitted well to Freundlich isotherm model thus showing heterogeneous adsorption. XPS and FTIR spectroscopy were applied to investigate adsorption mechanism and it was found that the

229

hydrophobic portion of propranolol penetrated completely into cyclodextrin cavity and amino group of propranolol interacted through hydrogen bond formation with the secondary hydroxyl group of cyclodextrin cavity. Flurometric studies revealed high binding constant between propranolol and CMCD which might have resulted in adsorption of adsorbate. Finally, desorption studies showed that the nanoadsorbents could be regenerated using methanol solution and using 50% methanol solution almost complete regeneration of the adsorbent was achieved. Thus, the as-synthesized CMCD functionalized magnetic nanoparticles with all significant properties would have great potentials in adsorptive separation/ removal of beta-blocker.

Chapter 9: Conclusions and recommendations

9.1 Conclusions

The main aim of the study is to present a systematic and comprehensive study on the application of cyclodextrin derivative functionalized magnetic nanoparticles for separation of chiral biomolecules and environmental pollutants. Initially, silica and cyclodextrin derivative functionalized magnetic nanoparticles (CMCD coated MNPs) were synthesized and applied for adsorption separation of single Trp, Phe and Tyr enantiomers and separation from racemic mixture as well. Later on, another cyclodextrin derivative functionalized MNPs (β-CDen MNPs) were synthesized and applied for separation of pharmaceuticals. Sorption separation of two different kinds of chemicals/ compounds (amino acid and PhACs/EDC) with different types of β-CD derivatives was explored. For this reason, adsorption/separation study of PhACs and EDC was not done using CMCD functionalized MNPs and β-CDen MNPs were not utilized for chiral separation of amino acids. The results are divided into five parts and presented in five separate chapters. These are silica and CMCD coated magnetic nanoparticles characterization results, adsorption and desorption results of single chiral amino acid enantiomers on silica and CMCD coated magnetic nanoparticles, chiral separation of amino acids using silica and CMCD coated magnetic nanoparticles, characterization results of amino-cyclodextrin functionalized magnetic nanoparticle and adsorption/desorption results of environmental pollutants (carbamazepine, naproxen and bisphenol A) on amino-cyclodextrin functionalized magnetic nanoparticle, detailed study of adsorption/desorption of beta-blocker propranolol using silica and CMCD coated magnetic nanoparticles.

The first part of experiment deals with synthesis of bare magnetic nanoparticles and functionalization of the surface with silica and CMCD followed by characterization of the chemical, physical and magnetic properties of the magnetic nanoparticles. Bare magnetic nanoparticles were synthesized and their surface was functionalized with silica and CMCD (Chapter 4). FTIR results showed the presence of Fe-O-Si stretching band and C-H stretching band, which indicated surface of the magnetic particles, was successfully functionalized with silica and CMCD. XRD patterns indicated that the silica and CMCD coated magnetic nanoparticles constitute iron oxide (Fe_3O_4). The XRD pattern also showed the characteristic peaks at 2θ of 30.22°, 35.56°, 43.08°, 57.48°, 63.08°. Superparamagnetic behaviour of bare and coated magnetic nanoparticles was observed by VSM with saturation magnetization of 75 emu/g and 45 emu/g, respectively. The size of silica and CMCD coated particles were measured by TEM and the result showed the particles were in nano scale with an average diameter of 29 nm. Moreover, the specific surface area of the silica and CMCD modified nano-particles was calculated as 74 m^2/g using BET (Chapter 4).

These nano-sized magnetic particles were scrutinized for adsorption of certain chiral aromatic amino acid enantiomers namely, D- and L-tryptophan (Trp), D- and L-phenylalanine (Phe) and D- and L-tyrosine (Tyr) from phosphate buffer solutions under different conditions (Chapter 5). Adsorption capacities of the coated magnetic nanoparticles toward amino acid enantiomers were in the order: L-Trp>L-Phe>L-Tyr and under the same condition, adsorption capacities were higher for L-enantiomers than the corresponding D-enantiomers. Structure and hydrophobicity of amino acid molecules emphasized the interactions between amino acid molecules and the nano-adsorbents bearing cyclodextrin, thus played important roles in the difference of their adsorption behaviors. All the equilibrium adsorption isotherms were fitted well to

Freundlich model. Higher amount of adsorption for the amino acid enantiomers was observed at pH close to the isoelectric point. Adsorption study results at different temperatures showed that maximum amount of adsorption occurred at 25°C and the amount decreased as temperature increased. Kinetic study results showed that the adsorption process was governed by pseudo second order kinetics. FTIR studies depicted significant changes after adsorption of amino acids onto nanoparticles. The stretching vibration frequencies of N-H bonds of the amino acid molecules were changed with complex formation through host-guest interaction.

These as-synthesized silica and CMCD functionalized Fe_3O_4 magnetic nanoparticles were utilized for enantioselective separation of racemic aromatic amino acid solution (Chapter 6). The magnetic nanoparticles preferentially adsorbed L-enantiomers of Trp, Phe and Tyr than the D-enantiomers and offered 94%, 73% and 58% enantiomeric excesses toward Trp, Phe and Tyr enantiomers, respectively. Hydrophobicities of the amino acids influenced interaction with cyclodextrin molecules to different degrees and thus resulted in different enantiomeric excesses. Several analytical techniques such as XPS and FTIR spectroscopy were applied to investigate the enantioselective mechanism and it was observed that hydrophobic portion of amino acid molecules penetrated into cyclodextrin cavity and amino group of the amino acid molecules formed hydrogen bonds with secondary hydroxyl groups of cyclodextrins. Flurometric studies also supported the observation of higher binding of CMCD to L-enantiomer compared to D-enantiomers. Thus, the as-synthesized CMCD functionalized magnetic nanoparticles with all significant properties would have great potentials in chiral separation technologies.

Afterwards, synthesis of amino-CD (β-CDen) functionalized magnetic nanoparticles and characterization of the chemical, physical and magnetic properties of the magnetic nanoparticles were carried out (Chapter 7). FTIR results showed the presence of C=O stretching band, antisymmetric glycosidic v_a(C–O–C) vibrations and the coupled v(C–C/C–O) stretch vibration, which indicated that surface of the magnetic particles was successfully functionalized with amino-CD. XRD patterns indicated that the composition of the coated magnetic nanoparticles was pure Fe_3O_4. The XRD patterns also showed the characteristic peaks at 2θ of 30.5°, 35.9°, 43.4°, 53.4° 57°, and 63.1°. It was observed that TDGA and CDen coated magnetic nanoparticles were superparamagnetic particles by VSM with saturation magnetization of 75 and 57.1 emu/g, respectively. The size of TDGA-CDen coated particles were measured by TEM and the result showed the particles were in nano scale with an average diameter of around 11.5 nm (Chapter 7).

Amino-CD functionalized magnetic nanoparticles were utilized for adsorption of two pharmaceuticals (carbamazepine, naproxen) and one EDC (bisphenol-A) (Chapter 7). Adsorption kinetics showed that the process could be explained by pseudo-second-order kinetics. Adsorption capacities of the coated magnetic nanoparticles toward the three above mentioned chemicals were in the order: carbamazepine> naproxen> bisphenol A (under the same conditions) and adsorption capacities were moderated by hydrophobicity of the target molecules. The equilibrium adsorption isotherms were fitted well to Freundlich model. For carbamazepine, there was not much effect of solution pH on the adsorption capacity. Whereas, for naproxen as solution pH increased, adsorption capacity decreased and for bisphenol A, adsorption capacity of the adsorbent decreased slightly in the range of pH 9-11. These results from adsorption study at different pH showed that adsorption was dependent on the ionization of

PhACs/EDC and CDen MNPs. FTIR studies of the nanoparticles after adsorption of the chemicals depicted significant changes in νCH_2 bands which indicated that inclusion complex formation had occurred between the PhACs/EDC and β-CDen. Moreover, desorption study showed that around 80%, 75% and 89% desorption of CBZ, NAP and BPA from the magnetic nanoparticles surface was achieved using ethanol as eluent.

Later part of this PhD project dealt with utilization of silica and carboxymethyl-β-cyclodextrin functionalized Fe_3O_4 magnetic nanoparticles for adsorption of propranolol from aqueous solution. Effect of pH study results showed that adsorption capacities of the particles increased as solution pH increased and the behavior was dominated by hydrophobic interaction between propranolol and the nanoadsorbents. When compared, adsorption capacities of silica and carboxymethyl-β-cyclodextrin functionalized particles were found to be three times higher than that of bare particles. Results from kinetic studies showed that the adsorption process was very fast, adsorption equilibrium reached within 1 hr and the kinetics data followed pseudo-second-order model. Adsorption equilibrium data were fitted well to Freundlich adsorption isotherm thus showing heterogeneous adsorption. Furthermore, XPS and FTIR spectroscopy were applied to investigate the adsorption mechanism and it was found that the hydrophobic portion of propranolol interacted with the cyclodextrin cavity and nitrogen molecule was involved in hydrogen bond formation. High binding constant between propranolol and CMCD was obtained when analyzed with fluorometric titrations which might have resulted in good adsorption capacity of the adsorbent. Finally, desorption studies show that the nanoadsorbents could be regenerated using methanol solution and using 50% methanol solution almost complete regeneration of the adsorbent was achieved.

In summary, nano-sized magnetic particles were prepared by chemical precipitation method and further modification of the particles' surface was done successfully. These surface functionalized magnetic nanoparticles can be used for separation of chiral biomolecules and environmental pollutants. The unique chemical, physical and magnetic properties of magnetic particles, such as nano-size, superparamagnetism, large specific surface area, and easy manipulation of surface modification make them suitable tool for the separation of chiral biomolecules and environmental pollutants. The results displayed the merits of easy synthesis of sorbents, rapid analysis and reliable quantitative detection. Because of the increasing demand for pure compounds, efficient strategies for analytical and preparative separations of chiral biomolecules and pharmaceuticals, endocrine disruptors and beta-blockers are required. Nearly all aspects of this technology, including synthesis, adsorption and analysis, can benefit greatly from the use of magnetic nanoparticles. Therefore, it is clear that in near future a variety of new approaches for chiral separation and removal of pharmaceuticals, EDCs and beta-blockers based on superparamagnetic nanoparticle will be developed, and this work will be a part of the general trend in development of this methodology.

9.2 Recommendations

In this work, synthesis of magnetite coated with cyclodextrin derivatives has been demonstrated. These as-prepared magnetic nanoparticles have been successfully utilized for separation of chiral biomolecules and other environmental pollutants. This thesis work is only a preliminary study. There are also several interesting directions for future research in the field of chiral separation and separation of environmental pollutants. Proposed future works are:

9.2.1 Separation of chiral biomolecules:

(a) In Chapter 6, enantioseparation of single and racemic aromatic amino acids was achieved utilizing CMCD coated magnetic nanoparticles. Adsorption study was focused on mainly three aromatic essential amino acids, tryptophan, phenylalanine and tyrosine since they are frequently used as food additives. Detailed adsorption study of these six amino acid enantiomers were time consuming too. Tests could not be carried out to study adsorption of other amino acids due to lack of time. Further work should be directed to study adsorption of single non-aromatic amino acids for example (D-/L-alanine, D-/L-valine, D-/L-leucine, D-/L-isoleucine) and enantioseparation of racemic amino acids (DL-alanine, DL-valine, DL-leucine, DL-isoleucine) etc. using cyclodextrin derivative conjugated magnetic nanoparticles. Investigation should be carried out to explore the adsorption mechanism of non-aromatic amino acids on CMCD coated magnetites. Moreover, regeneration possibilities of the modified magnetite should be studied.

(b) Desorption/regeneration possibilities of single amino acids (L-/D-Trp, L-/D-Phe, L-/D-Tyr) were verified in Chapter 5. Desorption of D-enantiomers were less compared to corresponding L-enantiomers which could eb due to less affinity of D-enantiomers to methanol. Some future work should be done using different desorbing agents (ethanol, IPA) and multiple desorption steps to increase regeneration possibilities.

(c) One important characteristic of amino acid enantiomers are their optical rotation. After release of separated enantiomers of amino acids from magnetic nanoparticles' surface, purity of the enantiomers should be characterized using optical activity measurement. Optical rotation of racemic amino acids as well as pure enantiomers can be determined. After separation of chiral racemic amino acids, optical rotation of the

separated enantiomers can be measured and compared to that of pure enantiomers. Furthermore, measurements with circular dichroism can be utilized to verify the purity of separated enantiomers.

(d) It has been observed that for chiral drugs, there may be three to five stereoselective receptors, each of which triggers a different physiological response. The use of specific isomers could allow one to elicit more exact therapeutic effects. It is true for approximately 25 percent of pharmaceutical products; only racemic mixtures of propranolol and methadone are available for clinical use while rest of the pharmaceuticals should be used in pure enantiomeric form. Thus chiral resolution of racemic drugs should be studied utilizing the CD modified magnetite nanoparticles.

(e) Enantioseparation was studied in low concentration of the aromatic amino acids (2 mM) and method for quantification was done using HPLC in abovementioned concentration. Future work should focus on developing a method to quantify enantioseparation of amino acids in high concentration level (> 2mM).

9.2.2 Removal of environmental pollutants:

(a) In Chapter 7, adsorptive removal of two pharmaceuticals (carbamazepine, naproxen) and one EDC (bisphenol A) using amino-CD conjugated magnetic nanoparticles were done. Presence of hundreds of organic and inorganic pollutants has been reported in water along with the microbial population. It is found that some organic pollutants and metal ions are not biodegradable and biotransformable hence they persist in environment. Toxic organic pollutants include pesticides, phenols, polynuclear aromatic hydrocarbons (PAHs), polychlorinated biphenyls (PCBs), plasticizers, and drug residues whereas toxic metal ions include arsenic, cadmium, platinum and chromium. Some researchers have worked on development of low cost adsorbents for removal of these pollutants from waste-water [462]. Advance works should be done utilizing cyclodextrin modified magnetite for removal of other toxic organic pollutants and toxic metal ions applying magnetic separation technique.

(b) In this thesis, desorption study was done for removal of CBZ, NAP and BPA from aqueous water. Adsorption-desorption studies of the pharmaceuticals and EDC from cyclodextrin modified magnetic nanoparticles should be carried out in few cycles and recyclability of the particles should be checked. Recyclability of the magnetic nanoparticles depends on the desorption condition. Generally desorption is carried out either using some other chemical which has high affinity toward the sorbate or by changing the operating condition (temperature/ pressure). After desorption, surface properties of the magnetic nanoparticles can be examined using different analytical techniques (XPS spectroscopy, FTIR spectroscopy etc). To protect the magnetic core and improve regeneration possibility of the magnetic nanoparticles, carbon layer can be deposited on the magnetic core which will increase chemical and thermal stability of the particles.

9.2.3 Multifunctional nanoparticles:

In recent years, the advent of multifunctional nanomaterials attracted enormous interest of biomedical research community. Rational combination of diverse building blocks such as metallic or semiconductor nanomotifs, organic molecules/polymers, biomolecules give rise to composite nanomaterials which exhibit a wide range of diagnostic and therapeutic capabilities; bioimaging, specific cell targeting, drug storage and controlled drug release etc., rendering them extremely intriguing and promising in biomedical research. Magnetic nanoparticles evidently are becoming prominent inorganic building blocks of such multifunctional nanocomposites because colloidal magnetic nanoparticles (MNPs), typically iron oxide (Fe_3O_4), exhibit superparamagnetism which can respond to external magnetic field. The fact that these superparamagnetic materials do not retain any magnetization after removal of the external magnetic field, and thus avoid aggregation, is a clear advantage for any in vivo application. Silica, (SiO_2) has been extensively utilized as a coating material of MNPs, providing Fe_3O_4@Silica core-shell nanocomposites, because silica is known to have low-toxicity and is less prone to degradation in biological environment. Recently we have developed silica based multifunctional magnetic nanoparticles [Fe_3O_4@SiO_2(FITC)-FA/CMCD NPs] which can be effectively used in fluorescence imaging, specific cell targeting and hydrophobic anticancer drug delivery. Confocal microscopic imaging studies show that the Fe_3O_4@SiO_2(FITC)-FA/CMCD NPs could specifically target cancer cells due to the high expression of folate receptor on cancer cells such as HeLa cells. These Fe_3O_4@SiO_2(FITC)-FA/CMCD nanoparticles should be used as an efficient adsorbent in controlled drug release applications.

9.2.4 Magnetic nanoparticles for separation of bio-molecules and waste-water purification in large scale using High Gradient Magnetic Separation (HGMS) system:

Future trend on magnetic separation should focus on large scale operation. High gradient magnetic separation (HGMS) for separation and purification purposes can be developed.

Separation of chiral bio-molecules, pharmaceuticals (PhACs) and EDC utilizing magnetic nanoparticles has not been studied extensively in large scale utilizing magnetic nanoparticles. So, further work should be done on separation of bio-molecules in large scale operation using HGMS system. However, recycling of waste-water has always been expensive. Hence, magnetic separation should be applied to removal of pharmaceuticals, EDC from waste-water on a practical use scale. In the conventional methods (mainly biological decomposition process) large-scale equipment is necessary to process a large amount of waste-water and hence a large amount of capital investment is needed. Even if the sewage system is used, large expense for usage of the sewage is required.

Figure 9-1 shows the possible use of HGMS system for chiral separation and removal of PhACs and EDC from waste-water. For HGMS system, the magnetic seeding technique can be developed for chemical species [463]. Magnetic seeding is a technique that the ferromagnetic particles are attached to the chemical species and then enable to separate them magnetically. This technique is called a colloid chemical method. For the large scale separation and purification purpose, magnetite nanoparticles can be synthesized first from iron oxides. The synthesized magnetite will absorb the chemical species and will form flocs. On the other hand, ferromagnetic filaments (magnetic filter) can be arranged in the magnetic field, and a high gradient magnetic field can be

generated in the neighbourhood. Though higher gradient of magnetic field can be generated by thinner magnetic filter, the achieved area is supposed to be small. For this purpose, 40-50 magnetic filters axially stacked in the superconducting magnet bore can be used. The system can be designed to wash the magnetic filter without discharging the magnet. The magnetic filter should have diameter large enough to withstand the magnetic force. The magnetic filter should endure hydraulic force for a long term. Thus, thickness of the ferromagnetic filament should be fat from the viewpoint of mechanical strength.

In the magnetic separation system, ferromagnetic particles will be attached to chemical species in seeding tank. As the larger sized magnetic seeded flocs sediment in a short time, the separation tank where the floc precipitates should be installed. Afterwards the remaining water containing biomolecules, PhAC/ EDC will be introduced into the superconducting magnetic separation unit, and a magnetic separation is performed. For advanced separation process, second magnetic seeding tank can be installed. This process has been depicted in Figure 9-1.
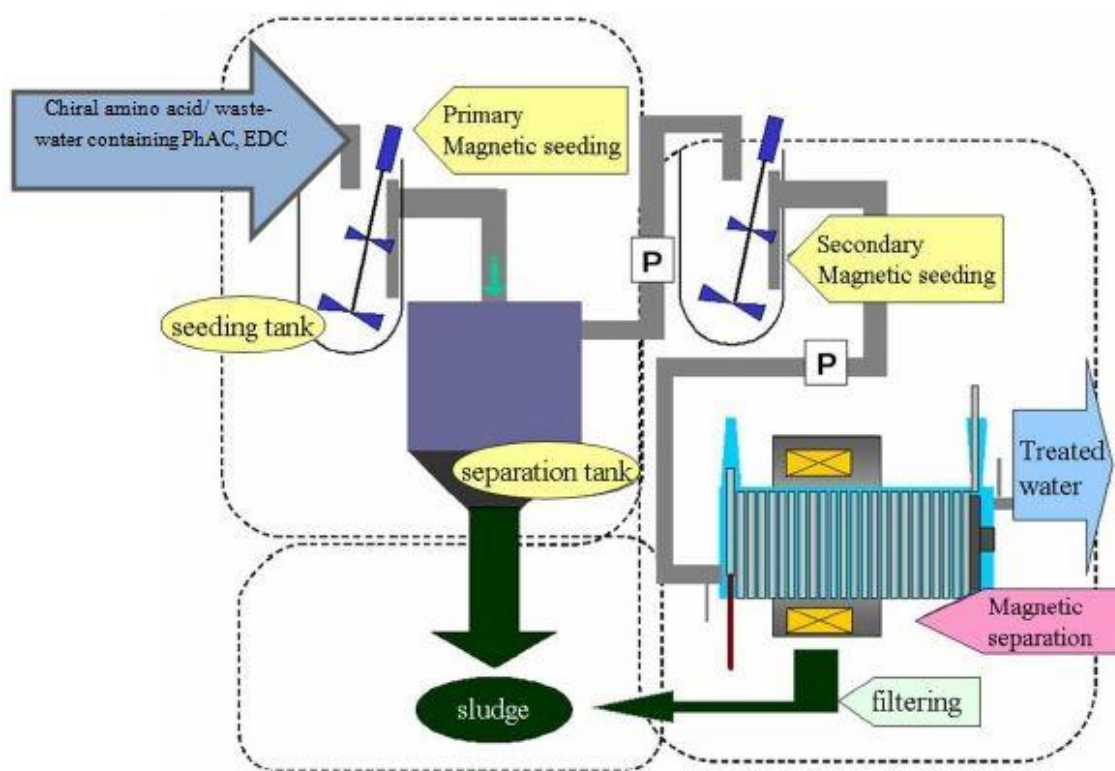
Figure 9-1 Overview of HGMS system [463].

References

[1] P. Wikström, S. Flygare, A. Gröndalen, P. O. Larsson, Magnetic aqueous two-phase separation: a new technique to increase rate of phase-separation, using dextran-ferrofluid or larger iron oxide particles. Anal. Biochem. 167 (1987) 331.

[2] Y. Deng, C. Deng, D. Qi, C. Liu, J. Liu, X. Zhang, D. Zhao, Synthesis of Core/Shell Colloidal Magnetic Zeolite Microspheres for the Immobilization of Trypsin. Adv. Mater. 21 (2009) 1377.

[3] M. Feyen, C. Weidenthaler, F. Schüth, A.-H. Lu, Synthesis of Structurally Stable Colloidal Composites as Magnetically Recyclable Acid Catalysts. Chem. Mater. 22 (2010) 2955.

[4] U. Jeong, X. Teng, Y. Wang, H. Yang, Y. Xia, Superparamagnetic Colloids: Controlled Synthesis and Niche Applications. Adv. Mater. 19 (2007) 33.

[5] R. Hao, R. Xing, Z. Xu, Y. Hou, S. Gao, S. Sun, Synthesis, functionalization, and biomedical applications of multifunctional magnetic nanoparticles. Adv. Mater. 22 (2010) 2729.

[6] J. Park, M. K. Yu, Y. Y. Jeong, J. W. Kim, K. Lee, V. N. Phan, S. Jon, Antibiofouling amphiphilic polymer-coated superparamagnetic iron oxide nanoparticles: synthesis, characterization, and use in cancer imaging in vivo. J. Mater. Chem. 19 (2009) 6412.

[7] D. Shi, H.S. Cho, Y. Chen, H. Xu, H. Gu, J. Lian, W. Wang, G. Liu, C. Huth, L. Wang, R.C. Ewing, S. Budko, G.M. Pauletti, Z. Dong, Fluorescent Polystyrene-Fe_3O_4 Composite Nanospheres for In Vivo Imaging and Hyperthermia. Adv. Mater. 21 (2009) 2170.

[8] J. Bao, W. Chen, T. Liu, Y. Zhu, P. Jin, L. Wang, J. Liu, Y. Wei, Y. Li, Bifunctional Au-Fe_3O_4 nanoparticles for protein separation. ACS Nano 1 (2007) 293.

[9] Y. Lee, H. Lee, Y.B. Kim, J. Kim, T. Hyeon, H. Park, P.B. Messersmith, T.G. Park, Bioinspired Surface Immobilization of Hyaluronic Acid on Monodisperse Magnetite Nanocrystals for Targeted Cancer Imaging. Adv. Mater. 20 (2008) 4154.

[10] I. Willner, Z. Cheglakov, Y. Weizmann, E. Sharon, Analysis of DNA and single-base mutations using magnetic particles for purification, amplification and DNAzyme detection. Analyst 133 (2008) 923.

[11] Y. Kang, L. Zhou, X. Li, J. Yuan, β-Cyclodextrin-modified hybrid magnetic nanoparticles for catalysis and adsorption. J. Mater. Chem. 21 (2011) 3704.

[12] W. Wang, Y. Xu, D.I.C. Wang, Z. Li, Recyclable nanobiocatalyst for enantioselective sulfoxidation: facile fabrication and high performance of chloroperoxidase-coated magnetic nanoparticles with iron oxide core and polymer shell. J. Am. Chem. Soc. 131 (2009) 12892.

[13] A. H. Lu, E. L. Salabas, F. Schuth, Magnetic nanoparticles: synthesis, protection, functionalization, and application. Angew. Chem. Int. Ed. 46 (2007) 1222.

[14] A. Corma, From Microporous to Mesoporous Molecular Sieve Materials and Their Use in Catalysis. Chem. Rev. 97 (1997) 2373.

[15] A.H. Lu, F. Schüth, Nanocasting: A Versatile Strategy for Creating Nanostructured Porous Materials. Adv. Mater. 18 (2006) 1793.

[16] J. Y. Ying, Christian P. Mehnert, Michael S. Wong, Synthesis and Applications of Supramolecular-Templated Mesoporous Materials. Angew. Chem. Int. Ed. 38 (1999) 56.

[17] T.K. Jain, I. Roy, T.K. De, A. Maitra, Nanometer Silica Particles Encapsulating Active Compounds: A Novel Ceramic Drug Carrier. J. Am. Chem. Soc. 120 (1998) 11092.

[18] J. Szejtli, Introduction and General Overview of Cyclodextrin Chemistry. Chem. Rev. 98 (1998) 1743.

[19] H. Dodziuk, Cyclodextrins and Their Complexes: Chemistry, Analytical Methods Applications. Wiley-VCH, New York (2006).

[20] M. E. Davis, M. E. Brewster, Cyclodextrin-based pharmaceutics: past, present and future. Nat. Rev. Drug Discov. 3 (2004) 1023.

[21] D. W. Pack, A. S. Hoffman, S. Pun, P. S. Stayton, Design and development of polymers for gene delivery. Nat. Rev. Drug Discov. 4 (2005) 581.

[22] Y. Liu, Y. Chen, Cooperative binding and multiple recognition by bridged bis(beta-cyclodextrin)s with functional linkers. Acc. Chem. Res. 39 (2006) 681.

[23] R. Villalonga, R. Cao, A. Fragoso, Supramolecular chemistry of cyclodextrins in enzyme technology. Chem. Rev. 107 (2007) 3088.

[24] S. Li, W. C. Purdy, Cyclodextrins and Their Applications in Analytical Chemistry. Chem. Rev. 92 (1992) 1457.

[25] K. A. Connors, The Stability of Cyclodextrin Complexes in Solution. Chem. Rev. 97 (1997) 1325.

[26] W.C. Bowman, Neuromuscular block. Br. J. Pharmarcol. 147 (2006) S277.

[27] K. Mori, H. Yamashita, Design of Colloidal and Supported Metal Nanoparticles: Their Synthesis, Characterization, and Catalytic Application. J. Jpn. Petrol. Ins. 54 (2011) 1.

[28] M. M. Yallapu, S. F. Othman, E. T. Curtis, B. K. Gupta, M. Jaggi, S. C. Chauhan, Multi-functional magnetic nanoparticles for magnetic resonance imaging and cancer therapy. Biomaterials 32 (2011) 1890.

[29] K. Hayashi, K. Ono, H. Suzuki, M. Sawada, M. Moriya, T. Yogo, High-Frequency, Magnetic-Field-Responsive Drug Release from Magnetic Nanoparticle/Organic Hybrid Based on Hyperthermic Effect. ACS App. Mater. Interface 2 (2010) 1903.

[30] S. S. Banerjee, D.-H. Chen, Grafting of 2-Hydroxypropyl-beta-Cyclodextrin on Gum Arabic-Modified Iron Oxide Nanoparticles as a Magnetic Carrier for Targeted Delivery of Hydrophobic Anticancer Drug. Int. J. App. Ceram. Technol. 7 (2010) 111.

[31] H. Bierau, Z. Zhang, A. Lyddiatt, Direct process integration of cell disruption and fluidised bed adsorption for the recovery of intracellular proteins. Curr. Opin. Biotechnol. 74 (1999) 208.

[32] R. Hjorth, Expanded-bed adsorption in industrial bioprocessing: recent developments. Trends Biotechnol. 15 (1997) 230.

[33] I. Safarik, M. Safarikova, Use of magnetic techniques for the isolation of cells. J. Chromatogr. B 722 (1999) 33.

[34] Z. Zhang, D.A. O'Sullivan, A. Lyddiatt, Magnetically stabilised fluidised bed adsorption: Practical benefit of uncoupling bed expansion from fluid velocities in the purification of a recombinant protein from Escherichia coli. J. Chem. Technol. Biotechnol. 74 (1999) 270.

[35] R. R. Dauer, E. H. Dunlop, High gradient magnetic separation of yeast. Biotechnol. Bioengg. 37 (1991) 1021.

[36] R. Hartig, M. Hausmann, G. Luers, M. Kraus, G. Weber, C. Cremer, Continuous sorting of magnetizable particles by means of specific deviation. Rev. Sci. Instrum. 66 (1995) 3289.

[37] C. B. Fuh, S.Y. Chen, Magnetic split-flow thin fractionation of magnetically susceptible particles. J. Chromatogr. A 857 (1999) 193.

[38] H. Kolm, J. Oberteuffer, D. Kelland, High Gradiant Magnetic Separation. Sci. Am. 233 (1975) 46.

[39] G. M. Whitesides, R. J. Kazlauskas, L. Josephson, Magnetic separations in biotechnology. Trends Biotechnol. 1 (1983) 144.

[40] D. Melville, F. Paul, S. Roath, Direct magnetic separation of red cells from whole blood. Nature 255 (1975) 706.

[41] C. S. Owen, High gradient magnetic separation of erythrocytes. Biophys. J. 22 (1978) 171.

[42] R. P. Blakemore, R. B. Frankel, Magnetic navigation in bacteria. Sci. Am. 245 (1981) 58.

[43] P. Dunnil, M. D. Lilly, Purification of Enzymes Using Magnetic Bio-Afinity Materials. Biotechnol. Bioengg. 16 (1974) 987.

[44] B. L. Hirschbein, G. M. Whitesides, Affinity Separation of Enzymes from Mixtures Containing Suspended Solids Comparisons of Magnetic and Nonmagnetic Techniques. App. Biocehm. Biotechnol. 7 (1982) 157.

[45] C. H. Setchell, Magnetic Separations in Biotechnology-a Review. J. Chem. Technol. Biotechnol. 35B (1985) 175.

[46] Y. Tamaura, K. Takahashi, Y. Kodera, Y. Saito, Y. Inada, Chemical Modification Of Lipase With Ferromagnetic Modifier -A Ferromagnetic Modified Lipase. Biotechnol. Lett. 8 (1986) 877.

[47] T. Lea, F. Vartdal, K. Nustad, S. Funderud, A. Berge, T. Ellingsen, R. Schmid, P. Stenstad, J. Ugelstad, Monosized, magnetic polymer particles: their use in separation of cells and subcellular components, and in the study of lymphocyte function in vitro. J. Mol. Recognit. 1 (1988) 9.

[48] M. Uhlen, Magnetic separation of DNA. Nature 340 (1989) 733.

[49] V. Goetz, M. Remaud, D. J. Graves, A novel magnetic silica support for use in chromatographic and enzymatic bioprocessing. Biotechnol. Bioengg. 37 (1991) 614.

[50] S. M. O'Brien, R. P. Sloane, O. R. T. Thomas, P. Dunnill, Characterisation of non-porous magnetic chelator supports and their use to recover polyhistidine-tailed T4 lysozyme from a crude E. coli extract. J. Biotechnol. 54 (1997) 53.

[51] O. Diettrich, K. Mills, A. W. Johnson, A. Hasilik, B. G. Winchester, Application of magnetic chromatography to the isolation of lysosomes from fibroblasts of patients with lysosomal storage disorders. FEBS Lett. 441 (1998) 369.

[52] M. D. Saikia, Studies on adsorption of amino acids on cyclodextrin bonded to silica particles. Colloids Surf. A 329 (2008) 177.

[53] S. Tang, L. Kong, J. Ou, Y. Liu, X. Li, H. Zou, Application of cross-linked beta-cyclodextrin polymer for adsorption of aromatic amino acids. J. Mol. Recognit. 19 (2006) 39.

[54] H. Li, P. A. Helm, G. Paterson, C. D. Metcalfe, The effects of dissolved organic matter and pH on sampling rates for polar organic chemical integrative samplers (POCIS). Chemosphere 83 (2011) 271.

[55] S. A. Piletsky, H. A. Andersson, I. A. Nicholls, Combined Hydrophobic and Electrostatic Interaction-Based Recognition in Molecularly Imprinted Polymers. Macromolecules 32 (1999) 633.

[56] D. S. Grzegorczyk, G. Carta, Adsorption of amino acids on porous polymeric adsorbents--I. Equilibrium. Chem. Eng. Sci. 51 (1996) 807.

[57] J. R. Domínguez, T. González, P. Palo, E. M. Cuerda-Correa, Removal of common pharmaceuticals present in surface waters by Amberlite XAD-7 acrylic-ester-resin: Influence of pH and presence of other drugs. Desalination 269 (2011) 231.

[58] Y. Deng, F. Wu, B. Liu, X. Hu, C. Sun, Sorptive removal of β-blocker propranolol from aqueous solution by modified attapulgite: Effect factors and sorption mechanisms. Chem. Eng. J. 174 (2011) 571.

[59] C. F. Brewer, van der Waals' induced 13C NMR shifts in crystalline amino acids and peptides. Eur. J. Biochem. 143 (1984) 363.

[60] C. Gazpio, M. Sanchez, J. Isasi, I. Velaz, C. Martin, C. Martinez Oharriz, A. Zornoza, Sorption of pindolol and related compounds by a β-cyclodextrin polymer: Isosteric heat of sorption. Carbohyd. Polym. 71 (2008) 140.

[61] D. -H. Chen, M. H. Liao, Preparation and characterization of YADH-bound magnetic nanoparticles. J. Mol. Catalysis B Enzymatic 16 (2002) 283.

[62] J. C. Janson, L. Ryden, Protein purification: Principles, high-resolution methods, and applications. VCH Publishers:Weinheim (1989).

[63] R. C. O'Handley, Modern Magnetic Materials: Principles and Applications. Wiley, New York 38 (2000) 41.

[64] N. Spaldin, Magnetic Materials: Fundamentals and Device Applications. Cambridge University Press, Cambridge, UK (2003).

[65] R. M. Cornell, U. Schwertmann, The iron oxides: Structure, properties, reactions, occurrences, and uses. Wiley-VCH:Weinheim, Germany (2003).

[66] D. R. Lide, CRC Handbook of Chemistry and Physics. Taylor & Francis CRC Press, Boca Raton, FL (2004).

[67] H. J. Williams, R. M. Bozroth, Magnetic Anisotropy of Nickel at 20 degree K. Phys. Rev. 56 (1939) 837.

[68] S. Sun, C. B. Murray, D. Weller, L. Folks, Monodisperse FePt Nanoparticles and Ferromagnetic FePt Nanocrystal Superlattices. Science 287 (2000) 1989.

[69] D. Weller, M. F. Doerner, Extremely high-density longitudinal magnetic recording media. Annu. Rev. Mater. Sci. 30 (2000) 611.

[70] Z. Kakol, J.M. Honig, Influence of deviations from ideal stoichiometry on the anisotropy parameters of magnetite $Fe_{3(1-\delta)}O_4$. Phys. Rev. B: Condens. Matter Mater. Phys. 40 (1989) 9090.

[71] R. S. Weisz, Magnetic Anisotropy Constants of Ferromagnetic Spinels. Phys. Rev. 96 (1954) 800.

[72] R. Valenzuela, Magnetic Ceramics. Cambridge University Press, Cambridge, UK (1994).

[73] A. B. Chin, I. D. Yaacob, Synthesis and characterization of magnetic iron oxide nanoparticles via w/o microemulsion and Massart's procedure. J. Mater. Pro. Technol. 191 (2007) 235.

[74] C. Albonoz, S. Jacobo, Preparation of a biocompatible magnetic film from an aqueous ferrofluid. J. Magn. Magn. Mater. 305 (2006) 12.

[75] E. H. Kim, H. L. Sook, B.K. Kwak, B. K. Kim, Synthesis of ferrofluid with magnetic nanoparticles by sonochemical method for MRI contrast agent. J. Magn. Magn. Mater. 289 (2005) 328.

[76] J. Wan, X. Chen, Z. Wang, X. Yang, Y. Qian, A soft-template-assisted hydrothermal approach to single-crystal Fe_3O_4 nanorods. J. Crys. Gro. 276 (2005) 571.

[77] M. Kimata, D. Nakagawa, M. Hasegawa, Preparation of monodisperse magnetic particles by hydrolysis of iron alkoxide. Powder Technol. 132 (2003) 112.

[78] G. S.-Alvarez, M. Muhammed, A. Zagorodni, Novel flow injection synthesis of iron oxide nanoparticles with narrow size distribution. Chem. Eng. Sci. 61 (2006) 4625.

[79] S. Basak, D. Chen, P. Biswas, Electrospray of ionic precursor solutions to synthesize iron oxide nanoparticles: Modified scaling law. Chem. Eng. Sci. 62 (2007) 1263.

[80] C. E. Sjogren, C. Johansson, A. Naevestad, P. C. Sontum, K. Briley-Saebo, A. K. Fahlvik, Crystal size and properties of superparamagnetic iron oxide (SPIO) particles. Magn. Reson. Imaging 15 (1997) 55.

[81] A. C. Nunes, Z. C. Yu, Fractionation of a water-based ferrofluid. J. Magn. Magn. Mater. 65 (1987) 265.

[82] L. Babes, B. Denizot, G. Tanguy, J. J. Le Jeune, P. Jallet, Synthesis of Iron Oxide Nanoparticles Used as MRI Contrast Agents: A Parametric Study. J. Colloid Interface Sci. 212474.

[83] S. Thurm, S. Odenbach, Magnetic separation of ferrofluids. J. Magn. Magn. Mater. 252 (2002) 247.

[84] I. Martínez-Mera, M. E. Espinosa-Pesqueira, R. Pérez-Hernández, J. Arenas-Alatorre, Synthesis of magnetite (Fe_3O_4) nanoparticles without surfactants at room temperature. Mater. Lett. 61 (2007) 4447.

[85] Y.-k. Su, M. Ma, Y. Zhang, N. Gu, Synthesis of nanometer-size maghemite particles from magnetite. Colloid Surf. A; Physicochemical and Engg. Aspects 245 (2004) 15.

[86] J. Qiu, R. Yang, M. Li, N. Jiang, Preparation and characterization of porous ultrafine FeO particles. Mater. Res. Bull. 40 (2005) 1968.

[87] R. Nagarajan, Nanoparticles: Building Blocks for Nanotechnology. ACS Publisher (2008) 2.

[88] Y. Sahoo, A. Goodarzi, M. T. Swihart, T. Ohulchanskyy, N. Kaur, E. P. Furlani., P. N. Prasad, Aqueous ferrofluid of magnetite nanoparticles: Fluorescence labeling and magnetophoretic control. J. Phys. Chem. B 109 (2005) 3879.

[89] A. Bee, R. Massart, S. Neveu, Synthesis of very fine maghemite particles. J. Magn. Magn. Mater. 149 (1995) 6.

[90] G. S. R. krishnamurti, P. M. Huang, Influence of citrate on the kinetics of Fe(II) oxidation and the formation of iron oxyhydroxides. Clays Clay Miner. 39 (1991) 28.

[91] C. Liu, P. M. Huang, Atomic Force Microscopy and Surface Characteristics of Iron Oxides Formed in Citrate Solutions. Soil Sci. Soc. Am. J. 63 (1999) 65.

[92] N. Fauconnier, J. N. Pons, J. Roger, A. Bee, Thiolation of Maghemite Nanoparticles by Dimercaptosuccinic Acid. J. Colloid Interface Sci. 194 (1997) 427.

[93] B. Denizot, G. Tanguy, F. Hindre, E. Rump, J. J. Le Jeune, P. Jallet, Phosphorylcholine Coating of Iron Oxide Nanoparticles. J. Colloid Interface Sci. 209 (1999) 66.

[94] D. Portet, B. Denizot, E. Rump, F. Hindre, Le J. J.-L. Jeune, P. Jallet, Comparative biodistribution of thin-coated iron oxide nanoparticles TCION: Effect of different bisphosphonate coatings. Drug Dev. Res. 54 (2001) 173.

[95] P. H. Mutin, G. G. AndréVioux, Organic/inorganic hybrid materials based on organophosphorus coupling molecules: from metal phosphonates to surface modification of oxides. C. R. Chimie 6 (2003) 1153.

[96] C. Yee, G. Kataby, A. Ulman, T. Prozorov, H. White, A. King, M. Rafailovich, J. Sokolov, A. Gedanken, Self-Assembled Monolayers of Alkanesulfonic and -phosphonic Acids on Amorphous Iron Oxide Nanoparticles. Langmuir 15 (1999) 7111.

[97] Y. Sahoo, H. Pizem, T. Fried, D. Golodnitsky, L. Burstein, C. N. Sukenik, G. Markovich, Alkyl Phosphonate/Phosphate Coating on Magnetite Nanoparticles: A Comparison with Fatty Acids. Langmuir 17 (2001) 7907.

[98] S. Mohapatra, N. Pramanik, S. K. Ghosh, P. Pramanik, Synthesis and characterization of ultrafine poly(vinylalcohol phosphate) coated magnetite nanoparticles. J. Nanosci. Nanotechnol. 6 (2006) 823.

[99] D. Roberts, W. L. Zhu, C. M. Frommen, Z. Rosenzweig, Synthesis of gadolinium oxide magnetoliposomes for magnetic resonance imaging. J. App. Phys. 87 (2000) 6208.

[100] M. D. Alcala, C. Real, Synthesis based on the wet impregnation method and characterization of iron and iron oxide-silica nanocomposites. Solid State Ionics 177 (2006) 955.

[101] K. Woo, J. Hong, J. -P. Ahn, Synthesis and surface modification of hydrophobic magnetite to processible magnetite@silica-propylamine. J. Magn. Magn. Mater. 293 (2005) 177.

[102] Y. Sun, L. Duan, Z. Guo, Y. DuanMu, M. Ma, L. Xu, Y. Zhang, N. Gu, An improved way to prepare superparamagnetic magnetite-silica core-shell nanoparticles for possible biological application. J. Magn. Magn. Mater. 285 (2005) 65.

[103] W. Stober, A. Fink, E. Bohn, Controlled growth of monodisperse silica spheres in the micron size range. J. Colloid Interface Sci. 26 (1968) 62.

[104] A. P. Philipse, M. P. B. van Bruggen, C. Pathmamanoharan, Magnetic Silica Dispersions: Preparation and Stability of Surface-Modified Silica Particles with a Magnetic Core. Langmuir 10 (1994) 92.

[105] Y. Lu, Y. Yin, B. T. Mayers, Y. Xia, Modifying the Surface Properties of Superparamagnetic Iron Oxide Nanoparticles through A Sol−Gel Approach. Nano Lett. 2 (2002) 183.

[106] X. Liu, Z. Ma, J. Xing, H. Liu, Preparation and characterization of amino−silane modified superparamagnetic silica nanospheres. J. Magn. Magn. Mater. 270 (2004) 1.

[107] M. D. Buttermouth, S. A. Bell, S. P. Armes, A. W. Simpson, Synthesis and Characterization of Polypyrrole− Magnetite–Silica Particles. J. Colloid Interface Sci. 183 (1996) 91.

[108] P. Tartaj, C. J. Serna, Synthesis of monodisperse superparamagnetic Fe/silica nanospherical composites. J. Am. Chem. Soc. 125 (2003) 15754.

[109] P. Tartaj, C. J. Serna, Microemulsion-Assisted Synthesis of Tunable Superparamagnetic Composites. Chem. Mater. 14 (2002) 4396.

[110] H. -H. Yang, S. -Q. Zhang, X. -L. Chen, Z. -X. Zhuang, J. -G. Xu, X. -R. Wang, Magnetite-containing spherical silica nanoparticles for biocatalysis and bioseparations. Anal. Chem. 76 (2004) 1316.

[111] P. Tartaj, T. González-Carreño, C. J. Serna, Synthesis of Nanomagnets Dispersed in Colloidal Silica Cages with Applications in Chemical Separation. Langmuir 18 (2002) 4556.

[112] M. Chen, S. Yamamuro, D. Farrell, S. A. Majetich, Gold-coated iron nanoparticles for biomedical applications. J. App. Phys. 93 (2003) 7551.

[113] J. Lin, W. Zhou, A. Kumbhar, J. Wiemann, J. Fang, E. E. Carpenter, C. J. O'Connor, Gold-Coated Iron (Fe@Au) Nanoparticles: Synthesis, Characterization, and Magnetic Field-Induced Self-Assembly. J. Am. Chem. Soc. 159 (2001) 26.

[114] J. L. Lyon, D. A. Fleming, M. B. Stone, P. Schiffer, M. E. Williams, Synthesis of Fe Oxide Core/Au Shell Nanoparticles by Iterative Hydroxylamine Seeding. Nano Lett. 4 (2004) 719.

[115] C. C. Berry, S. Wells, S. Charles, A. S. G. Curtis, Dextran and albumin derivatised iron oxide nanoparticles: influence on fibroblasts in vitro. Biomaterials 24 (2003) 4551.

[116] K. M. Lee, S. G. Kim, W. S. Kim, S. S. Kim, Properties of iron oxide particles prepared in the presence of dextran. Korean J. Chem. Engg. 19 (2002) 480.

[117] L.F. Gamarra, G.E.S.Brito, W. M. Pontuschka, E. Amaro, A. H. C. Parma, G. F. Goya, Biocompatible superparamagnetic iron oxide nanoparticles used for contrast agents: a structural and magnetic study. J. Magn. Magn. Mater. 289 (2005) 439.

[118] R. S. Molday, D. Mackenzie, Immunospecific ferromagnetic iron-dextran reagents for the labeling and magnetic separation of cells. J. Immunol. Methods 52 (1982) 353.

[119] H. Pardoe, W. Chua-anusorn, T. G. St Pierre, J. Dobson, Structural and magnetic properties of nanoscale iron oxide particles synthesized in the presence of dextran or polyvinyl alcohol. J. Magn. Magn. Mater. 225 (2001) 41.

[120] M. C. Bautista, O. Bomati-Miguel, M. P. Morales, C. J. Serna, S. Veintemillas-Verdaguer, Surface characterisation of dextran-coated iron oxide nanoparticles prepared by laser pyrolysis and coprecipitation. J. Magn. Magn. Mater. 293 (2005) 20.

[121] D. K. Kim, Y. Zhang, J. Kehr, T. Klason, B. Bjelke, M. Muhammed, Characterization and MRI study of surfactant-coated superparamagnetic nanoparticles administered into the rat brain. J. Magn. Magn. Mater. 225 (2001) 256.

[122] M. D. Butterworth, L. Illum, S. S. Davis, Preparation of ultrafine silica-and PEG-coated magnetite particles. Colloid Surface A: Physicochemical and Eng. Aspects 179 (2001) 93.

[123] K. G. Paul, T. B. Frigo, J. Y. Groman, E. V. Groman, Synthesis of ultrasmall superparamagnetic iron oxides using reduced polysaccharides. Bioconjugate Chem. 15 (2004) 394.

[124] M. D. Shultza, S. Calvin, P. P. Fatouros, E. E. Carpenter, Enhanced ferrite nanoparticles as MRI contrast agents. J. Magn. Magn. Mater. 311 (2007) 464.

[125] M. Sairam, B. V. K. Naidu, S. K. Nataraj, B. Sreedhar, T. M. Aminabhavi, Poly(vinyl alcohol)-iron oxide nanocomposite membranes for pervaporation dehydration of isopropanol, 1,4-dioxane and tetrahydrofuran. J. Membrane Sci. 283 (2006) 65.

[126] B. Schopf, T. Neuberger, K. Schulze, A. Petri, M. Chastellan, M. Hofmann, H. Hofmann, B. Vonrechenberg, Methodology description for detection of cellular uptake of PVA coated superparamagnetic iron oxide nanoparticles (SPION) in synovial cells of sheep. J. Magn. Magn. Mater. 293 (2005) 411.

[127] J. Lee, T. Isobe, M. Senna, Preparation of Ultrafine Fe_3O_4 Particles by Precipitation in the Presence of PVA at High pH. J. Colloid Interface Sci. 177 (1996) 490.

[128] M. Chastellan, A. Petri, H. Hofmann, Particle size investigations of a multistep synthesis of PVA coated superparamagnetic nanoparticles. J. Colloid Interface Sci. 278 (2004) 353.

[129] C. Albornoz, S. E. Jacobo, Preparation of a biocompatible magnetic film from an aqueous ferrofluid. J. Magn. Magn. Mater. 305 (2006) 12.

[130] F. Llanes, D. H. Ryan, R. H. Marchessault, Magnetic nanostructured composites using alginates of different M/G ratios as polymeric matrix. Int. J. Biol. Macromol. 27 (2000) 35.

[131] S. Laurent, D. Forge, M. Port, A. Roch, C. Robic, L. V. Elst, Luce, R. N. Muller, Magnetic iron oxide nanoparticles: synthesis, stabilization, vectorization, physicochemical characterizations, and biological applications. Chem. Rev. 108 (2008) 2064.

[132] Y. Nishio, A. Yamada, K. Ezaki, Y. Miyahsita, H. Furukawa, K. Horie, Preparation and magnetometric characterization of iron oxide-containing alginate/poly(vinyl alcohol) networks. Polymer 45 (2004) 7129.

[133] P. Sipos, O. Berkesi, E. Tombacz, T. G. St. Pierre, J. Webb, Formation of spherical iron(III) oxyhydroxide nanoparticles sterically stabilized by chitosan in aqueous solutions. J. Inorg. Biochem. 95 (2003) 55.

[134] S. R. Bhattarai, R. Bahadur K.C, S. Aryal, M. S. Khil, H. Y. Kim, N-Acylated chitosan stabilized iron oxide nanoparticles as a novel nano-matrix and ceramic modification. Carb. Polym. 69 (2007) 467.

[135] E. H. Kim, H. S. Lee, B. K. Kwak, B. -K. Kim, Synthesis of ferrofluid with magnetic nanoparticles by sonochemical method for MRI contrast agent. J. Magn. Magn. Mater. 289 (2005) 328.

[136] H. S. Lee, E. H. Kim, H. Shao, B. K. Kwak, Synthesis of SPIO-chitosan microspheres for MRI-detectable embolotherapy. J. Magn. Magn. Mater. 293 (2005) 102.

[137] A. Kondo, H. Fukuda, Preparation of thermo-sensitive magnetic hydrogel microspheres and application to enzyme immobilization. J. Ferment. Bioeng. 84 (1997) 337.

[138] N. Shamim, L. Hong, K. Hidajat, M.S. Uddin, Thermosensitive-polymer-coated magnetic nanoparticles: adsorption and desorption of bovine serum albumin. J. Colloid Interface Sci. 304 (2006) 1.

[139] A. Kondo, H. Kamura, K. Higashitani, Development and application of thermo-sensitive magnetic immunomicrospheres for antibody purification. App. Microbiol. Biotechnol. 41 (1994) 99.

[140] D. Schmaljohann, Thermo- and pH-responsive polymers in drug delivery. Adv. Drug Deliv. Rev. 58 (2006) 1655.

[141] K. Naa, J. H. Park, S. W. Kim, B. K. Sun, D. G. Woo, K.-H. Park, Delivery of dexamethasone, ascorbate, and growth factor (TGF beta-3) in thermo-reversible hydrogel constructs embedded with rabbit chondrocytes. Biomaterials 27 (2006) 5951.

[142] G. D. Mendenhall, Y. Geng, J. Hwang, Optimization of Long-Term Stability of Magnetic Fluids from Magnetite and Synthetic Polyelectrolytes. J. Colloid Interface Sci. 184 (1996) 519.

[143] K. Wormuth, Superparamagnetic Latex via Inverse Emulsion Polymerization. J. Colloid Interface Sci. 241 (2001) 366.

[144] M. Iijima, Y. Yonemochi, M. Tsukada, H. Kamiya, Microstructure control of iron hydroxide nanoparticles using surfactants with different molecular structures. J. Colloid Interface Sci. 298 (2006) 202.

[145] S. A. Gómez-Lopera, J. L. Arias, V. Gallardo, A. V. Delgado, Colloidal stability of magnetite/poly(lactic acid) core/shell nanoparticles. Langmuir 22 (2006) 2816.

[146] C. Flesch, C. Delaite, P. Dumas, E. Bourgeat-Lami, E. Duguet, Grafting of poly(e-caprolactone) onto maghemite nanoparticles. J. Polym. Sci. Part A: Polym. Chem. 42 (2004) 6011.

[147] R. Lawaczeck, M. Menzel, H. Pietsch, Superparamagnetic iron oxide particles: contrast media for magnetic resonance imaging. App. Organometal. Chem. 18 (2004) 506.

[148] L. Yuan, J. Li, W. Gang, S. LiQing, H. Bin, L. Li, N. Yu, W. Yao, G. ZhongWei, Study on the α-cyclodextrin/poly(ethylene glycol) self-assembly supramolecular nanoparticles for drug delivery. Sci. China Chem. 53 (2010) 495.

[149] Y. Chen, Y. Zhang, Y. Liu, Multidimensional nanoarchitectures based on cyclodextrins. Chem. Commun. 46 (2010) 5622.

[150] A.Z.M. Badruddoza, A.S.H. Tay, P.Y. Tan, K. Hidajat, M.S. Uddin, Carboxymethyl-beta-cyclodextrin conjugated magnetic nanoparticles as nano-adsorbents for removal of copper ions: Synthesis and adsorption studies. J. Hazard. Mater. 185 (2011) 1177.

[151] H. Cao, J. He, L. Deng, X. Gao, Fabrication of cyclodextrin-functionalized superparamagnetic Fe_3O_4/amino-silane core–shell nanoparticles via layer-by-layer method. App. Surface Sci. 255 (2009) 7974.

[152] Y. Wang, J. F. Wong, X. Teng, X. Z. Lin, H. Yang, "Pulling" Nanoparticles into Water: Phase Transfer of Oleic Acid Stabilized Monodisperse Nanoparticles into Aqueous Solutions of alfa-Cyclodextrin. Nano Lett. 3 (2003) 1555.

[153] S. He, W. Shi, X. Zhang, J. Li, Y. Huang, Beta-cyclodextrins-based inclusion complexes of $CoFe_2O_4$ magnetic nanoparticles as catalyst for the luminol chemiluminescence system and their applications in hydrogen peroxide detection. Talanta 82 (2010) 377.

[154] K. Mori, N. Yoshioka, Y. Kondo, T. Takeuchi, H. Yamashita, Catalytically active, magnetically separable, and water-soluble FePt nanoparticles modified with cyclodextrin for aqueous hydrogenation reactions. Green Chem. 11 (2009) 1337.

[155] H. -B. Xia, P. Foo, J. Yi, Water-Dispersible Spherically Hollow Clusters of Magnetic Nanoparticles. Chem. Mater. 21 (2009) 2442.

[156] H. Zhang, M.-L. Peng, Y.-L. Cui, C. Chen, Magnetic HP-β-CD Composite Nanoparticle: Synthesis, Characterization and Application as a Carrier of Doxorubicin in vitro. Chin. J. Chem. 26 (2008) 1737.

[157] I. Nedkov, L. Slavov, T. Merodiiska, P. Lukanov, Ph. Tailhades, M. Gougeon, R. E. Vandenberghe, Size effects in monodomain magnetite based ferrofluids. J. Nanopart. Res. 10 (2008) 877.

[158] Y. Hou, H. Kondoh, M. Shimojo, E. O. Sako, N. Ozaki, T. Kogure, T. Ohta, Inorganic nanocrystal self-assembly via the inclusion interaction of beta-cyclodextrins: toward 3D spherical magnetite. J. Phys. Chem. B 109 (2005) 4845.

[159] D. Bonacchi, A. Caneschi, D. Dorignac, A. Falqui, D. Gatteschi, D. Rovai, C. Sangregorio, R. Sessoli, Nanosized Iron Oxide Particles Entrapped in Pseudo-Single Crystals of γ-Cyclodextrin. Chem. Mater. 16 (2004) 2016.

[160] H.-B. Xia, J. Yi, P.-S. Foo, B. Liu, Facile Fabrication of Water-Soluble Magnetic Nanoparticles and Their Spherical Aggregates. Chem. Mater. 19 (2007) 4087.

[161] J. Hu, D. Shao, C. Chen, G. Sheng, J. Li, X. Wang, M. Nagatsu, Plasma-induced grafting of cyclodextrin onto multiwall carbon nanotube/iron oxides for adsorbent application. J. Phys. Chem. B 114 (2010) 6779.

[162] L.A. C. Cruz, C. A. M. Perez, H. A. M. Romero, P. E. G. Casillas, Synthesis of magnetite nanoparticles–β-cyclodextrin complex. J. Alloy. Compd. 466 (2008) 330.

[163] S. S. Banerjee, D. -H. Chen, Magnetic Nanoparticles Grafted with Cyclodextrin for Hydrophobic Drug Delivery. Chem. Mater. 19 (2007) 6345.

[164] Y. Ji, X. Liu, M. Guan, C. Zhao, H. Huang, H. Zhang, C. Wang, Preparation of functionalized magnetic nanoparticulate sorbents for rapid extraction of biphenolic pollutants from environmental samples. J. Sep. Sci. 32 (2009) 2139.

[165] X. Sun, C. Zheng, F. Zhang, L. Li, Y. Yang, G. Wu, N. Guan, β-Cyclodextrin-Assisted Synthesis of Superparamagnetic Magnetite Nanoparticles from a Single Fe(III) Precursor. J. Phys. Chem. C 112 (2008) 17148.

[166] R. X. Li, S. M. Liu, J. Q. Zhao, H. Otsuka, A. Takahara, Preparation and characterization of cross-linked β-cyclodextrin polymer/Fe_3O_4 composite nanoparticles with core-shell structures. Chin. Chem. Lett 22 (2011) 217.

[167] R. V. Kumar, Y. Koltypin, X. N. Xu, Y. Yeshurun, A. Gedanken, I. Felner, Fabrication of magnetite nanorods by ultrasound irradiation. J. App. Phys. 89 (2001) 6324.

[168] M.Racuciu, D.E. Creanga, N. Sulitanu, Dimensional analysis of aqueous magnetic fluids. App. Phys. A 89 (2007) 565.

[169] S. Moore, W. H. Stein, Chromatographic determination of amino acids by the use of automatic recording equipment. Methods Enzymol 6 (1963) 819.

[170] M. Rekharsky, Y. Inoue, Chiral Recognition Thermodynamics of β-Cyclodextrin: The Thermodynamic Origin of Enantioselectivity and the Enthalpy−Entropy Compensation Effect. J. Am. Chem. Soc. 122 (2000) 4418.

[171] J. L. Clark, J. L. Stezowski, Molecular Recognition in Cyclodextrin Complexes of Amino Acid Derivatives. 1. Crystallographic Studies of β-Cyclodextrin Complexes with N-Acetyl-l-phenylalanine Methyl Ester and N -Acetyl-l-phenylalanine Amide Pseudopeptides. J. Am. Chem. Soc. 123 (2001) 9880.

[172] K. B. Lipkowitz, S. Raghothama, J. Yang, Enantioselective Binding of Tryptophan by alfa-Cyclodextrin. J. Am. Chem. Soc 114 (1992) 1554.

[173] M. Roth, Fluorescence Reaction for Amino Acids. Anal. Chem. 43 (1971) 880.

[174] Y. Tapuhi, D. E. Schmidt, W. Lindner, B. L. Karger, Dansylation of amino acids for high-performance liquid chromatography analysis. Anal. Biochem. 115 (1981) 123.

[175] B. A. Bidlingmeyer, S. A. Cohen, T. L. Tarvin, Rapid analysis of amino acids using pre-column derivatization. J. Chromatogr. B: Biomed. Sci. and Appl. 336 (1984) 93.

[176] P.A. Haynes, D. Sheumack, J. Kibby, J. W. Redmond, Amino acid analysis using derivatisation with 9-fluorenylmethyl chloroformate and reversed-phase high-performance liquid chromatography. J. Chromatogr. A 540 (1991) 177.

[177] C. Cooper, N. Packer, K. Williams, Amino acid analysis protocols. Humana Press, Totowa, NJ , pp 1-7 (2001).

[178] D. W. Armstrong, X. Yang, S. M. Han, R. A. Menges, Direct liquid chromatographic separation of racemates with an .alpha.-cyclodextrin bonded phase. Anal. Chem. 59 (1987) 2594.

[179] W. A. Tao, D. Zhang, E. N. Nikolaev, C.R. Graham, Copper(II)-Assisted Enantiomeric Analysis of D,L-Amino Acids Using the Kinetic Method: Chiral Recognition and Quantification in the Gas Phase. J. Am. Chem. Soc. 122 (2000) 10598.

[180] O. Hofstetter, H. Lindstrom, H. Hofstetter, Direct Resolution of Enantiomers in High-Performance Immunoaffinity Chromatography under Isocratic Conditions. Anal. Chem. 74 (2002) 2119.

[181] I. Ali, V. K. Gupta, H. Y. Aboul-Enein, Chiral Resolution of Racemic Environmental Pollutants by Capillary Electrophoresis. Crit. Rev. Anal. Chem. 38 (2008) 132.

[182] H. J. Issaq, K. C. Chan, Separation and detection of amino acids and their enantiomers by capillary electrophoresis: A review. Electrophoresis 16 (1995) 467.

[183] B. Chankvetadze, Capillary electrophoresis in chiral analysis. Wiley, Chichester (1997).

[184] Z. -P. Yao, T. S. M. Wan, K.-P. Kwong, C.-T. Che, Chiral Analysis by Electrospray Ionization Mass Spectrometry/Mass Spectrometry. 1. Chiral Recognition of 19 Common Amino Acids. Anal. Chem. 72 (2000) 5383.

[185] C. -F. Tsai, C.-F. Li, H.-M. Chang, Enantiomeric Separation of Dansyl-Derivatized dl-Amino Acids by β-Cyclodextrin-Modified Micellar Electrokinetic Chromatography. J. Agric. Food Chem. 46 (1998) 979.

[186] A. Mie, M. Jörntén-Karlsson, B.-O. Axelsson, A. Ray, C. T. Reimann, Enantiomer separation of amino acids by complexation with chiral reference compounds and high-field asymmetric waveform ion mobility spectrometry: preliminary results and possible limitations. Anal. Chem. 79 (2007) 2850.

[187] J. L. Wachtel, H. G. Cassidy, Chromatography as a Means of Separating Amino Acids. J. Am. Chem. Soc. 65 (1943) 665.

[188] C. H. W. Hirs, S. Moore, W.H. Stein, The Chromatography of Amino Acids on Ion Exchange Resins. Use of Volatile Acids for Elution. J. Am. Chem. Soc. 76 (1954) 6063.

[189] D. E.Johnson, S. J. Scott, A. Meister, Gas-Liquid Chromatography of Amino Acid Derivatives. Anal. Chem. 33 (1961) 669.

[190] W. Parr, P. Y. Howard, Structural effect of selected dipeptides as stationary phases for the chromatographic separation of enantiomeric amino acids. Anal. Chem. 45 (1973) 711.

[191] W. A. Koenig, G.J. Nicholson, Glass capillaries for fast gas chromatographic separation of amino acid enantiomers. Anal. Chem. 47 (1975) 951.

[192] E. Bayer, E. Grom, B. Kaltenegger, R. Uhmann, Separation of amino acids by high performance liquid chromatography. Anal. Chem. 48 (1976) 1106.

[193] A. Dobashi, K. Oka, S. Hara, Optical resolution of the D- and L-amino acid family by liquid-solid chromatography. J. Am. Chem. Soc. 102 (1980) 7122.

[194] N. Nimura, T. Suzuki, Y. Kasahara, T. Kinoshita, Reversed-phase liquid chromatographic resolution of amino acid enantiomers by mixed chelate complexation. Anal. Chem. 53 (1981) 1380.

[195] W.L. Hinze, T.E. Riehl, D.W. Armstrong, W. DeMond, A. Alak, T. Ward, Liquid chromatographic separation of enantiomers using a chiral .beta.-cyclodextrin-bonded stationary phase and conventional aqueous-organic mobile phases. Anal. Chem. 57 (1985) 237.

[196] K. Fujimura, S. Suzuki, K. Hayashi, S. Masuda, Retention behavior and chiral recognition mechanism of several cyclodextrin-bonded stationary phases for dansyl amino acids. Anal. Chem. 62 (1990) 2198.

[197] R.K. Gilpin, S.E. Ehtesham, R.B. Gregory, Liquid chromatographic studies of the effect of temperature on the chiral recognition of tryptophan by silica-immobilized bovine albumin. Anal. Chem. 63 (1991) 2825.

[198] A. Messina, A.M. Girelli, M. Flieger, M. Sinibaldi, P. Sedmera, L. Cvak, Direct resolution of optically active isomers on chiral packings containing ergoline skeletons. 5. Enantioseparation of amino Acid derivatives. Anal. Chem. 68 (1996) 1191.

[199] T. Iida, H. Matsunaga, T. Fukushima, T. Santa, H. Homma, K. Imai, Complete enantiomeric separation of phenylthiocarbamoylated amino acids on a tandem column of reversed and chiral stationary phases. Anal. Chem. 69 (1997) 4463.

[200] A. Berthod, A. Valleix, V. Tizon, E. Leonce, C. Caussignac, D.W. Armstrong, Retention and Selectivity of Teicoplanin Stationary Phases after Copper Complexation and Isotopic Exchange. Anal. Chem. 73 (2001) 5499.

[201] M. del Mar Caja López, G.P. Blanch, M. Herraiz, Derivatization of chiral amino acids in supercritical carbon dioxide. Anal. Chem. 76 (2004) 736.

[202] C.V. Hoffmann, R. Pell, M. Lämmerhofer, W. Lindner, Synergistic effects on enantioselectivity of zwitterionic chiral stationary phases for separations of chiral acids, bases, and amino acids by HPLC. Anal. Chem. 80 (2008) 8780.

[203] P. Gozel, E. Gassmann, H. Michelsen, R.N. Zare, Electrokinetic resolution of amino acid enantiomers with copper(II)-aspartame support electrolyte. Anal. Chem. 59 (1987) 44.

[204] R. Kuhn, F. Erni, T. Bereuter, J. Haeusler, Chiral recognition and enantiomeric resolution based on host-guest complexation with crown ethers in capillary zone electrophoresis. Anal. Chem. 64 (1992) 2815.

[205] K.H. Gahm, A.M. Stalcup, Capillary Zone Electrophoresis Study of Naphthylethylcarbamoylated .beta.-Cyclodextrins. Anal. Chem. 67 (1995) 19.

[206] H.M. Chang, C.F. Tsai, C.F. Li, Enantiomeric Separation of Dns- dl-amino Acids by γ-Cyclodextrin-Modified Micellar Capillary Electrophoresis. J. Agric. Food Chem. 46 (1998) 4598.

[207] N. Budanova, E. Shapovalova, S. Lopatin, V. Varlamov, O. Shpigun, Heptakis(6-amino-6-deoxy)-beta-cyclodextrin as a chiral selector for the separation of anionic analyte enantiomers by capillary electrophoresis. Electrophoresis 25 (2004) 2795.

[208] D.L. Kirschner, M. Jaramillo, T.K. Green, Enantioseparation and stacking of Cyanobenz[f]isoindole-amino acids by reverse polarity capillary electrophoresis and sulfated beta-cyclodextrin. Anal. Chem. 79 (2007) 736.

[209] T. Zhang, Q. Fang, W.B. Du, J.L. Fu, Microfluidic picoliter-scale translational spontaneous sample introduction for high-speed capillary electrophoresis. Anal. Chem. 81 (2009) 3693.

[210] X. Sun, D. Li, M.L. Lee, Poly(ethylene glycol)-functionalized polymeric microchips for capillary electrophoresis. Anal. Chem. 81 (2009) 6278.

[211] T. Ueda, F. Kitamura, R. Mitchell, T. Metcalf, T. Kuwana, A. Nakamoto, Chiral separation of naphthalene- 2,3-dicarboxaldehyde-labeled amino acid enantiomers by cyclodextrin-modified micellar electrokinetic chromatography with laser- induced fluorescence detection. Anal. Chem. 63 (1991) 2979.

[212] A. Dobashi, M. Hamada, Y. Dobashi, J. Yamaguchi, Enantiomeric separation with sodium dodecanoyl-L-amino acidate micelles and poly(sodium (10-undecenoyl)-L-valinate) by electrokinetic chromatography. Anal. Chem. 67 (1995) 3011.

[213] F. von Heeren, E. Verpoorte, A. Manz, W. Thormann, Micellar electrokinetic chromatography separations and analyses of biological samples on a cyclic planar microstructure. Anal. Chem. 68 (1996) 2044.

[214] M. Lammerhofer, W. Lindner, High-efficiency chiral separations of N-derivatized amino acids by packed-capillary electrochromatography with a quinine-based chiral anion-exchange type stationary phase1. J. Chromatogr. A 829 (1998) 115.

[215] Z. Chen, T. Hobo, Chemically l-phenylalaninamide-modified monolithic silica column prepared by a sol−gel process for enantioseparation of dansyl amino acids by ligand exchange-capillary electrochromatography. Anal. Chem. 73 (2001) 3348.

[216] S.A. Shamsi, B.C. Valle, F. Billiot, I.M. Warner, Polysodium N-undecanoyl-l-leucylvalinate: a versatile chiral selector for micellar electrokinetic chromatography. Anal. Chem. 75 (2003) 379.

[217] B.C. Valle, K.F. Morris, K.A. Fletcher, V. Fernand, D.M. Sword, S. Eldridge, C.K. Larive, I.M. Warner, Understanding chiral molecular micellar separations using steady-state fluorescence anisotropy, capillary electrophoresis, and NMR. Langmuir 23 (2007) 425.

[218] B.Y. Kim, J. Yang, M. Gong, B.R. Flachsbart, M.A. Shannon, P.W. Bohn, J.V. Sweedler, Multidimensional separation of chiral amino acid mixtures in a multilayered three-dimensional hybrid microfluidic/nanofluidic device. Anal. Chem. 81 (2009) 2715.

[219] A. Maruyama, N. Adachi, T. Takatsuki, M. Torii, K. Sanui, N. Ogata, Enantioselective permeation of α-amino acid isomers through poly(amino acid)-derived membranes. Macromolecules 23 (1990) 2748.

[220] M. Yoshikawa, J.I. Izumi, T. Kitao, S. Sakamoto, Molecularly imprinted polymeric membranes containing DIDE derivatives for optical resolution of amino acids. Macromolecules 29 (1996) 8197.

[221] H.H. Rmaile, J.B. Schlenoff, Optically active polyelectrolyte multilayers as membranes for chiral separations. J. Am. Chem. Soc. 125 (2003) 6602.

[222] E. Miyako, T. Maruyama, F. Kubota, N. Kamiya, M. Goto, Optical resolution of various amino acids using a supported liquid membrane encapsulating a surfactant−protease complex. Langmuir 21 (2005) 4674.

[223] Y. Xiao, H.M. Lim, T.S. Chung, R. Rajagopalan, Acetylation of beta-cyclodextrin surface-functionalized cellulose dialysis membranes with enhanced chiral separation. Langmuir 23 (2007) 12990.

[224] Q. Liu, S. Zhang, B. Wu, J. Guo, J. Xie, M. Gu, Y. Zhao, L. Yun, K. Liu, Chiral melamine derivatives: design, synthesis, and application to mass spectrometry-based chiral analysis. Anal. Chem. 77 (2005) 5302.

[225] P. Dwivedi, C. Wu, L.M. Matz, B.H. Clowers, W.F. Siems, H.H. Hill, Gas-phase chiral separations by ion mobility spectrometry. Anal. Chem. 78 (2006) 8200.

[226] H. Tsukube, S. Shinoda, J. Uenishi, T. Kanatani, H. Itoh, T. Iwachido, O. Yonemitsu, Molecular recognition with lanthanide(III) tris(betadiketonate) complexes: extraction, transport, and chiral recognition of unprotected amino acids. Inorg. Chem. 37 (1998) 1585.

[227] T.J.M. de Bruin, A.T.M. Marcelis, H. Zuilhof, E.J.R. Sudhölter, Enantioselectivity measurements of copper(II) amino acid complexes using isothermal titration calorimetry. Langmuir 16 (2000) 8270.

[228] H. Okuno, T. Kitano, H. Yakabe, M. Kishimoto, H. Siigi, T. Nagaoka, Characterization of overoxidized polypyrrole colloids imprinted with l-lactate and their application to enantioseparation of amino acids. Anal. Chem. 74 (2002) 4184.

[229] M. Yokota, N. Doki, K. Shimizu, Chiral separation of a racemic compound induced by transformation of racemic crystal structures: DL-glutamic acid. Crystal Growth & Design 6 (2006) 1588.

[230] A. Gabashvili, D.D. Medina, A. Gedanken, Y. Mastai, Templating mesoporous silica with chiral block copolymers and its application for enantioselective separation. J. Phys. Chem. B 111 (2007) 11105.

[231] B. Schuur, J. Floure, A.J. Hallett, J.G.M. Winkelman, J.G. deVries, H.J. Heeres, Continuous chiral separation of amino acid derivatives by enantioselective liquid−liquid extraction in centrifugal contactor separators. Org. Process Res. Dev. 12 (2008) 950.

[232] R. Freeman, T. Finder, L. Bahshi, I. Willner, Beta-cyclodextrin-modified CdSe/ZnS quantum dots for sensing and chiroselective analysis. Nano Lett. 9 (2009) 2073.

[233] K. Kummerer, Pharmaceuticals in the environment: sources, fate, effects and risks. Springer-Verlag: Berlin (2001).

[234] C.G. Daughton, T.A. Ternes, Pharmaceuticals and personal care products in the environment: agents of subtle change? Environ. Health Perspect. 107 Suppl 6 (1999) 907.

[235] D.W. Kolpin, E.T. Furlong, M.T. Meyer, E.M. Thurman, S.D. Zaugg, L.B. Barber, H.T. Buxton, Pharmaceuticals, hormones, and other organic wastewater contaminants in U.S. Streams, 1999−2000: a national reconnaissance. Environ. Sci. Technol. 36 (2002) 1202.

[236] T. V. Madureira, J.C. Barreiro, M. J. Rocha, E. Rocha, Q. B. Cass, M.E. Tiritan, Spatiotemporal distribution of pharmaceuticals in the Douro River estuary (Portugal). Sci. Total Environ. 408 (2010) 5513.

[237] J. Oaks, M. Gilbert, M. Virani, R. Watson, C. Meteyer, B. Rideout, H. Shivaprasad, S. Ahmed, M. Chaudhry, M. Arshad, Diclofenac residues as the cause of vulture population decline in Pakistan. Nature 427 (2004) 630.

[238] J. Lawrence, B. Zhu, G. Swerhone, J. Roy, L. Wassenaar, E. Topp, D. Korber, Comparative microscale analysis of the effects of triclosan and triclocarban on the structure and function of river biofilm communities. Sci. Total Environ. 407 (2009) 3307.

[239] V. Winder, Y. Sapozhnikova, P. Pennington, E. Wirth, Effects of fluoxetine exposure on serotonin-related activity in the sheepshead minnow (Cyprinodon variegatus) using LC/MS/MS detection and quantitation. Comp. Biochem. Physiol. Part C: Toxicol. Pharmacol. 149 (2009) 559.

[240] F.A. Caliman, M. Gavrilescu, Pharmaceuticals, personal care products and endocrine disrupting agents in the environment – a review. Clean-Soil, Air, Water 37 (2009) 277.

[241] D. Grover, J. Zhou, P. Frickers, J. Readman, Improved removal of estrogenic and pharmaceutical compounds in sewage effluent by full scale granular activated carbon: impact on receiving river water. J. Hazard. Mater. 185 (2011) 1005.

[242] D. B. Huggett, B. W. Brooks, B. Peterson, C. M. Foran, D. Schlenk, Toxicity of select beta adrenergic receptor-blocking pharmaceuticals (B-blockers) on aquatic organisms. Arch Environ Contam Toxicol 43 (2002) 229.

[243] A. Villegas-Navarro, E. Rosas-L, J. L. Reyes, The heart of Daphnia magna: effects of four cardioactive drugs. Comp. Biochem. Physiol. Part C: Toxicol. Pharmacol. 136 (2003) 127.

[244] B. Ferrari, R. Mons, B. Vollat, B. Fraysse, N. Paxéus, R. L. Giudice, A. Pollio, J. Garric, Environmental risk assessment of six human pharmaceuticals: are the current environmental risk assessment procedures sufficient for the protection of the aquatic environment? Environ. Toxicol. Chem. 23 (2004) 1344.

[245] K. Fent, A. Weston, D. Caminada, Ecotoxicology of human pharmaceuticals. Aquat Toxicol 76 (2006) 122.

[246] B. I. Escher, N. Bramaz, R. L. Eggen, M. Richter, In Vitro Assessment of Modes of Toxic Action of Pharmaceuticals in Aquatic Life. Environ. Sci. Technol. 39 (2005) 3090.

[247] S.A. Snyder, S. Adham, A.M. Redding, F.S. Cannon, J. DeCarolis, J. Oppenheimer, E.C. Wert, Y. Yoon, Role of membranes and activated carbon in the removal of endocrine disruptors and pharmaceuticals. Desalination 202 (2007) 156.

[248] T.A. Ternes, M. Meisenheimer, D. McDowell, F. Sacher, H.J. Brauch, B. Haist-Gulde, G. Preuss, U. Wilme, N. Zulei-Seibert, Removal of pharmaceuticals during drinking water treatment. Environ. Sci. Technol. 36 (2002) 3855.

[249] P. E. Stackelberg, E. T. Furlong, M. T. Meyer, S. D. Zaugg, A. K. Henderson, D. B. Reissman, Persistence of pharmaceutical compounds and other organic wastewater contaminants in a conventional drinking-water-treatment plant. Sci. Total Environ. 329 (2004) 99.

[250] J. Hollender, S.G. Zimmermann, S. Koepke, M. Krauss, C.S. McArdell, C. Ort, H. Singer, U. von Gunten, H. Siegrist, Elimination of organic micropollutants in a municipal wastewater treatment plant upgraded with a full-scale post-ozonation followed by sand filtration. Environ. Sci. Technol. 43 (2009) 7862.

[251] T. X. Bui, S. -Y. Kang, S. -Y. Lee, H. Choi, Organically functionalized mesoporous SBA-15 as sorbents for removal of selected pharmaceuticals from water. J. Hazard. Mater. 193 (2011) 156.

[252] J. L. Sotelo, A. R. Rodríguez, M. M. Mateos, S. D. Hernández, S. A. Torrellas, J. G. Rodríguez, Adsorption of pharmaceutical compounds and an endocrine disruptor from aqueous solutions by carbon materials. J. Environ. Sci. Heal. B 47 (2012) 640.

[253] P. Oleszczuk, B. Pan, B. Xing, Adsorption and desorption of oxytetracycline and carbamazepine by multiwalled carbon nanotubes. Environ. Sci. Technol. 43 (2009) 9167.

[254] T.A. Ternes, J. Stüber, N. Herrmann, D. McDowell, A. Ried, M. Kampmann, B. Teiser, Ozonation: a tool for removal of pharmaceuticals, contrast media and musk fragrances from wastewater? Water Res. 37 (2003) 1976.

[255] M.M. Huber, S. Canonica, G.Y. Park, U. von Gunten, Oxidation of pharmaceuticals during ozonation and advanced oxidation processes. Environ. Sci. Technol. 37 (2003) 1016.

[256] M.M. Huber, A. GÖbel, A. Joss, N. Hermann, D. LÖffler, C.S. McArdell, A. Ried, H. Siegrist, T.A. Ternes, U. von Gunten, Oxidation of pharmaceuticals during ozonation of municipal wastewater effluents: a pilot study. Environ. Sci. Technol. 39 (2005) 4290.

[257] M.M. Huber, T.A. Ternes, U. von Gunten, Removal of estrogenic activity and formation of oxidation products during ozonation of 17α-ethinylestradiol. Environ. Sci. Technol. 38 (2004) 5177.

[258] M. C. Dodo, H. -P. E. Kohler, U. von Gunten, Oxidation of antibacterial compounds by ozone and hydroxyl radical: elimination of biological activity during aqueous ozonation processes. Environ. Sci. Technol. 43 (2009) 2498.

[259] S. Cole, The emergence of treatment wetlands. Environ. Sci. Technol. 32 (1998) 218A.

[260] R.M. Gersberg, B.V. Elkins, S.R. Lyon, C.R. Goldman, Role of aquatic plants in wastewater treatment by artificial wetlands. Water Res. 20 (1986) 363.

[261] D.Q. Zhang, S.K. Tan, R.M. Gersberg, S. Sadreddini, J. Zhu, N.A. Tuan, Removal of pharmaceutical compounds in tropical constructed wetlands. Ecol. Eng. 37 (2011) 460.

[262] H. Brix, C. A. Arias, The use of vertical flow constructed wetlands for on-site treatment of domestic wastewater: New Danish guidelines. Ecol. Eng. 25 (2005) 491.

[263] S. Judd, The status of membrane bioreactor technology. Trends Biotechnol. 26 (2008) 109.

[264] M. Clara, B. Strenn, O. Gans, E. Martinez, N. Kreuzinger, H. Kroiss, Removal of selected pharmaceuticals, fragrances and endocrine disrupting compounds in a membrane bioreactor and conventional wastewater treatment plants. Water Res. 39 (2005) 4797.

[265] K. Kimura, H. Hara, Y. Watanabe, Removal of pharmaceutical compounds by submerged membrane bioreactors (MBRs). Desalination 178 (2005) 135.

[266] L. D. Nghiem, N. Tadkaew, M. Sivakumar, Removal of trace organic contaminants by submerged membrane bioreactors. Desalination 236 (2009) 127.

[267] M. Cirja, P. Ivashechkin, A. Schäffer, P.F.X. Corvini, Factors affecting the removal of organic micropollutants from wastewater in conventional treatment plants (CTP) and membrane bioreactors (MBR). Rev. Environ. Sci. Biotechnol. 7 (2008) 61.

[268] D. F. Ollis, H. Al-Ekabi, Photocatalytic purification and treatment of water and air. Amsterdam: Elsevier Science (1993).

[269] M. R. Hoffmann, S. T. Martin, W. Choi, D. W. Bahnemannt, Environmental applications of semiconductor photocatalysis. Chem. Rev. 95 (1995) 69.

[270] M. R. Prairie, L. R. Evans, B. M. Stange, S. L. Marlinez, An investigation of Ti02 photocatalysis for the treatment of water contaminated with metals and organic chemicals. Environ. Sci. Technol. 27 (1993) 1776.

[271] S. Malato, J. Blanco, A. Vidal, C. Richter, Photocatalysis with solar energy at a pilot-plant scale: an overview. App. Catal. B: Environ. 37 (2002) 1.

[272] C. S. Turchi, D. F. Ollis, Photocatalytic degradation of organic water contaminants: mechanisms involving hydroxyl radical attack. J. Catal. 122 (1990) 178.

[273] G. R. Boyd, H. Reemtsma, D. A. Grimm, S. Mitra, Pharmaceuticals and personal care products (PPCPs) in surface and treated waters of Louisiana, USA and Ontario, Canada. Sci. Total Environ. 311 (2003) 135.

[274] M .A. C. Adams, Y. Wang, K. Loftin, M. Meyer, Removal of antibiotics from surface and distilled water in conventional water treatment processes. J. Environ. Eng. 128 (2002) 253.

[275] N. Vieno, T. Tuhkanen, L. Kronberg, Removal of pharmaceuticals in drinking water treatment: effect of chemical coagulation. Environ. Technol. 27 (2006) 183.

[276] K. Stein, M. Ramil, G. Fink, M. Sander, T.A. Ternes, Analysis and sorption of psychoactive drugs onto sediment. Environ. Sci. Technol. 42 (2008) 6415.

[277] J.R. Domínguez, T. González, P. Palo, E.M. Cuerda-Correa, Removal of common pharmaceuticals present in surface waters by Amberlite XAD-7 acrylic-ester-resin: Influence of pH and presence of other drugs. Desalination 269 (2011) 231.

[278] T. X. Bui, H. Choi, Adsorptive removal of selected pharmaceuticals by mesoporous silica SBA-15. J. Hazard. Mater. 168 (2009) 602.

[279] S.M. Rivera-Jimenez, M.M. Lehner, W.A. Cabrera-Lafaurie, A.J. Hernández-Maldonado, Removal of naproxen, salicylic acid, clofibric acid, and carbamazepine by water phase adsorption onto inorganic–organic-intercalated bentonites modified with transition metal cations. Environ. Eng. Sci. 28 (2011) 171.

[280] A.C. Hari, R.A. Paruchuri, D.A. Sabatini, T.C.G. Kibbey, Effects of pH and cationic and nonionic surfactants on the adsorption of pharmaceuticals to a natural aquifer material. Environ. Sci. Technol. 39 (2005) 2592.

[281] Z. Yu, S. Peldszus, P. M. Huck, Adsorption of selected pharmaceuticals and an endocrine disrupting compound by granular activated carbon. 1. adsorption capacity and kinetics. Environ. Sci. Technol. 43 (2009) 1467.

[282] Z. Yu, S. Peldszus, P. M. Huck, Adsorption characteristics of selected pharmaceuticals and an endocrine disrupting compound-Naproxen, carbamazepine and nonylphenol-on activated carbon. Water Res. 42 (2008) 2873.

[283] V. Matamoros, C. Arias, H. Brix, J.M. Bayona, Removal of pharmaceuticals and personal pare Products (PPCPs) from urban wastewater in a pilot vertical flow constructed wetland and a sand filter. Environ. Sci. Technol. 41 (2007) 8171.

[284] X. Li, F.I. Hai, L.D. Nghiem, Simultaneous activated carbon adsorption within a membrane bioreactor for an enhanced micropollutant removal. Bioresour. Technol. 102 (2011) 5319.

[285] G. Laera, B. Jin, H. Zhu, A. Lopez, Photocatalytic activity of TiO2 nanofibers in simulated and real municipal effluents. Catal. Today 161 (2011) 147.

[286] S. Kleywegt, V. Pileggi, P. Yang, C. Hao, X. Zhao, C. Rocks, S. Thach, P. Cheung, B. Whitehead, Pharmaceuticals, hormones and bisphenol A in untreated source and finished drinking water in Ontario, Canada--occurrence and treatment efficiency. Sci. Total Environ. 409 (2011) 1481.

[287] D. Vogna, R. Marotta, R. Andreozzi, M. d'Ischia, Kinetic and chemical assessment of the UV/H_2O_2 treatment of antiepileptic drug carbamazepine. Chemosphere 54 (2004) 497.

[288] Y. Yoon, P. Westerhoff, S. Snyder, E. Wert, Nanofiltration and ultrafiltration of endocrine disrupting compounds, pharmaceuticals and personal care products. J. Membr. Sci. 270 (2006) 88.

[289] S. Castiglioni, R. Bagnati, R. Fanelli, F. Pomati, D. Calamari, E. Zuccato, Removal of Pharmaceuticals in Sewage Treatment Plants in Italy. Environ. Sci. Technol. 40 (2006) 357.

[290] M. Carballa, F. Omil, J.M. Lema, Removal of cosmetic ingredients and pharmaceuticals in sewage primary treatment. Water Res. 39 (2005) 4790.

[291] N. Nakada, T. Tanishima, H. Shinohara, K. Kiri, H. Takada, Pharmaceutical chemicals and endocrine disrupters in municipal wastewater in Tokyo and their removal during activated sludge treatment. Water Res. 40 (2006) 3297.

[292] J. Radjenovic, M. Petrovic, D. Barceló, Analysis of pharmaceuticals in wastewater and removal using a membrane bioreactor. Anal. Bioanal. Chem. 387 (2007) 1365.

[293] A. M. Comerton, R. C. Andrews, D. M. Bagley, P.Yang, Membrane adsorption of endocrine disrupting compounds and pharmaceutically active compounds. J. Membr. Sci. 303 (2007) 267.

[294] T.E. Doll, F.H. Frimmel,) Photocatalytic degradation of carbamazepine, clofibric acid and iomeprol with P25 and Hombikat UV100 in the presence of natural organic matter (NOM) and other organic water constituents. Water Res. 39 (2005) 403.

[295] H. Shemer, Y. K. Kunukcu, K.G. Linden, Degradation of the pharmaceutical metronidazole via UV, Fenton and photo-Fenton processes. Chemosphere 63 (2006) 269.

[296] V. Matamoros, J. García, J.M. Bayona, Organic micropollutant removal in a full-scale surface flow constructed wetland fed with secondary effluent. Water Res. 42 (2008) 653.

[297] N. Nakada, H. Shinohara, A. Murata, K. Kiri, S. Managaki, N. Sato, H. Takada, Removal of selected pharmaceuticals and personal care products (PPCPs) and endocrine-disrupting chemicals (EDCs) during sand filtration and ozonation at a municipal sewage treatment plant. Water Res. 41 (2007) 4373.

[298] Y. Zhang, S. -U. Geisen, C. Gal, Carbamazepine and diclofenac: removal in wastewater treatment plants and occurrence in water bodies. Chemosphere 73 (2008) 1151.

[299] M. Whelehan, U. von Stockar, I.W. Marison, Removal of pharmaceuticals from water: using liquid-core microcapsules as a novel approach. Water Res. 44 (2010) 2314.

[300] N. Tadkaew, M. Sivakumar, S.J. Khan, J.A. McDonald, L.D. Nghiem, Effect of mixed liquor pH on the removal of trace organic contaminants in a membrane bioreactor. Bioresour. Technol. 101 (2010) 1494.

[301] N. Tadkaew, F.I. Hai, J.A. McDonald, S.J. Khan, L.D. Nghiem, Removal of trace organics by MBR treatment: The role of molecular properties. Water Res. 45 (2011) 2439.

[302] D. Vogna, R. Marotta, A. Napolitano, R. Andreozzi, M. d'Ischia, Advanced oxidation of the pharmaceutical drug diclofenac with UV/H2O2 and ozone. Water Res. 38 (2004) 414.

[303] R. Andreozzi, V. Caprio, R. Marotta, A. Radovnikovic, Ozonation and H_2O_2/UV treatment of clofibric acid in water: a kinetic investigation. J. Hazard. Mater. B 103 (2003) 233.

[304] C. Zwiener, F. H. Frimmel, Oxidative treatment of pharmaceuticals in water. Water Res. 34 (2000) 1881.

[305] D. Fatta-Kassinos, E. Hapeshi, A. Achilleos, S. Meric, M. Gros, M. Petrovic, D. Barcelo, Existence of Pharmaceutical Compounds in Tertiary Treated Urban Wastewater that is Utilized for Reuse Applications. Water Resour. Manage. 25 (2011) 1183.

[306] W. Xue, C. Wu, K. Xiao, X. Huang, H. Zhou, H. Tsuno, H. Tanaka, Elimination and fate of selected micro-organic pollutants in a full-scale anaerobic/anoxic/aerobic process combined with membrane bioreactor for municipal wastewater reclamation. Water Res. 44 (2010) 5999.

[307] R. Andreozzi, M. Canterino, R. Marotta, N. Paxeus, Antibiotic removal from wastewaters: The ozonation of amoxicillin. J. Hazard. Mater. 122 (2005) 243.

[308] M. A. C. Adams, Y. Wang, K. Loftin, M. Meyer, Removal of antibiotics from surface and distilled water in conventional water treatment processes. J. Environ. Eng. 128 (2002) 253.

[309] R. Andreozzia, V. Caprio, R. Marotta, D. Vogna, Paracetamol oxidation from aqueous solutions by means of ozonation and H_2O_2/UV system. Water Res. 37 (2003) 993.

[310] H.M. Coleman, M. Troester, S.J. Khan, J.A. McDonald, G. Watkins, R.M. Stuetz, Assessment of trace organic chemical removal by a membrane bioreactor using gas chromatography/mass spectometry and a yeast screen bioassay. Environ. Toxicol. Chem. 28 (2009) 2537.

[311] A. Rossner, S. A. Snyder, D. R. U. Knappe, Removal of emerging contaminants of concern by alternative adsorbents. Water Res. 43 (2009) 3787.

[312] M.J. Benotti, B.D. Stanford, E.C. Wert, S.A. Snyder, Evaluation of a photocatalytic reactor membrane pilot system for the removal of pharmaceuticals and endocrine disrupting compounds from water. Water Res. 43 (2009) 1513.

[313] S. Zorita, L. Mårtensson, L. Mathiasson, Occurrence and removal of pharmaceuticals in a municipal sewage treatment system in the south of Sweden. Sci. Total Environ. 407 (2009) 2760.

[314] W. Hua, E.R. Bennett, R.J. Letcher, Ozone treatment and the depletion of detectable pharmaceuticals and atrazine herbicide in drinking water sourced from the upper Detroit River, Ontario, Canada. Water Res. 40 (2006) 2259.

[315] N. Park, B.J. Vanderford, S.A. Snyder, S. Sarp, S.D. Kim, J. Cho, Effective controls of micropollutants included in wastewater effluent using constructed wetlands under anoxic condition. Ecol. Eng. 35 (2009) 418.

[316] S. Snyder, Occurrence, treatment, and toxicological relevance of EDCs and wharmaceuticals in Water. Ozone: Sci. Eng. 30 (2008) 65.

[317] G.F. Upelaar, R.T. Meijers, R. Hopman, J.C. Kruithof, Oxidation of herbicides in groundwater by the fenton process: a realistic alternative for O_3/H_2O_2 treatment? Ozone: Sci. Eng. 22 (2000) 607.

[318] R. Andreozzi, R. Marotta, G. Pinto, A. Pollio, Carbamazepine in water: persistence in the environment, ozonation treatment and preliminary assessment on algal toxicity. Water Res. 36 (2002) 2869.

[319] A. Alum, Y. Yoon, P. Westerhoff, M. Abbaszadegan, Oxidation of bisphenol A, 17beta-estradiol, and 17alpha-ethynyl estradiol and byproduct estrogenicity. Environ. Toxicol. 19 (2004) 257.

[320] S. Irmak, O. Erbatur, A. Akgerman, Degradation of 17beta-estradiol and bisphenol A in aqueous medium by using ozone and ozone/UV techniques. J. Hazard. Mater. 126 (2005) 54.

[321] Y. Ohko, I. Ando, C. Niwa, T. Tatsuma, T. Yamamura, T. Nakashima, Y. Kubota, A. Fujishima, Degradation of bisphenol A in water by TiO_2 photocatalyst. Enviorn. Sci. Technol. 35 (2001) 2365.

[322] T. Nakashima, Y. Ohko, D. Tryk, A. Fujishima, Decomposition of endocrine-disrupting chemicals in water by use of TiO_2 photocatalysts immobilized on polytetrafluoroethylene mesh sheets. J. Photochem. Photobiol. A: Chem. 151 (2002) 207.

[323] E.J. Rosenfeldt, K.G. Linden, Degradation of endocrine disrupting chemicals bisphenol A, ethinyl estradiol, and estradiol during UV photolysis and advanced oxidation processes. Environ. Sci. Technol. 38 (2004) 5476.

[324] P. -J. Chen, K. J. Linden, D. E. Hinton, S. Kashiwada, E. J. Rosenfeldt, S. W. Kullman,) Biological assessment of bisphenol A degradation in water following direct photolysis and UV advanced oxidation. Chemosphere 65 (2006) 1094.

[325] I. Langmuir, The constitution and fundamental properties of solids and liquids. J. Am. Chem. Soc. 38 (1916) 2221.

[326] H. Freundlich, Über die adsorption in lösungen. Z. Phys. Chem. 57 (2011) 385.

[327] A.W. Adamson, Physical chemistry of surfaces. New York, Wiley (1990).

[328] I. Quinones, G. Guiochon, Extension of a Jovanovic-Freundlich isotherm model to multicomponent adsorption on heterogeneous surfaces. J. Chromatogr. A 796 (1998) 15.

[329] D. F. Siqueira, M. Stamm, U. Breiner, R. Stadler, Adsorption of di-and triblock copolymers with functionalized butadiene-styrene blocks from dilute solution. Polymer 36 (1995) 3229.

[330] A. K. Bajpai, Adsorption of bovine serum albumin onto glass powder surfaces coated with polyvinyl alcohol. J. App. Polm. Sci. 78 (2000) 933.

[331] Y. S. Ho, G. Mckay, A comparison of chemisorption kinetic models applied to pollutant removal on various sorbents. Proc. Saf. Environ. 76 (1998) 332.

[332] Y. S. Ho, G. McKay, Pseudo-second order model for sorption processes. Process Biochem. 34 (1999) 451.

[333] N. Shamim, H. Liang, K. Hidajat, M. S. Uddin, Adsorption, desorption, and conformational changes of lysozyme from thermosensitive nanomagnetic particles. J. Colloid Interface Sci. 320 (2008) 15.

[334] Z. G. Peng, K. Hidajat, M.S. Uddin, Selective and sequential adsorption of bovine serum albumin and lysozyme from a binary mixture on nanosized magnetic particles. J. Colloid Interface Sci. 281 (2005) 11.

[335] S. -Y. Mak, D. -H. Chen, Fast adsorption of methylene blue on polyacrylic acid-bound iron oxide magnetic nanoparticles. Dyes and Pigments 61 (2004) 93.

[336] M. Zhao, Z. Tang, P. Liu, Removal of methylene blue from aqueous solution with silica nano-sheets derived from vermiculite. J. Hazard. Mater. 158 (2008) 43.

[337] D. Bendz, N.A. Paxéus, T. R. Ginn., F. J. Loge, Occurrence and fate of pharmaceutically active compounds in the environment, a case study: Höje River in Sweden. J. Hazard. Mater. 122 (2005) 195.

[338] L. J. Fono, D. L. Sedlak, Use of the Chiral Pharmaceutical propranolol to identify sewage discharges into asurface waters. Environ. Sci. Technol. 39 (2005) 9244.

[339] D.B. Huggett, I. A. Khan, C. M. Foran, D. Schlenk, Determination of beta-adrenergic receptor blocking pharmaceuticals in United States wastewater effluent. Environ. Pollut. 121 (2003) 199.

[340] P. Roberts, K. Thomas, The occurrence of selected pharmaceuticals in wastewater effluent and surface waters of the lower Tyne catchment. Sci. Total Environ. 356 (2006) 143.

[341] T. A. Ternes, Occurrence of drugs in German sewage treatment plants and rivers1. Water Res. 32 (1998) 3245.

[342] S. Wiegel, R. Brockmeyer, H. Harms, J. Loffer, H. Reincke, R. Schmidt, B. Stachel, W. von Tumpling, A. Wanke, Pharmaceuticals in the river Elbe and its tributaries. Chemosphere 57 (2004) 107.

[343] Z.G. Peng, K. Hidajat, M.S. Uddin, Adsorption of bovine serum albumin on nanosized magnetic particles. J. Colloid Interface Sci. 271 (2004) 277.

[344] F. H. Chen, Q. Gao, J. Z. Ni, The grafting and release behavior of doxorubincin from $Fe_3O_4@SiO_2$ core–shell structure nanoparticles via an acid cleaving amide bond: the potential for magnetic targeting drug delivery. Nanotechnology 19 (2008) 165103.

[345] M. Prabaharan, R. Jayakumar, Chitosan-graft-beta-cyclodextrin scaffolds with controlled drug release capability for tissue engineering applications. Int. J. Biol. Macromol. 44 (2009) 320.

[346] M. -H. Liao, D. -H. Chen, Preparation and characterization of a novel magnetic nano-adsorbent. J. Mater. Chem. 12 (2002) 3654.

[347] L. A. Belyakova, K. A. Kazdobin, V.N. Belyakov, S. V. Ryabov, A. F. Danil de Namor, Synthesis and properties of supramolecular systems based on silica. J. Colloid Interface Sci. 283 (2005) 488.

[348] B. L. May, S. D. Kean, C. J. Easton, S. F. Lincoln, Preparation and characterization of 6A-polyaminemono- substituted β-cyclodextrins. J. Chem. Soc. Perkin Transactions 1 (1997) 3157.

[349] N. Shamim, L. Hong, K. Hidajat, M. S. Uddin, Thermosensitive polymer (N-isopropylacrylamide) coated nanomagnetic particles: preparation and characterization. Colloids Surf. B 55 (2007) 51.

[350] Y. Wang, T. -T. Ong, L. -S. Li, T. T. Y. Tan, S. -C. Ng, Enantioseparation of a novel "click" chemistry derived native beta-cyclodextrin chiral stationary phase for high-performance liquid chromatography. J. Chromatogr. A 1216 (2009) 2388.

[351] H. -D. Wang, R. Xie, C. H. Niu, H. Song, M. Yang, S. Liu, L. -Y. Chu, Chitosan chiral ligand exchange membranes for sorption resolution of amino acids. Chem. Eng. Sci. 64 (2009) 1462.

[352] E. J. W. Verwey, J. T. G. Overbeek, Theory of the stability of lyophobic colloids. Elsevier: Amsterdam, The Netherlands (1948).

[353] B. Vincent, J. Edwards, S. Emmett, A. Jones, Depletion flocculation in dispersions of sterically-stabilised particles. Colloid Surface. 18 (1986) 261.

[354] R. M. Cornell, U. Schertmann, Iron oxides in the laboratory: preparation and characterization. VCH Publishers: Weinheim, Germany (1991).

[355] J. Deng, X. Ding, W. Zhang, Y. Peng, J. Wang, X. Long, P. Li, A. S. C. Chan, Magnetic and conducting Fe_3O_4-cross-linked polyaniline nanoparticles with core-shell structure. Polymer 43 (2002) 2179.

[356] X. Xu, G. Friedman, K. D. Humfeld, S. A. Asher, Superparamagnetic photonic crystals. Adv. Mater. 13 (2001) 1681.

[357] C.R. Vestal, Z.J. Zhang, Atom transfer radical polymerization synthesis and magnetic characterization of $MnFe_2O_4$/polystyrene core/dhell nanoparticles. J. Am. Chem. Soc. 124 (2002) 14312.

[358] Y.A. Shchipunov, Sol–gel-derived biomaterials of silica and carrageenans. J. Colloid Interface Sci. 268 (2003) 68.

[359] H. Wang, H. Nakamura, Y. Yao, H. Maeda, E. Abe, Effect of solvents on the preparation of silica-coated magnetic particles. Chem. Lett. 11 (2001) 1168.

[360] F. G. Aliev, M. A. Correa-Duarte, J. W. Ostrander, M. Giersig, N. A. Kotov, Layer-by-layer assembly of core-shell magnetite nanoparticles: effect of silica coating on interparticle interactions and magnetic properties. Adv. Mater. 11 (1999) 1006.

[361] A. Bocanegra-Diaz, N. D. S. Mohallem, M. A. Novak, R. D. Sinisterra, Preparation of ferrofluid from cyclodextrin and magnetite. J. Magn. Magn. Mater. 272 (2004) 2395.

[362] Y. Fan, Y. -Q. Feng, S. -L. Da, On-line selective solid-phase extraction of 4-nitrophenol with beta-cyclodextrin bonded silica. Anal. Chim. Acta 484 (2003) 145.

[363] S.D. Kim, J. Cho, I.S. Kim, B.J. Vanderford, S.A. Snyder, Occurrence and removal of pharmaceuticals and endocrine disruptors in South Korean surface, drinking, and waste waters. J. Phys. Chem. C 41 (2007) 1013.

[364] R. D. Palma, S. Peeters, M. J. V. Bael., H. V. den Rul, K. Bonroy, W. Laureyn, J. Mullens, G. Borghs, G. Maes, Silane ligand exchange to make hydrophobic superparamagnetic nanoparticles water-dispersible. Chem. Mater. 19 (2007) 1821.

[365] O. Gleeson, R. Tekoriute, Y. K. Gun'ko, S. J. Connon, The first magnetic nanoparticle-supported chiral DMAP analogue: highly enantioselective acylation and excellent recyclability. Chem. Eur. J. 15 (2009) 5669.

[366] P. M. Arnal, C. Weidenthaler, F. Schüth, Highly monodisperse zirconia-coated silica spheres and zirconia/silica hollow spheres with remarkable textural properties. Chem. Mater. 18 (2006) 2733.

[367] V. S. Zaitsev, D. S. Filimonov, I. A. Presnyakov, R. J. Gambino, B. Chu, Physical and chemical properties of magnetite and magnetite-polymer nanoparticles and their colloidal dispersions. J. Colloid Interface Sci. 212 (1999) 49.

[368] D. -H. Chen, S. -H. Wu, Synthesis of nickel nanoparticles in water-in-oil microemulsions. Chem. Mater. 12 (2000) 1354.

[369] D. A. van Leeuwen, J. M. van Ruitenbeek, L. J. de Jongh, A. Ceriotti, G. Pacchioni, O. D. Haberlen, N. Rosch, Quenching of magnetic moments by ligand-metal interactions in nanosized magnetic metal clusters. Phys. Rev. Lett. 73 (1994) 1432.

[370] M. Kosmulski, Compilation of PZC and IEP of sparingly soluble metal oxides and hydroxides from literature. Adv. Colloid Interface Sci. 152 (2009) 14.

[371] M.H. Kalavathy, L.R. Miranda, Comparison of copper adsorption from aqueous solution using modified and unmodified Hevea brasiliensis saw dust. Desalination 255 (2010) 165.

[372] Y. Kamatani, H. Minakata, P. T. M. Kenny, T. Iwashita, K. Watanabe, K. Funase, X. P. Sun, A. Yongsiri, K. H. Kim, P. Novales-Li, E. T. Novales, C. G. Kanapi, H. Takeuchi, K. Nomoto, Achatin-I, an endogenous neuroexcitatory tetrapeptide from Achatina fulica Férussac containing a D-amino acid residue. Biochem. Biophys. Res. Commun. 160 (1989) 1015.

[373] H. Brückner, T. Westhauser, Chromatographic determination of D-amino acids as native constituents of vegetables and fruits. Chromatographia 39 (1994) 419.

[374] E. Okuma, H. Abe, Simultaneous determination of D- and L-amino acids in the nervous tissues of crustaceans using precolumn derivatization with (+)-1-(9-fluorenyl)ethyl chloroformate and reversed-phase ion-pair high-performance liquid chromatography. J. Chromatogr. B 660 (1994) 243.

[375] Y. Nagata, K. Horiike, T. Maeda, Distribution of free D-serine in vertebrate brains. Brain Res. 634 (1994) 291.

[376] A. Hashimoto, T. Nishikawa, T. Oka, T. Hayashi, K. Takahashi, Widespread distribution of free D-aspartate in rat periphery. FEBS Lett. 331 (1993) 4.

[377] X. -C. Wang, C. Lee, Adsorption and desorption of aliphatic amines, amino acids and acetate by clay minerals and marine sediments. Marine Chem. 44 (1993) 1.

[378] K. Imamura, T. Mimura, M. Okamoto, T. Sakiyama, K. Nakanishi, Adsorption behavior of amino acids on a stainless steel surface. J. Colloid Interface Sci. 229 (2000) 237.

[379] B. Liedberg, I. Lundstörm, C. R. Wu, W. R. Salaneck, Adsorption of glycine on hydrophilic gold. J. Colloid Interface Sci. 108 (1985) 123.

[380] A. Ihs, B. Liedberg, K. Udval, C. Törnkvist, P. Bodö, I. Lundstörm, Infrared and photoelectron spectroscopy of amino acids on copper: glycine, L-alanine and β-alanine. J. Colloid Interface Sci. 140 (1990) 192.

[381] D. W. Armstrong, T. J. Ward, R. D. Armstrong, T. E. Beesley, Separation of drug stereoisomers by the formation of beta cyclodextrin inclusion complexes. Science 232 (1986) 1132.

[382] T. N. Sorrell, Organic Chemistry (2nd Edition). University Science Books, USA (2006).

[383] S. Ghosh, A. Z. M. Badruddoza, M.S. Uddin, K. Hidajat, Adsorption of chiral aromatic amino acids onto carboxymethyl-β-cyclodextrin bonded Fe_3O_4/SiO_2 core-shell nanoparticles. J. Colloid Interface Sci. 354 (2011) 483.

[384] W. C. Yang, W. G. Shim, J. W. Lee, H. Moon, Adsorption and desorption dynamics of amino acids in a nonionic polymeric sorbent XAD-16 column. Korean J. Chem. Engg. 20 (2003) 922.

[385] Ö. Altun, S. Bilcen, Spectroscopic characterization of Cu(II) complex of L-phenylalanine and D,L-tryptophan. Spectrochim. Acta A 75 (2010) 789.

[386] A. A. Younes, D. Mangelings, Y. V. Heyden, Chiral separations in normal-phase liquid chromatography: Enantioselectivity of recently commercialized polysaccharide-based selectors. Part II. Optimization of enantioselectivity. J. Pharm. Biomed. Anal. 56 (2011) 521.

[387] M. C. Waldhier, M. F. Almstetter, N. Nürnberger, M.A. Gruber, K. Dettmer, P. J. Oefner, Improved enantiomer resolution and quantification of free D-amino acids in serum and urine by comprehensive two-dimensional gas chromatography-time-of-flight mass spectrometry. J. Chromatogr. A 1218 (2011) 4537.

[388] V. Pérez-Fernández, M. A. García, M. L. Marina, Chiral separation of agricultural fungicides. J. Chromatogr. A 1218 (2011) 6561.

[389] J. Li, F. Dong, J. Xu, X. Liu, Y. Li, W. Shan, Y. Zheng, Enantioselective determination of triazole fungicide simeconazole in vegetables, fruits, and cereals using modified QuEChERS (quick, easy, cheap, effective, rugged and safe) coupled to gas chromatography/tandem mass spectrometry. Anal. Chim. Acta 702 (2011) 127.

[390] P. S. Baran, K. Li, D. P. O'Malley, C. Mitsos, Short, Enantioselective Total Synthesis of Sceptrin and Ageliferin by Programmed Oxaquadricyclane Fragmentation. Angew. Chem. Int. Ed. 45 (2006) 249.

[391] R. Ferretti, A. Mai, B. Gallinella, L. Zanitti, S. Valente, R. Cirilli, Application of 3μm particle-based amylose-derived chiral stationary phases for the enantioseparation of potential histone deacetylase inhibitors. J. Chromatogr. A 1218 (2011) 8394.

[392] C. Hamman, D. E. Schmidt, M. Wong, M. Hayes, The use of ammonium hydroxide as an additive in supercritical fluid chromatography for achiral and chiral separations and purifications of small, basic medicinal molecules. J. Chromatogr. A 1218 (2011) 7886.

[393] A. E. Ribeiro, P. S. Gomes, L. S. Pais, A. E. Rodrigues, Chiral separation of flurbiprofen enantiomers by preparative and simulated moving bed chromatography. Chirality 23 (2011) 602.

[394] B. Preinerstorfer, M. L. Mmerhofer, W. Lindner, Advances in enantioselective separations using electromigration capillary techniques. Electrophoresis 30 (2009) 100.

[395] H. Pellissier, Recent developments in dynamic kinetic resolution. Tetrahedron 64 (2008) 1563.

[396] H. Wu, Y. Zhao, M. Nie, Z. Jiang, Molecularly imprinted organic–inorganic hybrid membranes for selective separation of phenylalanine isomers and its analogue. Sep. Pur. Technol. 68 (2009) 97.

[397] M. Yokota, N. Doki, K. Shimizu, Chiral separation of a racemic compound induced by transformation of racemic crystal structures: dl -glutamic acid. Crystal Growth & Design 6 (2006) 1588.

[398] L. Xu, M.-J. Kim, K.-D. Kim, Y.-H. Choa, H.-T. Kim, Surface modified Fe_3O_4 nanoparticles as a protein delivery vehicle. Colloids Surface A: Physicochem. Eng. Aspects 350 (2009) 8.

[399] H. J. Choi, M. H. Hyun, Separation of enantiomers with magnetic silica nanoparticles modified by a chiral selector: enantioselective fishing. Chem. Commun. (2009) 6454.

[400] A. Hu, G. T. Yee, W. Lin, Magnetically recoverable chiral catalysts immobilized on magnetite nanoparticles for asymmetric hydrogenation of aromatic ketones. J. Am. Chem. Soc. 127 (2005) 12486.

[401] A. R. Khan, P. Forgo, K. J. Stine, V. T. D'Souza, Methods for selective modifications of cyclodextrins. Chem. Rev. 98 (1998) 1977.

[402] X. Lai, W. Tang, S. -C. Ng, Novel cyclodextrin chiral stationary phases for high performance liquid chromatography enantioseparation: effect of cyclodextrin type. J. Chromatogr. A 1218 (2011) 5597.

[403] C. Gu, S. A. Shamsi, Evaluation of a methacrylate-bonded cyclodextrins as a monolithic chiral stationary phase for capillary electrochromatography (CEC)-UV and CEC coupled to mass spectrometry. Electrophoresis 32 (2011) 2727.

[404] S. S. Banerjee, D. -H. Chen, Cyclodextrin-conjugated nanocarrier for magnetically guided delivery of hydrophobic drugs. J. Nanopart. Res. 11 (2009) 2071.

[405] E. Y. Ozmen, M. Sezgin, A. Yilmaz, M. Yilmaz, Synthesis of beta-cyclodextrin and starch based polymers for sorption of azo dyes from aqueous solutions. Bioresour. Technol. 99 (2008) 526.

[406] W. Tang, I. W. Muderawan, S. -C. Ng, H. S. O. Chan, Enantioselective separation in capillary electrophoresis using a novel mono-6A-propylammonium-β-cyclodextrin as chiral selector. Anal. Chim. Acta 555 (2006) 63.

[407] Y. -C. Guillaume, C. Andre, A novel chiral column for the HPLC separation of a series of dansyl amino and arylalkanoic acids. Talanta 76 (2008) 1261.

[408] N. Thuaud, B. Sebille, A. Deratani, G. Lelievre, Retention behavior and chiral recognition of [beta]-cyclodextrinderivative polymer adsorbed on silica for warfarin, structurally related compounds and Dns-amino acids. J. Chromatogr. A 555 (1991) 53.

[409] Z. Zhou, J. -H. Cheng, T. -S. Chung, T. A. Hatton, The exploration of the reversed enantioselectivity of a chitosan functionalized cellulose acetate membranes in an electric field driven process. J. Membr. Sci. 389 (2012) 372.

[410] K. Singh, H.C. Bajaj, P. Ingole, A. Bhattacharya, Comparative study of enantioseparation of racemic tryptophan by ultrafiltration using BSA-immobilized and BSA-interpenetrating network polysulfone membranes. Sep. Sci. Technol. 45 (2010) 346.

[411] E. Van der Ent, P. Van Hee, J. Keurentjes, K. Van't Riet, A. Van der Padt, Multistage electrodialysis for large-scale separation of racemic mixtures. J. Mem. Sci. 204 (2002) 173.

[412] F. Tang, Q. Zhang, D. Ren, Z. Nie, Q. Liu, S. Yao, Functional amino acid ionic liquids as solvent and selector in chiral extraction. J. Chromatogr. A 1217 (2010) 4669.

[413] A. Studenov, D. Szalda, Y. Ding, Synthesis of no-carrier-added C-11 labeled D- and L-enantiomers of phenylalanine and tyrosine for comparative PET Studies. Nucl. Med. Biol. 30 (2003) 39.

[414] K. Singh, P.G. Ingole, H.C. Bajaj, H. Gupta, Preparation, characterization and application of β-cyclodextrin-glutaraldehyde crosslinked membrane for the enantiomeric separation of amino acids. Desalination 298 (2012) 13.

[415] Y.D. Jiang, J.H. Zhang, S.M. Xie, Y.C. Lv, M. Zhang, C. Ma, L.M. Yuan, Chiral separation of D,L-tyrosine through nitrocellulose membrane. J. App. Polym. Sci. (2011) n/a.

[416] W. Zhang, V. Carravetta, O. Plekan, V. Feyer, R. Richter, M. Coreno, K.C. Prince, Electronic structure of aromatic amino acids studied by soft x-ray spectroscopy. J Chem Phys 131 (2009) 035103.

[417] M. Shanmugam, D. Ramesh, V. Nagalakshmi, R. Kavitha, R. Rajamohan, T. Stalin, Host–guest interaction of l-tyrosine with β-cyclodextrin. Spectrochim Acta Part A 71 (2008) 125.

[418] N. Phuong, K. Lee, K. Kim, J. Choi, J. Kim, J. Kang, Determination of stability constants of the inclusion complexes of beta-blockers in heptakis (2,3-dimethyl-6-sulfato)-beta-cyclodextrin. Arch Pharm Res 27 (2004) 1290.

[419] L. Huang, J. He, X. Ge, R. Lu, J. Guo, Fluorimetric investigation of supramolecular system by modified β-cyclodextrin and its analytical application. Spectrochimica Acta Part A: Molecular and Biomolecular Spectroscopy 78 (2011) 1553.

[420] Y. Liu, B. Li, T. Wada, Y. Inoue, Fluorometric Studies on Inclusion Complexation of L/D-Tryptophan by beta-Cyclodextrin 6-O-Pyridinecarboxylates. Bioorg. Chem. 29 (2001) 19.

[421] M. J. Benotti, R. A. Trenholm, B. J. Vanderford, J. C. Holady, B. D. Stanford, S. A. Snyder, Pharmaceuticals and Endocrine Disrupting Compounds in U.S. Drinking Water. Environ. Sci. Technol. 43 (2009) 597.

[422] T. A. Ternes, M. Stumpf, J. Mueller, K. Haberer, R. D. Wilken, M. Servos, Behavior and occurrence of estrogens in municipal sewage treatment plants--I. Investigations in Germany, Canada and Brazil. Sci. Total Environ. 225 (1999) 81.

[423] Y. Dong, D. Wu, X. Chen, Y. Lin, Adsorption of bisphenol A from water by surfactant-modified zeolite. J. Colloid Interface Sci. 348 (2010) 585.

[424] N. Vieno, T. Tuhkanen, L. Kronberg, Removal of pharmaceuticals in drinking water treatment: effect of chemical coagulation. Environ. Technol. 27 (2006) 183.

[425] S. Esplugas, D. M. Bila, L. G. T. Krause, M. Dezotti, Ozonation and advanced oxidation technologies to remove endocrine disrupting chemicals (EDCs) and pharmaceuticals and personal care products (PPCPs) in water effluents. J. Hazard. Mater. 149 (2007) 631.

[426] T. E. Doll, F. H. Frimmel, Kinetic study of photocatalytic degradation of carbamazepine, clofibric acid, iomeprol and iopromide assisted by different TiO_2

materials--determination of intermediates and reaction pathways. Water Res. 38 (2004) 955.

[427] G. Liu, J. Ma, X. Li, Q. Qin, Adsorption of bisphenol A from aqueous solution onto activated carbons with different modification treatments. J. Hazard. Mater. 164 (2009) 1275.

[428] S. Suarez, M. C. Dodd, F. Omil, U. von Gunten, Kinetics of triclosan oxidation by aqueous ozone and consequent loss of antibacterial activity: relevance to municipal wastewater ozonation. Water Res. 41 (2007) 2481.

[429] B. Pan, D. Lin, H. Mashayekhi, B. Xing, Adsorption and hysteresis of bisphenol A and 17α-ethinyl estradiol on carbon nanomaterials. Environ. Sci. Technol. 42 (2008) 5480.

[430] W. -T. Tsai, C. -W. Lai, T. -Y. Su, Adsorption of bisphenol-A from aqueous solution onto minerals and carbon adsorbents. J. Hazard. Mater. 134 (2006) 169.

[431] F. Cao, P. Bai, H. Li, Y. Ma, X. Deng, C. Zhao, Preparation of polyethersulfone-organophilic montmorillonite hybrid particles for the removal of bisphenol A. J. Hazard. Mater. 162 (2009) 791.

[432] C. Cheng, L. Ma, J. Ren, L. Li, G. Zhang, Q. Yang, C. Zhao, Preparation of polyethersulfone-modified sepiolite hybrid particles for the removal of environmental toxins. Chem. Eng. J. 171 (2011) 1132.

[433] S.M. Rivera-Jiménez, A. Hernández-Maldonado, 18-Nickel(II) grafted MCM-41: A novel sorbent for the removal of Naproxen from water. Micropor. Mesopor. Mater. 116 (2008) 246.

[434] H. Wang, Y.F. Yu, Q.W. Chen, K. Cheng, Carboxyl-functionalized nanoparticles with magnetic core and mesopore carbon shell as adsorbents for the removal of heavy metal ions from aqueous solution. Dalton Trans 40 (2011) 559.

[435] X. Zhao, Y. Shi, Y. Cai, S. Mou, Cetyltrimethylammonium bromide-coated magnetic nanoparticles for the preconcentration of phenolic compounds from environmental water samples. Environ. Sci. Technol. 42 (2008) 1201.

[436] W. Guo, W. Hu, J. Pan, H. Zhou, W. Guan, X. Wang, J. Dai, L. Xu, Selective adsorption and separation of BPA from aqueous solution using novel molecularly imprinted polymers based on kaolinite/Fe_3O_4 composites. Chem. Eng. J. 171 (2011) 603.

[437] C. R. Ispas, M. T. Ravalli, A. Steere, S. Andreescu, Multifunctional biomagnetic capsules for easy removal of phenol and bisphenol A. Water Res. 44 (2010) 1961.

[438] A. Badruddoza, K. Hidajat, M. Uddin, Synthesis and characterization of beta-cyclodextrin-conjugated magnetic nanoparticles and their uses as solid-phase artificial chaperones in refolding of carbonic anhydrase bovine. J. Colloid Interface Sci. 346 (2010) 337.

[439] S.M. Rivera-Jiménez, S. Méndez-González, A. Hernández-Maldonado, Metal (M=Co2+, Ni2+, and Cu2+) grafted mesoporous SBA-15: Effect of transition metal incorporation and pH conditions on the adsorption of Naproxen from water. Micropor. Mesopor. Mat. 132 (2010) 470.

[440] M. Ike, M. -Y. Chen, C. -S. Jin, M. Fujita, Acute toxicity, mutagenicity, and estrogenicity of biodegradation products of bisphenol-A. Environ. Toxicol. 17 (2002) 457.

[441] E. Loffredo, C. Eliana Gattullo, A. Traversa, N. Senesi, Potential of various herbaceous species to remove the endocrine disruptor bisphenol A from aqueous media. Chemosphere 80 (2010) 1274.

[442] J. -H. Kim, S. -J. Kim, C. -H. Lee, H. -H. Kwon, Removal of toxic organic micropollutants with FeTsPc-immobilized amberlite/H_2O_2 : effect of physicochemical properties of toxic chemicals. Ind. Eng. Chem. Res. 48 (2009) 1586.

[443] W. Su-Hua, D. Bing-zhi, H. Yu, Adsorption of bisphenol A by polysulphone membrane. Desalination 253 (2010) 22.

[444] M. Yamamura, R.L. Camiloa, L.C. Sampaio, M.A. Macedo, N. Nakamura, H.E. Toma, Preparation and characterization of (3-aminopropyl)triethoxysilane-coated magnetite nanoparticles. J. Magn. Magn. Mater. 279 (2004) 210.

[445] N. Aoki, K. Kinoshita, K. Mikuni, K. Nakanishi, K. Hattori, Adsorption of 4-nonylphenol ethoxylates onto insoluble chitosan beads bearing cyclodextrin moieties. J. Incl. Phenom. Macrocycl. Chem. 57 (2007) 237.

[446] M. Kitaoka, K. Hayashi, Adsorption of bisphenol A by cross-linked beta-cyclodextrin polymer. J. Inclusion Phenom. Macrocyclic Chem. 44 (2002) 429.

[447] P. Xiao, Y. Dudal, F. -X. Philippe Corvini, P. Shahgaldian, Polymeric cyclodextrin-based nanoparticles: synthesis, characterization and sorption properties of three selected pharmaceutically active ingredients. Polym. Chem. 2 (2010) 120.

[448] D. Bonenfant, P. Niquette, M. Mimeault, A. Furtos-Matei, R. Hausler, UV-VIS and FTIR spectroscopic analyses of inclusion complexes of nonylphenol and nonylphenol ethoxylate with beta-cyclodextrin. Water Res. 43 (2009) 3575.

[449] E. Alvira, J. A. Mayoral, J. I. Garcia, Molecular modelling study of [beta]-cyclodextrin inclusion complexes. Chem. Phys. Lett. 271 (1997) 178.

[450] M. Mimeault, D. Bonenfant, FTIR spectroscopic analyses of the temperature and pH influences on stratum corneum lipid phase behaviors and interactions. Talanta 56 (2002) 395.

[451] M. Maurer, B. Escher, P. Richile, C. Schaffner, A. Alder, Elimination of beta-blockers in sewage treatment plants. Water Res. 41 (2007) 1614.

[452] D. Ashton, M. Hilton, K. V. Thomas, Investigating the environmental transport of human pharmaceuticals to streams in the United Kingdom. Sci. Total Environ. 333 (2004) 167.

[453] A. Wick, G. Fink, A. Joss, H. Siegristi, T.A. Ternes, Fate of beta blockers and psycho-active drugs in conventional wastewater treatment. Water Res. 43 (2009) 1060.

[454] A. A. M. Stolker, W. Niesing, E. A. Hogendoorn, J. F. M. Versteegh, R. Fuchs, U. A. Th. Brinkman, Liquid chromatography with triple-quadrupole or quadrupole-time of flight mass spectrometry for screening and confirmation of residues of pharmaceuticals in water. Anal. Bioanal. Chem. 378 (2004) 955.

[455] T. V. Madureira, M. J. Rocha, C. Cruzeiro, M. H. Galante, R.A. F. Monteiro, E. Rocha, The toxicity potential of pharmaceuticals found in the Douro River estuary (Portugal): assessing impacts on gonadal maturation with a histopathological and stereological study of zebrafish ovary and testis after sub-acute exposures. Aquat. Toxicol. 105 (2011) 292.

[456] M. Cleuvers, Initial risk assessment for three beta-blockers found in the aquatic environment. Chemosphere 59 (2005) 199.

[457] B. I. Escher, N. Bramaz, M. Richter, J. Lienert, Comparative ecotoxicological hazard assessment of beta-blockers and their human metabolites using a mode-of-action-based test battery and a QSAR approach. Environ. Sci. Technol. 40 (2006) 7402.

[458] H. Ericson, G. Thorsén, L. Kumblad, Physiological effects of diclofenac, ibuprofen and propranolol on Baltic Sea blue mussels. Aquat. Toxicol. 99 (2010) 223.

[459] E. Giltrow, P.D. Eccles, M. J. Winter, P. J. McCormack, M. Rand-Weaver, T. H. Hutchinson, J. P. Sumpter, Chronic effects assessment and plasma concentrations of the beta-blocker propranolol in fathead minnows (Pimephales promelas). Aquat. Toxicol. 95 (2009) 195.

[460] E. Isarain-Chávez, R. M. Rodríguez, P. L. Cabot, F. Centellas, C. Arias, J. A. Garrido, E. Brillas, Degradation of pharmaceutical beta-blockers by electrochemical advanced oxidation processes using a flow plant with a solar compound parabolic collector. Water Res. 45 (2011) 4119.

[461] H. Yang, T. An, G. Li, W. Song, W. J. Cooper, H. Luo, X.Guo, Photocatalytic degradation kinetics and mechanism of environmental pharmaceuticals in aqueous suspension of TiO_2: a case of beta-blockers. J. Hazard. Mater. 179 (2010) 834.

[462] I. Ali, V. K. Gupta, Advances in water treatment by adsorption technology. Nat Protoc 1 (2007) 2661.

[463] S. Nishijima, S. -I. Takeda, Research and development of superconducting high gradient magnetic separation for purification of wastewater from paper factory. IEEE T. App. Superconduc. 17 (2007) 2311.

List of publications

Journal Articles

<u>Sudipa Ghosh</u>, A.Z.M. Badruddoza, M.S. Uddin, K. Hidajat, Adsorption of chiral aromatic amino acids onto carboxymethyl-β-cyclodextrin bonded Fe_3O_4/SiO_2 core-shell nanoparticles, *J. Colloid Interface Sci*. 354(2) (2011) 483-492.

A. Z. M. Badruddoza, <u>Sudipa Ghosh</u>, Md. Taifur Rahman, Zakir Hossain, K. Hidajat, M.S. Uddin, Multifunctional silica core-shell nanoparticles with magnetic, fluorescent, cell targeting and drug-inclusion functionalities for biomedical applications, *Manuscript in preparation.*

<u>Sudipa Ghosh</u>, A.Z.M. Badruddoza, M.S. Uddin, K. Hidajat, Adsorptive removal of emerging contaminants from aqueous solutions using superparamagnetic Fe_3O_4 nanoparticles bearing aminated β-cyclodextrin, *Manuscript in preparation.*

<u>Sudipa Ghosh</u>, Tan Hui Fang, M. S. Uddin, K. Hidajat, Enantioselective separation of chiral aromatic amino acids with surface functionalized magnetic nanoparticles, *Submitted to Colloids and Surfaces B: Biointerfaces (under revision)*.

<u>Sudipa Ghosh</u>, Quek Jee Teck, M. S. Uddin, K. Hidajat, Sorption separation of beta-blocker propranolol from aqueous solution by surface functionalized magnetic nanoparticles, *Manuscript in Preparation*.

Conference Presentations

<u>Sudipa Ghosh</u>, A. Z. M. Badruddoza, M. S. Uddin, K. Hidajat, Surface Functionalized Magnetic Nanoparticles for separation of chiral amino acids, *ChemBiotech*, National University of Singapore, Singapore, January 28-29, 2010.

<u>Sudipa Ghosh</u>, Won Guon Xiang, A. Z. M. Badruddoza, M. S. Uddin, K. Hidajat, Surface Functionalized Magnetic Nanoparticles for separation of chiral biomolecules, The 5th

SBE International Conference on Bioengineering and Nanotechnology *(ICBN)*, Bioplois, Singapore, August 1-4, 2010.

Sudipa Ghosh, Tan Hui Fang, M. S. Uddin, K. Hidajat, Enantioselective separation of chiral aromatic amino acids with surface functionalized magnetic nanoparticles, 14th Asia Pacific Confederation of Chemical Engineering Congress *(APCCHE)*, Suntech City, Singapore, February 21-24, 2012.